The Role of the Adaptor Protein ADAP in different T cell Subsets and Pathogen-specific Immune Responses against *Listeria monocytogenes*

Dissertation

zur Erlangung des akademischen Grades

doctor rerum naturalium

(Dr. rer. nat.)

genehmigt durch die Fakultät für Naturwissenschaften
der Otto-von-Guericke-Universität Magdeburg

von

Gerald Peter Parzmair, MSc, BSc

geb. am 14. Dezember 1981 in Hallein, Österreich

Gutachter

Prof. Dr. Dunja Bruder

Prof. Dr. Wiebke Hansen

eingereicht am: 24. Mai 2016

verteidigt am: 21. September 2016

Supervisors:

Prof. Dr. Dunja Bruder
Prof. Dr. Burkhart Schraven

Meiner Mutter,
Sonja Parzmair,
gewidmet.

"The most exciting phrase to hear in science,
the one that heralds new discoveries,
is not 'Eureka' but 'That's funny...'."
— Isaac Asimov (1920–1992)

Danksagung

Contents

List of Figures

List of Tables

List of Abbreviations

aa	amino acids
ACK	ammonium chloride potassium
ADAP	adhesion and degranulation-promoting adaptor protein
ADCC	antibody-dependent cell-mediated cytotoxicity
Ag	antigen
ALT	alanine aminotransferase
APC	antigen presenting cell
APC	allophycocyanin
Bcl10	B-cell CLL-lymphoma 10
BHI	brain heart infusion
BMDC	bone marrow-derived dendritic cell
BSA	bovine serum albumin
BV	Brilliant Violet$^{\text{TM}}$
CARMA1	caspase recruitment domain-containing membrane-associated guanylate kinase protein 1
CARST	congenital autosomal recessive small-platelet thrombocytopenia
CBA	cytometric bead array
Cdk	cyclin dependent kinase
CFDA	carboxyfluorescein diacetate
CFSE	carboxyfluorescein succinimidyl ester
CFU	colony forming units
CNS	central nervous system
CTL	cytotoxic T lymphocyte
Cy	Cyanine
DC	dendritic cell
DMSO	dimethyl sulfoxide
DNA	desoxyribonucleic acid
EAE	experimental autoimmune encephalomyelitis
EDTA	ethylenediaminetetraacetic acid
ELISA	enzyme-linked immunosorbent assay
EVH1	Ena/VASP homology 1
FACS	fluorescence-activated cell sorting
FBS	fetal bovine serum
FITC	fluorescein isothiocyanate
FMO	fluorescence minus one
FSC	forward scatter
Fyb	Fyn-binding protein

Gads	Grb2-related adapter downstream of Shc
GEF	guanine nucleotide exchange factor
HGF	hepatocyte growth factor
HRP	horse radish peroxidase
hSH3	SH3 domein with an N-terminal α-helix
i.v.	*intravenous*
IFN-γ	interferon γ
IκBα	inhibitor of κB-α
IKK	IκB kinase
IL-2Rα	interleukin 2 receptor α chain
IMDM	Iscove's modified Dulbecco's medium
Inl	internalin
inLN	inguinal lymph nodes
iNOS	inducible nitroc oxide synthase
IS	immunological synapse
LAT	Linker of activated T cells
ldLN	liver-draining lymph nodes
LFA-1	lymphocyte function-associated antigen 1
LLO	listeriolysin O
Lm	*Listeria monocytogenes*
LPS	lipopolysaccharide
LTA	lipoteichoic acid
MACS	magnetic-activated cell sorting
MALT1	mucosa-associated lymphoid tissue lymphoma translocation gene 1
MFI	mean fluorescence intensity
MHC	major histocompatiblity complex
mRNA	messenger ribonucleic acid
MS	multiple sklerosis
Mst1	mammalian Ste20-like kinase
Nck	non-catalytic region of tyrosine kinase adapter protein 1
NETs	neutrophil extracellular traps
NF-κB	nuclear factor kappa-light-chain-enhancer of activated B cells
o/n	over night
OD	optical density
OVA	ovalbumin
PALS	periarterial lymphatic sheath
PB	pacific blue
PBS	phosphate buffered saline
PCR	polymerase chain reaction
PD-1	programmed death receptor 1
PE	phycoerythrin
PerCP	peridinin chlorophyll protein
PFA	paraformaldehyde
PKCθ	protein kinase C theta
PLC	phospholipase C
PRR	pattern recognition receptor
RAPL	Regulator for cell Adhesion and Polarization enriched in Lymphoid tissues

RIAM	Rap1 Interacting Adapter Molecule
RT	room temperature
SAV	streptavidin
SDS	sodium dodecyl sulfate
SH2	Src Homolgy 2
SH3	Src Homolgy 3
SKAP55	Src kinase-associated phosphoprotein of 55 kDa
SKAP-HOM	SKAP55 homologue
SLAP-130	SLP-76-associated phosphoprotein of 130 kDa
SLP-76	SH2-domain-containing leukocyte protein of 76 kDa
SMAC	supramolecular activation cluster
SSC	side scatter
T1D	type 1 diabetes
TAK1	TGF-β-activated protein kinase
TCR	T cell receptor
TGF-β	transforming growth factor β
TLR	Toll-like receptor
TMB	tetramethylbenzidine
TNF-α	tumor necrosis factor α
TRAF6	TNF receptor associated factor 6
UV	ultraviolet
VASP	vasodilator-stimulated phosphoprotein
VLA	very late antigen
vWF	von Willebrandt factor
WASp	WiskottAldrich syndrome protein
ZAP-70	Zeta-chain-associated protein kinase 70

"In the beginning the Universe was created. This made a lot of people very angry and been widely regarded as a bad move."

— Douglas Adams

1

Introduction

1.1 Adhesion and degranulation-promoting adaptor protein

Signaling processes in immune cells rely on adaptor proteins. These have no enzymatic activity themselves but serve as scaffolds for macromolecular signaling complexes (signalosomes). They contain specialized protein-protein and protein-lipid interaction domains that facilitate the binding to other parts of the signaling machinery and can be divided into two major groups: transmembrane and cytosolic adapter proteins [1, 2, 3].

The *adhesion and degranulation-promoting adapter protein* (ADAP) — also known as *Fyn-binding protein* (Fyb) or *SH2-domain-containing leukocyte protein of 76 kDa (SLP-76)-associated phosphoprotein of 130 kDa* (SLAP-130) — belongs to the group of cytosolic adaptors and was first discovered as an interaction partner for the T cell signaling proteins Fyn and SLP-76, as its alternative names indicate. The latter itself is a cytosolic adaptor while Fyn belongs to the Src family of kinases [4, 5]. In mice it is encoded on chromosome 15: 6,579,871–6,663,304 (Ensembl: ENSMUSG00000022148), while in humans it is found on chromosome 5: 39,105,236–39,274,528 (Ensembl: ENSG00000082074). The encoded protein has 783 amino acids (aa) in humans and 819 aa in mice and shares sequence identity of 72 % according to the BLAST algorithm [6]. ADAP expression has been shown in T cells [4], NK cells [7], platelets [8], myeloid cells [9] — like neutrophils, monocytes and *dendritic cells* (DCs) — and pre-B

cells, but not in mature splenic B cells [10]. Furthermore, it is also expressed in unconventional T cells like NKT, CD8$\alpha\alpha$ and TCR$\gamma\delta$ T cells [11].

In order to understand its role in signaling, its importance for cellular functions and its overall effects on the immune system, a closer look at its structural features is necessary.

1.1.1 Structure of ADAP

ADAP contains several structural features which enable it to fulfill its scaffold function (Figure 1.1). Among these are particular tyrosine phosphorylation motives that facilitate binding to *Src homology 2* (SH2) domains of other signaling proteins. Y^{595}DDV and Y^{651}DDV are responsible for the binding to the aforementioned SLP-76. Y^{625}DGI facilitates binding to the Fyn kinase and Y^{595}DDV has a double-function and also mediates binding to non-catalytic region of tyrosine kinase adaptor protein 1 (Nck) [12, 5, 13, 14].

Furthermore ADAP contains two unusual Src Homology 3 domains with an α-helix on the N-terminal end (hSH3). These two domains — the N-terminal hSH3^N and the C-terminal hSH3^C — mediate transient interactions with lipid membranes and the additional α-helices enhance the binding [15, 16]. Between these two hSH3 domains a binding site for *Ena/vasodilator-stimulated phosphoprotein (VASP) homology 1* (EVH1) is located [17], and ahead of the hSH3^N domain is a proline-rich region, which is responsible for the binding of ADAP to *Src kinase-associated phosphoprotein of 55 kDa* (SKAP55; also known as SKAP1) and its homologue (SKAP-HOM; also known as SKAP2) [18, 5, 14].

Recently, two more binding sites have been identified. One is located in the area of the hSH3^N domain and the EVH1 binding site and mediates interaction with *caspase recruitment domain-containing membrane-associated guanylate kinase protein 1* (CARMA1), while the other is located around the hSH3^C domain and binds to *transforming growth factor β* (TGF-β)-*activated protein kinase* (TAK1) [19, 20].

There are several other potential tyrosine phosphorylation motives in ADAP (at positions 559, 571, 755, 771 and 780) and in *in vitro* kinase assays mutation of the tyrosines to phenylalanines (rendering it non-functional) had moderate to significant effects on T cells adhesion and migration [14]. However, potential binding partners have yet to be identified and for the sake of simplicity these sites were left out of Figure 1.1.

The specific structural features of ADAP and its binding partners also determine its role in various signaling events that will be discussed in more details in the following sections.
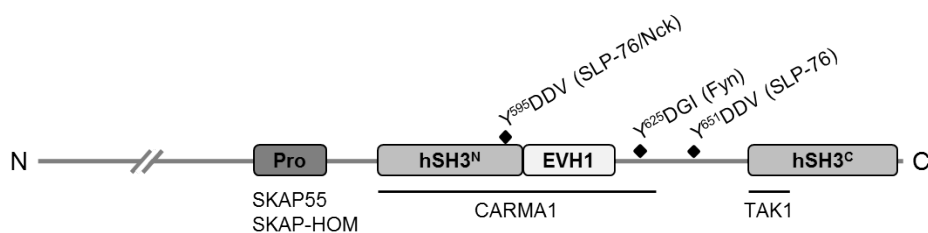
Figure 1.1: Structural features of ADAP that mediate binding to other signaling proteins.
ADAP contains several structural features mediating binding to other proteins of the signaling machinery.
The tyrosine phosphorylation motives Y^{595}DDV and Y^{651}DDV facilitate the binding to SLP-76, while
Y^{625}DGI is necessary for interaction with Fyn. Y^{595}DDV is also responsible for Nck-binding. Two hSH3
domains are important for the transient binding of the lipid membrane and an interaction site for EVH1
is located between these two. Binding to SKAP55 and SKAP-HOM is mediated by a proline-rich region
(PRO) and CARMA1 and TAK1 binding sites are found in the two hSH3 domains. The scheme was
adapted from Witte, et *al.* [21].

1.1.2 The role of ADAP in integrin activation

After its first description, ADAP was soon recognized as an important mediator of integrin
activation in T cells following TCR engagement [22, 23]. Important interaction partners for
ADAP in this respect are the aforementioned SKAP55 and SKAP-HOM. Approx. 70 % of
ADAP are constitutively bound to SKAP55 whereas all of SKAP55 is associated with ADAP
[24]. ADAP deficiency results in concomitant absence of SKAP55/SKAP-HOM on the protein
level, while mRNA levels were not affected [25], indicating that ADAP is necessary for stable
expression of these proteins [26, 27, 28]. On the other hand, knock-down of SKAP55/SKAP-
HOM had no effect on ADAP expression [29, 27].

After *T cell receptor* (TCR) activation the ADAP/SKAP55 module gets recruited to a plat-
form formed by *linker of activation of T cells* (LAT), *Grb2-related adapter downstream of Shc*
(Gads) and SLP-76, after the first has been phosphorylated by *zeta-chain-associated protein
kinase 70* (ZAP-70) [30, 31]. The ADAP/SKAP55 module then can bind the two Rap1 in-
teracting proteins, *Rap1 interacting adapter molecule* (RIAM) and *regulator for cell adhesion
and polarization enriched in lymphoid tissues* (RAPL) [32, 33]. Rap1 has been shown as a cru-
cial regulator of TCR-mediated integrin activation [34]. Loss of interaction of the latter with
ADAP/SKAP55 reduced the binding of Rap1 to CD11a (α_L), one chain of the integrin lympho-
cyte function-associated antigen 1 (LFA-1; CD11a/CD18), and, subsequently, reduces adhesion
[35]. Important for this interaction is also *mammalian Ste20-like kinase* (Mst1), which has been
shown to interact with RAPL [36], completing the so termed ADAP/SKAP55/RAPL/Mst1
complex. RIAM on the other hand interacts with Rap1, Mst1 and Kindlin-3, which is neces-
sary for binding and activation of CD18 (β_2), the second part of LFA-1) [35]. Both modules
— ADAP/SKAP55/RAPL/Mst1 and ADAP/SKAP55/Mst1/RIAM/Kindlin-3 — are crucial
for proper integrin activation in T cells (Figure 1.2A).
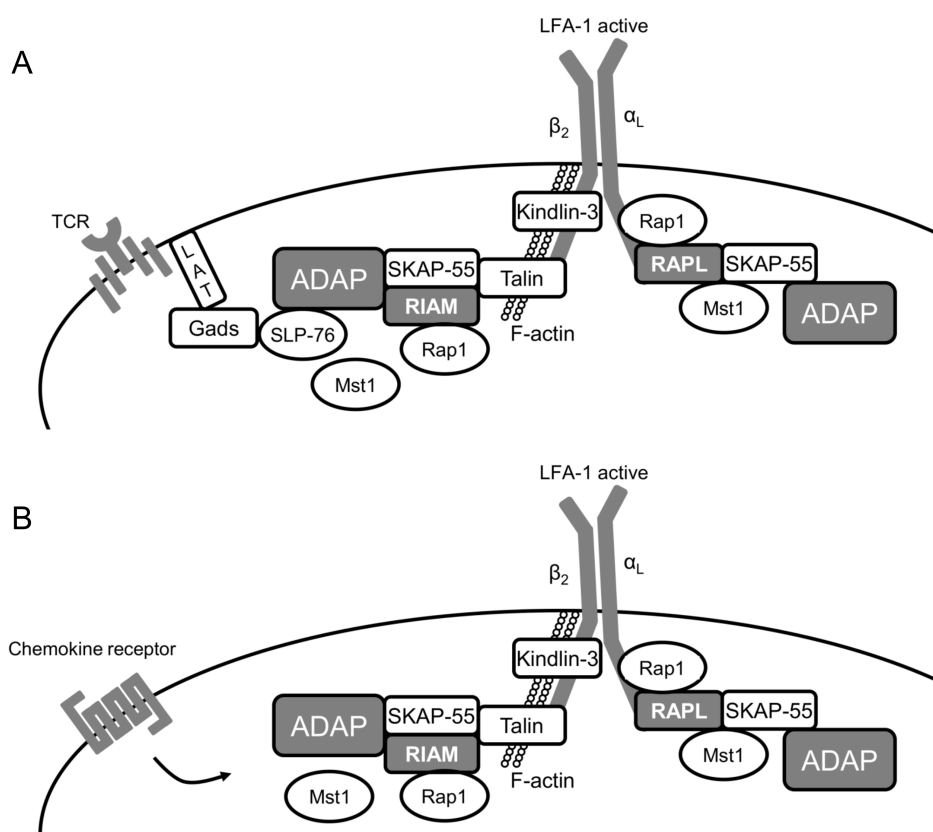
Figure 1.2: The role of ADAP in activation of integrins in T cells following TCR or chemokine receptor stimulation. (A) Following TCR-stimulation the ADAP/SKAP55 module is responsible for forming two distinct complexes that each exclusively interact with one of the chains of the integrin LFA-1 ($\alpha_L\beta_2$). Together with RAPL/Mst1/Rap1 it is responsible for the interaction with the α_L-chain, while in complex with the RIAM/Rap1/Mst1/Kindlin-3/Talin binding to the β_2-chain is mediated. This combined action leads to a conformational change in the structure of the integrin that subsequently activates it. (B) For the chemokine receptor induced activation of the integrin the modules are basically the same, although the direct mediators between the GPCR and the complexes remain elusive. The schemes were adapted from Witte, et *al.* [21].

Both modules have also been shown to play crucial roles in the signaling downstream of chemokine receptors CCR7 and CXCR4, also leading to integrin activation and highlighting the versatility of ADAP. Again, two complexes have been shown to be involved in the activation of integrin LFA-1 ($\alpha_L\beta_2$) in response to chemokine ligation, namely RAPL/Mst1/Rap1 and RIAM/Rap1/Mst1/Kindlin-3/Talin. Both complexes require the ADAP/SKAP55-module for the activation of this integrin in response to chemokine receptor mediated activation and each of these two complexes seems to interact with one of the two integrin chains exclusively [37]. While the RAPL/Mst1/Rap1 complex probably interacts with the α_L-chain via RAPL [33], the RIAM/Rap1/Mst1/Kindlin-3/Talin complex utilizes Kindlin-3 for the interaction with the β_2-chain [38] (Figure 1.2B).

Furthermore, rather recently the importance of ADAP has also been shown in the chemokine

receptor-mediated activation of the integrin *very late antigen-4* (VLA-4; $\alpha_4\beta_1$; CD49d/CD29), where it serves as a scaffold in recruiting the *guanine nucleotide exchange factor* (GEF) Vav1 [39]. The transient complex ADAP/SLP-76/Vav1 stimulates Rac1 activation; a crucial GTPase involved in the activation of the VLA-4 integrin [40].

Apart from T cells, the pivotal role of ADAP in adhesion regulation via integrins has also been demonstrated in neutrophil granulocytes. Here, ADAP and SLP-76 mediate E-selectin-mediated integrin activation, and subsequently, the recruitment of neutrophils in a mouse kidney ischemia-reperfusion injury model [41].

Taken together, these findings clearly demonstrate the paramount role of ADAP in integrin-associated adhesion and leukocyte recruitment. Nevertheless, key mechanisms as well as its role in other leukocytes remain elusive.

1.1.3 ADAP in NF-κB signaling

As mentioned above 70 % of ADAP are constitutively bound to SKAP55. The other 30 % belong to another module that serves an important role in *nuclear factor kappa-light-chain-enhancer of activated B cells* (NF-κB) activation; an important transcription factor for the activation and proliferation of T cells [42, 43]. NF-κB is usually found in an inactive state in the cytoplasm. This is maintained by the binding of *inhibitor of κB-α* (IκBα). A trimeric complex, called the *IκB kinase* (IKK) complex, consisting of IKKα, IKKβ and IKKγ, is needed to phosphorylate IκBα, facilitating the release of NF-κB. Upon this, NF-κB translocates to the nucleus and initiates the transcription of its target genes [44].

However, IKK is inactive under steady-state conditions. Upon TCR activation CARMA1 is recruited to the plasma membrane after phosphorylation by *protein kinase C theta* (PKCθ). CARMA1 then binds *B-cell CLL-lymphoma 10* (Bcl10) and *mucosa-associated lymphoid tissue lymphoma translocation gene 1* (MALT1); forming the CBM complex. In turn, this complex recruits the E3 ubiquitin protein ligase *TNF receptor associated factor 6* (TRAF6), which polyubiquitinates the inhibitory IKKγ subunit, leading to its degradation. Furthermore, the aforementioned TAK1 is recruited to the complex and phosphorylates IKKβ. All of this is fundamental for IKK activation, and subsequently, IκBα-release from NF-κB and translocation of the transcription factor to the nucleus [45, 44, 42].

Both, TRAF6 and TAK1 recruitment, have been shown to be impaired in $Adap^{-/-}$ T cells, signifying an important role for ADAP in these processes [46]. As a matter of fact, ADAP is required for the formation of the CBM complex that recruits TRAF6 and also directly binds TAK1, bringing it in close vicinity to the complex [46, 20]. Taken together, this demonstrates
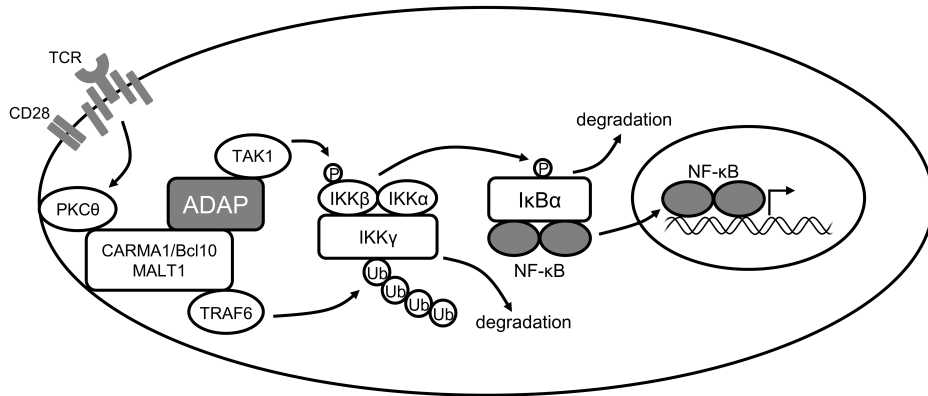
Figure 1.3: The role of ADAP in NF-κB signaling following TCR activation. Upon TCR and CD28 ligation CARMA1 is phosphorylated by PKCθ and recruited to the plasma membrane. In turn, CARMA1 binds Bcl10 and MALT1, forming the CBM complex, which is necessary for TRAF6 mobilization. TRAF6 polyubiquitinates the inhibitory γ-subunit of IKK, leading to its degradation. ADAP has a pivotal role in stabalizing this CBM complex, but also recruits TAK1. This kinase, on the other hand, is needed for the phosphorylation of IKKβ, rendering the IKK kinase functional. Subsequently IKK phosphorylates the inhibitory protein IκBα, which leads to the release of NF-κB. Finally, the transcription factor is able to translocate to the nucleus, where it initiates the transcription of its target genes. The scheme was adapted from Witte, et *al.* [21].

the formation of a PKCθ/CBM/TRAF6/ADAP/TAK1 signalosome that promotes NF-κB activation. This is depicted in Figure 1.3.

1.1.4 ADAP in cell cycle progression

The proliferation of T cells is not only affected by loss of ADAP due to impaired NF-κB signaling. It has also been recognized that ADAP serves an important role in cell cycle progression during the G1-S transition phase after TCR activation. Temporary accumulation of cyclin and *cyclin-dependent kinases* (CDKs) is needed for cell cycle progression. Following TCR activation the usual sequence is as follows: Cdk4 and Cdk6 are activated during the G1 phase. This leads to cyclin E induction and at the G1 late phase restriction point Cdk2 is activated [19].

However, cyclin E is only transiently expressed after TCR activation, probably due to increased ubiquitination and subsequent degradation. The interaction of ADAP with CARMA1 and TAK1 is necessary for proper cyclin E expression. Interestingly, only the interaction with CARMA1 seems to be crucial for Cdk2 activation. Taken together, this demonstrates ADAP's paramount role in the induction of T cell proliferation [19].

1.1.5 The role of ADAP in the reorganization of the actin cytoskeleton

Rearrangement of the actin cytoskeleton is a prerequisite for proper formation of the *immunological synapse* (IS). This term refers to a cellular structure that is formed at the interface of a T cell and an APC or target cells. It is characterized by accumulation of signaling proteins, receptors and machinery for exocytosis [47]. As mentioned above (see section 1.1.2), upon TCR ligation, several tyrosine kinases become activated and in turn activate and recruit LAT and SLP-76, together forming the base of a signalosome. These proteins, together with Vav1, also play an important role in mediating TCR-induced actin cytoskeletal reorganization [48, 49, 17, 50].

Furthermore, two additional proteins, *Wiskott-Aldrich syndrome protein* (WASp) and WAVE2, are pivotal in several crucial cellular roles of the actin cytoskeleton [51, 52, 53]. Furthermore, the interaction of SLP-76/Vav1 and Nck has been identified as necessary for WASp recruitment to the IS [54]. However it soon became apparent that Nck alone was not able to mediate this recruitment of WASp to the IS. ADAP has been shown to constitutively interact with WASp and only a joint action of ADAP with Nck was able to induce proper actin cytoskeletal reorganization [55].

1.1.6 ADAP in TGF-β signaling

TGF-β1 — the most abundant isoform of TGF-β — is an important cytokine that controls the initiation and resolution of inflammation during infections [56]. It is usually secreted as an inactive precursor that is bound to *latency associated peptide* (LAP) and latent *TGF-β-binding protein* (LTBP), and due to this, not able to ligate with its receptor [57]. It is activated in several ways, including (i) protease-mediated cleavage by matrix metalloproteinases MMP-9 and MMP-2 [58] and (ii) by release from the latency complex mediated by α_V-integrin, with or without proteolytic help form metalloproteinases [59, 57, 60, 61]. Upon its activation, TGF-β is able to bind to its receptor, TβRI/II; a heterodimer. This ligation leads to the activation of SMAD-dependent and -independent pathways and subsequently to an increase in the expression of the integrins CD103 ($\alpha_E\beta_7$) and *very late antigen-1* (VLA-1; $\alpha_1\beta_1$; CD49a/CD29) [62].

It has recently been shown by Li, et *al.* [62] that ADAP plays a pivotal role in these processes by taking part in a pathway downstream of the TβRI/II. This pathway includes the aforementioned TRAF6, ADAP itself, TAK1 and the rector-regulated (R-) SMAD3 transcription factor. Furthermore, together with TRAF6 and TAK1 it mediates the TGF-β1-induced expression of

CD103 and there is also evidence that ADAP is involved in the control of the surface expression levels of VLA-1 [62].

1.1.7 ADAP in PD-1 expression

Programmed cell death protein 1 (PD-1), also known as CD279, is an inhibitory receptor expressed on activated T cells. Its natural ligands are PD-1L and PD-2L, and upon ligation, the receptor reduces the response of the cell in a regulatory manner and is important for the control of T cell responses [63].

Recently, ADAP has been identified as a key player in the induction of PD-1 expression following T cell activation. Li, et *al.* [64] demonstrated that the ADAP/SKAP55 module is necessary for the expression and activation of the transcription factor *nuclear factor of activated T cells c1* (NFATc1), which in turn is responsible for the expression of PD-1.

1.1.8 Cellular effects of ADAP deficiency

The importance of ADAP in the above mentioned cellular processes has direct effects on the function of cells when they are devoid of ADAP. These ramifications will be discussed in the paragraphs to follow, and as discussed earlier, T cells were the first cell type that was investigated for the role of ADAP in their function.

The conventional $Adap^{-/-}$ mouse

Most of the studies mentioned above were performed with cells from the conventional $Adap^{-/-}$ mouse that was created and first described by Peterson, et *al.* [23]. They performed a detailed analysis of the hematopoietic cellularity in these mice (summarized in Table 1.1).

$Adap^{-/-}$ mice showed reduced numbers of T cells. More specifically, CD4$^+$ and CD8$^+$ T cells were reduced. The number of B220$^+$ B cells was increased, while the number of DX-5$^+$ NK cells was comparable to the numbers found in wild type littermates. In the blood of the knock-out mice, the white blood cell count was unaffected, as was the hematocrit. Interestingly, the number of platelets was significantly reduced in $Adap^{-/-}$ mice. Furthermore, thymocyte numbers were also significantly reduced [23]. Wu, et *al.* [65] analyzed the thymocyte compartment in more detail and this will be discussed below.

Table 1.1: Hematopoietic cellularity of wild type and $Adap^{-/-}$ mice. $\bar{x}$ represents means and SD the standard deviation of the mean. T cells were identified by CD3 staining. CD4$^+$ T cells by CD4 and CD8$^+$ by CD8. B220 identified B cells, wheras NK cells were defined as DX-5$^+$. WBC stands for white blood cells. The table was adapted from Peterson, et *al.* [23].

	Hematopoietic cellularity of wild type and $Adap^{-/-}$ mice				
	$Adap^{+/+}$		$Adap^{-/-}$		
	$\bar{x}$	$\pm$ SD	$\bar{x}$	$\pm$ SD	p value
Thymocytes [$\times 10^6$]	254	88	188	66	0.001
Splenocytes [$\times 10^6$]	94	22	82	9	*NS*
CD3$^+$ [%]	35	5	22	4	0.0001
CD4$^+$ [%]	29	5	19	2.8	0.002
CD8$^+$ [%]	13.5	3.1	7.8	2.2	0.0004
B220$^+$ [%]	52	6.8	69	1.5	0.001
DX-5$^+$ [%]	3.8	1.2	2.9	0.14	*NS*
WBC per µL[$\times 10^3$]	7.8	4.1	6.9	3.3	*NS*
Hematocrit [%]	49	8	51	5	*NS*
Platelets per µL[$\times 10^3$]	721	275	410	74	0.01

ADAP during the development of T cells

ADAP is found in developing T cells in the thymus throughout their maturation. However the extent of its expression is variable. The early stage *double-negative* (DN) thymocytes, that neither express CD4 nor CD8, have considerable amounts of ADAP. This decreases by approx. 2.2-fold when the cells progress towards the *double-positive* (DP) stage and express CD4 as well as CD8. Following that, thymocytes progress to a *single-positive* (SP) stage, where they only express either CD4 or CD8 and ADAP expression in SP thymocytes increases again by about 2.5-fold. Comparison between SP CD4$^+$ thymocytes and mature splenic CD4$^+$ T cells revealed no differences in ADAP expression levels. However, following TCR-activation and progression of the T cells towards effector and memory phenotype, the amount of ADAP in the cells increases again 1.7-fold [11].

Analysis of the cellularity of T cells in $Adap^{-/-}$ animals revealed that these mice have significantly less thymocytes [22, 23, 65]. There is no difference in the numbers of DN thymocytes between $Adap^{-/-}$ and wild type animals. However, there are significantly less DP and SP thymocytes in the $Adap^{-/-}$ mice. This can be attributed to a reduced proliferation capability of DP thymocytes, and not to reduced survival of the cells. *Ex vivo* survival of the knock-out DP cells was comparable to their wild type counterparts. Furthermore, there is clear evidence that $Adap^{-/-}$ thymocytes exhibit inefficient positive selection of MHC-II-restricted cells, as well as

severely impaired negative selection [65].

Interestingly, ADAP seems not to be required in the development of unconventional thymic T cells subsets, like NKT, TCR$\gamma\delta$ and CD8$\alpha\alpha$ T cells, although its expression levels in these cells are comparable to conventional TCR$\alpha\beta$ T cells [11].

ADAP also seems to play a role in the development of memory phenotype (MP) T cells. These are cells that exhibit a memory phenotype, even though the organism never encountered antigen. This cell type can be identified as being CD44$^{\text{hi}}$ and either CD62L$^{\text{hi}}$ or CD62L$^{\text{lo}}$, depending on the literature [66, 67, 68], and arises usually during lymphopenic situations, such as neonatal development, chemotherapy or late-stage HIV infection [66]. According to Fiege, et *al.* [67], *Adap*$^{-/-}$ mice have approx. twice as many MP CD8^{+} T cells then their wild type littermates, and this most likely due to the reason that ADAP seems to dampen interleukin 15 (IL-15) signaling which together with IL-7 signaling is a prerequisite to become MP T cells.

Impact of ADAP on T cell activation and function

Very early studies focusing on the role of ADAP in T cells revealed that *Adap*$^{-/-}$ T cells were impaired in their activation and function. Peterson, et *al.* [23] as well as Griffiths, et *al.* [22] demonstrated already in 2001 that, upon TCR-stimulation, less *Adap*$^{-/-}$ T cell responded with expression of the early activation marker CD69, up-regulation of the high-affinity α chain of the *interleukin 2 receptor* (IL-2Rα; CD25), proliferation as well as production of the cytokines IL-2 and *interferon γ* (IFN-γ). Mueller, et *al.* [69] analyzed the impact of ADAP-deficiency in a CD4^{+} T cell TCR-transgenic mouse model in more detail. These DO11.10 mice produce CD4^{+} T cells with a TCR specific for a peptide from ovalbumin, OVA$_{323-339}$ (N–ISQAVHAAHAEINEAGR–C). *In vitro* stimulation of *Adap*$^{-/-}$ CD4^{+} DO11.10 cells revealed strongly reduced proliferation and impaired up-regulation of the early activation markers CD69 and CD25. Furthermore, they were able to show in an adoptive transfer model that *Adap*$^{-/-}$ CD4^{+} T cells are also impaired in their proliferation *in vivo*, while interestingly the expression of CD69, CD25 and CD62L was normal.

The aforementioned role of ADAP in the activation of integrins (see section 1.1.2) results in impaired adhesion of *Adap*$^{-/-}$ cells to integrin ligands. The induced conjugation of T cells with APCs, and hence the formation of the immunological synapse, is in part mediated by adhesion of LFA-1 to its ligands ICAM-1 and 2. After the binding of the integrins the *supermolecular activation cluster* (SMAC) is formed at the synapse, a region where receptors are clustered and rearranged [70, 71, 72, 73]. This process also involves a complex reorganization of the actin cytoskeleton, and the role of ADAP in this process has been discussed in section 1.1.5. Thus, it comes as no surprise that *Adap*$^{-/-}$ T cells have been reported to show impaired IS formation

[43, 28, 69] and ADAP provides the necessary stability and duration of the IS needed for the adequate activation of CD4$^+$ T cells [74].

The role of ADAP in NK cell function

Fostel, et *al.* [7] were able to detect ADAP in NK cells and analyzed $Adap^{-/-}$ NK cells from $Adap^{-/-}$ mice by applying different stimulation schemes. Mouse NK cells show a natural cytotoxicity against YAC-1 cells [75] and NK cells devoid of ADAP showed similar cytotoxicity as wild type cells. Also in an *antigen-dependent cellular cytotoxicity* (ADCC) model [76], $Adap^{-/-}$ NK cells displayed wild type killing capacity. Stimulation via the activating receptors Ly49D and 2B4 [77, 78] also revealed no significant differences. IFN-γ production was also not affected by loss of ADAP when the cells were stimulated with an antibody against 2B4 or the cytokine IL-12 [79]. The authors also assessed the ability of $Adap^{-/-}$ NK cells to suppress tumors in the metastatic model B16. Tumor growth is markedly increased when NK cells were depleted with an αNK1.1 antibody, which confirmed their involvement [80]. However, in the study presented by Fostel, et *al.* [7] ADAP deficiency had no effect on the suppression of tumor growth.

May, et *al.* [81] demonstrated in 2013 that NK cells relied on ADAP for their activation, quite to the contrary to the results published by Fostel, et *al.* [7]. They stimulated wild type and $Adap^{-/-}$ NK cells with anti-Ly49D treatment — as did Fostel and colleagues — and found that the $Adap^{-/-}$ NK cells produced less IFN-γ and showed reduced expression of the degranulation and cytotoxicity marker CD107a. Interestingly, they reported that the proliferation of the cells under these circumstances was not affected by loss of ADAP. Also in 2013, a few months later, Rajasekaran, et *al.* [82] published a comprehensive analysis of the signaling machinery involved in NK cell activation. They reported that ADAP exclusively regulates — together with Fyn and via the CBM signalosome (see section 1.1.3) — the production of IFN-γ, GM-CSF, CCL3, CCL4 and CCL5 upon stimulation via NKG2D and CD137. When the cells were stimulated with a cocktail of IL-12 and IL-18, $Adap^{-/-}$ NK cells responded with less cytokine production only for CCL3 and CCL4. Of note, the cytotoxicity of the NK cells was not affected by loss of ADAP.

Together these data suggest an important role for ADAP in the regulation of cytokine production in killer cells (CD8$^+$ cytotoxic lymphocytes and NK cells), while it seems dispensable for their cytotoxicity. The former is mediated via formation of the CBM signalosome, while the latter is independent of ADAP, and likely, the induction of proliferation and cytotoxicity is found upstream of ADAP, though Fyn is involved in this process [82, 83].

ADAP in Neutrophils

Neutrophil granulocytes have been shown to utilize ADAP for migration purposes. Block, et *al.* [41] used an ischemia-reperfusion induced *acute kidney injury* (AKI) model to study the recruitment of neutrophils to the kidneys in wild type and $Adap^{-/-}$ mice. They were able to demonstrate that ADAP is involved in E-selectin-mediated integrin activation. Loss of ADAP results in impaired rolling and adhesion to the endothelium and subsequent transmigration. This rendered $Adap^{-/-}$ mice less susceptible to AKI.

ADAP in dendritic cells (DCs)

Dendritic cells are important for the antigen-specific activation of T cells. ADAP has been shown to play only a marginal role in this cell type. *Bone marrow-derived dendritic cells* (BMDCs) showed normal skin colonization, spontaneous motility and antigen-induced migration in $Adap^{-/-}$ mice. Furthermore, antigen-uptake, maturation and adhesion of the $Adap^{-/-}$ dendritic cells were not aberrant *in vitro*. Despite the lack of ADAP, they also expressed wild type amounts of the cytokines *tumor necrosis factor alpha* (TNF-α) and IL-6. Moreover, *in vivo* the cells were able to fully activate T cells. However, conjugate formation with T cells was significantly impaired *in vitro*, but also this had no effect on the activation of T cells. As mentioned before, ADAP is also involved in the integrin outside-in signaling, and CD11c-mediated responses were clearly altered in $Adap^{-/-}$ BMDCs. The production of the cytokines TNF-α, IL-6 and IL-10 was markedly reduced upon activation via the integrin. On the other hand, the integrin-induced actin polymerization was significantly increased in the $Adap^{-/-}$ BMDCs [84].

ADAP in platelets

Platelets, also called thrombocytes, play an important role in blood coagulation and clotting blood vessel injuries [85]. The integrin *glycoprotein IIb/IIIa* (GPIIb/IIIa), also termed as $\alpha_{IIb}\beta_3$ (CD41/CD61), binds the ligands fibrinogen and *von Willebrand factor* (vWF), and is responsible for the capturing of platelets to the extracellular matrix of injured blood vessels [86, 87, 88]. ADAP has been shown to play a role downstream of tyrosine-kinase-coupled and G-protein coupled receptor mediated $\alpha_{IIb}\beta_3$ activation. Its deletion in mouse platelets does not completely abrogate the activation of the integrin, but significantly decreases it [89]. The ADAP/SKAP55 module cannot be responsible for this effect, since SKAP55 is not expressed in platelets. Only its homologue, SKAP-HOM, is found in platelets [90, 25, 89]. However, even this might not be involved in this process, since Kasirer-Friede, et *al.* [91] have shown integrin

activation even in the absence of this adaptor protein. Furthermore, the aforementioned proteins, RIAM and RAPL, seem not to be involved in the coupling of ADAP to the integrin, as it was the case in T cells (see section 1.1.2). However, talin and kindlin-3, both known to be involved in the coupling of ADAP to integrins in T cells, are also essential in platelets [91].

ADAP has also been implied in integrin outside-in signaling in platelets, where it mediates the activation of the cells via the binding of collagen to the integrin *very late antigen-2* (VLA-2; $\alpha_2\beta_1$; CD49b/CD29) [92]. But also the mechanotransduction, which is mediated by integrin $\alpha_{\mathrm{IIb}}\beta_3$ and leads to F-actin assembly and thereby promotes platelet spreading and thrombus stabilization, relies on ADAP [93].

ADAP in eosinophils

Eosinophil granulocytes are major contributors to the symptoms of allergic asthma, when they are recruited to the lung of affected individuals. In order to survive in the lung, the cells need activation- and survival-promoting signals derived from cytokines, such as GM-CSF, IL-5 and IL-3 [94, 95, 96]. The Mac-1 and LFA-1 ligand ICAM-1 is expressed on eosinophils following their activation with TNF-α, IFN-γ, IL-1 or GM-CSF [97, 98, 99, 100], and has been reported to modulate IL-5- and GM-CSF-induced activation of the cells [101, 102, 103, 104].

Pazdrak, et *al.* [105] reported an ADAP-dependent mechanism behind the modulation of the GM-CSF signaling by ICAM-1 ligation. The receptor for GM-CSF consists of a common β-chain, GMRβ — that is also part of the receptor complexes for IL-5 and IL-3 — and a high-affinity α-chain [106]. ADAP, together with Shc, Grb2 and Sos, was found to be a part in a complex that bridges ICAM-1 and GMRβ and is necessary in the modulation of the receptor by ICAM-1 [105].

ADAP in other cell types

As the role of ADAP is well described in T cells, and there are accumulating data for its function in other immune cells, it is surprising that findings in other cell types are scarce. To date there are no reports on the importance of ADAP in monocytes. Evidence for the role of ADAP in macrophages is only indirect, since its interaction partner SKAP-HOM (a.k.a. Skap-2) is required for the integrin-stimulated cytoskeletal rearrangement in these cells and phosphorylation of ADAP is dependent on this molecule [107].

Furthermore, a role for ADAP in the genesis of osteoclasts has been reported. These cells break down bone material and are essential in the homeostasis of the skeleton. The non-receptor tyrosine kinase c-Src is involved in signaling processes controlling proliferation, differentiation and transformation [108]. Mice that lack c-Src suffer from osteopetrosis — the failure to

break down bone — which is attributed to the reliance of osteoclasts on this kinase [109, 110]. Koga, et *al.* [111] were able to show that ADAP interacts with the aforementioned kinase and knock-down of ADAP severely impairs the differentiation of progenitor cells to osteoclasts.

1.1.9 The role of ADAP in disease mechanisms

As discussed above, ADAP deficiency has a variety of ramifications for a broad spectrum of cell types. Thus, ADAP has been implied in various disease settings in different animal models and also in humans with alterations in the gene responsible for its expression. The effects of ADAP deficiency will be discussed in the following paragraphs, and can be explained by ADAP's role as a positive regulator of immune cell function, but also of negative control mechanisms.

Loss of ADAP leads to CARST in humans

Recently, Levin, et *al.* [112] reported a case of *congenital autosomal recessive small-platelet thrombocytopenia* (CARST) in a family of five individuals of Arab Christian ancestry. The individuals had a nonsense mutation (c.G393A; p.W131X) in the *FYB* gene encoding for ADAP in humans, which is predicted to cause premature transcription termination. The disease manifested itself by smaller and less platelets in the blood stream of the patients and the cells responded less to stimuli. Overall the individuals suffer from an increased bleeding tendency that was partially predicted by the findings in $Adap^{-/-}$ mice. However the extent of the thrombocytopenia and the bleeding was more severe in the human patients. Interestingly, the patients showed no abnormal white blood cell count, and during 17 years of follow-up examinations, no incidence of enhanced susceptibility to infections was reported.

ADAP deficiency promotes allograft survival

ADAP deficiency has been convincingly implied in increased survival of xenogeneic allografts. Tian, et *al.* have shown in 2007 that heart transplants exhibited prolonged survival in $Adap^{-/-}$ mice [113]. Three years later they replicated their findings in an intestinal allograft model [114]. Intestinal transplants are considered especially challenging. Blockage of costimulatory signals by αCD40L monoclonal antibodies proofed to be a successful strategy in various transplantation models [115, 116]. However, this approach failed in mouse models of intestinal allografts.

Tian, et *al.* [114] were able to demonstrate that abrogation of co-stimulation together with ADAP deficiency protected intestinal transplants in mice. They attributed this fact to impaired T cell function, since $Adap^{-/-}$ T cells proliferated less in response to exposure to allo-

genic dendritic cells. Furthermore, $Adap^{-/-}$ host T cells infiltrated less into the transplanted intestinal allograft and were also less activated. Interestingly, the killing capacity of $Adap^{-/-}$ CTLs was not impaired when confronted with allogenic target cells.

ADAP improves HIV replication and propagation

The *human immunodeficiency virus 1* (HIV-1) infects and depletes selectively CD4$^+$ T cells, and by this, drastically impairs the immune system of affected individuals [117, 118]. Viral penetration into the cells necessitates binding to the receptors CD4, CXCR4 and CCR5 and the replication of the viral particles is mainly mediated by the transcription factors NFAT, AP1 and NF-κB [119, 120]. Viral replication requires activation of T cells and is severely impaired in quiescent cells [121]. The virus can also utilize cell-to-cell transmission with membrane nanotubes or the formation of a *virological synapse* (VS) between infected and uninfected cells [122, 123, 124]. This propagation mode is at least 500-fold more efficient than infection by free virus particles [125, 124, 126]. VS-mediated viral propagation requires the localization of the aforementioned receptors, plus the integrin LFA-1 and its ligand ICAM-1 at the cell-to-cell contact site and blockage of integrin ligation abrogates VS formation and subsequently transfer of virus from infected to uninfected cells [127, 124, 122, 125, 128, 129, 130].

Wei, et *al.* [131] analyzed the role of ADAP in viral replication and propagation, since it has been known to be involved in NF-κB and integrin signaling (see section 1.1.3 and section 1.1.2). They were able to identify ADAP as an important regulator of the two aforementioned processes: (i) it is required for the activation of NF-κB following CD3/CD28-mediated stimulation and subsequent initiation of viral replication, and (ii) ADAP-deficiency severely affected formation of the VS and markedly impaired viral propagation to uninfected cells.

ADAP deficiency enhances anti-tumor immune response

It has been recognized that expression of the PD-1 receptor reduces CD8$^+$ CTL-mediated anti-tumor responses [132, 133] and blockage of the interaction between the receptor and its ligand PD-L1 presents a potential clinical strategy for tumor treatment [134, 135, 136, 137]. Since ADAP is involved in the activation of integrins, which are necessary for the formation of the cytotoxic synapse, it came as a surprise that Li, et *al.* [64] were able to show that ADAP deficiency improved the killing capacity of CD8$^+$ CTLs. This was attributed to the aforementioned fact (see section 1.1.7) that ADAP is involved in the expression of PD-1 via a pathway including SKAP55, and the transcription factor NFATc1. ADAP deficiency actually significantly enhanced DC-based anti-tumor vaccine approaches in mice. This is a clear indication that ADAP is not only involved in positive regulatory mechanisms of the immune system, but also plays a role in negative ones.

ADAP protects from influenza A virus infection

The first data on the role of ADAP in an immune response during an infection was reported by Li, et *al.* [62]. As mentioned above (see section 1.1.6) ADAP is involved in the signaling downstream of TβRI. ADAP deficiency leads to impaired TGF-β production which has drastic effects if $Adap^{-/-}$ mice are infected with influenza A virus. The authors reported that $Adap^{-/-}$ mice exhibited enhanced mortality after infection with H5N1 and H1N1 influenza A viruses. The knock-out mice lost significantly more weight during the course of the infection. Furthermore, massively more $CD8^{+}$ T cells infiltrated into the bronchial lumen, and the mice experienced a cytokine storm with vastly increased amounts of IL-1β, IL-6, TNF-α, IFN-γ, and the chemokines CCL2 (MCP-1), CCL3 (MIP-1α), CCL5 (RANTES) and CXCL10 (IP-10). Histological scoring revealed severe lung damage and higher viral load. This further highlights the importance of ADAP not only in the positive regulation of immune responses, but also in the negative control mechanisms that keep the immune system in check.

Absence of ADAP attenuates EAE in mice

Experimental autoimmune encephalomyelitis (EAE) is an eponymous autoimmune disorder affecting the *central nervous system* (CNS) and serves as an animal model for the human disease *multiple sclerosis* (MS) [138]. It is mainly mediated by T cells and a proinflammatory cascade involving T_H17 cells, IL-6 and TGF-β [139, 140]. In order to analyze the impact of ADAP deficiency on EAE disease progression, Engelmann, et *al.* [141] induced EAE by immunizing wild type and $Adap^{-/-}$ mice with MOG_{35-55}-peptide. The $Adap^{-/-}$ mice showed an attenuated clinical course of the disease. Moreover, less proinflammatory cells invaded the spinal cord and significantly lower amounts of MOG-specific antibodies were found in the serum of the $Adap^{-/-}$ mice.

It was reasonable to assume that this phenotype was caused by above described impaired T cell function. However, $Adap^{-/-}$ T cells transferred into T cell-deficient $Lck^{-/-}$ mice were able to induce EAE at comparable levels to their wild type counterparts. Furthermore, MOG-peptide specific TCR-transgenic 2D2 T cells failed to induce EAE when transferred to $Adap^{-/-}$ mice. Hence, it is likely that the effects of ADAP deficiency were not T cell intrinsic. Even more interesting, bone marrow chimeras demonstrated that the observed effects were likely not caused by hematopoietic cell types. The authors also reported that T cells accumulate in peripheral lymph nodes, although the cause for this remains elusive.

ADAP deficiency increases diabetes incidence due to lymphopenia

Type 1 diabetes (T1D) is a disease that develops due to autoimmune targeting of self-antigens on β-islet cells [142, 143]. One identified cause for increased T1D risk is T cell lymphopenia. An explanation for this might be, that the T lymphocytes are subjected to less competition for growth and activation signals, which leads to increased expansion and activation of autoreactive T cell clones [144, 145, 146, 147, 148]. Zou, et *al.* [149] bred $Adap^{-/-}$ mice to BCD2.5 mice to analyze the effects of ADAP deficiency on the development of diabetes. BCD2.5 mice generate $CD4^+$ T cells with a TCR specific for islet cell-specific antigen [150]. With this model Zou, et *al.* found that ADAP deficiency led to a drastically increased incidence of diabetes and this was most likely due to the fact that the $Adap^{-/-}$ mice exhibited a markedly reduced thymic $CD4^+$ T cell output, which resulted in lymphopenia induced diabetes.

Taken together, the presented studies show that ADAP is involved in a plethora of functions of different aspects of the immune systems and its absence can have diverse effects in various disease models.

1.2 Murine listeriosis as a model for probing immune responses

The Gram-positive bacterium *Listeria monocytogenes* was first described in 1926 by Murray, et *al.* [151] as *Bacterium monocytogenes* after being isolated from rabbits, where it caused a lethal infection and the eponymous increase in monocyte numbers in circulating blood (Figure 1.4A). A year later it was also found in gerbils by Pirie and was renamed *Listerella hepatolytica*, to honor the British surgeon Joseph Lister (1827–1912) [152]. Its final name was adopted in 1940. At first seen only as an animal pathogen that was also able to sometimes infect humans, it was recognized as a human pathogen in the 1970s [153] and, later in the 1980s, it became clear that the usual transmission route was ingestion of contaminated food [154].

The disease caused by the bacterium was termed listeriosis (ICD-10 A32) and its clinical manifestations include gastroenteritis, septic abortions in pregnant women, meningitis and encephalitis [157]. Although its incidence is rather low, with 0.26 cases per 100,000 individuals and estimated 1600 illnesses per year in the United States of America [158, 159], its lethality rate is astonishingly high — up to 30 % worldwide — in immunocompromised individuals, neonates and fetuses [160].

The bacterium itself is a facultative intracellular pathogen and was already used in the 1960s as a means to study cellular immune responses against these kinds of infections [161, 162]. And
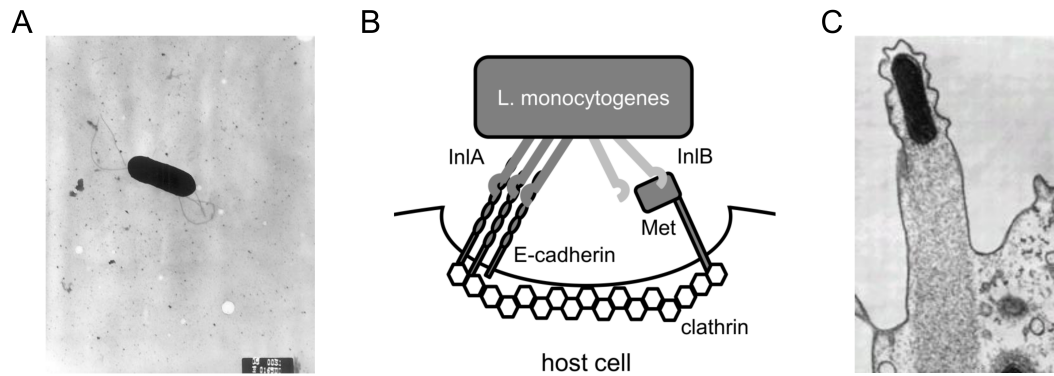
Figure 1.4: Electron micrograph and propagation mechanisms of *Listeria monocytogenes*. (A) Electron micograph of *L. monocytogenes*. Picture taken from the Centers for Disease Control and Prevention's Public Health Image Library. (B) Voluntary uptake of *L. monocytogenes* via the to two virulence factors InlA and InlB. Binding of InlA to host E-cadherin, or binding of InlB to the receptor tyrosine kinase Met initiates clathrin mediated endocytosis of the pathogen. Schema adapted from Stavru, et *al.* [155]. (C) Actin "comet tail" formation and resulting membrane protrusions that facilitate the propagation of the bacterium to neighboring host cells. Taken from Kuo & McGrath [156].

since then it established itself as a model system and contributed extensively to our current knowledge of the immune system.

1.2.1 Pathophysiology and cell biology of *L. monocytogenes* infection

The pathogen usually enters the body via the digestive tract. This is where it shows for the first time one of its key pathological features: crossing barriers. After it crosses the intestinal epithelium, it disseminates into lymph and blood stream. From there it is able to spread into deeper tissues, but the primary sites for bacterial replication are the spleen and the liver. However, at later stages it is able to cross two other barriers. After crossing the feto-placental barrier it infects the fetus which can lead to abortion or stillbirth. The third barrier is the blood-brain barrier, and after crossing it, *L. monocytogenes* can cause meningitis and encephalitis [155].

The ability of the pathogen to easily cross epithelial barriers can be attributed to certain molecular features with which it utilizes host machinery for its purposes. These include induced uptake into host cells, escape from phagosomes and propagation into other cells. These will be discussed in the following sections.

Induced *L. monocytogenes* uptake by host cells

The voluntary uptake of the pathogen is mediated by two bacterial surface proteins — *internalin A* (InlA) and InlB — that belong to the leucine-rich repeat containing internalin family [163]. InlA binds to E-cadherin, an adherence junction protein on epithelial cells, which is also its own ligand [164], while InlB interacts with the receptor tyrosine kinase Met, with the endogenous ligand *hepatocyte growth factor* (HGF) [165]. Ubiquitous expression of Met facilitates the broad spectrum of cells that can be infected by the pathogen [155]. However, on the species-level there are restrictions. For example, the reason for the poor oral infection capacity in mice, compared to humans, is a different amino acid at position 16 of the murine E-cadherin, which impairs the binding of InlB at the intestinal level [166, 155]. Ultimately, the ligation of the internalins with the host receptors leads to clathrin-mediated engulfment of the bacterium and its entry into the cell [155, 167] (Figure 1.4B).

Escape of *L. monocytogenes* from phagosomes to the cytosol

Once inside the host cell, the bacterium finds itself inside a phagosome with a mildly acidic pH [168], but it needs to escape from it before it fuses with a lysosome, since this would mean its degradation. The pathogen has evolved machinery that facilitates this. The concerted action of two phospholipases — PI-PLC and PC-PLC — and *listeriolysin O* (LLO) disrupts the membrane of the phagosome, inhibits its fusion with the lysosome and releases the bacterium into the cytosol [155]. After entering the cytosol the pathogen starts its replication.

Motility and spreading from cell to cell

After replication the bacterium needs to spread to other cells. Listeria evolved an intricate mechanism to do so by polar expression of *actin-assembly-inducing protein* (ActA). ActA is structurally similar to the above mentioned WASp (see section 1.1.5), and can bind actin-related protein 2/3 (Arp2/3). This serves as a nucleation point for host actin polymerization, forming an actin "comet tail" due to the polar expression of ActA that propels the bacterium through the cell [169, 170, 171, 172] (Figure 1.4C). Upon reaching the host cell outer membrane, cell protrusions containing bacteria, are formed that are invaginated by neighboring cells. Via this mechanism *L. monocytogenes* can spread to other cells without cell lysis and never actually entering extracellular space, which leaves it protected form humoral aspects of the immune system, such as complement and antibodies [155]. Once inside the newly infected cells it uses its escape machinery (PI-PLC, PC-PLC and LLO) to exit the double-membrane vesicle that was created during the invagination process, and the cycle starts again [155]. The above

Table 1.2: Innate immune genes and *Listeria monocytogenes*. Innate immune gene knock-out mice and their response to *L. monocytogenes* infection. Taken from Pamer [157].

Mouse strain	Description	Response to infection
SCID	severe combined immunudeficiency	chronic infection, ultimately lethal
$Tnfr55^{-/-}$	tumor-necrosis factor receptor p55	highly susceptible, early lethality
$Ifn\text{-}\gamma^{-/-}$	interferon-γ	highly susceptible, early lethality
$Lt^{-/-}$	lymphotoxin	reduced resistance
$Trail^{-/-}$	TNF-related apoptosis-inducing ligand	increased resistance
$Ifn\text{-}\alpha r^{-/-}$	interferon-α receptor	increased resistance
$Irf3^{-/-}$	interferon-regulatory factor 3	increased resistance
$p47^{phox-/-}$	phagocyte oxidase of 47 kDa	mildly increased susceptibility
$Nos2^{-/-}$	inducible nitric-oxide synthase	moderately increased susceptibility
$Lfa1^{-/-}$	lymphocyte function-associated antigen 1	increased resistance
$Ccr2^{-/-}$	CC-chemokine receptor 2	very susceptible, early lethality
$Ccl2^{-/-}$	CC-chemokine ligand 2	moderately increased susceptibility
$Ccr5^{-/-}$	CC-chemokine receptor 5	normal resistance
$Tlr2^{-/-}$	Toll-like receptor 2	normal resistance
$Tlr4^{-/-}$	Toll-like receptor 4	normal resistance
$Myd88^{-/-}$	myeloid differentiation primary-response gene 88	very susceptible, early lethality
$Casp1^{-/-}$	caspase 1	mildly increased susceptibility
$Rip2^{-/-}$	receptor-interacting protein 2	increased susceptibility, delayed lethality
$Nf\text{-}\kappa b^{-/-}$	nuclear factor-κB	highly susceptible

described process is also responsible for the crossing of the blood-brain and feto-placental barriers [173, 174].

1.2.2 Innate immune responses against *L. monocytogenes* infection

Upon infection with *Listeria* the innate immune system is the first to respond to the pathogen. It is necessary for the survival of the mice [175] and its effectiveness has been proven in a plethora of knock-out mice models, reviewed by Pamer [157] and summarized in Table 1.2. Moreover, mice lacking T cell-mediated and humoral immunity were rather resistant to infection with this bacterial pathogen, further highlighting the importance of the innate immune system during the early phase of murine listeriosis [176].

Following introduction into the blood stream the bacteria primarily reside in macrophages and monocytes that finally end up in the marginal zone of the spleen that is located between the T cell-containing white pulp and the red pulp, dominated by B cells [177, 178]. The infected macrophages and monocytes gradually move to the white pulp area where the bacteria can infect surrounding cells by intercellular spreading as described above [177, 178]. From here,

the bacteria can spread systemically, especially to the liver. The innate immune system has a paramount role in preventing this and controlling bacterial proliferation and dissemination. Details of the involved mechanisms will be discussed in the following sections.

Inflammatory cytokines involved in the innate immune responses against *L. monocytogenes* infection

Certain cytokines play a paramount role during the early phase immune response against *L. monocytogenes* infection. IFN-γ seems to be a major player, since mice lacking the cytokine or the corresponding receptor were reported to be highly susceptible to the pathogen and succumbed quickly to it [179, 180]. During the innate response phase the cytokine is necessary for the activation of infected macrophages, which then are able to eradicate the intracellular pathogen [181]. But it has also been reported that high amounts of IFN-γ produced by NK cells can inhibit neutrophil migration towards foci of infection and severely affect survival of infected mice [182].

TNF-α also plays an important role in the innate immune response against *L. monocytogenes*. This has been shown by use of a mutant TNF receptor that cannot be downregulated during the infection. This drastically increased the resistance to *L. monocytogenes* infection [183]. Furthermore, mice deficient of the *TNF receptor protein 55* (TNFRp55) — a major molecule in TNF-α signaling — were highly susceptible to infection and died quickly [184, 185].

Interestingly, type I interferons (IFN-α and -β) seem to have detrimental effects during an infection with *L. monocytogenes*, even though they are known to be of paramount importance during viral infections. Mice lacking type I interferon receptors, as well as mice devoid of the transcription factor *IFN-regulatory factor 3* (IRF3), showed increased resistance against *L. monocytogenes*. This has been attributed to the type I interferon induced apoptosis of T cells, loss of TNF-producing cells and decreased viability of *L. monocytogenes*-infected macrophages [186, 187, 188, 189, 157].

Neutrophils during listeriosis

Neutrophils are among the first responders to infection and are able to control bacterial pathogens by phagocytosis and subsequent killing by production of reactive nitrogen and oxygen species [190]. These processes are also highly relevant during infection with *L. monocytogenes*, since mice in which *phagocyte oxidase of 47 kD*a (p47phox) or inducible nitric oxide synthase (iNOS, NOS2) were deleted, showed increased susceptibility [191, 192, 193]. This mode of killing is highly effective. But at the very beginning of the infection, neutrophils engulf relatively few bacteria. However at later stages of the infection they are among the cell

types that show the most bactericidal activity [194, 195]. Moreover, they can combat pathogens by formation of *neutrophil extracellular traps* (NETs). These are structures composed of DNA and anti-microbial proteins that are proficiently bactericidal [196].

In a recently published study by Carr, et *al.* [197] the importance of neutrophils during murine listeriosis was assessed by specific antibody-mediated depletion of these granulocytes with αLy6G treatment. This revealed that neutrophils play an important role in the immune response in the liver, where they are necessary for the control of bacterial growth even when low infection doses were used. On the other hand, neutrophils were only needed in the spleens for protection against high dose infections, while at lower doses they seemed not to play a vital role. Generally, at higher doses neutrophil-depleted animals quickly succumbed to the infection. $Lfa1^{-/-}$ mice showed increased neutrophil numbers in their blood streams — probably due to reduced endothelial adhesion — and increased resistance. This indicates that the LFA1-ICAM interaction does not play a vital role for neutrophils during listeriosis [198].

During the infection neutrophils produced considerable amounts of TNF-α which is known to play a pivotal role in the immune response and has been shown to be able to lyse infected hepatocytes [199, 200]. Production of IFN-γ by neutrophils during *Listeria* infection has been described earlier, but with a low-virulence strain (LM/OVA ΔactA) [201]. This could not be replicated by Carr, et *al.* [197], that used the wild type strain 10403S.

Monocytes, macrophages and dendritic cells during listeriosis

Macrophages are not only the primary site of bacterial replication, but also — especially in the liver in the form of resident Kupffer cells — responsible for the majority of the eradication of the pathogen in the early phase of the infection. These cells produce considerable amounts of TNF-α and IL-12, cytokines that elicit the production of IFN-γ by NK cells. In turn, this cytokine stimulates the infected resident macrophages to kill the intracellular bacteria [202, 181, 203, 178]. Furthermore, the recruitment of monocytes is a hallmark of listeriosis and eponymous for the pathogen. Mice deficient of the *CC chemokine receptor 2* (CCR2) or its ligand *CC chemokine ligand 2* (CCL2) were highly susceptible to infection with the pathogen and showed early lethality [204, 205]. And as with neutrophils, killing by production of reactive oxygen and nitrogen species is crucial in the innate immune response against *L. monocytogenes*, as shown by increased susceptibility and higher bacterial burdens in mice deficient of phagocyte oxidase and nitric oxide synthase [206, 192]. Interestingly, a monocyte-derived dendritic cell population has been identified, that is recruited to the spleen. These cells are not themselves infected by the bacteria but produce considerable amounts of TNF-α and iNOS, and were hence called TipDCs. Their recruitment is strongly dependent on CCR2-CCL2 signaling and they are essential for early control of the bacterial pathogen [191].

However, as described above, *L. monocytogenes* manages to quickly move from the marginal zone in the spleen to *periarteriolar lymphoid sheaths* (PALS) in the T cell zones and this migration is pivotal for its later systemic spreading. $CD8\alpha^+CD11c^+$ DCs are responsible for the transport of the bacteria to the PALS, as the pathogen seems to have evolved to take advantage of them [207, 194, 208]. 1 to 2 min after the bacteria have entered the blood stream they are taken up by myeloid cells. Opsonization with complement 3 and aggregation with $CD41^+$ platelets via GPIb facilitates their uptake by $CD8\alpha^+CD11c^+$ DCs. This was further proven by impaired targeting of the bacteria to this DC subset and bacterial replication when platelets were depleted from infected mice [209, 195].

Toll-like receptors (TLRs) are responsible for recognition of viral and bacterial patterns and induce activation of DCs and macrophages. Since *L. monocytogenes* is a Gram-positive bacterium, it does not contain *lipopolysaccharide* (LPS) in its outer membrane and hence lacks the ligand for TLR4. However, involvement of TLR2 and the downstream mediator MyD88 have been shown in knock-out mouse models. TLR2 recognizes, among others, *lipoteichoic acid* (LTA). Although TLR2 knock-out mice only showed slightly increased bacterial burden, signaling via this receptor also significantly increased phagocytosis of the pathogen. However, knock-out of MyD88, which is involved in a plethora of signaling pathways, leads to massively increased susceptibility and early lethality [210, 211, 212, 213]. Cytosolic microbial products are sensed by *nucleotide-binding oligomerization domain* (NOD) proteins and *NACHT-, LRR- and pyrin-domain-containing proteins* (NALPs) [214]. NOD2-deficient mice are more susceptible to oral, but interestingly, not to intravenous infection with *L. monocytogenes*. NOD2 recognizes *muramyl dipeptide* (MDP), which is present in Gram-positive as well as -negative bacteria [215, 216]. NALP3 (also known as cryopyrin), on the other hand, is responsible for the activation of caspase 1, a proteolytic enzyme that processes the cytokines IL-1β and IL-18, important for the activation of innate and adaptive immune mechanisms. Thus, NALP3-deficient macrophages showed decreased IL-1β-production in response to *L. monocytogenes*-infection [217].

NK cells during *L. monocytogenes* infection

The migration of infected $CD8\alpha^+CD11c^+$ DCs to the PALS coincides with migration of NK cells to this region, and when both are clustered the activation and IFN-γ production of the NK cells peaks at around 24 hours post infection [218, 219]. Proof for the activation of NK cells by DCs has been provided in the former studies where $CD11c^+$ cells were depleted and this drastically impaired NK cell activation during *L. monocytogenes* infection [220, 218]. Furthermore, infected bone marrow-derived DCs (BMDCs) were able to stimulate NK cells to produce IFN-γ *in vitro* [221]. Direct cell-to-cell contact seems not to be necessary for the mediation of this activation. An abundantly produced bacterial protein termed p60 is

responsible for most of the NK cell activation during *L. monocytogenes* infection [219], and purified p60 was able to activate the cells even the absence of other *L. monocytogenes* factors [222]. Nevertheless, DCs and also the cytokine IL-18 are important for the proper activation of the killer cells [221].

However, the overall role and function of NK cells is controversial, since they have been shown to be detrimental during *L. monocytogenes* infection. While on the other hand depletion of this cell type resulted in reduced bacterial burden [223], another study documented survival of otherwise lethal infections in the absence of NK cells [182]. The authors of the latter study were able to attribute this to the high amounts of IFN-γ produced by the NK cells, which in turn led to the downregulation of the chemokine receptor CXCR2 on neutrophils, and hence, impaired the recruitment of these cells. Moreover, as already stated above, NK cells produce considerable amounts of type I interferons that negatively impact the killing by phagocytes. Additionally, they have been shown to serve immune-suppressive roles during neuroinflammation, which leads to the speculation that they also might serve regulatory roles during systemic *L. monocytogenes* infection [224, 225].

1.2.3 Adaptive immune responses against *L. monocytogenes* infection

Innate immunity initiates and is followed by the adaptive immune response. CD8α^+CD11c$^+$ DCs — themselves part of the innate immune system — play an integral part in inducing the adaptive response [226]. Previously mentioned TLR and other *pattern recognition receptor* (PRR) signaling leads to the activation of DCs, and hence, promotes antigen presentation, leads to expression of co-stimulatory molecules and increased production of "signal 3" cytokines [227]. The crucial role of DCs in these processes has been shown by depleting them, which left mice unable to mount a CD8$^+$ T cells response to infection [228]. Ultimately, the importance of an adaptive T cell response for the overall clearance of the pathogen has been shown [229, 176]. The involved cell types and mechanisms of the adaptive immune response will be discussed in the following paragraphs.

Role of CD8$^+$ T cells during *L. monocytogenes* infection

The number of naïve CD8$^+$ T cells specific for a particular *antigen* (Ag) is usually rather small, ranging from 10 to 1,000 cells per mouse [230, 231, 232]. In order to combat the invading pathogen sufficient numbers of specific CD8$^+$ T cells must be produced. When a naïve T cell is stimulated by a DC with all three necessary signals (TCR engagement, co-receptor
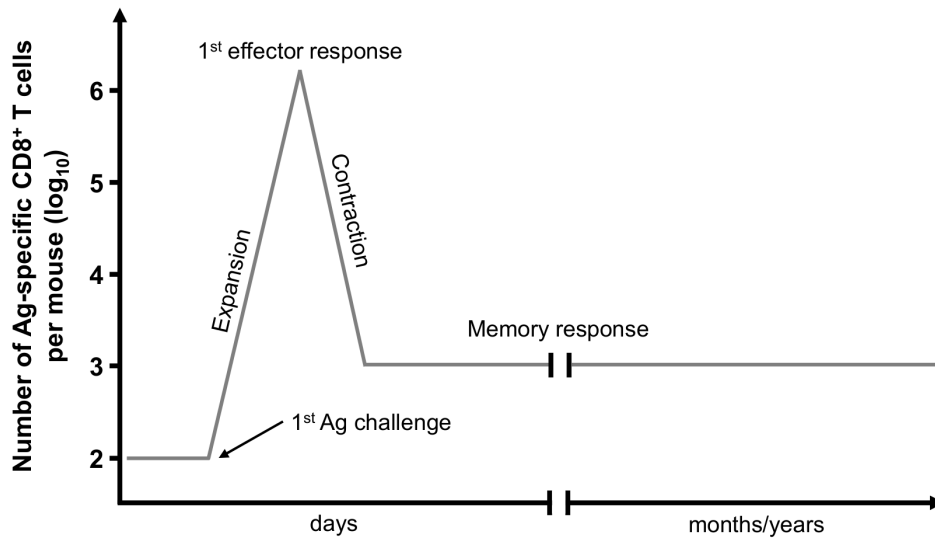
Figure 1.5: Kinetics of the CD8$^+$ T cell response during infection with *L. monocytogenes*. When naïve CD8$^+$ T cells are stimulated by mature DCs with the three obligatory signals (TCR engagement, co-stimulatory receptor ligation, cytokine signals), they respond with massive proliferation, resulting in up to 10,000-fold multiplication of their initial numbers (expansion phase). During this process the cells acquire effector function (1st effector response). Following this, the cells enter the contraction phase where 90–95 % undergo apoptosis. The remaining cells will become memory CD8$^+$ T cells that will provide the host with life-long protection (memory response).

ligation, cytokine signals) it starts proliferating and their number can increase up to 10,000-fold [233, 234, 235]. This phase is generally referred to as expansion phase, and induction of it seems to happen rather early (Figure 1.5). Interestingly, later presence of the antigen — or pathogen — is not required for expansion, since antibiotics-mediated termination of the *L. monocytogenes* infection 24 hours post infection had little impact on the nature of CD8$^+$ T cell expansion [236]. The "signal 3" cytokine IL-12 seems to play a pivotal role in the induction of expansion, since mice that are not able to respond to IL-12 showed decreased CD8$^+$ T cells expansion during infection with the intracellular pathogen [237]. Surprisingly, perforin expression, which is induced upon activation of CD8$^+$ T cells, is negatively regulating the expansion phase, indicated by its increase in perforin-deficient mice during listeriosis [238].

During the phase of expansion the cells acquire effector function (Figure 1.5). This includes the production of the cytolytic proteins granzyme B and perforin, as well as the secretion of TNF-α and IFN-γ. However, the production of the latter cytokines seems to be dispensable for protection during listeriosis [239, 240], as is the perforin- and FAS-mediated killing of infected cells [241]. But a closer look revealed that CD8$^+$ T cells from mice that lack TNF-α and perforin were protective in livers, but failed to confer protection in the spleen [239]. However, it seems that antigen-specific CD8$^+$ T cells are required for the recruitment of macrophages and neutrophils [157].

Following the effector response 90–95 % of the CD8$^+$ T cells undergo apoptosis and die. This

is referred to as the contraction phase (Figure 1.5) [242]. This massive reduction of effector cell numbers seems to be as early programmed as the expansion phase [243, 238], and is usually initiated approx. 5 days after peak of the Ag presentation by DCs [244]. Early production of IFN-γ is important for the later contraction phase, since IFN-γ-irresponsive mice showed a decreased contraction phase [238].

The remaining 5–10 % of the CD8$^+$ T cells account for the memory population. The memory response is a hallmark of the adaptive immune system and usually leads to life-long protection from reinfection (Figure 1.5) [245, 246, 247, 248]. These cells are usually split into two groups according to certain expression profiles: (i) *effector memory T cells* (T$_{EM}$) being CD62L^{lo}, CCR7^{lo}, Il-7Rα^{hi}, IFN-γ^{hi}, IL-2$^{lo/hi}$, and (ii) *central memory T cells* (T$_{CM}$) being CD62L^{hi}, CCR7^{hi}, Il-7Rα^{hi}, IFN-γ^{hi}, IL-2$^{lo/hi}$. While the former remain in peripheral tissue, the latter retain the ability to circle through the lymphatic system [249, 250, 251]. Their maintenance relies on IL-7 and IL-15 signaling, which keeps them at higher numbers as the initial naïve population. Upon re-encounter with the pathogen, they can quickly proliferate to massive numbers and acquire effector function [157].

CD4$^+$ T cells during listeriosis

CD4$^+$ T cells expand in a similar manner during *L. monocytogenes* infection as do their CD8$^+$ counterparts [252]. However, their role during the primary immune response is limited, as their absence has no effects on the 1st CD8$^+$effector response [253]. So far only reduced granuloma formation was detectable when CD4$^+$ T cells were depleted [254]. Generally, *L. monocytogenes* infection induces a strong T$_H$1 response and the IFN-γ produced by T$_H$1 cells might incite macrophages to kill phagocytosed bacteria [255].

Although CD4$^+$ T helper cells might only play a marginal role during the primary immune response against *L. monocytogenes*, they serve an important function in the memory response. Without CD4$^+$ T cells present, the memory CD8$^+$ T cell response gradually deteriorates and protective immunity is ultimately lost [256]. Although most of the contribution of CD4$^+$ T cells to the sustaining of the CD8$^+$ T cell response comes after the clearance of the pathogen [257], they are also needed during the primary response, since CD8$^+$ T cells activated in the absence of CD4$^+$ T cell help are prone to undergo "activation induced cell death" upon restimulation during the secondary response [258].

However, there is a subset of CD25$^+$CD4$^+$ T cells that have a suppressive effect that inhibits CD8$^+$ T cell responses against infection with *L. monocytogenes* [259]. Although these *regulatory T cells* (T$_{reg}$) do not expand during the infection with the pathogen [260], they are limiting the secondary CD8$^+$ T cell responses [259].

B cell mediated immunity during *L. monocytogenes* infection

Early in *Listeria* research it became clear that antibody-mediated immunity only serves a minor role in the defense against this pathogen, since transfer of serum did not provide recipient mice with immunity. Only transfer of cells was able to do that [161]. This comes as no surprise, since these intracellular bacteria are most of the time not accessible to complement factors or antibodies. This limits the effectiveness of B cell-mediated immune responses markedly. However, B cell-produced natural antibodies might play an important role in the early phase of the infection and seem to be able to keep the pathogen from disseminating [261]. Furthermore, B cells seem to play a role in the maintenance of CD8$^+$ T cell memory [262].

Murine listeriosis is an established model infection and a versatile tool for probing immune responses against intracellular pathogens. Key aspects are well described and allow for detailed analysis of effects in genetically modified mice.

1.3 Aims of the thesis

The adaptor protein ADAP has been extensively characterized in T cells and myeloid cells. However certain aspects of this scaffold protein still remain elusive. The role of ADAP in T cell activation and function has been intensively studied. However, these studies rarely distinguished between the two major subsets, CD4$^+$ and CD8$^+$ T cells. Furthermore, its role in immune responses during infections is largely unknown. Thus, to further elucidate the significance of ADAP comprehensive *in vitro* and *in vivo* models based on the use of genetically modified mice will be used, that either serve as donors for certain immune cell types, or are subjected to infection with recombinant *L. monocytogenes*. These approaches were used to address the two central aims of this thesis:

Aim 1 Identifying potential differences between CD4$^+$ and CD8$^+$ T cells in terms of their dependency on ADAP for their activation and function.

Aim 2 Deciphering the role of ADAP in pathogen-specific immunity during an infection with *L. monocytogenes*.

In order to elucidate potentially different roles of ADAP in T cell subsets (aim 1), first the expression level of the adaptor protein in CD4$^+$ and CD8$^+$ T cells needs to be assessed. Differences in expression could already have a massive influence on the respective T cell subset. Furthermore, *in vitro* activation assays will be used to determine, whether ADAP deficiency has different effects on CD4$^+$ and CD8$^+$ T cells. To this end, selected activation markers and the proliferative response of the cells will be analyzed and compared. Adhesion assays will be utilized to assess whether the two T cell subsets rely differently on ADAP for this important

feature. To analyze the effects of ADAP deficiency on CD4$^+$ and CD8$^+$ T cell activation and function *in vivo*, $Adap^{-/-}$ T cells from either $Adap^{-/-} \times$ OT-I $\times$ CD90.1 (CD8$^+$ T cells) or $Adap^{-/-} \times$ OT-II $\times$ CD90.1 (CD4$^+$ T cells) will be adoptively transferred to wild type recipient mice. These transgenic T cells express a TCR specific for immunodominant peptides of the model antigen ovalbumin. In order to activate the transferred T cells *in vivo*, the recipient mice will be infected with *L. monocytogenes* or influenza A virus. Both pathogens are genetically engineered to express the corresponding ovalbumin peptides. After certain time points the activation status and function of the cells will be assessed.

Although ADAP plays important and multifaceted roles in different immune cells, its function during infection with pathogens is largely unknown. In order to further analyze the role of ADAP during infections, this thesis will utilize *L. monocytogenes* infection in order to probe the effects of ADAP deficiency on the immune response against this pathogen (aim 2). As described above murine listeriosis is an excellent tool for probing CD8$^+$ T cell-mediated immune responses, but also other cell types, such as neutrophils, monocytes and NK cells play important parts in defense against the bacterium. The first milestone of this part of the thesis will be to assess whether ADAP deficiency has an impact on the susceptibility of mice to this intracellular pathogen. Histology of the main target organs — spleen and liver — will be used to determine potential differences between $Adap^{-/-}$ and wild type mice with respect to pathology. The cellularity and activation/maturation status of CD8$^+$ T cells, neutrophils, monocytes and NK cells that are all known to fulfill important functions in immune defense against *L. monocytogenes*, will be analyzed at different time points post infection to obtain a better understanding of the role of ADAP in the nature and kinetics of the immune response to the pathogen. This data will be complemented with cytokine and chemokine data from the sera of the infected $Adap^{-/-}$ and wild type mice. The clearance of the pathogen will be assessed by determining the bacterial burden in spleen and liver at certain time points after the infection.

Together this comprehensive investigation should uncover the potential contribution of ADAP in the innate and adaptive immunity against *L. monocytogenes*.

"If you wish to make an apple pie from scratch, you must first invent the universe."

— Carl Sagan

2

Materials

This chapter provides a register for the mouse lines, materials, appliances and buffers used during the course of this thesis. Materials are classified into consumables and antibodies.

2.1 Mouse models

The thesis at hand used standard transgenic laboratory mouse models. The transgenic mouse lines were all bred in-house, while standard C57Bl/6J mice — used as recipients for the adoptive transfer models described later in this thesis — were bought from Harlan Laboratories Ltd. (Rossdorf, Germany). The transgenic mouse models used in this thesis will be explained in more details in the following paragraphs.

2.1.1 Conventional ADAP knock-out mouse ($Adap^{-/-}$)

The conventional $Adap^{-/-}$ mouse used in this thesis was provided by Prof. Burkhart Schraven from the Otto-von-Guericke-University of Madgeburg, Germany. The transgenic mouse was first described as SLAP-130/Fyb$^{-/-}$ and generated by Peterson, et *al.* in 2001 [23], who generated these mice by introducing a neomycin cassette into the ADAP gene locus, rendering it non-functional. These mice were on the C57Bl/6J background.

The provided mice were introduced into the animal facility of the Helmholtz Centre for Infection research (HZI) by embryo transfer to ensure a proper hygienic status. The resulting mice were bred with wild type in-house C57Bl6/J mice; giving rise to heterozygous offspring. These were mated with each other, subsequently giving rise to wild type, heterozygous and knock-out offspring. All wild type control mice in these thesis — except when stated otherwise — were taken from the own in-house breeding and originated from the same breeding as the knock-out and heterozygous mice.

2.1.2 OT-I TCR CD90.1 double-transgenic $Adap^{-/-}$ mice ($Adap^{-/-}$ × OT-I × CD90.1)

OT-I T cell receptor transgenic mice expressing exclusively one TCR variant on their CD8$^+$ T cells, recognizing the MHC-I-restricted ovalbumin$_{257-264}$ peptide SIINFEKL and co-expressing the CD90.1 variant — not the CD90.2 that is found in normal C57Bl/6J mice — were bred with the in-house generated $Adap^{-/-}$ mice to create the $Adap^{-/-}$ × OT-I × CD90.1 mouse line. The MHC-II-restricted $Adap^{-/-}$ × OT-II × CD90.1 mice were created in the same manner. Corresponding wild type control animals were taken from these breedings for all experiments.

2.2 Consumables

Table 2.1: Consumables used in this study.

Product	Company
10 mL Syringe Luer-Lok^{TM} Tip	BD, Franklin Lakes, NJ, USA
2-propanol	Avantor Performance Materials B.V., Deventer, The Netherlands
Ammonium chloride (NH$_4$Cl)	Carl Roth GmbH + Co. KG, Karlsruhe, Germany
Bacto^{TM} Agar	Becton, Dickinson and Company, Sparks, MD, USA
Bacto^{TM} Brain Heart Infusion	Becton, Dickinson and Company, Sparks, MD, USA
BD FACS^{TM} Lysing Solution	Becton, Dickinson and Company, Sparks, MD, USA
BD Vacutainer$^®$ 9NC (Sodium citrate)	BD, Franklin Lakes, NJ, USA
β-mercaptoethanol	Sigma-Aldrich, St. Louis, MO, USA
Biozyme LE Agarose	Biozym Scientific GmbH, Hess. Oldendorf, Germany
Brefeldin A (from *Penicillium brefeldianum*)	Sigma-Aldrich, St. Louis, MO, USA
CD8a$^+$ T Cell Isolation Kit, mouse	Miltenyi Biotec GmbH, Bergisch Gladbach, Germany
Collagenase D from *Clostridium histolyticum*	Sigma-Aldrich, St. Louis, MO, USA
CompBeads Anti-Mouse Ig, κ	BD, Franklin Lakes, NJ, USA
CompBeads Anti-Rat and Anti-Hamster Ig, κ	BD, Franklin Lakes, NJ, USA

Table 2.1: continued

Product	Company
CompBeads Negative Control (FBS)	BD, Franklin Lakes, NJ, USA
Desoxyribonuclease I (DNase I; from bovine pancreas)	Sigma-Aldrich, St. Louis, MO, USA
Easycoll Separating Solution (density 1.124 g/mL)	Biochrom GmbH, Berlin, Germany
EASYstrainer^{TM} 100 μm	Greiner Bio-One GmbH, Bad Nenndorf, Germany
EASYstrainer^{TM} 70 μm	Greiner Bio-One GmbH, Bad Nenndorf, Germany
Ethylenediamine tetraacetic acid disodium salt dihydrate (EDTA)	Carl Roth GmbH + Co. KG, Karlsruhe, Germany
Fetal Bovine Serum (FBS) Good Forte	PAN-Biotech GmbH, Aidenbach, Germany
Ficoll-Paque^{TM} PLUS	GE Healthcare, Buckinghamshire, UK
Genotyping primers (ADAP-fw, ADAP-rv, Neo-rv)	Eurofins MWG Operon LLC, Huntsville, AL, USA
Gentamycin-Solution	Carl Roth GmbH + Co. KG, Karlsruhe, Germany
Heparin Sodium 25000	ratiopharm GmbH, Ulm, Germany
Inoculation loops 10 μL, blue	Sarstedt AG & Co., Nümbrecht, Germany
Ionomycin	Sigma-Aldrich, St. Louis, MO, USA
IPEGAL$^®$ CA-630	Sigma-Aldrich, St. Louis, MO, USA
Iscove's Modified Dulbecco's Medium (IMDM)	Thermo Fisher Scientific Inc., Darmstadt, Germany
Isoflurane	Curamed Pharma GmbH, Karlsruhe, Germany
LIVE/DEAD$^®$ Fixable Blue Dead Cell Stain Kit, for UV excitation	Fisher Scientific GmbH, Darmstadt, Germany
Low Range DNA Ladder (Peqlab)	VWR International GmbH, Erlangen, Germany
Nunc MaxiSorp$^®$ flat-bottom 96 well plate	eBioscience Inc., San Diego, CA, USA
Omnican$^®$-F fine dosage 1 mL syringe	B. Braun Melsungen AG, Melsungen, Germany
Omnifix$^®$-F Tuberculin 1 mL syringe	B. Braun Melsungen AG, Melsungen, Germany
peptideOVA$_{257-264}$	synthetizded by Dr. Dr. Werner Tegge (HZI)
Pan T Cell Isolation Kit II, mouse	Miltenyi Biotec GmbH, Bergisch Gladbach, Germany
Paraformaldehyde (PFA)	Sigma-Aldrich, St. Louis, MO, USA
PBS Tablets	Thermo Fisher Scientific Inc., Darmstadt, Germany
Penicillin-Streptomycin	Fisher Scientific GmbH, Darmstadt, Germany
phorbol 12-myristate 13-acetate (PMA)	Sigma-Aldrich, St. Louis, MO, USA
Potassium bicarbonate (KHCO$_3$)	Merck KGaA, Darmstadt, Germany
Proteinase K, recombinant, PCR Grade	Roche Diagnostics GmbH, Mannheim, Germany
2× Red PCR Master Mix	PJK GmbH, Kleinblittersdorf, Germany
Roti$^®$-Safe GelStain	Carl Roth GmbH + Co. KG, Karlsruhe, Germany
Sodium carbonate anhydrous (Na$_2$CO$_3$)	Merck KGaA, Darmstadt, Germany
Sodium hydrogen carbonate (NaHCO$_3$)	Carl Roth GmbH + Co. KG, Karlsruhe, Germany
Sterican$^®$ 26G disposable insulin needle	B. Braun Melsungen AG, Melsungen, Germany
50× TAE Buffer	Eppendorf AG, Hamburg, Germany
TMB Substrate Set	BioLegend$^®$, San Diego, CA, USA
Vibrant$^®$ CFDA SE Cell Tracer Kit	Fisher Scientific GmbH, Darmstadt, Germany

2.3 Appliances

Table 2.2: Appliances used in this study.

Product	Company
AutoFlow NU-4750 Water Jacket CO_2 Incubator	NuAire, Plymouth, MN, USA
AutoMACS	Miltenyi Biotec GmbH, Bergisch Gladbach, Germany
BD LSRFortessa™	BD, Franklin Lakes, NJ, USA
Eclipse TS100 Inverted Routine Microscope	Nikon GmbH, Düsseldorf, Germany
Geliance 600 Imaging System	PerkinElmer Life and Analytical Sciences, Shelton, CT, USA
Heraeus™ Fresco™ 21 centrifuge	Fisher Scientific GmbH, Darmstadt, Germany
Heraeus™ Multifuge™ X3FR centrifuge	Fisher Scientific GmbH, Darmstadt, Germany
HORIZON 11.14 Electrophoresis System	Biometra GmbH, Göttingen, Germany
Infinite® M200 Microplate Reader	Tecan Group Ltd., Männedorf, Switzerland
Maxisafe 2020 Class II Biological Safety Cabinet	Fisher Scientific GmbH, Darmstadt, Germany
Polytron PT 1300 D homogenizer	KINEMATICA AG, Luzern, Switzerland
PowerPac™ Basic Power Supply	Bio-Rad Laboratories GmbH, Munich, Germany
T3 Thermocycler	Biometra GmbH, Göttingen, Germany
Thermomixer Comfort	Eppendorf AG, Hamburg, Germany
Waterbath SUB 14	Grant Instruments, Cambridge, UK

2.4 Antibodies

Table 2.3: Antibodies and antisera used in this study.

Specificity	Synonym	Conjugate	Clone	Isotype	Manufacturer
ADAP	Fyb, SLAP-130	n/a	polyclonal	sheep serum	Dr. Gary Koretzky, Philadelphia, USA
CD11b	α_M integrin, Mac-1	Pacific blue	M1/70	Rat IgG2b, κ	BioLegend®, San Diego, CA, USA
CD16/32	Fcγ R III/II, Ly-17	n/a	93	Rat IgG2a, λ	BioLegend®, San Diego, CA, USA
CD161b/c	NK1.1, Ly-55	PE	PK136	Mouse IgG2a, κ	BioLegend®, San Diego, CA, USA
CD19	B4	PerCP-Cy5.5	6D5	Rat IgG2a, κ	BioLegend®, San Diego, CA, USA
CD25	IL-2Rα, Ly-43	PerCP-Cy5.5	PC61	Rat IgG1, λ	BioLegend®, San Diego, CA, USA
CD27	TNFRSF7	PE-Cy7	LG.7F9	Armenian hamster IgG	eBioscience®, San Diego, CA, USA
CD274	PD-L1, B7-H1	Biotin	MIH5	Rat IgG2a, λ	eBioscience®, San Diego, CA, USA
CD279	PD-1	PE	J43	Armenian hamster IgG	eBioscience®, San Diego, CA, USA
CD28	Tp44, T44	n/a	37.51	Syrian Hamster IgG	BioLegend®, San Diego, CA, USA
CD3e	T3	n/a	145-2C11	Hamster IgG1, κ	BioLegend®, San Diego, CA, USA
CD3e	T3	APC	145-2C11	Hamster IgG1, κ	BioLegend®, San Diego, CA, USA
CD335	NKp46	eFluor®660	29A1.4	Rat IgG2a, κ	eBioscience®, San Diego, CA, USA
CD4	L3T4, T4	BV510	RM4-5	Rat IgG2a, κ	BioLegend®, San Diego, CA, USA
CD43	Ly-48, Leukosialin	APC-Cy7	1B11	Rat IgG2a, κ	BioLegend®, San Diego, CA, USA
CD44	Hermes, Pgp-1, Ly-24	Biotin	IM7	Rat IgG2b, κ	BioLegend®, San Diego, CA, USA
CD62L	L-selectin, LECAM-1, Ly-22	Biotin	MEL-14	Rat IgG2a, κ	eBioscience®, San Diego, CA, USA
CD69	Very early activation antigen	Biotin	H1.2F3	Hamster IgG1, λ	BD, Franklin Lakes, NJ, USA
CD69	Very early activation antigen	PE	H1.2F3	Hamster IgG1, λ	BD, Franklin Lakes, NJ, USA
CD8a	T8, Lyt2, Ly-2	BV421	53-6.7	Rat IgG2a, κ	BioLegend®, San Diego, CA, USA
CD8a	T8, Lyt2, Ly-2	FITC	53-6.7	Rat IgG2a, κ	BioLegend®, San Diego, CA, USA
CD90.1	Thy1.1	PE-Cy7	OX-7	Mouse IgG1, κ	BioLegend®, San Diego, CA, USA
CD90.2	Thy1.2	PerCP-eFluor710	30-H12	Rat IgG2b, κ	eBioscience®, San Diego, CA, USA
Gr-1		PerCP-Cy5.5	RB6-8C6	Rat IgG2b, κ	BioLegend®, San Diego, CA, USA
Granzyme B		Alexa Fluor 647	GB11	Mouse IgG1, κ	BioLegend®, San Diego, CA, USA
IFN-γ		Pacific blue	XMG1.2	Rat IgG1, κ	BioLegend®, San Diego, CA, USA

Table 2.3: continued

Specificity	Synonym	Conjugate	Clone	Isotype	Manufacturer
IFN-γ		PE	XMG1.2	Rat IgG1, κ	BioLegend®, San Diego, CA, USA
Ly-6G		PE-Cy7	1A8	Rat IgG2a, κ	BioLegend®, San Diego, CA, USA
SAV $\rightarrow$ Biotin		BV605	n/a	n/a	BioLegend®, San Diego, CA, USA
sheep IgG		Alexa Fluor 488	polyclonal	Donkey IgG	Abcam®PLC, Cambridge, UK
TCR Vα2		FITC	B20.1	Rat IgG2a, λ	BioLegend®, San Diego, CA, USA
TCR Vβ5.1, 5.2		PE	MR9-4	Mouse IgG1, κ	BioLegend®, San Diego, CA, USA

2.5 Buffer and media composition

FACS Buffer

Component	Stock	Volume/Mass	Final concentration
FBS	n/a	20 mL	2 % (v/v)
EDTA, pH = 8.0	$0.5 \; \text{mol} \cdot \text{L}^{-1}$	4 mL	$2 \; \text{mmol} \cdot \text{L}^{-1}$

ad 1000 mL with PBS

ACK Buffer

Component	Stock	Volume/Mass	Final concentration
FBS	n/a	20 mL	2 % (v/v)
EDTA, pH = 8.0	$0.5 \; \text{mol} \cdot \text{L}^{-1}$	4 mL	$2 \; \text{mmol} \cdot \text{L}^{-1}$

ad 1000 mL with PBS

Rapid Tail Digest Buffer

Component	Stock	Volume/Mass	Final concentration
Tris-HCl	$0.5 \; \text{mol} \cdot \text{L}^{-1}$	40 mL	$100 \; \text{mmol} \cdot \text{L}^{-1}$
NaCl	$5 \; \text{mol} \cdot \text{L}^{-1}$	8 mL	$200 \; \text{mmol} \cdot \text{L}^{-1}$
SDS	10 % (v/v)	4 mL	0.2 % (v/v)
EDTA, pH = 8.0	$0.5 \; \text{mol} \cdot \text{L}^{-1}$	2 mL	$5 \; \text{mmol} \cdot \text{L}^{-1}$

ad 200 mL with MilliQ

ELISA Coating Buffer

Component	Stock	Volume/Mass	Final concentration
$NaHCO_3$	n/a	8.40 g	$100 \; \text{mmol} \cdot \text{L}^{-1}$
Na_2CO_3	n/a	3.56 g	$34 \; \text{mmol} \cdot \text{L}^{-1}$

ad 1000 mL with MilliQ and set pH to 9.5

ELISA Wash Buffer

Component	Stock	Volume/Mass	Final concentration
PBS	n/a	1000 mL	n/a
Tween-20	n/a	500 µL	0.05 % (v/v)

ELISA Assay Diluent

Component	Stock	Volume/Mass	Final concentration
PBS	n/a	100 mL	n/a
BSA	n/a	1 g	1 % (w/v)

IMDM compl.

Component	Stock	Volume/Mass	Final concentration
IMDM + GlutaMAX$^{\text{TM}}$-I	n/a	500.00 mL	n/a
FBS	n/a	55.00 mL	10 % (v/v)
Penicillin	$10000 \text{ U} \cdot \text{mL}^{-1}$	5.00 mL	$100 \text{ U} \cdot \text{mL}^{-1}$
Streptamycin	$10000 \text{ µg} \cdot \text{mL}^{-1}$	5.00 mL	$100 \text{ µg} \cdot \text{mL}^{-1}$
Gentamycin	$50 \text{ mg} \cdot \text{mL}^{-1}$	1.10 mL	$500 \text{ µg} \cdot \text{mL}^{-1}$
β-mercaptoethanol	$0.25 \text{ mmol} \cdot \text{L}^{-1}$	0.55 mL	$0.25 \text{ µmol} \cdot \text{L}^{-1}$

Tissue Digest Medium

Component	Stock	Volume/Mass	Final concentration
Collagenease D	$0.5 \text{ mg} \cdot \text{L}^{-1}$	2.20 mL	$0.02 \text{ mg} \cdot \text{L}^{-1}$
DNase I	$1.0 \text{ mg} \cdot \text{L}^{-1}$	0.55 mL	$0.01 \text{ mg} \cdot \text{L}^{-1}$
IMDM compl.	n/a	550 mL	n/a

"If you try and take a cat apart to see how it works, the first thing you have on your hands is a non-working cat."

— Douglas Adams

3

Methods

This chapter will describe the methods and protocols that were used during the course of these studies. For better understanding this chapter was divided into *General techniques and protocols* and *Investigative assays*. While the former covers more common techniques, the latter usually describes a combination of these general techniques used to investigate a certain problem.

3.1 General techniques and protocols

Several general techniques and protocols were used in this thesis repeatedly and in a number of different investigative assays. These methods will be described in the following paragraphs and referred to from the respective investigative assays that utilize these techniques.

3.1.1 Genotyping of mice from in-house breedings

Determination of the actual genotype of the in-house breeding mice was necessary. The mice from the $Adap^{-/-}$ breedings were genotyped using PCR, while the genotype of mice from the OT-I $\times$ CD90.1 breedings was determined by use of flow cytometry.

Table 3.1: PCR Master Mix for ADAP genotyping.

Volume	Reagent
10 µL	2 × PCR Master mix (by PJK)
1 µL	primer mix
8 µL	MilliQ H$_2$O
19 µL	total mix

ADAP-specific genotyping using PCR

For ADAP-specific genotyping tail biopsies were taken when the mice were 4 weeks old, but also *postmortem* when sacrificing the animals during the investigative assays. 100 µL of Rapid Tail Digest buffer with 100 µg · mL^{-1} Proteinase K were added to the tails and the digestion was performed usually over night at 56 °C while vigorously shaking in a Thermomixer Comfort. The minimum duration for this digestion was 3 h. The reaction was stopped afterwards by heating the samples for 10 min at 95 °C. The rest of the tissue was pelleted by centrifugation for 5 min at 14,000 rpm and 4 °C in a table top centrifuge. The supernatant was carefully transferred to a new Eppendorf tube that already contained 600 µL of 2-propanol. The tube was inverted immediately several times until precipitation was clearly visible. This precipitate was pelleted by centrifugation for 5 min at 12,000 rpm and 4 °C. This time the supernatant was discarded and the DNA-pellet was washed by adding 500 µL of 70 % ethanol and centrifuging again as mentioned above. The supernatant was again discarded and an additional centrifugation was performed to eliminate any residual supernatant. After drying the pellet for approx. 10 min at room temperature (RT) with open lid, the pellet was solved in 50 µL MilliQ water. A 1:10 dilution was prepared for the following PCR.

The following primers were used in the ADAP genotyping PCR:

ADAP forward primer:	CCG TGG GGC CAA AGT CAG GAG AA	(23 bp)
ADAP reverse primer:	CCC ACC CCA AGG TCC TTT CTT AC	(23 bp)
Neomycin reverse primer:	GCG CTA CCG GTG GAT GTG GAA TGT	(24 bp)

The composition of the mix for the genotyping PCR is found in Table 3.1. The primer mix consisted of all three primers with a concentration 5 µmol · L^{-1} each. To this mix 1 µL of previously prepared template DNA from the tail digest was added. The program for the T3 Thermocycler is found in Table 3.2.

After completion of the thermocycler program the samples were applied to a 2 % agarose gel containing 5 % Roti$^{®}$-GelStain. The gel ran in a HORIZON 11.14 electrophoresis system for approx. 25 min at a constant voltage of $\Delta U = 160V$, provided by a PowerPac$^{\text{TM}}$ Basic

Table 3.2: Thermocycler programm for ADAP genotyping PCR.

Step	Temperature [°C]	Duration [s]	Go to	Cycles
1	95	600		
2	95	30		
3	60	90		
4	72	90	2	10
5	95	15		
6	60	45		
7	72	90	5	27
8	4	∞		
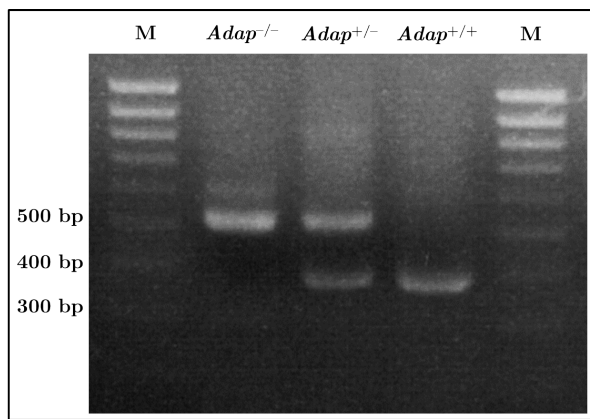
Figure 3.1: Representative ADAP genotyping gel electropherogram. DNA extracted from tail biopsies of $Adap^{-/-}$, $Adap^{+/-}$ and $Adap^{+/+}$ mice was used as template in an ADAP genotyping PCR. Amplicons from knock-out animals were approx. 550 bp long, while wild type templates gave rise to approx. 350 bp long amplicons. Heterozygous animals showed both bands. M indicates the PeqGold Low Range DNA Ladder.

Power Supply. DNA-bands were detected in a Geliance 600 Imaging system with UV light and documented. Amplified sequences of $Adap^{+/+}$ mice were approx. 350 bp long; those of $Adap^{-/-}$ 550 bp. Heterozygous animals showed both bands. A representative gel electropherogram is shown in Figure 3.1.

CD90 allele and OT-I T cell receptor genotyping using flow cytometry

In order to determine whether the $Adap^{-/-}$ × OT-I × CD90.1 and $Adap^{-/-}$ × OT-II × CD90.1 animals were truly TCR-transgenic and expressed the CD90.1 isoform, blood was taken retro bulbar and was stabilized with heparin (250 I.E.). During this procedure the mice were anesthetized with isoflurane (2-chloro-2-(difluoromethoxy)-1,1,1-trifluoro-ethane). 80 µL of the stabilized blood were mixed with an antibody staining mix. The contents thereof can be found in Table 3.3. The dilution factor for each antibody was determined by titration on splenocytes. The cells were stained for 15 min at room temperature in the dark. Since the erythrocytes would affect the flow cytometric measurement, they were lysed by adding 480 µL BD FACS Lysis solution (diluted 1:10 in MilliQ water) and incubating for 15 min at room temperature. Afterwards, the cells were immediately measured with the BD LSRFortessa.

Table 3.3: Flow Cytometry Panel for OT-I TCR and CD90 genotyping.

Specificity	Conjugate	Isotype	Clone
CD8a	BV421	Rat IgG2a, κ	53-6.7
TCR Vα2	FITC	Rat IgG2a, λ	B20.1
TCR Vβ5.1, 5.2	PE	Mouse IgG1, κ	MR9-4
CD90.1	PE-Cy7	Mouse IgG1, κ	OX-7
CD90.2	PerCP-eFluor710	Rat IgG2b, κ	30-H12
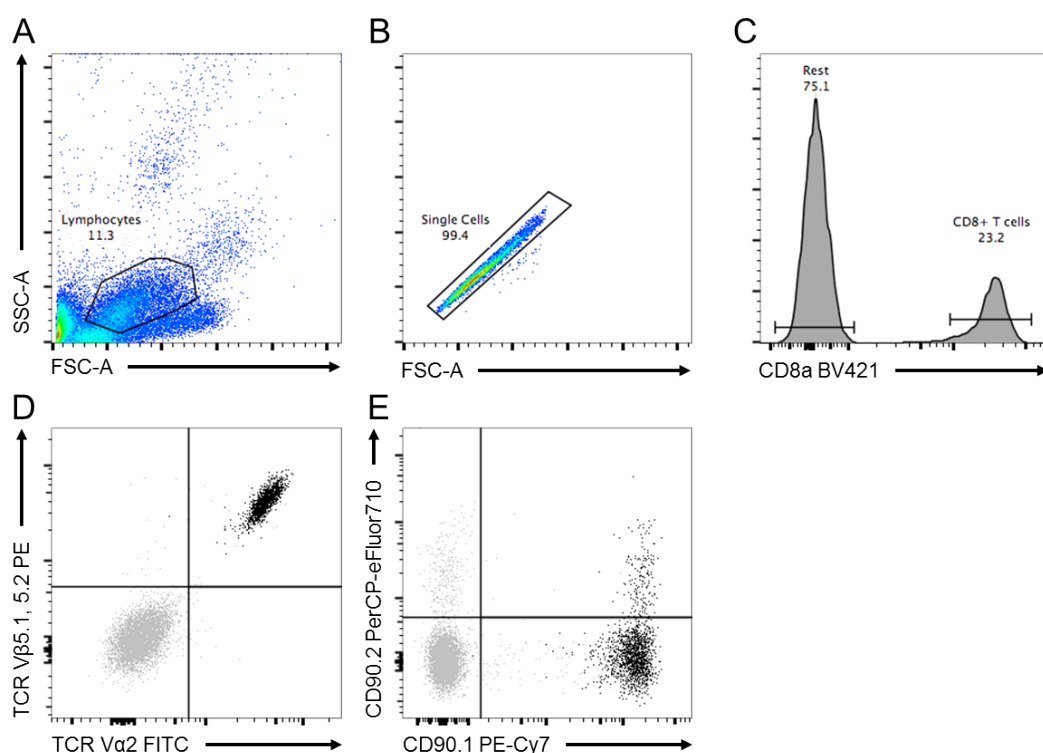
Figure 3.2: Gating strategy used for OT-I TCR and CD90 flow cytometric genotyping. Stained leukocytes from lysed blood were measeured with a BD LSRFortessa. For data analysis the following gating strategy was applied: (A) Lymphocytes were identfied by FSC-A and SSC-A. (B) Single cells were defined by the correlation of FSC-A and FSC-H. (C) CD8$^+$ T cells were distinguished from other cells. (D) CD8$^+$ T cells (black) and other cells (gray) plotted for TCR Vα2 vs. TCR Vβ5.1, 5.2, and CD90.1 vs. CD90.2 expression.

αCD8 was used to identify CD8$^+$ T cells. OT-I TCR transgenic cells are double-positive for TCR Vα2 and TCR Vβ5.1, 5.2. αCD90.1 and αCD90.2 were used to ensure that the animals were CD90.1$^+$CD90.2$^-$. The gating strategy used in this study can be found in Figure 3.2. Spectral overlap was compensated with single stainings.

3.1.2 Infection of mice with *Listeria monocytogenes*

Since a major aim of this study was to elucidate *in vivo* the role of ADAP during an infection, mice were infected intravenously (*i.v.*) with ovalbumin-expressing *Listeria monocytogenes*. This led to a systemic infection that would mainly affect the spleens and livers of the animals. In order to reproducibly infect the mice, *Listeria* needed to be grown and a precise infectious dose had to be applied to the mice.

Growth and preparation of *Listeria*

Listeria monocytogenes (strain 10403s), expressing the model antigen ovalbumin were taken up with an inoculating loop from the –70 °C glycerol stocks and struck out on brain-heart-infusion (BHI) Petri dishes. The bacteria were grown over night at 37 °C in the incubator and later stored in the fridge for further use.

On the evening prior to an infection a 5 mL BHI starting culture was inoculated with a swipe of an inoculating loop over the previously prepared plate. This starting culture was incubated over night at 37 °C while shaking at 180 rpm. The lid of the tube was not fully closed to allow for ventilation of the culture. In the morning of the following day 1 mL of the starting culture was transferred to 4 fresh mL BHI. This main culture was also incubated at 37 °C while shaking at 180 rpm for 3 h. At this time point the Listeria were in the log-phase and metabolically most active. 1 mL of the bacterial suspension was taken after that and transferred to an Eppendorf tube. The bacteria were centrifuged for 3 min at 3,000 rpm and room temperature. The resulting supernatant was aspirated, the remaining bacterial pellet was washed with 1 mL sterile, cold PBS, and centrifuged again with the aforementioned settings. This washing step was repeated and the bacteria were taken up in 1 mL of PBS.

In order to approximate the colony forming units per mL (CFU $\cdot$ mL^{-1}) the bacterial suspension was diluted 1:10 and the optical density at 600 nm (OD$_{600}$) was measured. Usually, the OD$_{600}$ ranged between 1.2 and 1.5. Next, the suspension was diluted to an OD$_{600}$ of 1. Here equation 3.1 was used to determine the volume x (in µL) of the bacterial suspension that was transferred into a new Eppendorf tube and diluted with y µL ($y = 1000 - x$) of PBS.

$$x = \frac{0.1}{\text{OD}_{600}} \cdot 1000 \tag{3.1}$$

A measurement of the newly diluted suspension was performed to confirm the desired optical density. Prior assays showed that a suspension with an OD$_{600}$ of 1 holds approx. $1.25 \cdot 10^9$ CFU $\cdot$ mL^{-1} *Listeria*. The bacteria were again diluted to correct for this and 1:10 serial dilutions from $1 \cdot 10^8$ to $1 \cdot 10^6$ CFU $\cdot$ mL^{-1} were prepared. Since the animals were usually

infected with 2 or $4 \cdot 10^4$ CFU $\cdot$ mL^{-1}, and 100 µL per mouse were needed for this, a 2 or $4 \cdot 10^5$ CFU $\cdot$ mL^{-1} suspension was prepared. 1:10 serial dilutions from this suspension were made to 2 or $4 \cdot 10^2$ CFU $\cdot$ mL^{-1}.

To determine the actual infectious dose, 50 µL of the 10^3 and 100 µL of the 10^2 dilution were plated on BHI Petri dishes and incubated over night at 37 °C in the incubator. The colonies were counted on the next day which, corrected for the dilution factor, showed the actual amount of bacteria that had been applied to the mice.

Intravenous infection

The prepared infection inoculum was taken on ice to the infection unit of the animal facility. This should limit unwanted bacterial growth. The mice were placed shortly under an infrared heat lamp to dilate the tail veins. To infect a mouse, it was placed into a mouse restrainer and 100 µL of the infection inoculum were injected *i.v.* into the *Vena caudalis*. Blood loss was limited by pressing on the entry wound with sterile gauze for several seconds.

Over the following days the mice were monitored. If a mouse showed signs of severe pain — hunched back, closed eyes, reduced movement — it was euthanized according to the animal protection regulations.

3.1.3 Influenza A virus infection

For the viral infection of mice, virus stocks were diluted to the desired amount with sterile PBS and transferred to the infection unit of the animal facility. The mice were anesthetized by intraperitoneal (*i.p.*) injection of 100 µL per g of bodyweight of the narcotic solution (10 % ketamine, 2 % xylazine, in 0.9 % saline) provided by the animal facility. Proper depth of the anesthesia was determined by testing for the interdigital reflex. After this 25 µL of the virus solution were applied to the anesthetized mice intranasally by use of a micropipette and they were monitored for their well-being during the recovery phase of the anesthesia as well as the days following the infection until the experiment was terminated.

3.1.4 Sacrificing and dissection of mice

In order to gain access to the several organs and the cells of interest therein, the subject mice were euthanized and dissected. All procedures were performed according to the animals protection act and animal suffering was kept to an absolute minimum.

Euthanasia

Sacrificing of the mice was generally done by carbon dioxide (CO_2) inhalation. Therefore, the mice were placed individually into a 2 L beaker with tissue bedding. The beaker was closed with aluminum foil and CO_2 was slowly led into the vessel with a pressure of $P = 50$ kPa to minimize animal suffering. To confirm the actual death of the animal, the corneal and interdigital reflexes were checked. Furthermore, after the animal was opened during the sectio (see below), the diaphragm was pierced to ensure that the animal would not reanimate or even gain consciousness.

Sectio

For the dissection the mouse was pinned through the limbs onto a board and sprayed with 70 % ethanol. A long median incision from pelvis to mandible and two relieving incisions in the direction of the forelimbs as well as two in the direction of the hind limbs were made. The skin was pulled aside and when needed, the inguinal lymph nodes (inLN) could be excised in the lower third of the pulled open skin. Next, the peritoneum was opened by cutting from the pelvis to the caudal end of the sternum. Again, four relieving incisions were made and the peritoneum was pulled aside to access the coelom.

Cardiac blood As soon as the death of the animal was confirmed and the thorax exposed, a syringe with a 26 G cannula was introduced into the heart ventricle through the thorax sinister lateral of the sternum. The cardiac blood was slowly taken in order to not collapse the ventricle. If the blood was needed for flow cytometric analysis the syringe was pre-filled with 100 µL heparin (250 I.E.) and after the draw transferred to an Eppendorf tube already containing 100 µL heparin (250 I.E.) to prevent coagulation. If the blood was needed for the evaluation of serum cytokines, ALT or TGF-β levels, two different protocols were applied that can be found in section 3.1.6.

Spleen The spleen was found sinister lateral and caudal of the thorax. The afferent and efferent blood vessels were severed and the tissue connecting the spleen to the pancreas was removed. The organ was stored in either cold PBS or IMDM compl.

Liver In order to remove the liver, first the gall bladder had to be excised carefully. Then, the connective tissue and vessels cranial and dorsal of the liver were severed and the liver was taken out and stored in cold IMDM compl.

Lung The lung of the animals was harvested by opening the thorax. To this end the thorax was cut open with two lateral incisions; this exposed the lung, heart and thymus. The lung was carefully removed each of the 5 lobes at a time. Special attention was necessary to avoid accidental removal of thymus parts or bronchial lymph nodes. The lung lobes were stored in IMDM compl. on ice until further use.

The liver draining lymph nodes were found dorsal of the liver close to the hepatic veins. After removal they were stored in cold IMDM compl.

Thymus After opening the thorax with lateral incisions the two-lobed thymus was found cranial of the heart. It was excised carefully to make sure that no bronchial lymph nodes were taken by accident. The thymus was stored in cold IMDM compl. until further use.

Tail biopsy For the final postmortem genotyping of the mice, tail biopsies were taken. Therefore, approx. 2 mm of the tail tip were cut off, put into an Eppendorf tube and stored for further use (see section 3.1.1) at –20 °C.

3.1.5 Cell preparation methods

For this study leukocytes of several tissues were prepared and enriched. This included spleen, lymph nodes, liver, lung and blood leukocytes. This was necessary to be able to analyze different cell types and their activation status and functionality by flow cytometry. All steps were performed on ice as much as possible, except when noted differently.

Preparation of splenocytes

The excised spleen was either pressed through a 100 μm diameter cell strainer into 10 mL PBS (fast but lesser yield) or rinsed with a 10 mL syringe and a 26 G cannula. For the latter method the spleen was placed into a Petri dish and perfused with 10 mL ice-cold PBS while it was gently squeezed with a blunt forceps.

The resulting splenocyte suspension was centrifuged (400 rcf; 10 min; 4 °C), the supernatant aspirated and the pellet resuspended in 2 mL ACK buffer for erythrocyte lysis. After 2 min the lysis was stopped by addition of 12 mL FACS buffer. This suspension was passed through a 100 μm cell strainer and centrifuged (400 rcf; 10 min; 4 °C). Afterwards, the pellet was usually resuspended in either FACS buffer or IMDM compl. and stored on ice until further use.

Preparation of lymph node cells

Excised lymph nodes were pressed through 100 μm cell strainers into 10 mL IMDM compl. The resulting cell suspension was centrifuged (400 rcf; 10 min; 4 °C) and the cell lymphocytes pellet resuspended in IMDM compl. and stored on ice until further use.

Preparation of liver leukocytes

The harvested livers were transferred to Petri dishes and minced with scissors. Afterwards they were taken up in 3 mL digest medium (0.2 mg · mL^{-1} collagenase D, 0.01 mg · mL^{-1} DNAse I in IMDM compl.), transferred to 15 mL falcon tubes and incubated for 30 min at 37 °C. Every 5 min the suspension was sheared with a disposable Pasteur pipette. After the first incubation (30 min) 2 ml of fresh digest medium were added to the tubes and the minced livers were further digested for additional 15 min. Again, every 5 min the samples were sheared. Afterwards, 60 μL of 0.5 mol · L^{-1} EDTA (pH= 8.0) were added (f.c. = 5 mmol · L^{-1}) and the samples rested for 5 min at 37 °C to stop the digestion.

The digested liver suspension was passed through 100 μm cell strainers. Remaining tissue debris were pressed through with a syringe plunger and the cell strainer was washed with 14 mL ice-cold PBS. The resulting 20 mL single cell suspension was passed through a 70 μm cell strainer, followed by centrifugation (300 rcf; 6 min; RT).

The supernatant was aspirated and the cell pellet resuspended in 10 mL of 0.2 % NaCl/MilliQ for erythrocyte lysis. After approx. 20 s the lysis was abrogated by addition of 10 mL 1.6 % NaCl/MilliQ, bringing the suspension back to physiological osmolar levels (approx. 0.9 % NaCl). After adding 10 mL PBS the suspension was centrifuged again (300 rcf; 6 min; RT) and the resulting pellet was resuspended in 10 mL of 35 % Easycoll/PBS. The Easycoll Separating Solution has a defined density ($\rho = 1.124$ g · mL^{-1}). The suspension was centrifuged (360 rcf; 10 min; RT; no break).

This differential density centrifugation resulted in pelleted liver leukocytes on the bottom of the falcon, while the hepatocytes and other cells floated on top of the Easycoll layer. The latter was aspirated and discarded, while the leukocyte pellet was resuspended in IMDM compl. and stored on ice until further use.

This protocol was adapted from Cotter and Muruve (2006)[263].

Preparation of lung lymphocytes

Lung lymphocytes were isolated from excised lungs by a protocol similar to the liver leukocyte isolation protocol described above. The lungs were minced with scissors and resuspended in

3 mL digest medium and digested as described above. After this procedure everything was transferred to fresh 50 mL Falcon tubes through 100 µm cell strainers. After centrifugation (400 rcf; 10 min; 4 °C) erythrocyte lysis was performed by resuspending the pellet in 2 mL ACK buffer. After stopping the lysis with approx. 12 mL FACS Buffer the cells were resuspended in 4 mL IMDM compl. and layered on 4 mL Ficoll in 15 mL Falcon tubes. After centrifugation at room temperature for 20 min at 400 rcf the interphase — comprising the lymphocytes — was carefully transferred to a fresh 15 mL falcon tube and washed by adding approx. 10 mL FACS buffer, centrifuging (400 rcf; 10 min; 4 °C), and aspiration of the resulting supernatant. The remaining cell pellet was resuspended in IMDM compl. and stored on ice until further use.

Preparation of blood leukocytes

500 µL heparinized blood were transferred into a fresh 50 mL falcon tube. Erythrocyte lysis was facilitated by adding 10 mL 0.2 % NaCl/MilliQ and stopped approx. 20 s later with 10 mL 1.6 % NaCl/MilliQ. Additional 10 mL of PBS were added and the resulting suspension was centrifuged (400 rcf; 10 min; 4 °C). After the centrifugation the supernatant was aspirated and if necessary the pellet was lysed again. Otherwise the pellet was resuspended in IMDM compl. and the suspension stored on ice for later use.

Isolation of specific cell types from splenocytes using Magnetic-Activated Cell Sorting (MACS)

In order to isolate splenic T cells or just CD8$^+$ T cells magnetic-activated cell sorting (MACS) was used. Therefore the Pan T Cell Isolation Kit II or the CD8$^+$ T Cell Isolation Kit by Miltenyi were used according to the protocol provided by the manufacturer.

10^8 splenocytes of each mouse were used and resuspended in 400 µL FACS Buffer (40 µL per 10^7 cells). 100 µL (10 µL per 10^7 cells) of the provided biotin-antibody cocktail were added and the cells were incubated for 10 min in at 4 °C. After this incubation 300 µL FACS Buffer and 200 µL provided streptavidin-microbeads (20 µL per 10^7 cells) were added and another incubation for 15 min at 4 °C followed. The cells were washed by adding 10 mL FACS Buffer and centrifuging (400 rcf; 10 min; 4 °C) and afterwards resuspended in 1 mL FACS Buffer.

For the actual separation the Miltenyi autoMACS system was used. The negative selection program "deplete" eluated the desired unlabeled cell population in 3 mL FACS Buffer at the "neg" port.

Isolation of specific cell types from splenocytes using Fluorescence-Activated Cell Sorting

More sophisticated isolation of highly specific cell sub types was accomplished by fluorescence-activated cell sorting (FACS) using a BD FACSAria II SORP or a Beckman Coulter MoFlo™ XDP.

To this end splenocytes were prepared (see section 3.1.5 on page 44) and resuspended in 1 mL FACS Buffer. The cells were blocked and stained for specific markers as described in section 3.1.11 on page 51 and given to the Flow Cytometry Core Facility. The identified cells are packed in droplets that are directed in to their respective tubes. The resulting suspensions were centrifuged (400 rcf; 20 min; 4 °C) and stored on ice until further use.

3.1.6 Serum and plasma preparation

For analysis of serum cytokines and ALT-levels, blood was drawn and kept without any anti-coagulants. After incubation for 30 min at 37 °C the blood had coagulated. The samples were put on ice for 30 min and afterwards centrifuged (1000 rcf; 10 min; °C). The serum was removed carefully with a pipette, transferred to a fresh Eppendorf tube and stored at –70 °C until further use.

Analysis of TGF-β levels required platelet-free plasma (PFP). It was prepared by taking 400 μL cardiac blood and immediately mixing it with 100 μL 0.105 mol · L^{-1} sodium citrate to prevent coagulation. The stabilized blood was centrifuged (400 rcf; 5 min; 4 °C) and the platelet-rich plasma (PRP) was carefully transferred to a fresh Eppendorf tube. The PRP was centrifuged again (6800 rcf; 10 min; 4 °C) to pellet the platelets. The resulting PFP was carefully transferred to a fresh Eppendorf tube and stored at –70 °C until further use.

3.1.7 Determination of cell numbers in suspension by use of a hemocytometer

The cell concentration (and subsequently the absolute cell number) of a suspension was determined by using a hemocytometer. Therefore the cell suspension was diluted in trypan blue (usually 1:10) and approx. 10 μL were pipetted on the hemocytometer.

A hemocytometer has a grid that usually delimits 4 big squares. These squares are also subdivided into 4 × 4 smaller squares. To determine the cell number, all living cells (bright and not blue stained) in each big square are counted (x). Usually all 4 big squares are counted

($n = 4$). Equation 3.2 was used to calculate the number of cells per mL (c), where a is the aforementioned dilution factor.

$$c = \frac{1}{a} \cdot \left(\frac{1}{n} \sum_{i=1}^{n} x_i \right) \cdot 10^4 \tag{3.2}$$

Absolute cell numbers were calculated by multiplying by the actual volume of the cell suspension.

3.1.8 Assessment of colony forming units (CFU) in organs of *Listeria* infected mice

The bacterial burden in spleens and livers of *Listeria* infected mice was determined. To this end the organs of the mice were transferred to sterile tubes with 1 mL (spleens) or 2 mL (livers) of 0.2 % (v/v) IGEPAL® CA-630/PBS (also termed NP-40/PBS) and thoroughly homogenized using a Polytron PT 1300 D homogenizer.

10-fold serial dilutions of each homogenized organ were prepared (100 µL + 900 µL) to a dilution factor of 10^{-6}. For these dilutions also 0.2 % (v/v) IGEPAL® CA-630/PBS was used. The dilutions were kept on ice at all times. At least three different dilutions were plated in duplicates on BHI Petri dishes by pipetting 50 µL of the dilution on the plate and thoroughly spreading it with a sterile inoculation loop. The dishes were incubated over night at 37 °C.

On the next day the colonies on the dishes were counted and — taking into account the dilution factor and the initial volume — the CFU in the respective organs were calculated.

3.1.9 Enzyme-linked immunosorbent assay (ELISA)

To determine the concentration of several cytokines in the sera of infected $Adap^{-/-}$ mice and their wild type counterparts ELISAs were performed. In this study ELISA kits by BioLegend were used. The protocols for the different cytokines were identical and followed precisely.

Assay procedure

One day prior to the actual assay the Nunc MaxiSorp® flat-bottom 96 well plates needed to be coated. Therefore, the capture antibody was diluted 1:200 in Coating Buffer and 100 µL were pipetted in each well. The plates were sealed and incubated o/n at 4 °C. On the next day, the plates were washed 4 times with 300 µL Wash Buffer for each well. In order to

minimize non-specific binding, the wells were blocked with 200 μL Assay Diluent by sealing and incubating them for 1 h at RT and 200 rpm on a shaker. Afterwards the wells were washed again with 4 times with 300 μL Wash Buffer.

The standard dilutions were prepared as stated by the manufacturer, ranging from 500 pg · mL^{-1} to 7.8 pg · mL^{-1}, and 100 μL of each dilution were pipetted into the wells. Assay Diluent served as a negative control. The actual serum samples were diluted to fit the range and also 100 μL were added to the in the respective wells. All standards, negative controls and samples were done in duplicates. The plates were sealed again and incubated at RT for 2 h while shaking at 200 rpm.

After the incubation, the plates were washed again 4 times with 300 μL Wash Buffer. The Detection Antibody was diluted 1:200 in Assay Diluent and 100 μL were pipetted into each well. After incubation for 1 h at RT and 200 rpm shaking, the plates were washed 4 times with 300 μL Wash Buffer. The avidin-conjugated horse radish peroxidase (HRP) was diluted in 1:1000 in Assay Diluent and 100 μL were added to the wells. The plates were incubated for 30 min at RT while shaking.

For the desired color-reaction the TMB Substrate Solution was prepared by mixing the provided solutions A and B in a 1:1 ratio. 100 μL of the resulting solution were added to the wells and plates were kept for approx. 15–30 min in the dark to develop the desired colour. The reaction was stopped by addition of 100 μL 2 N H$_2$SO$_4$, turning the solution from blue to yellow.

To acquire the respective OD values the plates were read by an Infinite$^{®}$ M200 Microplate Reader by Tecan. The measurement wavelength was set to 450 nm, while the reference wavelength was 570 nm. The absorbance of at the reference wavelength was subtracted from the one at the measurement wavelength. The data was exported for further analysis.

Data transformation and concentration calculation

In order to determine the actual concentration of the cytokines in the sera, first, a standard curve was calculated from the OD values of the standard dilutions. For all following calculations, GraphPad Prims v5.02 was used. The concentration (c) of each standard dilution was log-transformed ($c = \log_{10} c$) and a standard curve was modeled with a sigmoidal dose-response (variable slope) equation (see equation 3.3).

$$OD = B + \frac{T - B}{1 + 10^{(\log EC_{50} - c) \cdot a}} \tag{3.3}$$

Here, OD is the OD measured at the respective concentration (c). B is the OD at the bottom plateau, while T is the OD at the top plateau. $\log EC_{50}$ is the concentration c halfway between B and T. a is the slope factor. The parameters B, T, $\log EC_{50}$ and a are automatically determined by the software.

With this standard curve the software is able to interpolate the unknown c of the ODs of the samples. These calculated c-values have to be transformed back again ($c = 10^c$) to yield concentrations in $pg \cdot mL^{-1}$.

3.1.10 CFDA SE staining for proliferation analysis

To analyze the proliferative behavior of cells, CFDA SE (carboxyfluorescein diacetate, succinimidyl ester) staining was used. This compound can passively enter cells, where intracellular esterases cleave the acetate groups, rendering it fluorescent and reactive to cellular amine groups, with which it forms stable conjugates. This facilitates that the dye remains in the cells and is also fixable with aldehyde fixatives.

The fact that it is covalently bound to cellular amines, and not transferable to adjacent cells, makes it an ideal means to analyze the proliferation of cells. When a cell undergoes division all cellular components are divided equally between it and its daughter cells. This results in the bisection of the dye amount in each of the descendant cells, rendering both half as fluorescent as the mother cell before the division. If these cells divide again, the fluorescence of their descendants is bisected again. This is often referred to as CFSE dilution [264, 265].

Staining procedure

The cells for the CFDA SE staining were resuspended in 4 mL pure IMDM, since FBS would scavenge the dye and drastically reduce the efficiency of the staining. Maximally $1 \cdot 10^7$ cells $\cdot$ mL^{-1} were stained at once. The CFDA SE in DMSO stock solution ($c = 10$ mmol $\cdot$ L^{-1}) was diluted 1:1000 in pure IMDM with a resulting concentration of $c = 10$ µmol $\cdot$ L^{-1}. 444 µL of this dilution were added to each 4 mL preparation, yielding a final CFDA SE concentration of $c = 1$ µmol $\cdot$ L^{-1}.

The cells were vortexed and incubated for exactly 8 min at 37 °C with open lids in an incubator. The staining reaction was stopped by addition of 10 mL pure FBS. After centrifugation (400 rcf; 10 min; 4 °C) the supernatant was aspirated and the cells were washed with 14 mL IMDM compl. After this, the cells were kept in the dark and were ready for further use.
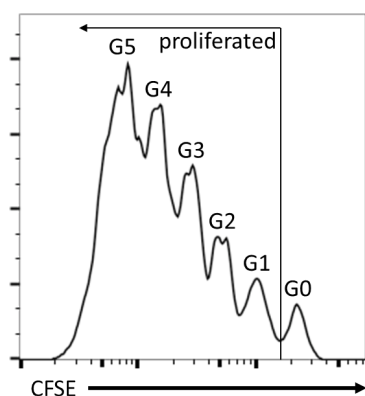
Figure 3.3: Representative histogram of CFSE dilution due to proliferation. Splenic lymphocytes were cultured for 72 h and activated with plate-bound αCD3 (0.25 μg $\cdot$ mL^{-1}) and soluble αCD28 (1 μg $\cdot$ mL^{-1}). The cells were stained for CD8 to identify CD8$^+$ T cells. Following flow cytometric acquisition the data was analyzed by gating on the CD8$^+$ cells and the CFSE signal was detected in bl525 channel. The right-most peak — designated G0 — represents the cells that have not undergone division. From there to the left follow the peaks for the different generation — G1...G5 — in increasing order.

Data acquisition and interpretation

The cellular CFSE dilution caused by the proliferation of the cells is detectable by flow cytometry. When the CFDA is cleaved into CFSE, it becomes fluorescent and its excitation peak is found at 494 nm, while its peak emission is at 521 nm. On the LSRFortessa the fluorochrome is excitable with the blue laser (488 nm) and detectable in the corresponding bl525 detector (525/50).

After gating on the desired cell population a histogram for the bl525 parameter shows the CFSE dilution pattern (Figure 3.3). The rightmost peak represents undivided cells. Here, the dye has not been diluted by cell divisions. This population is often referred to as G0 (generation 0). To the left of it, the cells that have undergone at least one round of division can be found. They are grouped into a series of peaks starting with cells that have only proliferated once (G1) and ranging up to the ones that have divided five times (G5). This allows for a thorough analysis of the proliferative behavior of cells.

3.1.11 Cell staining for flow cytometry

For the flow cytometric analysis of cells, usually fluorescent dyes and fluorochrome-conjugated antibodies are used to analyze the behavior of the cells and identify specific cellular features. The following protocols were applied for this task during the work for this thesis.

Extracellular stainings with fluorescently labeled antibodies and live/dead discrimination

Samples for staining were transferred to the wells of 96-well round-bottom plates. Also BD CompBeads — a 1:1 mixture of negative control and antibody-binding beads — were pipetted to the plates for the single stainings, necessary for the compensation. The cells and beads were washed by adding 150 μL PBS and centrifuging (400 rcf; 5 min; 4 °C) them.

For live/dead discrimination LIVE/DEAD® Fixable Blue was used. The compound in one vial provided by the manufacturer was dissolved in 50 μL anhydrous DMSO. This stock solution was diluted 1:1000 for the actual staining of the cells, where 100 μL per well were needed. To block unspecific binding of the antibodies that were used later on, an antibody against CD16/CD32 — the most prominent Fc binding receptors, responsible for most of the background — was also added to the dilution with a final concentration of $1\,\mu g \cdot mL^{-1}$. The cells were resuspended in the dilution and incubated for 30 min at RT in the dark. For compensation of the live/dead staining, an aliquot of control cells was exclusively stained with this dye. Afterwards, the cells were washed by adding 150 μL PBS and centrifuging (400 rcf; 5 min; 4 °C). The supernatant was discarded by emptying and tapping the pate on absorbent tissue.

For the staining with the fluorescently-labeled antibodies targeted against extracellular markers, antibody cocktails were made. The composition of the cocktails varied with every experiment and the markers of interest in that setting. Detailed tables of the antibodies used in each experiment can be found in the respective sections.

All antibodies used in this study have previously been titrated to find the most suitable dilution, showing on one hand a bright staining, while still having negligible amounts of background. Since the dilution factors varied with each new lot of the antibodies used, they will not be documented in this thesis. *Fluorescence minus one* (FMO) control dilutions were also prepared. These included all antibodies of the panel, except one. FMO stainings were used to determine the negative cells.

In order to stain the cells, they were resuspended in 100 μL of the respective antibody cocktails that were always prepared immediately before the staining procedure. For compensation later on, single staining dilutions — dilutions of each antibody in separate — were prepared and the CompBeads were stained with these. After an incubation of 10 min at 4 °C in the dark, the cells were washed with 150 μL PBS and centrifuged (400 rcf; 5 min; 4 °C). The supernatant was discarded as described above.

Most of the time biotinylated antibodies were used. In order to be able to detect them by flow cytometry they needed to be bound by streptavidin-conjugated (SAV) fluorochromes. These were titrated in advance, like the antibodies, and the corresponding dilutions were prepared. In order to stain the cells they were resuspended in a secondary staining step in 100 μL of the dilution and incubated for 10 min at 4 °C in the dark. Thereafter, the cells were washed again as already described above.

Fixation of the cells was performed to preserve and measure them later as well for intracellular stainings, usually done on the following day. The cells were resuspended in 100 μL 2 % (v/v) paraformaldehyde (PFA)/PBS and incubated for 20 min at RT in the dark. After washing, the cells were resuspended in PBS and stored at 4 °C in the dark until further use.

Cell permeabilization and intracellular staining with fluorescently labeled antibodies

Intracellular staining of cytokines is an excellent tool to determine the frequency of cytokine producing cells as well as the amount of cytokines that are produced per cell in a relative manner. For the antibodies specific for the certain cytokines to bind their targets, the cells had to be permeabilized. To achieve this, they were resuspended in 100 µL 0.1 % (v/v) IPEGAL® CA-630/PBS and incubated for exactly 4 min. The permeabilization was stopped by adding 150 µL PBS and centrifuging (400 rcf; 5 min; 4 °C).

After supernatant removal the cells were resuspended in 100 µL of the antibody cocktail directed against the cytokines of interest. These antibodies — as the ones before — were pre-titrated and the dilutions were prepared accordingly. Also, FMO control stainings were made for later gating. The cells were washed, resuspended in PBS and stored at 4 °C until they were measured with a flow cytometer.

3.2 Investigative assays

Several investigative assays were performed to elucidate the role of ADAP in pathogen-specific immune responses. Most of these assays used general techniques already described in the sections found above. The assays included *in vitro* activation systems as well as *in vivo* infection mouse models and are grouped as follows:

- *In vitro* assays
  - Analysis of lymphocyte and myeloid cellularity in wild type and $Adap^{-/-}$ mice
  - Flow cytometric evalutaion of ADAP expression levels in lymphocytes
  - *In vitro* activation of polyclonal CD4$^+$ and CD8$^+$ T cells
  - *In vitro* activation of monoclonal OT-I TCR-transgenic CD8$^+$ T cells
- *In vivo* assays
  - Adoptive transfer of OT-I TCR-transgenic CD8$^+$ T cells to wild type hosts followed by an infection with OVA-expressing *Listeria monocytogenes*
  - Adoptive transfer of OT-I TCR-transgenic CD8$^+$ T cells to wild type hosts followed by an infection with recombinant IAV-OVA
  - *In vivo* cytotoxicity assay after IAV infection
  - Survival, weight loss and bacterial burden after a *Listeria monocytogenes* infection

Table 3.4: Lymphocyte and myeloid panels used to determine the cellularity and activation status in wild type and $Adap^{-/-}$ mice. The utilized antibodies are described with their specificity, conjugation, clone and isotype.

Specificity	Conjugate	Clone	Isotype
Lymphocyte panel			
CD3ϵ	APC	145-2C11	Hamster IgG1, κ
CD4	BV510	RM4-5	Rat IgG2a, κ
CD8a	BV421	53-6.7	Rat IgG2a, κ
NK1.1	PE	PK136	Mouse IgG2a, κ
CD19	PerCP-Cy5.5	1D3	Rat IgG2a, κ
CD43	APC-Cy7	1B11	Rat IgG2a, κ
CD62L	Biotin	MEL-14	Rat IgG2a, κ
CD44	FITC	IM7	Rat IgG2b, κ
Myeloid panel			
CD11b	Pacific blue	M1/70	Rat IgG2b, κ
Ly-6G	PE-Cy7	1A8	Rat IgG2a, κ
Streptavidin			
SAV	BV605	n/a	n/a

– Cellularity, activation status and effector function of immune cells after a *Listeria monocytogenes* infection

– Serum cytokines and bacterial burden in spleens and livers following an infection with *Listeria monocytogenes*

3.2.1 Analysis of lymphocyte and myeloid cellularity in $Adap^{-/-}$ mice

The cellularity of lymphocyte subsets, and neutrophils and monocytes in spleen, blood and inguinal lymph nodes (inLN) of wild type and $Adap^{-/-}$ mice under steady-state conditions was assessed by flow cytometric staining. To this end, splenocytes, blood leukocytes and cells from inLN were isolated according to the protocols in section 3.1.5. The leukocyte cell numbers in each compartment were determined as described in section 3.1.7. The cells were stained for flow cytometry according to the protocol found in section 3.1.11 with the panels in Table 3.4.

After the staining the cells were measured with the BD LSRFortessa flow cytometer. CD4$^+$ and CD8$^+$ T cells were identified as CD3$^+$NK1.1$^-$CD19$^-$ and CD4$^+$ or CD8$^+$ respectively. NKT cells were defined as CD3$^+$NK1.1$^+$CD19$^-$, NK cells as CD3$^-$NK1.1$^+$CD19$^-$ and B

cells as CD3$^-$NK1.1$^-$CD19$^+$. Neutrophils and monocytes were identified by being CD11b$^+$. Neutrophils were CD11b^{hi}Ly-6G^{hi} and monocytes as CD11b^{hi}Ly-6G^{lo}. Activation marker gating was performed using the corresponding FMOs. The gating strategy for the lymphocyte panel can be found in the appendix A.1.1 on page 137 in Figure A.1.1. The gating strategy for the myeloid panel can be found in the appendix A.1.2 on page 138 in Figure A.1.2. Absolute cell numbers were calculated with the frequencies determined by flow cytometry and the previously acquired leukocyte numbers in the respective organs.

3.2.2 Flow cytometric evaluation of ADAP expression levels in lymphocytes

Intracellular ADAP expression was assessed by means of flow cytometry. To this end splenocytes from *Adap$^{+/+}$*, *Adap$^{+/-}$* and *Adap$^{-/-}$* mice were isolated as described in section 3.1.5 on page 44 and stained with the flow cytometry panel in Table 3.5 according to the protocol described in section 3.1.11 on page 51, and afterwards fixed. In order to stain intracellular ADAP, the cells were permeabilized with 0.1 % (v/v) IPEGAL$^®$ CA-630/PBS for 4 min at room temperature and washed afterwards. The cells were then stained either with αADAP polyclonal sheep serum provided by Gary Koretzky [5] or with the corresponding pre-immunization serum for 1 hour at room temperature in the dark. A FITC-conjugated donkey αsheep IgG polyclonal antibody was used to detect the sheep serum. Incubation with this secondary antibody lasted for 30 min. After washing, the cells were measured on the LSRFortessa flow cytometer. The gating strategy can be found in Figure A.1.3 in appendix A.1.3 on page 138.

CD4$^+$ and CD8$^+$ T cells were identified as CD3$^+$CD19$^-$NK1.1$^-$ and CD4$^+$ or CD8$^+$ respectively. NKT cells were defined as CD3$^+$CD19$^-$NK1.1$^+$, while NK cells were CD3$^-$CD19$^-$NK1.1$^+$. B cells on the other hand were identified by being CD3$^-$CD19$^+$NK1.1$^-$.

3.2.3 *In vitro* activation of polyclonal CD4$^+$ and CD8$^+$ T cells

To analyze how a loss of ADAP would affect the activation of a polyclonal pool of CD4$^+$ and CD8$^+$ T cells, splenocytes form wild type and *Adap$^{-/-}$* mice were prepared as described in section 3.1.5 on page 44 and T cells were isolated using MACS (see 3.1.5 on page 46). To analyze their proliferative behavior later on, they were also stained with CFSE (see section 3.1.10). These cells were resuspended in IMDM compl. and mixed with lethally irradiated splenocytes form a wild type donor mouse, so that 180 μL held $2 \cdot 10^5$ isolated T cells and $3 \cdot 10^5$ irradiated APCs.

Table 3.5: Panels used for the intracellular ADAP staining in in lymphocytes to determine its expression levels. The utilized antibodies are described with their specificity, conjugation, clone and isotype. The αADAP polyclonal sheep serum and the corresponding pre-immunization control serum was provided by Gary Koretzky.

Specificity	Conjugate	Clone	Isotype
Extracellular panel			
CD3ε	APC	145-2C11	Hamster IgG1, κ
CD4	BV510	RM4-5	Rat IgG2a, κ
CD8a	BV421	53-6.7	Rat IgG2a, κ
NK1.1	PE	PK136	Mouse IgG2a, κ
CD19	PerCP-Cy5.5	1D3	Rat IgG2a, κ
αADAP or control serum			
sheep αADAP serum	n/a	n/a	polyconal
or			
pre-immunization serum	n/a	n/a	polyconal
Secondary antibody			
donkey αsheep IgG	FITC	n/a	polyconal

The cells were left either unstimulated, stimulated with two different concentrations of plate-bound αCD3ε (Clone 145-2C11), plate-bound αCD3ε together with soluble αCD28 (Clone 37.51), or PMA+Ionomycin (P+I).

A day prior to the actual assay, 96-well round-bottom plates were coated with two different concentrations of αCD3ε antibody. To this end, two dilutions of the antibody were prepared with 0.25 µg · mL^{-1} and 0.75 µg · mL^{-1} in PBS. 100 µL of these dilutions were pipetted into their respective wells and the plates were incubated at 4 °C o/n. Before the previously prepared cells were added to the wells, the plate was washed twice with 300 µL IMDM compl. per well.

For the stimulation 180 µL of the prepared cell suspensions was transferred into each well. 20 µL of 10 µg · mL^{-1} αCD28 were added to the wells reserved for this combined treatment. 20 µL of 10 × P+I solution was added to the wells dedicated for this stimulation mode, leading to a final concentration for PMA of 50 ng · mL^{-1}, and 100 ng · mL^{-1} for ionomycin. To the rest of the wells 20 µL of IMDM compl. were added.

The plates were incubated for either 24 or 72 h at 37 °C in an incubator with 7.5 % CO$_2$. After the desired amount of time, the supernatant was harvested, transferred to an Eppendorf tube and stored for later cytokine analysis by ELISA at −70 °C. The cells were stained for activation markers (see section 3.1.11) and measured on a BD LSRFortessa. Table 3.6 lists the antibodies used for the staining procedure. The panel was split into three separate ones,

Table 3.6: Panels used for staining in the *in vitro* T cell activation assays. The utilized antibodies are described with their specificity, conjugation, clone and isotype. The ones listed in the core panel are present in the other panels.

Specificity	Conjugate	Clone	Isotype
Core Panel			
CD3ε	APC	145-2C11	Hamster IgG1, κ
CD4	BV510	RM4-5	Rat IgG2a, κ
CD8a	BV421	53-6.7	Rat IgG2a, κ
Panel 1			
CD69	PE	H1.2F3	Hamster IgG1, λ
CD43	APC-Cy7	1B11	Rat IgG2a, κ
Panel 2			
CD25	PerCP-Cy5.5	PC61	Rat IgG1, λ
CD44	Biotin	IM7	Rat IgG2b, κ
Panel 3			
CD62L	Biotin	MEL-14	Rat IgG2a, κ
Streptavidin			
SAV	BV605	n/a	n/a

to avoid spill-over.

The flow cytometry data was analyzed with FlowJo and the cells were gated as shown in Figure A.1.4 in appendix A.1.4 on page 139. Cells were first gated on low intensity in the uv450 detector were the live/dead staining allowed for selection of viable cells. These cells were gated for single cells by use of a FSC-A vs. FSC-H plot. Only cells with a strong correlation between these parameters were gated. Selection for singlets was further improved by using a SSC-H vs. SSC-W plot. Furthermore the selected cells were gated for lymphocytes in a FSC-A vs. SSC-A plot. T cells were selected for their expression of CD3 (detected at the rd670 detector). The two T cell subsets were identified by their expression of CD4 (vi525 detector) and CD8 (vi450 detector) respectively.

The signal intensities generated by the antibodies against the several activation markers were analyzed at the respective detectors. Expression of the early activation marker CD69 (yg582 detector), the memory markers CD43 (rd780 detector) and CD44 (vi605 detector), the IL-2Rα chain CD25 (bl852 detector), and the homing marker CD62L (vi605 detector) was analyzed by plotting their histograms. Negative cells were defined with the respective FMOs and positive cells were gated.

Table 3.7: Panel used for staining in the *in vitro* T cell activation assay with OT-I TCR-transgenic CD8$^+$ T cells. The utilized antibodies are described with their specificity, conjugation, clone and isotype.

Specificity	Conjugate	Clone	Isotype
Panel			
CD3ϵ	APC	145-2C11	Hamster IgG1, κ
CD8a	BV421	53-6.7	Rat IgG2a, κ
CD69	PE	H1.2F3	Hamster IgG1, λ
CD25	PerCP-Cy5.5	PC61	Rat IgG1, λ
CD62L	Biotin	MEL-14	Rat IgG2a, κ
Streptavidin			
SAV	BV605	n/a	n/a

3.2.4 *In vitro* activation of monoclonal OT-I TCR-transgenic CD8$^+$ T cells

In order to analyze the role of ADAP in the activation of CD8$^+$ T cells further, splenocytes from $Adap^{-/-} \times$ OT-I $\times$ CD90.1 and $Adap^{+/+} \times$ OT-I $\times$ CD90.1 mice were harvested (see section 3.1.5) and CD8$^+$ T cells isolated by MACS (see section 3.1.5) using the CD8$^+$ T cell Isolation Kit by Miltenyi. These cells were stained with CFSE (see section 3.1.10) to be able to analyze their proliferation behavior by CFSE dilution later on. The cells were activated with increasing amounts of the OT-I corresponding peptide OVA$_{257-264}$ (N-SIINFEKL-C) — 10, 100 and 1000 pg $\cdot$ mL^{-1} — or vehicle as a control. To this end, they were co-cultured with lethally irradiated APCs, as already mentioned above (see section 3.2.3). The cells were resuspended in 180 µL IMDM compl. and 20 µL of the respective 10-fold peptide solution were added. The peptide was produced in-house by Dr. Dr. Werner Tegge of the Peptide Synthesis Facility. After addition of the peptide the cells were incubated at 37 °C for either 24 or 72 h with 7.5 % CO$_2$.

After the respective amount of time, the supernatant was aspirated and stored at –70 °C for potential later analysis. The cells were washed with 150 µL PBS and after centrifugation (400 rcf; 5 min; 4 °C) stained according to a previously described protocol (see section 3.1.11) for activation markers. Table 3.7 lists the antibodies used in this experiment.

After the staining procedure the cells were measured with a BD LSRFortessa flow cytometer. The gating strategy is depicted in Figure A.1.5 in appendix A.1.6 on page 139. In short, lymphocytes were identified in the FSC-A vs SSC-A dot plot. Of these, singlets were gated on in an FSC-A vs FSC-H dot plot. Live cells were identified as being low for the viability dye (detected in uv450). The cells of interest were CD3$^+$CD8$^+$ (rd670 and vi450 respectively) and
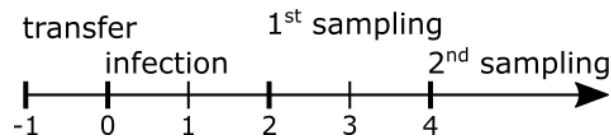
Figure 3.4: Time scheme for adoptive transfer experiments. One day prior to infection with *Lm*OVA either wild type or $Adap^{-/-}$ × OT-I × CD90.1 CD8$^+$ T cells were transferred to wild type recipient mice. 2 or 4 days after the infection, the mice were sacrificed, the transferred CD8$^+$ T cells isolated from their spleens, and assessed for their activation status and effector function.

positive gates for activation markers CD69 (yg582), CD25 (bl685) and CD62L (vi650) was set using the corresponding FMOs.

3.2.5 Adhesion assays

The adhesion assays for this thesis were performed in collaboration with Dr. Stefanie Kliche form the Otto von Guericke University Magdeburg. MACS-purified splenic T cells were stimulated with anti-CD3, PMA (50 ng $\cdot$ mL^{-1}), or MnCl$_2$ for 30 min at 37 °C before adhesion on Fc-ICAM-1 (10 µg$\cdot$ mL^{-1})-coated 96-well strips. Non-bound cells were removed by washing with HBSS and the bound cell fraction was determined by counting (in triplicates). To assess CXCR4/CCR7-mediated adhesion, T cells were incubated for 10 min at 37 °C on Fc-ICAM-1-coated 96-well strips co-immobilized with or without CXCL12 (100 ng $\cdot$ mL^{-1}) or CCL21 (500 ng $\cdot$ mL^{-1}); subsequently, non-bound cells were removed by washing with HBSS as described above. Adherent cells were calculated as percentage of input ($2 \cdot 10^5$ cells).

3.2.6 *In vivo* analysis of adoptively transferred OT-I TCR-transgenic CD8$^+$ T cells during an infection with OVA-expressing *L. monocytogenes*

The effects of ADAP deficiency on the activation, expansion and function of OT-I TCR-transgenic CD8$^+$ T cells was further investigated in an *in vivo* adoptive transfer system combined with an infection with ovalbumin-expressing *Listeria monocytogenes* (*Lm*OVA). The ovalbumin in these intracellular pathogenic bacteria contains the peptide OVA$_{257-264}$, and, hence, is able to activate them under proper inflammatory conditions.

To this end, splenocytes were isolated from $Adap^{+/+}$ × OT-I × CD90.1 and $Adap^{-/-}$ × OT-I × CD90.1 mice (see section 3.1.5) and OT-I TCR-transgenic CD8$^+$ T cells were isolated using MACS (see section 3.1.5). For subsequent proliferation analysis the cells were stained with CFSE (see section 3.1.10). After this, the purity was assessed by flow cytometry. Therefore, the cells were stained with αCD3ε APC (Clone: 145-2C11) and αCD8a PE (Clone: 53-6.7).

Table 3.8: Panel used for staining in the *in vivo* T cell activation assay with OT-I TCR-transgenic CD8$^+$ T cells in an adoptive transfer model with *Lm*OVA. The utilized antibodies are described with their specificity, conjugation, clone and isotype.

Specificity	Conjugate	Clone	Isotype
Extracellular panel			
CD8a	BV421	53-6.7	Rat IgG2a, κ
CD90.1	PE-Cy7	OX-7	Mouse IgG1, κ
CD25	PerCP-Cy5.5	PC61	Rat IgG1, λ
CD43	APC-Cy7	1B11	Rat IgG2a, κ
CD44	Biotin	IM7	Rat IgG2b, κ
Streptavidin			
SAV	BV605	n/a	n/a
Intracellular panel			
IFN-γ	PE	XMG1.2	Rat IgG1, κ
Granzyme B	Alexa Fluor 647	GB11	Mouse IgG1, κ

The purity of the cells was usually < 95 %. The cells were counted with a hemocytometer (see section 3.1.7), adjusted for purity, and every preparation for each genotype was diluted to yield the same cell concentration of $5.5 \cdot 10^6$ cells per 200 μL suspension. The suspensions were transferred to the infection unit of the animal facility and 200 μL of either $Adap^{+/+}$ or $Adap^{-/-}$ OT-I TCR-transgenic CD8$^+$ T cells were injected *i.v.* into the *Vena caudalis* of wild type, externally bred, C57Bl/6J recipient mice. On the following day the mice were infected with $2 \cdot 10^4$ CFU of *Lm*OVA per mouse via *i.v.* injection into the *Vena caudalis* (see section 3.1.2) and monitored on the consecutive days for their general well-being.

After 2 or 4 days post infection the mice were sacrificed and splenocytes were isolated as described above. In order to determine the level of IFN-γ production of the transferred OT-I TCR-transgenic CD8$^+$ T cells cells, isolated cells were restimulated with $1 \text{ μg} \cdot \text{mL}^{-1}$ of OVA$_{257-264}$ for 5 hours at 37 °C. After 1 hour of this incubation Brefeldin A was added to a final concentration of $5 \text{ μg} \cdot \text{mL}^{-1}$ to stop the vesicular transport from the Golgi apparatus and inhibit cytokine exocytosis. Subsequently they were stained (see section 3.1.11) for flow cytometric analysis. On the next day the cells were permeabilized and stained for IFN-γ and granzyme B intracellularly (see section 3.1.11). The utilized panels can be found in Table 3.8. After the staining procedure the cells were measured in a BD LSRFortessa and analyzed with FlowJo vX.

Since the wild type recipient mice express the CD90.2 variant, the transferred OT-I TCR-transgenic CD8$^+$ T cells— due to the expression of CD90.1 — were easily distinguishable from the host cells. The gating strategy used during these experiments can be found in Figure

A.1.6 in appendix A.1.6 on page 140. A schematic overview of the experimental procedure is shown in Figure 3.4.

3.2.7 *In vivo* analysis of adoptively transferred OT-I TCR-transgenic CD8$^+$ T cells during an infection with OVA$_{257-264}$-expressing influenza A virus

The aforementioned adoptive transfer model was also applied using an influenza A virus infection to investigate the role of ADAP in viral infections. For it to be able to effectively activate OT-I TCR-transgenic CD8$^+$ T cells the pathogen needed to encode the corresponding OVA$_{257-264}$-peptide. Therefore we used a recombinant IAV virus (IAV-OVA). Due to practical reasons the TCR-transgenic CD8$^+$ T cells were not sorted by MACS, but rather total splenocytes of the double-transgenic animals were transferred into the wild type recipient mice. Nevertheless the actual number of transferred OT-I TCR-transgenic CD8$^+$ T cells was set to approx. $5 \cdot 10^6$ cells. Apart from that, the procedure for preparation of the cells, as well as the method of injection into the recipient mice, was the same as described in the previous section (see section 3.2.6).

On the following day the mice were infected with a sublethal dose (1:1500 diluted) of the recombinant IAV-OVA virus as described previously (see section 3.1.3) and were monitored for their general well-being on a daily basis. On day 7 post infection the mice were sacrificed and their lungs harvested for the following cell isolation. The lungs were minced with scissors, taken up in digest medium and digested as described above (see section 3.1.5). After the digestion, the lungs were passed through a 100 µm cell strainer that was rinsed with ice-cold FACS buffer. After centrifugation (400 rcf; 10 min; 4 °C) the cell pellet was resuspended in 4 mL IMDM compl. and carefully pipetted on a 4 mL layer of Ficoll in a 15 mL falcon tube. The tubes were centrifuged at 900 rcf for 20 min at room temperature without any breaks, the interphase containing the lymphocytes were carefully transferred into a new 15 mL falcon tube and washed with IMDM compl. After centrifugation (400 rcf; 10 min; 4 °C) the cells were resuspended in IMDM compl. and restimulated as described above (see section 3.2.6).

As for the other adoptive transfer the cells were stained for activation markers, cytokine and granzyme B production as described earlier in section 3.1.11 on page 51 and 53. The flow cytometry panel that was used during these experiments is the same as found in Table 3.8 and the gating strategy is identical with the one in Figure A.1.6 in appendix A.1.6 on page 140.

3.2.8 *In vivo* cytotoxicity assay to determine the CD8$^+$ CTL response of previously IAV infected mice

The ability of CD8$^+$ T cells to kill target cells, and hence becoming cytotoxic T lymphocytes (CTLs), is a prerequisite for a successful immune response, especially against intracelluar pathogens like influenza A virus. To probe the development and function of CTLs in $Adap^{-/-}$ animals an *in vivo* CTL assay was used. To this end wild type and $Adap^{-/-}$ animals were infected with influenza A virus (strain A/Puerto Rico/8/1934 H1N1) as described in section 3.1.3 on page 42. After the infection the mice were monitored the following days for their general well-being.

On day 14 post infection, splenocytes from wild type mice were isolated (see section 3.1.5) and split into two fractions. One of these was pulsed with $1\mu g \cdot mL^{-1}$ of the immunodominant peptide NP$_{366-374}$ (N-ASNENMETM-C) of the nucleoprotein (NP) of the influenza A virus, while the other was mock treated. The pulsed cells were stained with a final concentration of $2.5\ \mu mol \cdot L^{-1}$ of CFSE; the unpulsed cells were stained with $0.25\ \mu mol \cdot L^{-1}$. This differential labeling allowed for later flow cytometric distinction. The stained cells were pooled again at a ratio of 1:1 and $2 \cdot 10^7$ total cells were injected *i.v.* into the *Vena caudalis* of the previously IAV infected mice. Two uninfected mice served as control and were also injected with the same amount of labeled and pulsed cells.

After 12 hours the mice were sacrificed, their splenocytes isolated as previously described (see section 3.1.5) and measured on the LSRFortessa flow cytometer. No additional stainings were needed. The gating strategy is shown in Figure A.1.7 in appendix A.1.7 on page 140. When gated on all CFSE$^+$ cells two distinct populations were detectable. The CFSE^{hi} population represented the pulsed cells that had been targets for the *in vivo* developed NP-specific CTLs of the recipient mice. The CFSE^{lo} population was the unpulsed cells that served as internal controls and should not have been lysed by the CTLs. The specific lysis of the pulsed target cells (in %) was calculated using equations taken from [266]. First the ratio r between the frequencies of pulsed (CFSE^{hi}) and unpulsed (CFSE^{lo}) was calculated (see equation 3.4).

$$r = \frac{\text{CFSE}^{lo}}{\text{CFSE}^{hi}} \tag{3.4}$$

The specific lysis L (in %) was than calculated with the ratio of the control mice r_{ctrl} and of each infected mouse r_{sample} according to equation 3.5.

$$L = \left(1 - \frac{r_{\text{ctrl}}}{r_{\text{sample}}}\right) \cdot 100 \tag{3.5}$$

3.2.9 Weight loss and survival of wild type and $Adap^{-/-}$ mice following an infection with *L. monocytogenes*

The impact of a *L. monocytogenes* infection on $Adap^{+/+}$ and $Adap^{-/-}$ mice was determined by their weight loss during the course of the infection as well as their overall survival. To this end male and female mice were infected (see section 3.1.2) with approx. $5 \cdot 10^4$ and $2.5 \cdot 10^4$ CFU, respectively, and monitored on a daily basis. The initial starting weight of each mouse was noted before the infection and also on each of the 14 consecutive days at approx. the same time of day. The humane endpoint was defined as either:

- loss of more than 25 % of the initial starting weight

- reduced grooming and resulting scruffy-looking fur

- ataxia

- closed eyes

- adenomatous abdomen

- apathy

- crooked posture

- social isolation

If a mouse met one of these criteria, it was euthanized by either cervical dislocation or CO_2 inhalation.

3.2.10 Cellular infiltration and T and NK cell function in livers and spleens following *L. monocytogenes* infection

The identity of infiltrating cells in spleens and livers of *Listeria*-infected wild type and $Adap^{-/-}$ animals was determined by flow cytometry. Animals were sacrificed at certain time points after the infection and spleens and livers were harvested. Leukocytes of these organs were isolated as described in section 3.1.5. The absolute cell numbers of leukocytes in the organs were determined as described in section 3.1.7 on page 47. The cells were unspecific restimulated with PMA ($1 \ \mu g \cdot mL^{-1}$) and ionomycin ($1 \ \mu g \cdot mL^{-1}$) for 5 hours at 37 °C. After 1 hour of this incubation Brefeldin A was added with a final concentration of $5 \ \mu g \cdot mL^{-1}$.

Following the restimulation, the cells were stained with the three flow cytometry panels found in Table 3.9 according to the protocols in section 3.1.11. The first panel identified CD8$^+$ T cells and stained for functional markers on these cells. The second panel identified NK

Table 3.9: Panels used to determine infiltrating cells and their functional status in livers and spleens of wild type and *Adap$^{-/-}$* mice after *Listeria monocytogenes* infection. Three panels were used to identify and distinguish CD8^{+} T cells, NK cells, neutrophils and monocytes. The intracellular staining was only used for CD8^{+} T cells and NK cells.

Specificity	Conjugate	Clone	Isotype
CD8^{+} T cell extracellular panel			
CD8a	FITC	53-6.7	Rat IgG2a, κ
CD25	PerCP-Cy5.5	PC61	Rat IgG1, λ
CD43	APC-Cy7	1B11	Rat IgG2a, κ
CD69	Biotin	H1.2F3	Hamster IgG1, λ
CD279 (PD-1)	PE	J43	Hamster IgG2, κ
NK cell extracellular panel			
CD335 (NKp46)	eFluor 660	29A1.4	Rat IgG2a, κ
CD69	Biotin	H1.2F3	Hamster IgG1, λ
CD279 (PD-1)	PE	J43	Hamster IgG2, κ
CD25	PerCP-Cy5.5	PC61	Rat IgG1, λ
CD27	PE-Cy7	LG.7F9	Hamster IgG
Neutrophil and monocyte extracellular panel			
CD11b	Pacific blue	M1/70	Rat IgG2b, κ
Ly-6G	PE-Cy7	1A8	Rat IgG2a, κ
Gr-1	PerCP-Cy5.5	RB6-8C5	Rat IgG2b, κ
CD274 (PD-L1)	Biotin	MIH5	Rat IgG2a, λ
Streptavidin			
SAV	BV605	n/a	n/a
Intracellular Panel			
IFN-γ	Pacific blue	XMG1.2	Rat IgG1, κ

cells by CD335 (NKp46) expression and stained for their functional markers. The third panel distinguished between neutrophils and monocytes. Neutrophils were defined as CD11b^{+}Gr-1^{+}Ly-6G^{+}and monocytes as CD11b^{+}Gr-1^{+}Ly-6G^{-}. The absolute cell numbers of each of the identified populations was calculated with the frequencies determined by the flow cytometric analysis performed on the BD LSRFortessa. The gating strategy can be found in Figure A.1.8 in appendix A.1.6 on page 140.

3.2.11 Serum cytokine and chemokine analysis using cytometric bead arrays

Concentrations of inflammation-related cytokines and proinflammatory chemokines in sera of *Listeria*-infected wild type and *Adap$^{-/-}$* mice was analyzed using BioLegend LEGENDplex$^{\text{TM}}$

Table 3.10: Inflammation-related cytokines and proinflammatory chemokines detected by Bi-oLegend LEGENDplex^{TM}cytometric bead arays. Inflammation-related cytokines were detected by the *Mouse Inflammation Panel* kit, while the chemokines were analyzed with the *Mouse Proinflammatory Chemokine Panel* kit.

BioLegend LEGENDplex^{TM} cytokines and chemokines		
Mouse Inflammation Panel	**Mouse Proinflammatory Chemokine Panel**	
Cytokine	*Chemokine*	*Alternative name*
CCL2 (MCP-1)	CCL2	MCP-1
GM-CSF	CCL3	MIP-1α
IFN-β	CCL4	MIP-1β
IFN-γ	CCL5	RANTES
IL-1α	CCL11	Eotaxin
IL-1β	CCL17	TARC
IL-6	CCL20	MIP-3α
IL-10	CCL22	MDC
IL-12p70	CXCL1	KC
IL-17A	CXCL5	LIX
IL-23	CXCL9	MIG
IL-27	CXCL10	IP-10
TNF-α	CXCL13	BLC

Mouse Inflammation Panel and *Mouse Proinflammatory Chemokine Panel* respectively. The cytometric bead array (CBA) assays are able to detect the cytokines and chemokines listed in Table 3.10.

Serum samples were prepared as descried in section 3.1.6 on page 3.1.6 from *Listeria*-infected mice at certain time points after the infection. The actual assay was performed according to the protocol provided by the manufacturer. In short, serum samples were diluted 1:2 with *Assay Buffer* (provided by the manufacturer) and the standard was diluted according to the protocol (ranging from 50 ng $\cdot$ mL^{-1}to 2.4 pg $\cdot$ mL^{-1}). The assay was performed in a 96-well U-bottom plate. The following reagents were pipetted into each well:

Volume	Reagent
25 µL	Matrix C (provided by the manufacturer)
25 µL	Assay Buffer (provided by the manufacturer)
25 µL	standard dilutions to the standard wells
or	
25 µL	diluted samples to the sample wells
25 µL	mixed beads (provided by the manufacturer)
25 µL	Detection Antibodies (provided by the manufacturer)

The plate was covered with aluminum foil to protect it from light and was incubated for 2 hours at room temperature on a shaking table set to 600 rpm. After the incubation 25 µL of the provided PE-conjugated streptavidin (SA-PE) were added to each well followed by another incubation of 30 min at room temperature while shaking at 600 rpm. The plate was again covered with aluminum foil to protect it from unwanted photo bleaching. The plate was centrifuged at 1000 rcf for 5 min and the supernatant was carefully removed with a multichannel pipette. Each well was washed with 200 µL of *Wash Buffer* (provided by the manufacturer) and centrifuged again at 1000 rcf for 5 min. After removal of the supernatant, the beads were resuspended in *Assay Buffer* and measured on the BD LSRFortessa flow cytometer. The gating strategy was performed as described by the manufacturer and can be found in Figure A.1.9 in appendix A.1.9 on page 142.

The data acquired by the flow cytometer was analyzed manually with FlowJo. The gating strategy shown in Figure A.1.9 in appendix A.1.9 on page 142 was used and geometric means of the fluorescence intensities (gMFI) in the PE-channel of each bead population — representing the several cytokines and chemokines — were exported. GraphPad Prism was used to calculate a fitted model for the standard curve. Richard's asymmetric five-parameter logistic equation was used for the model [267], and the unknown concentrations of the samples were calculated from that model by the software.

4

Results

As mentioned in the introduction, the aims of this thesis were to determine whether CD4$^+$ and CD8$^+$ T cells differently rely on ADAP, and what role the adapter protein plays in the immune responses against the intracellular pathogen *L. monocytogenes*. Several assays were performed to collect data and to answer these questions. However, for the later interpretation of the results, initial in depth analysis of the mouse models used in the frame of this thesis was necessary.

4.1 Basic characterization of the transgenic mouse lines used in this thesis

Three transgenic mouse lines and their respective wild type controls were used for this thesis: (i) the conventional $Adap^{-/-}$ mouse, (ii) the OT-I TCR-transgenic and (iii) the OT-II TCR-transgenic mice. The cellularity of these mice was determined to address whether ADAP deficiency itself has any impact on cell numbers.

4.1.1 Cellularity in the conventional $Adap^{-/-}$ mouse

The conventional ADAP knock-out mouse ($Adap^{-/-}$) was analyzed for its lymphocyte and myeloid cellularity in spleen, blood and inguinal lymph nodes (inLN). To this end, cells of

the respective compartments were isolated and stained according to the protocol described in section 3.2.1. The identified cell subsets were CD4$^+$ and CD8$^+$ T cells, NKT and NK cells, B cells, as well as neutrophils and monocytes in a separate panel. The absolute cell numbers of the leukocyte populations in the respective compartments were calculated and compared between wild type and $Adap^{-/-}$ mice (Figure 4.1). Table A.1 summarizing the determined cell numbers can be found in appendix A.2.1.

In general, there was a tendency in $Adap^{-/-}$ mice for more splenocytes in total, however, this did not reach significance. When the lymphocyte subsets were analyzed in more detail, there were no significant differences detectable for CD4$^+$ T cells, NKT and NK cells. However $Adap^{-/-}$ mice showed significantly reduced numbers of CD8$^+$ T cells and, contrariwise, B cell numbers were increased (Figure 4.1A). In blood, no significant differences were observable for all analyzed lymphocyte subsets (Figure 4.1B). The same was true for the inguinal lymph nodes (Figure 4.1C).

When the cellularity of the two analyzed myeloid cell types — neutrophils and monocytes — was determined, interesting differences became apparent. Although they did not reach significance, there seemed to be higher numbers of both cell types in the spleens of $Adap^{-/-}$ mice when compared to the wild type control mice (Figure 4.1D). This became even more striking in the blood, where both, neutrophil and monocyte numbers, were significantly increased in $Adap^{-/-}$ mice (Figure 4.1E).

Cellularity of memory phenotype T cells $Adap^{-/-}$ mice

The T cell compartment was further analyzed by distinguishing between naïve and memory phenotype (MP) T cells. The latter are found even in pathogen inexperienced mice and are described to have a more innate-like phenotype (see section 1.1.8). Staining for CD44 and CD62L differentiates between naïve (CD44^{lo}CD62L^{hi}), memory phenotype (CD44^{hi}CD62L^{lo}) and intermediary cells (CD44^{hi}CD62L^{hi}) (Figure 4.2A). Fiege, et *al.* [67] have recently shown that conventional $Adap^{-/-}$ mice produce more MP CD8$^+$ T cells than their wild type counterparts. This was confirmed in the experiments performed for this thesis. Furthermore, also the CD4$^+$ T cell compartment exhibited more MP cells in the spleen, while no significant differences were detectable in peripheral blood and inguinal lymph nodes. The difference between wild type and $Adap^{-/-}$ mice in the CD8$^+$ T cell compartment was detectable in every tested compartment (although only a tendency in inLNs) (Figure 4.2A and B) and was as well most pronounced in the spleen.

An intermediary T cell population was identified that successfully up-regulated CD44 but failed to sufficiently shed CD62L. In the CD4$^+$ T cell compartment this subpopulation was increased in spleens of $Adap^{-/-}$ animals compared to the wild type control mice. In blood
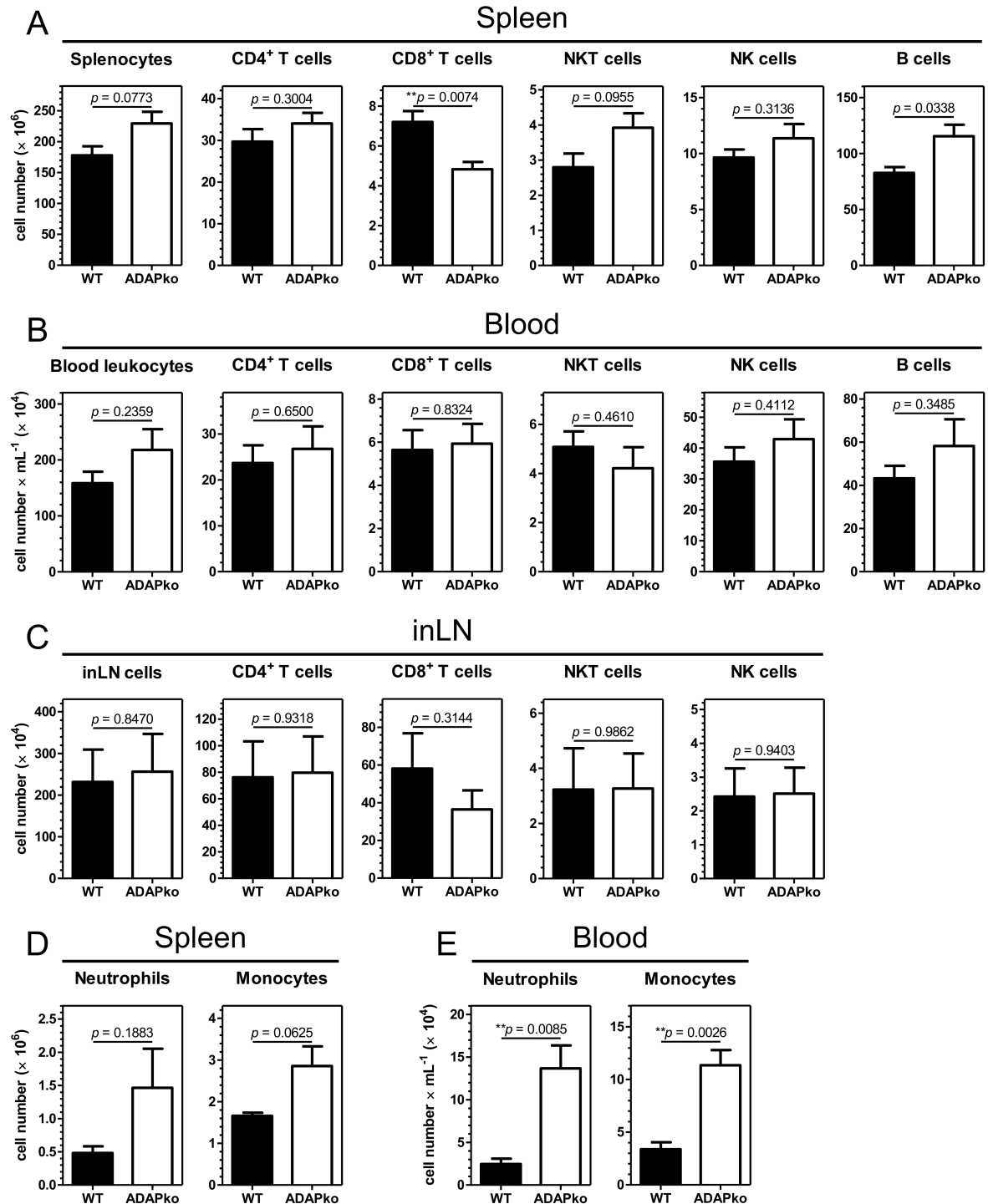
Figure 4.1: Comparative analysis of lymphocyte and myeloid cellularity in $Adap^{+/+}$ and conventional $Adap^{-/-}$ mice. Splenocytes, blood leukocytes and cells from inguinal lymph nodes (inLN) of $Adap^{+/+}$ (■) and $Adap^{-/-}$ (□) were isolated and stained for flow cytometry with αCD3, αCD4, αCD8, αNK1.1, αCD19, αCD11b, αGr-1 and αLy-6G to identify CD4$^+$ and CD8$^+$ T cells, NKT and NK cells, B cells, neutrophils and monocytes. The absolute cell numbers for the analyzed compartments were calculated. Absolute cell numbers of lymphocyte subsets in (A) spleens, (B) blood and (C) inLN of wild type and $Adap^{-/-}$ mice were determined; neutrophil and monocyte numbers in (D) spleen and (E) blood. Statistical analysis was performed using two-tailed, unpaired Student's t-test. $Adap^{+/+}$, N = 4; $Adap^{-/-}$, N = 5. Data represented as means ± SEM. *$p \leq 0.05$, **$p \leq 0.01$, ***$p \leq 0.001$.
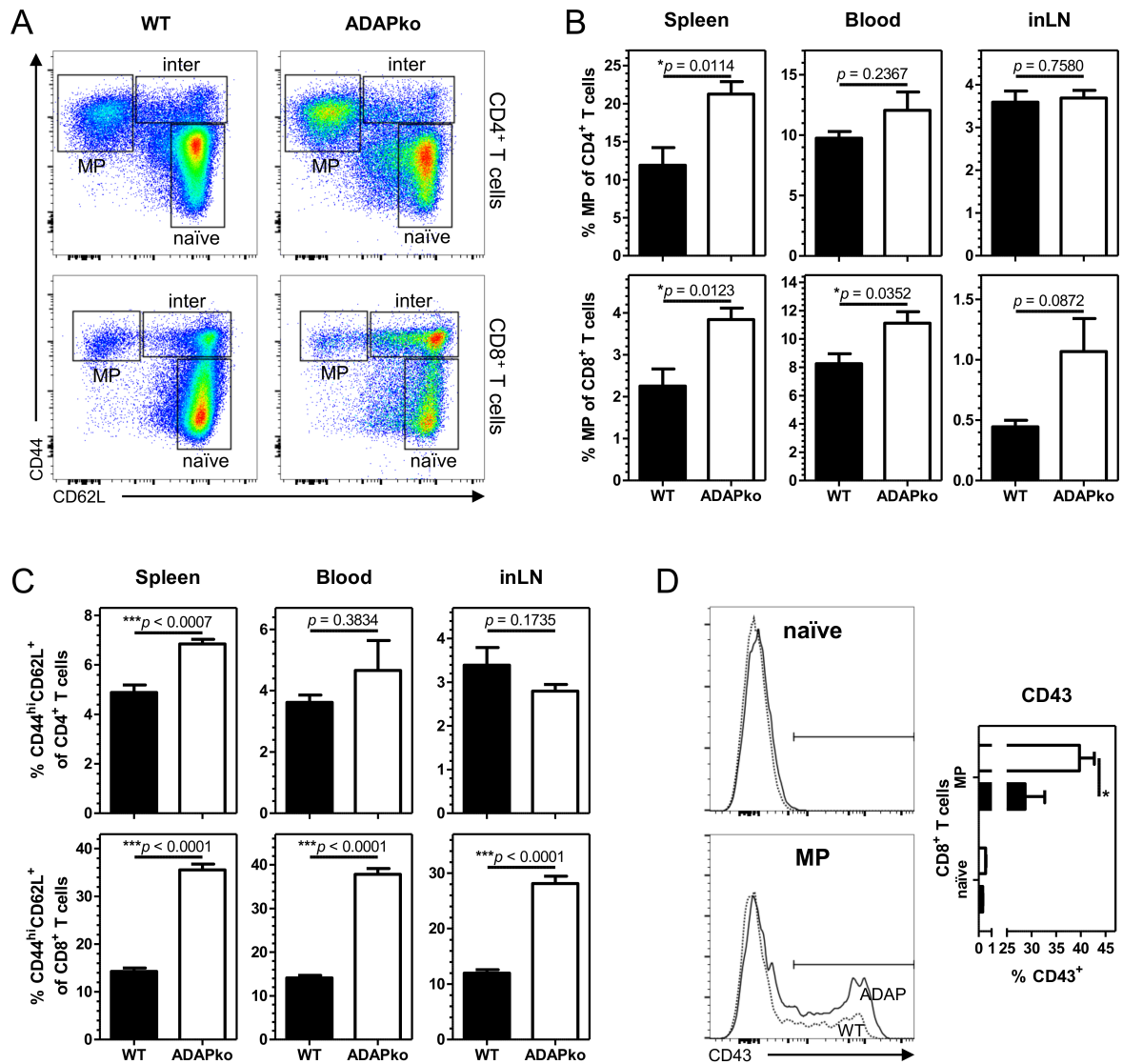
Figure 4.2: Frequency of intermediary and memory phenotype T cells in ADAP-deficient animals. Splenocytes, blood leukocytes and cells from inguinal lymph nodes (inLN) of $Adap^{+/+}$ (■) and $Adap^{-/-}$ (□) were isolated and stained for flow cytometry with αCD3, αCD4, αCD8a to identify CD4$^+$ and CD8$^+$ T cells. Furthermore, the cells were stained with αCD44 and αCD62L to differentiate between naïve (CD44^{lo}CD62L^{hi}), intermediary (CD44^{hi}CD62L^{hi}) and memory phenotype (MP; CD44^{hi}CD62L^{lo}) T cells. (A) Representative FACS plots for the CD44 vs CD62L staining on wild type and $Adap^{-/-}$ CD4$^+$ and CD8$^+$ T cells isolated from spleens. (B) Frequency of MP CD4$^+$ and CD8$^+$ T cells respectively in spleens, blood and inguinal lymph nodes (inLN). (C) Frequency of intermediary T cells in spleens, blood and inLN. (D) Expression of the memory and effector marker CD43 on naïve and MP CD8$^+$ T cells isolated from wild type and $Adap^{-/-}$ mice. Statistical analysis was performed using two-tailed, unpaired Student's t-test (B–C) and two-way ANOVA with Bonferroni's *post-hoc* test (D). $Adap^{+/+}$, N = 4; $Adap^{-/-}$, N = 5. Data represented as means ± SEM. *$p \leq 0.05$, **$p \leq 0.01$, ***$p \leq 0.001$.

and inLNs no significant differences were detectable. On the other hand, in the CD8$^+$ T cell compartment this intermediary population was strongly increased in spleen, blood and inLNs in $Adap^{-/-}$ mice (Figure 4.2C).

The expression of CD43 is increased on effector and memory CD8$^+$ T cells. As expected, while naïve CD8$^+$ T cells showed no detectable expression of CD43, a considerable proportion of MP CD8$^+$ T cells expressed this molecule. Interestingly, significantly more of the MP cells from $Adap^{-/-}$ animals expressed this marker (Figure 4.2D). Table A.2 summarizing all acquired frequencies can be found in appendix A.2.1.

4.1.2 Characterization of $Adap^{-/-} \times$ OT-I $\times$ CD90.1 mice

In order to analyze the role of ADAP in T cell subset activation in a monoclonal setting, wild type and $Adap^{-/-}$ OT-I and OT-II TCR-transgenic mice were generated (see section 2.1.2). OT-1 TCR-transgenic mice produce CD8$^+$ T cells that exclusively express one variant of the TCR that is specific for a certain peptide of the model antigen ovalbumin (OVA$_{257-264}$; N-SIINFEKL-C) that is restricted to the H-2Kb-MHC class I molecule. OT-II mice, on the other hand, produce exclusively CD4$^+$ T cells with a TCR specific for the I-Ad-MHC class II restricted peptide OVA$_{323-339}$ (N-ISQAVHAAHAEINEAGR-C).

Investigating the cellularity of the T cells in the two TCR-transgenic mouse lines by flow cytometric staining of blood leukocytes revealed that $Adap^{-/-}$ OT-II mice only produce very few CD4$^+$ T cells (Figure 4.3A). This was not entirely surprising, as similar effects have been previously reported for other MHC class II restricted TCR-transgenic mouse lines on ADAP-devoid background, like AND and H-Y mice [65]. $Adap^{-/-}$ OT-I TCR-transgenic mice, on the other hand, produced CD8$^+$ T cell numbers comparable to their wild type littermates (Figure 4.3A). Proper TCR-transgenicity was assessed by flow cytometric analysis for TCR Vα2 and TCR Vβ5.1, 5.2, which are specific for the OT-I and OT-II T cells (see section 3.1.1). Also in this respect $Adap^{-/-}$ CD4$^+$ T cells from OT-II mice showed aberrant TCR expression, while CD8$^+$ T cells from OT-I mice were not affected by loss of ADAP (Figure 4.3B). Due to the negligible numbers of CD4$^+$ T cells and their abnormal TCR expression, any further experiments with the $Adap^{-/-}$ OT-II TCR-transgenic mouse line were not reasonable and thus the breeding was terminated.

Analysis and proper characterization for the wild type and $Adap^{-/-}$ OT-I lines were further advanced. CD8$^+$ T cells in spleen and thymus of these animals were comparable (Figure 4.3C). Since Fiege, et *al.* [67] reported recently that conventional $Adap^{-/-}$ mice produced more memory phenotype CD8$^+$ T cells (characterized by CD44^{hi}CD122^{hi} expression) under steady-state conditions the numbers of this cell type was also assessed in our OT-I TCR-transgenic mouse line. When stained for a similar marker combination (CD44^{hi}CD62L^{lo}), less of this cell
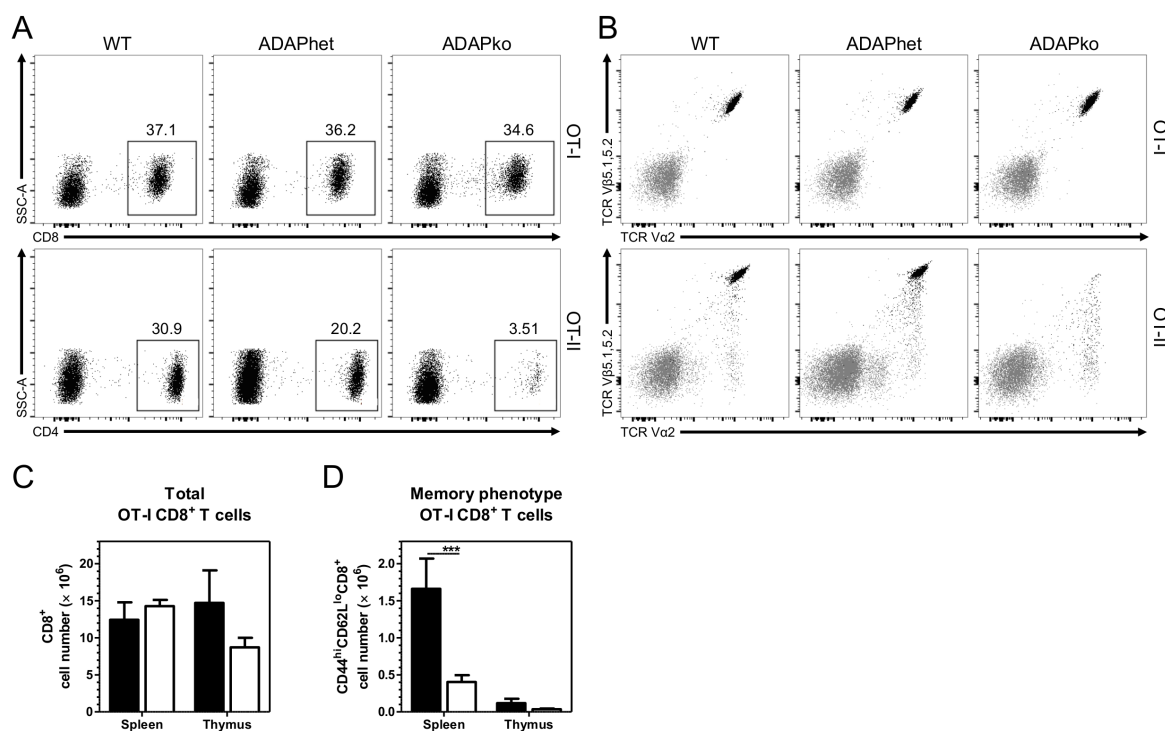
Figure 4.3: Cellular characterization of $Adap^{+/+}$ and $Adap^{-/-}$ OT-transgenic mice. Blood leukocytes form $Adap^{+/+}$ (■; WT), $Adap^{+/-}$ (ADAPhet) and $Adap^{-/-}$ (□; ADAPko) OT-I and OT-II transgenic mice were isolated and stained with αCD8 or αCD4 respectively. (A) shows the frequencies of OT-transgenic CD4$^+$ and CD8$^+$ T cells in relation to the ADAP genotype. (B) The cells were also stained for TCR Vα2 and TCR Vβ5.1, 5.2 to confirm the TCR-transgenicity. (C) Splenocytes and thymocytes of $Adap^{+/+}$ and $Adap^{-/-}$ × OT-I × CD90.1 mice were analyzed for CD8 expression and the absolute numbers of CD8$^+$ OT-I transgenic T cells in the respective organs were determined. (D) These cells were also analyzed for the memory marker CD44 and CD62L and the absolute numbers of memory phenotype cells were assessed. Statistical analysis was performed using two-way ANOVA with Bonferroni's *post-hoc* test. $Adap^{+/+}$, N = 4; $Adap^{-/-}$, N = 4. Data represented as means ± SEM. *$p \leq 0.05$, **$p \leq 0.01$, ***$p \leq 0.001$.

type was found (Figure 4.3D). Table A.3 summarizing the results of this experiment can be found in appendix A.2.2.

4.2 Subset-specific importance of ADAP for T cell activation and function

The first question addressed was, whether ADAP was equally important in the activation, adhesion, expansion and function of the two main T cell subsets, namely CD4$^+$ and CD8$^+$ T cells. Previous studies analyzed the role of ADAP in great detail, but omitted to distinguish between these subsets. On the following pages the data gathered for ADAP expression, activation marker regulation after *in vitro* activation, *in vitro* stimulated adhesion, and *in*

vivo activation in two adoptive transfer models with *L. monocytogenes* and influenza A virus infections are presented.

4.2.1 Expression of ADAP in lymphocyte subsets

The expression of ADAP in conventional and unconventional T cells and NK cells is a well-established fact in literature [4, 7, 11] and was already discussed in the introduction. Nevertheless, confirmation of these results was attempted and, for the first time, also a subset-specific analysis of CD4$^+$ and CD8$^+$ T cells was performed. Moreover, gene-dose effects of ADAP-heterozygosity and actual absence of the protein in the $Adap^{-/-}$ mice used in this study were also determined. To this end, splenocytes were isolated from $Adap^{+/+}$, $Adap^{+/-}$ and $Adap^{-/-}$ mice and stained for intracellular ADAP as described in section 3.2.2.

As expected and previously reported [10], mature, splenic B cells did not express detectable levels of ADAP and served as an internal negative control. T cells, NK cells and NKT cells on the other hand produced significant amounts of ADAP. While CD4$^+$ and CD8$^+$ T cells expressed comparable amounts of ADAP, NK and NKT cells expressed significantly lower ADAP levels. Furthermore, lymphocytes isolated from ADAP heterozygous animals showed significantly reduced ADAP expression compared to the wild type control mice, and cells from knock-out animals, as expected, completely lacked the adapter protein (Figure 4.4A and B). All expression values were calculated as folds over the gMFI of the pre-immunization serum staining. Table A.4 lists the calculated ADAP expression levels and can be found in appendix A.2.3.

4.2.2 CD3ϵ on wild type and $Adap^{-/-}$ CD4$^+$ and CD8$^+$ T cells

The subset-specific extent of CD3ϵ expression on wild type and $Adap^{-/-}$ T cells was determined from the data acquired in the experiments discussed in section 4.1.1. The amount of CD3ϵ was estimated by the gMFI of the signal in the channel for the CD3ϵ staining.

There is a clear difference in the expression of CD3ϵ on CD4$^+$ and CD8$^+$ T cells, with the latter only presenting approx. half of the amount of the former. This is in concordance with published results [268, 269, 270]. Interestingly, ADAP deficiency significantly reduced CD3ϵ expression on both T cell subtypes (Figure 4.5). The results of this experiment are summarized in Table A.5 in appendix A.2.4.
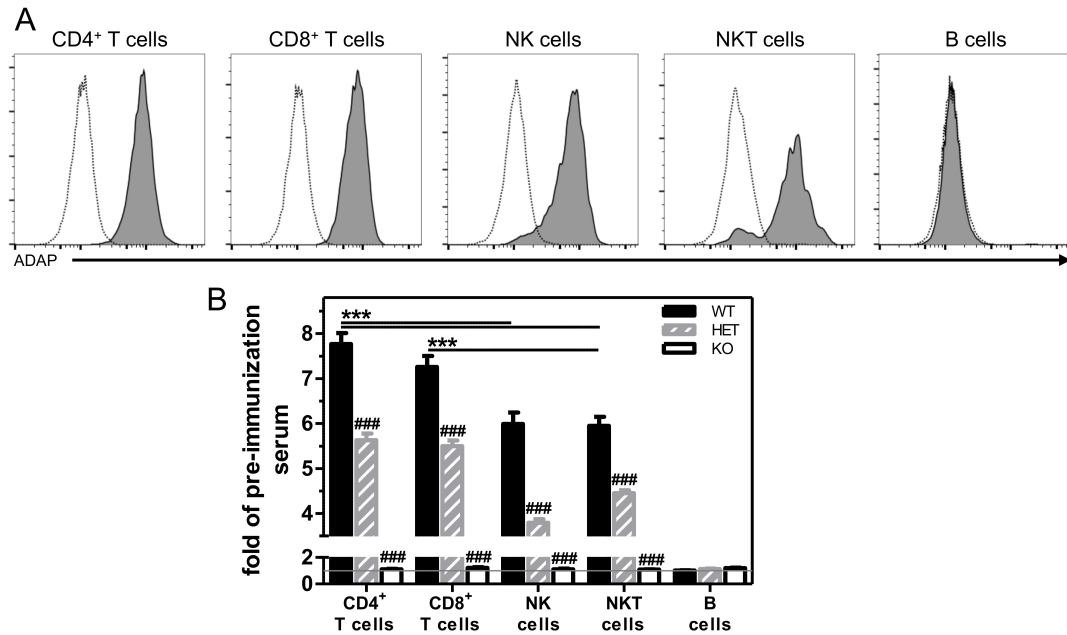
Figure 4.4: Splenic CD4$^+$ and CD8$^+$ T cells express comparable amounts of ADAP, while NK and NKT cells produce significantly less. Splenic lymphocytes were isolated from $Adap^{+/+}$ (WT), $Adap^{+/-}$ (HET) and $Adap^{-/-}$ (KO) mice. CD4$^+$, CD8$^+$, NKT cells and NK and B cells were identified by flow cytometric staining for extracellular markers and ADAP expression was assessed by intracellular staining with an ADAP-specific polyclonal sheep serum. For control purposes cells were also stained with a pre-immunization serum to calculate the specific ADAP staining as fold of the control gMFIs. (A) shows histograms of ADAP-stainings of the analyzed cell types. The gray histograms represent the ADAP stainings, while the dashed histograms depict the pre-immunization serum control stainings. (B) Graphical representation and statistical analysis of ADAP expression in lymphocyte subsets. While CD4$^+$ and CD8$^+$ T cells express comparable levels of ADAP, NK and NKT cells produce significantly less. Splenic B cells, as expected, lack ADAP. Moreover, ADAP-heterozygosity results in a clear reduction of ADAP expression, and ultimately, $Adap^{-/-}$ cells are completely devoid of ADAP. Statistical analysis was performed using two-way ANOVA with Bonferroni's *post hoc* test. $Adap^{+/+}$, N = 14; $Adap^{+/-}$, N = 5; $Adap^{-/-}$, N = 10. Data represented as means $\pm$ SEM. *$p \leq 0.05$, **$p \leq 0.01$, ***$p \leq 0.001$.
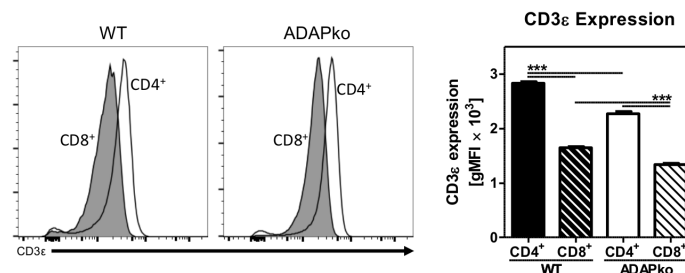
Figure 4.5: Subset-specific CD3ϵ expression analysis on wild type and $Adap^{-/-}$ T cells. The data collected in the experiments described in section 4.1.1 were further analyzed for the amount of CD3ϵ on the two T cell subsets and in regards to the ADAP genotype. Statistical analysis was performed using two-way ANOVA with Bonferroni's *post hoc* test. $Adap^{+/+}$, N = 4; $Adap^{-/-}$, N = 5. Data represented as means $\pm$ SEM. *$p \leq 0.05$, **$p \leq 0.01$, ***$p \leq 0.001$.

4.2.3 *In vitro* activation and proliferation of CD4$^+$ and CD8$^+$ T cells from wild type and *Adap*$^{-/-}$ mice

The importance of ADAP in T cell signaling downstream of the TCR leading to their activation has been demonstrated *in vitro* by staining for the expression of early activation marker CD69, the high affinity α-chain of the IL-2 receptor (IL-2Rα, CD25), as well as analyzing their proliferation behavior [23, 22]. However, the effect of ADAP deficiency on T cell activation was not investigated in a subset-specific manner. To clarify this, T cells were isolated from spleens of *Adap*$^{+/+}$ and *Adap*$^{-/-}$ mice and stimulated *in vitro* with plate-bound αCD3 and soluble αCD28 treatment (see section 3.2.3). At 24 and 72 hours post stimulation the activation and proliferation status of the cells was assessed by flow cytometry.

Both T cell subsets up-regulated the early activation marker CD69 after activation, and as expected, the *Adap*$^{-/-}$ T cells showed a significantly decreased response (Figure 4.6A). However, when the cells were analyzed for shedding of CD62L in response to their activation, CD8$^+$ T cells were clearly less affected by the loss of ADAP then their CD4$^+$ counterparts (Figure 4.6B). Furthermore, also the up-regulation of CD25 was hardly affected in CD8$^+$ T cells when ADAP was missing (Figure 4.6C). Most strikingly, while *Adap*$^{-/-}$ CD4$^+$ T cells showed an impaired proliferation response — in concordance with previously published results — CD8$^+$ T cells were not affected in their proliferation behavior (Figure 4.6D).

Though CD69 expression was affected by ADAP deficiency in CD8$^+$ T cells, the vast majority of activation markers does not seem to rely on this adapter protein in this T cell subset. CD4$^+$ T cells, on the other hand, seem to strongly rely on it. Table A.6 in appendix A.2.5 summarizes the data collected in these experiments.

4.2.4 ADAP is required for proper adhesion of CD4$^+$ T cells after TCR activation but not in their CD8$^+$ counterparts

Since the previous experiments indicated subset-specific relevance of ADAP in T cell activation, this aspect was addressed in the context of integrin-mediated adhesion. Previous studies have clearly shown the importance of ADAP in T cell adhesion in response to TCR stimulation [271]. Furthermore, a crucial role for ADAP in the chemokine receptor induced integrin activation has been demonstrated. For CXCR4 this has been shown in human primary T cells upon downregulation of ADAP, and for CCR7 in mouse splenic T cells [37, 272].

To clarify whether subset-specific effects of ADAP deficiency are also present in adhesion processes, splenic CD4$^+$ and CD8$^+$ T cells from either wild type or *Adap*$^{-/-}$ mice were sorted and their adhesion to ICAM-1, a LFA-1 ligand, in response to activation was assessed. The cells
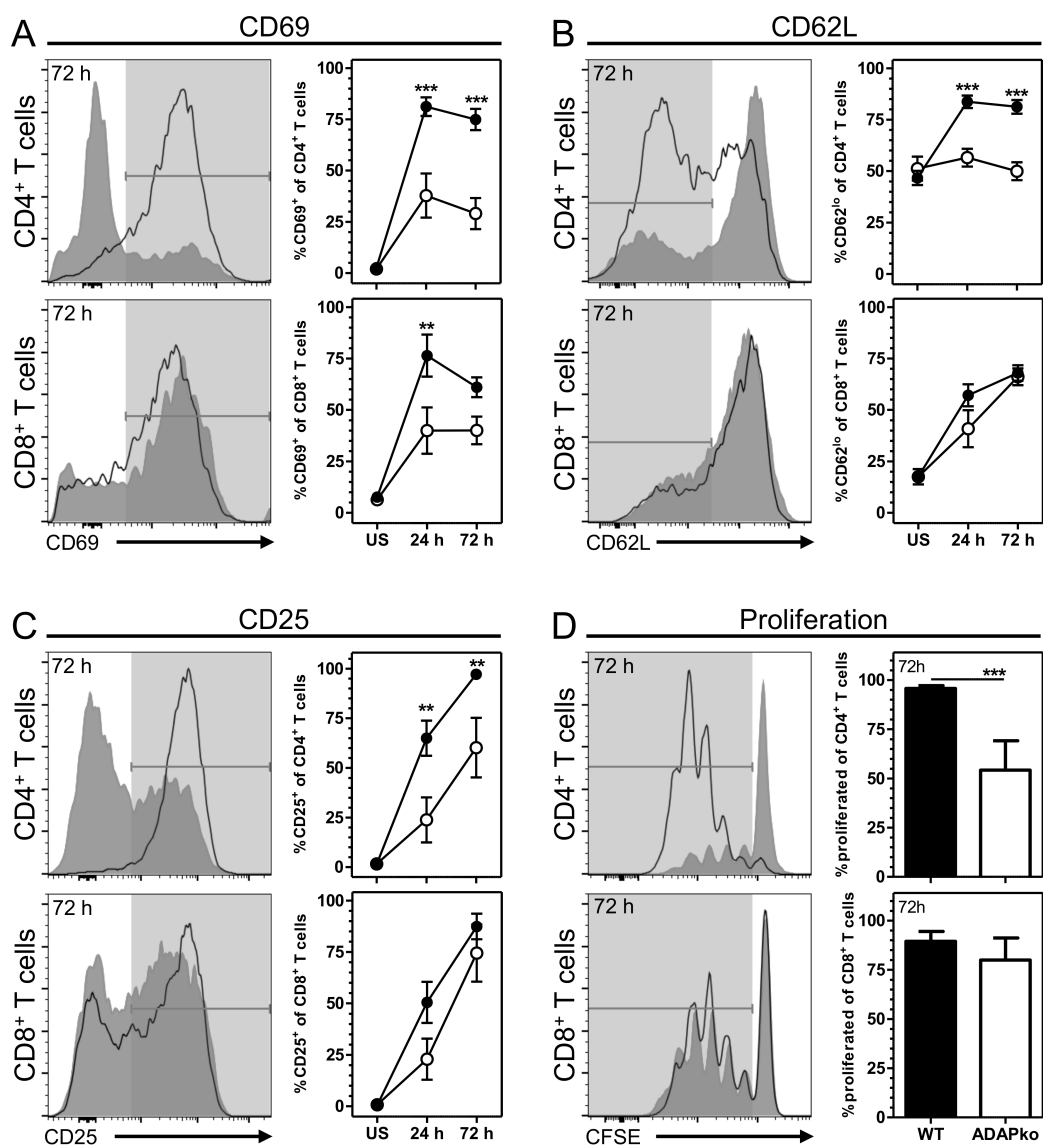
Figure 4.6: Activation and proliferation analysis of *in vitro* activated CD4$^+$ and CD8$^+$ wild type and *Adap*$^{-/-}$ T cells. Splenic T cells were isolated from *Adap*$^{+/+}$ (■) and *Adap*$^{-/-}$ (□) mice and *in vitro* activated by plate-bound αCD3 and soluble αCD28. 24 and 72 hours later the cells were subset-specifically — CD4$^+$ and CD8$^+$ — analyzed for the expression of activation markers and their proliferative response. (A) CD69 up-regulation was impaired in *Adap*$^{-/-}$ T cells, irrespective of their subtype. (B) CD62L shedding, (C) CD25 expression and (D) proliferation were only significantly affected by loss of ADAP in CD4$^+$ T cells, but not in their CD8$^+$ counterparts. Histograms show representative data. Gray histograms represent knock-out cells, while transparent histograms show wild type data. Statistical analysis was performed using two-way ANOVA with Bonferroni's *post hoc* test. *Adap*$^{+/+}$, N = 7; *Adap*$^{-/-}$, N = 5. Data represented as means ± SEM. *$p \leq 0.05$, **$p \leq 0.01$, ***$p \leq 0.001$.
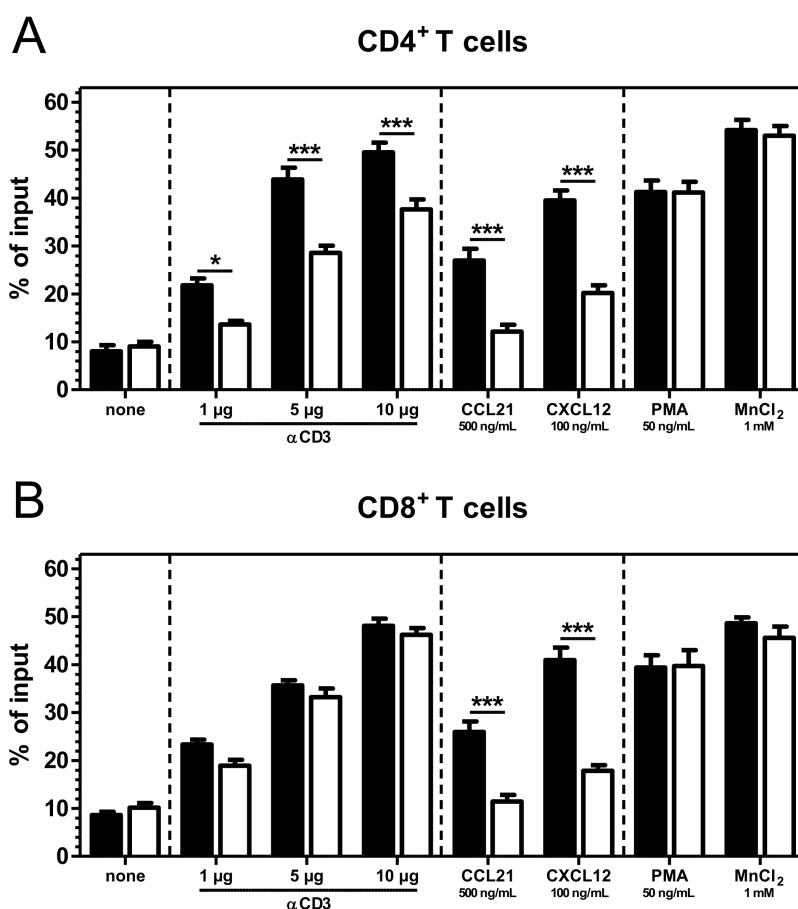
Figure 4.7: *In vitro* **adhesion behavior of wild type and** $Adap^{-/-}$ **CD4$^+$ and CD8$^+$ T cells.**
CD4$^+$ and CD8$^+$ T cells were sorted from $Adap^{+/+}$ (■) and $Adap^{-/-}$ (□) mice. Adhesion on ICAM-1 covered surfaces was either induced via the TCR by αCD3 treatment, or via the chemokine receptors CCR7 (by use of CCL21) and CXCR4 (by use of CXCL12). The percentage of cells that were adherent of the initially applied number was determined. (A) ADAP deficiency significantly decreased adhesion of CD4$^+$ T cells irrespective of TCR or chemokine receptor activation. (B) CD8$^+$ T cell adhesion induced via chemokine receptors was also significantly impaired in $Adap^{-/-}$ cells. However, TCR-induced adhesion was not affected. Statistical analysis was performed using two-way ANOVA with Bonferroni's *post hoc* test. $Adap^{+/+}$, N = 3; $Adap^{-/-}$, N = 3. Data represented as means $\pm$ SEM. *$p \leq 0.05$, **$p \leq 0.01$, ***$p \leq 0.001$.

were either activated via their TCR (αCD3 treatment) or their chemokine receptors, CCR7 (treatment with CCL21) and CXCR4 (treatment with CXCL12). Treatments with either PMA or MnCL$_2$ are known to induce T cell adhesion independent of cell surface receptor engagement, hence bypassing ADAP, and were used as positive controls. In this setting $Adap^{-/-}$ CD4$^+$ T cells showed a significantly reduced adhesion to ICAM-1-coated surfaces in response to increasing levels of TCR engagement. This was also the case when the cells were activated via their chemokine receptors (Figure 4.7A). On the other hand, their CD8$^+$ counterparts were not affected by loss of ADAP in response to TCR ligation, but clearly when activated with the chemokines (Figure 4.7B).

This shows that ADAP is required for mediating adhesion downstream of the TCR in CD4$^+$ T cells, while this is not the case in CD8$^+$ T cells. Interestingly, chemokine receptor stimulated adhesion seems to rely on ADAP, irrespective of the T cell subtype, since also the CD8$^+$ T cells showed a significant reduction of adhesion when ADAP was missing. The data from these experiments are summarized in Table A.7 in appendix A.2.6.

4.2.5 Activation of monoclonal CD8$^+$ OT-I TCR-transgenic T cells *in vitro*

Further analysis of the influence of ADAP deficiency on the activation and proliferation of CD8$^+$ T cells was performed using monoclonal OT-I TCR-transgenic CD8$^+$ T cells from the $Adap^{-/-} \times$ OT-I $\times$ CD90.1 mice. Unfortunately, the same analysis was not possible for CD4$^+$ T cells, since the $Adap^{-/-} \times$ OT-II $\times$ CD90.1 mice did not produce sufficient CD4$^+$ T cell numbers (see section 4.1.2). The advantage of this cell system is that there is only one monoclonal CD8$^+$ T cell type and it can be specifically activated with the cognate peptide OVA$_{257–264}$. This reduces background effects generated by the polyclonal pool of T cells in wild type mice. These monoclonal CD8$^+$ T cells were isolated from $Adap^{-/-} \times$ OT-I $\times$ CD90.1 mice and stimulated *in vitro* with increasing concentrations of OVA$_{257–264}$ according to the protocol found in section 3.2.4. After incubating the cells for 24 or 72 h the cells were stained for activation markers and their proliferation was analyzed by flow cytometry.

In contrast to the results obtained following polyclonal *in vitro* activation (see section 4.2.3), expression of the early activation marker CD69 was not affected by loss of ADAP in this monoclonal *in vitro* model (Figure 4.8A). CD62L shedding was also not significantly altered by ADAP deficiency, although the general response was lower, irrespective of the activation (Figure 4.8B). This was already detectable in the cellularity analysis of the mice in section 4.1.2 (Figure 4.3D), where less of the knock-out cells had a memory phenotype in the steady-state, hence, had not shedded CD62L. The up-regulation of the high-affinity IL-2Rα chain (CD25) was only affected by ADAP deficiency at minuscule amounts of OVA$_{257–264}$ — 10 pg $\cdot$ mL^{-1}. No significant differences were detectable at the other tested peptide concentrations (Figure 4.8C). And finally, the cells proliferated readily end extensively in response to the peptide, irrespective of the ADAP genotype (Figure 4.8D). Table A.8 in appendix A.2.7 summarizes the data compiled during these experiments.

Taken together, this data obtained in another *in vitro* setting confirmed that ADAP is dispensable for the activation and proliferation of CD8$^+$ T cells.
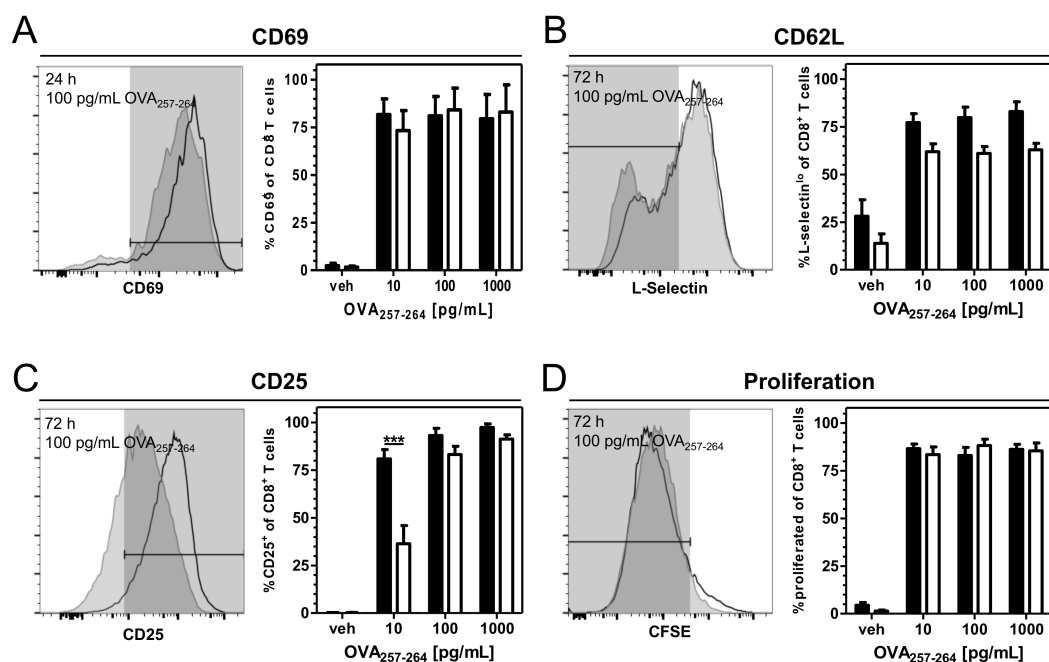
Figure 4.8: Activation and proliferation of OT-I TCR-transgenic $Adap^{-/-}$ CD8$^+$ T cells. Monoclonal OT-I TCR-transgenic CD8$^+$ T cells were isolated from wild type (■) and $Adap^{-/-}$ (□) mice by MACS, stained with CFSE for proliferation analysis and co-cultured with lethally irradiated APCs from wild type donor mice. The cells were activated with increasing concentrations of the OT-I cognate peptide OVA$_{257-264}$ and incubated for either 24 or 72 h. Thereafter, the cells were stained against CD8 and activation markers — (A) CD69, (B) CD62L and (C) CD25 — and analyzed by flow cytometry. (D) Proliferation was assessed by CFSE dilution. Statistical analysis was performed using two-way ANOVA with Bonferroni's *post hoc* test. $Adap^{+/+}$, N = 4; $Adap^{-/-}$, N = 4. Data represented as means $\pm$ SEM. *$p \leq 0.05$, **$p \leq 0.01$, ***$p \leq 0.001$.

4.2.6 Analysis of the activation and proliferation of CD8$^+$ OT-I TCR-transgenic T cells in an *in vivo* adoptive transfer model with *L. monocytogenes* infection

The next step was to confirm the *in vitro* findings *in vivo*. To this end, an adoptive transfer model was chosen. This allowed for the analysis of the OT-I TCR-transgenic CD8$^+$ T cell activation in an ADAP-sufficient organism (mouse). OT-I TCR-transgenic T cells also expressed the CD90.1 variant, which allowed for the identification of the cells in the CD90.2$^+$ wild type hosts. To activate the transferred T cells in the most relevant way, an infection of the recipient mice with *L. monocytogenes* was performed. The immune response against this intracellular pathogen relies heavily on the action of effector CD8$^+$ T cells. In order to be able to activate the OT-I TCR-transgenic T cells, the bacteria themselves were transgenic and expressed ovalbumin (*Lm*OVA) harboring the OVA$_{257-264}$ peptide recognized by the OT-I TCR-transgenic T cells.
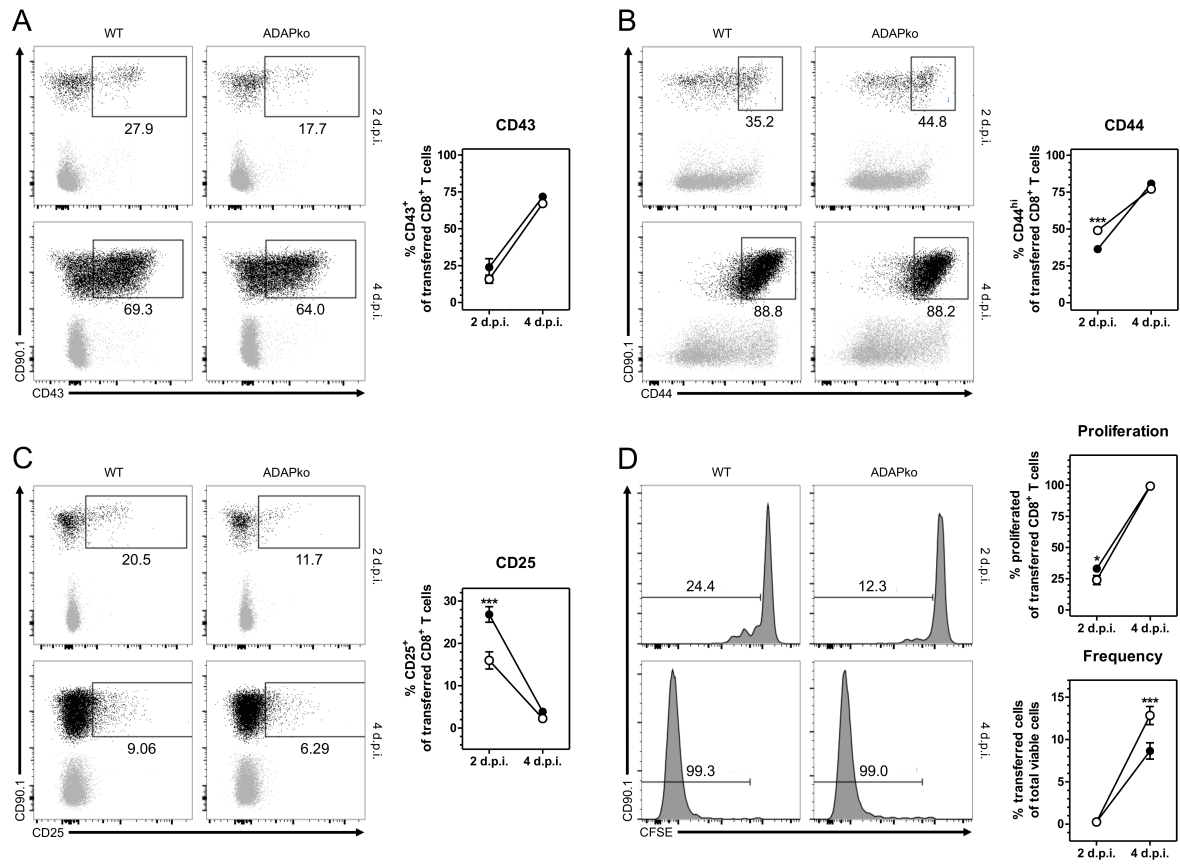
Figure 4.9: Activation and proliferation of OT-I TCR-transgenic wild type and $Adap^{-/-}$ CD8$^+$ T cells in an adoptive transfer model with LmOVA infection. Wild type (■) and $Adap^{-/-}$ (□) OT-I TCR-transgenic CD8$^+$ T cells were transferred to wild type recipient mice that were infected one day later with $2 \cdot 10^4$ CFU/mouse. 2 or 4 days post infection the mice were sacrificed, splenocytes isolated and stained for CD8 and CD90.1 to identify the transferred cells. Furthermore, the cells were stained against the activation markers (A) CD43, (B) CD44 and (C) CD25. The cells were also analyzed for their proliferation behavior and frequency (D). Statistical analysis was performed using two-way ANOVA with Bonferroni's *post hoc* test. $Adap^{+/+}$, N = 6; $Adap^{-/-}$, N = 6–7. Data represented as means ± SEM. *$p \leq 0.05$, **$p \leq 0.01$, ***$p \leq 0.001$.

To perform these experiments, wild type and $Adap^{-/-}$ OT-I TCR-transgenic CD8$^+$ T cells were isolated from the donor mice, stained with CFSE and approx. $5 \cdot 10^6$ cells were transferred *i.v.* to the wild type recipient mice. On the day following the transfer the mice were infected *i.v.* with LmOVA ($2 \cdot 10^4$ CFU/mouse). 2 or 4 days post infection, the animals were sacrificed, splenocytes isolated and stained for activation markers. The transferred cells were identified as CD8$^+$CD90.1$^+$ T cells. The experimental procedure is described in detail in section 3.2.6.

A clear activation of the transferred OT-I TCR-transgenic CD8$^+$ T cells was detectable, proving that the model was working. Progression to effector and memory cells was analyzed by the expression of CD43 and CD44. The level of CD43 was not significantly different between genotypes at any time point that was analyzed (Figure 4.9A). More $Adap^{-/-}$ cells were CD44$^{\text{hi}}$

compared to their wild type counterparts on day 2 post infection albeit this difference was gone on day 4 post infection (Figure 4.9B). Therefore, general progression to effector and memory phenotype seemed not to be impaired in transferred $Adap^{-/-}$ CD8$^+$ T cells. Markedly less transferred $Adap^{-/-}$ T cells were positive for CD25 on day 2 post infection. Since CD25 is only needed in the early phase of the T cell expansion, the frequency of CD25$^+$ T cells had drastically decreased on the later time point analyzed. Here, also the difference between the genotypes was lost (Figure 4.9C). Indicating the positive correlation of CD25 expression and proliferation, significantly less $Adap^{-/-}$ T cells had proliferated at the early time point following pathogen encounter although this phenotype was gone at day 4 post infection. Interestingly, when looking at the frequency of the transferred CD8$^+$ T cells, the $Adap^{-/-}$ cells seemed to even exceed the frequency of wild type cells (Figure 4.9D). These findings suggest that ADAP is dispensable for the activation and expansion of OT-I TCR-transgenic CD8$^+$ T cells *in vivo*.

The effector function of the transferred cells was assessed by staining for granzyme B and the proinflammatory cytokine IFN-γ. The former is an important effector molecule in the CD8$^+$ T cell mediated killing of target cells, while the latter is a key cytokine in the defense against intracellular pathogens. 2 days post infection, less of the $Adap^{-/-}$ transferred cells produced granzyme B when compared to their wild type counterparts. On day 4 after the infection, this phenotype was lost and most cells produced granzyme B, irrespective of the ADAP genotype (Figure 4.10A). Conversely, there was no significant difference in the frequency of IFN-γ producing T cells at the early time point post infection, but interestingly, a significantly smaller proportion of the cells was IFN-γ^+ at the later time point (Figure 4.10B).

However, also the $Adap^{-/-}$ T cells managed to battle the intracellular pathogen and to reduce the bacterial burden in the livers of the recipient animals (Figure 4.10C). Control mice were also infected with *Listeria* of the same strain (10403S) that did not express ovalbumin (*Lm* wt) and hence failed to activate the transgenic transferred cells (data not shown). The bacterial burden in these mice increased unhindered, since they were not controlled by the CD8$^+$ T cells transferred to the mice (Figure 4.10C).

Ultimately, ADAP appears to be dispensable for the effector function of CD8$^+$ T cells during *L. monocytogenes* infection, although less of them produce IFN-γ. Table A.9 presents the data acquired during the course of these experiments and can be found in appendix A.2.8.
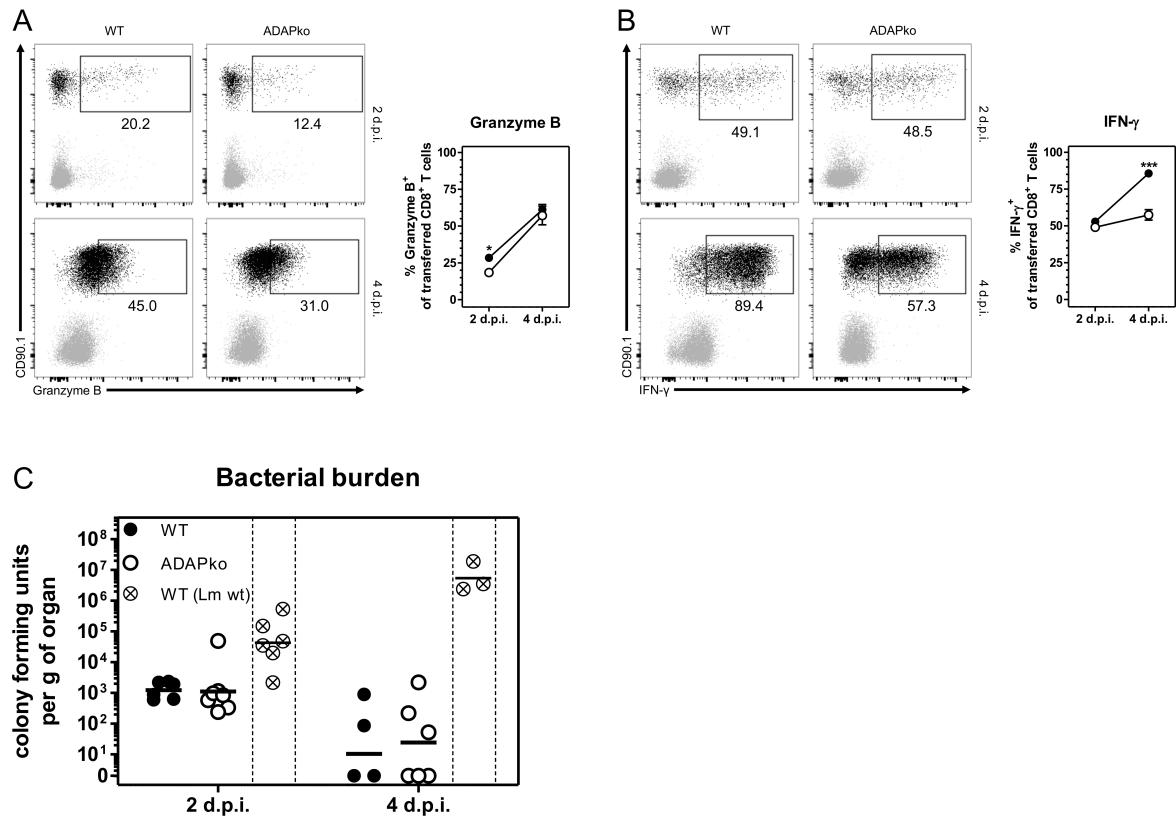
Figure 4.10: Effector function of OT-I TCR-transgenic wild type and $Adap^{-/-}$ CD8$^+$ T cells in an adoptive transfer model with LmOVA infection. Wild type (■) and $Adap^{-/-}$ (□) OT-I TCR-transgenic CD8$^+$ T cells were transferred to wild type recipient mice, that were infected one day later with $2 \cdot 10^4$ CFU/mouse. 2 or 4 days post infection the mice were sacrificed, splenocytes isolated and stained for CD8 and CD90.1 to identify the transferred cells. Furthermore, the cells were stained intracellularly against the effector function markers (A) granzyme B and (B) IFN-γ. (C) The livers of the infected animals were also homogenized, lysed and plated on BHI-agar Petri dishes to determine the bacterial load in the organ. Control mice were also infected with *Listeria* that do not express ovalbumin (Lm wt) and therefore failed to activate the transferred cells. Statistical analysis was performed using two-way ANOVA with Bonferroni's *post hoc* test. $Adap^{+/+}$, N = 6; $Adap^{-/-}$, N = 6–7. Data represented as means ± SEM. *$p \le 0.05$, **$p \le 0.01$, ***$p \le 0.001$.

4.2.7 Analysis of the activation and proliferation of CD8$^+$ OT-I TCR-transgenic T cells in an *in vivo* adoptive transfer model with influenza infection

The next aim was to confirm the aforementioned findings in another infection model. Infection with the influenza A virus leads to a local infection of the airways and the bronchi, in contrast to the systemic nature of the LmOVA infection. Nevertheless, the immune response against this viral pathogen relies strongly on the cytotoxic effects of pathogen-specific CD8$^+$ cells [273, 274]. $Adap^{-/-}$ OT-I TCR-transgenic CD8$^+$ T cells were again transferred to wild type recipient mice. On the day following the transfer, the mice were infected intranasally with influenza A virus
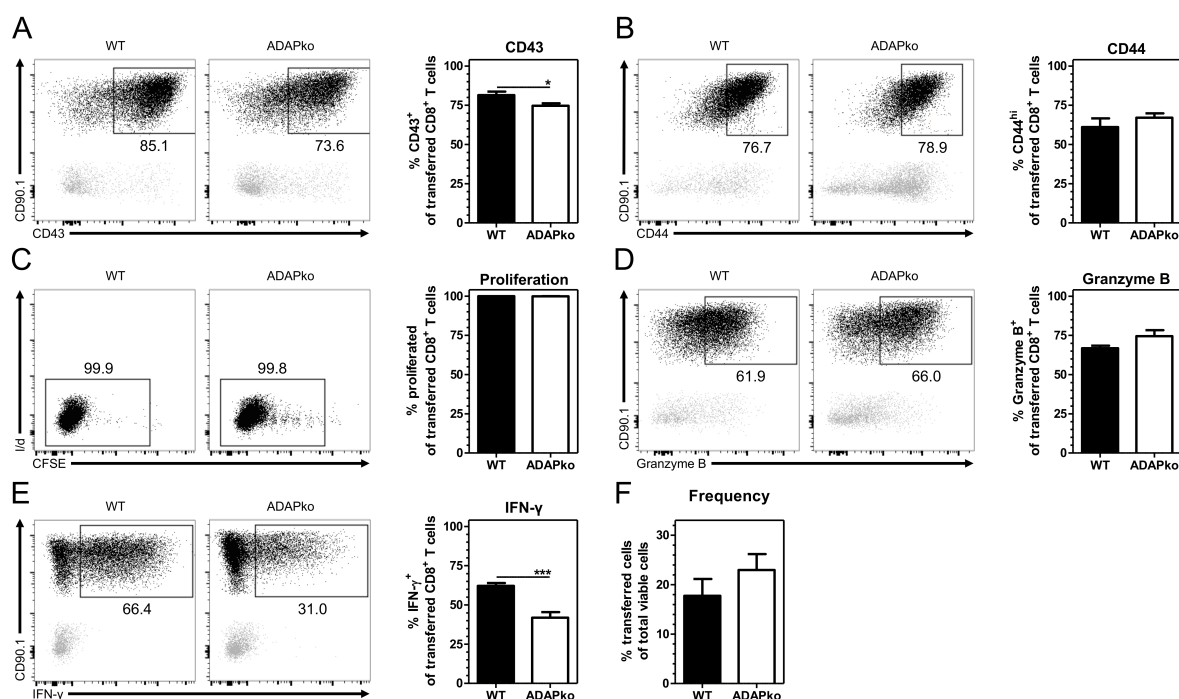
Figure 4.11: Activation and effector function of OT-I TCR-transgenic wild type and $Adap^{-/-}$ CD8$^+$ T cells in an adoptive transfer model with IAV-OVA infection. Wild type (■) and $Adap^{-/-}$ (□) OT-I TCR-transgenic CD8$^+$ T cells were transferred to wild type recipient mice, that were infected one day later with IAV-OVA. 7 days post infection the mice were sacrificed, lung lymphocytes isolated and stained for CD8 and CD90.1 to identify the transferred cells. Furthermore, the cells were stained for the activation markers (A) CD43 and (B) CD44. (C) The proliferation of the cells was also assessed by CFSE dilution. The effector function of the cells was determined by intracellular staining for (D) granzyme B and (E) IFN-γ production. (F) The frequency of the transferred cells was also determined. Statistical analysis was performed using two-way ANOVA with Bonferroni's *post hoc* test. $Adap^{+/+}$, N = 6; $Adap^{-/-}$, N = 6–7. Data represented as means ± SEM. $*p \leq 0.05$, $**p \leq 0.01$, $***p \leq 0.001$.

(IAV) expressing the OVA$_{257-264}$ peptide (IAV-OVA). 7 days post infection lymphocytes from the lungs of these animals were isolated, stained and analyzed by flow cytometry according to the protocol found in section 3.2.7.

The frequency of CD43$^+$ $Adap^{-/-}$ T cells was significantly reduced when compared to their wild type counterparts; although the reduction was only marginal (Figure 4.11A). The same amount of transferred T cells was CD44^{hi} (Figure 4.11B). Hence, progression to effector and memory phenotype seemed not to be affected by ADAP-deficiency, comparable to the results in the transfer model with the *Lm*OVA infection. Furthermore, both genotypes showed strong proliferation (Figure 4.11C) and no significant difference was detectable in the frequency of transferred CD8$^+$ T cells 7 days after the infection (Figure 4.11F).

The effector function of the cells was again assessed by intracellular staining for granzyme B and IFN-γ. While there were no differences detectable in the frequency of granzyme B producing T cells (Figure 4.11D), $Adap^{-/-}$ T cells showed a markedly decreased frequency of
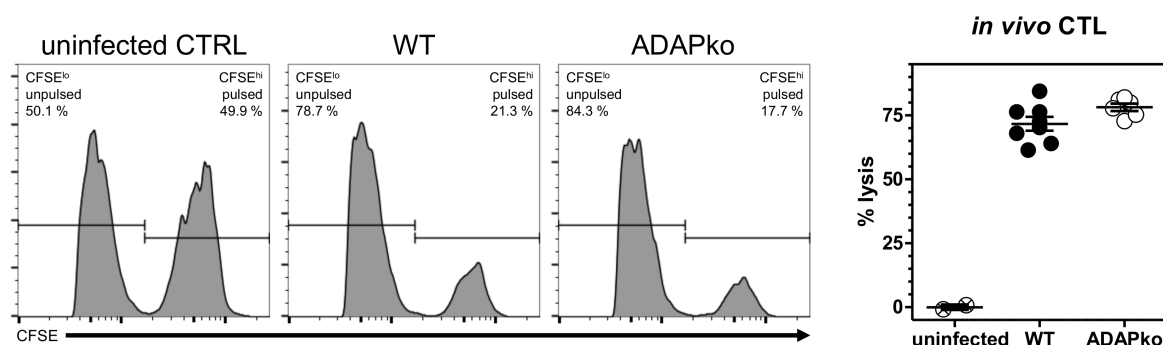
Figure 4.12: *In vivo* **analysis of CD8$^+$ T cell cytotoxicity in wild type and** *Adap$^{-/-}$* **mice following IAV infection.** Wild type (■) and *Adap$^{-/-}$* (□) mice were infected with influenza A virus strain A/Puerto Rico/8/1934 H1N1. 14 days after the infection, NP$_{366-374}$-pulsed or unpulsed, differentially CFSE-labeled splenocytes from wild type mice were transferred i.v. into the previously infected mice. Two control mice, that were not infected, also received target cells. 12 h after the transfer, the mice were sacrificed, their splenocytes isolated and the target cell frequencies were assessed by flow cytometry. The actual specific lysis was calculated. Statistical analysis was performed using one-way ANOVA with Bonferroni's *post hoc* test. *Adap$^{+/+}$*, N = 8; *Adap$^{-/-}$*, N = 6. Data represented as means ± SEM. *$p \leq 0.05$, **$p \leq 0.01$, ***$p \leq 0.001$.

IFN-γ^+ cells (Figure 4.11E), in concordance with the data obtained from the *Listeria* infection model.

These results are in accordance to the ones obtained in the other infection model and show that this phenotype in *Adap$^{-/-}$* CD8$^+$ T cells is irrespective of the pathogen used. Table A.10 lists the data collected in this experiment and can be found in section A.2.9.

4.2.8 *In vivo* analysis of the CTL activity in *Adap$^{-/-}$* mice following IAV infection

Since ADAP deficiency had little impact on the activation and effector function of CD8$^+$ T cells in the *in vitro* as well as *in vivo* OT-I TCR-transgenic system, we next wanted to analyze the cytotoxic capabilities of polyclonal CD8$^+$ T cells after an IAV infection *in vivo*. To this end, wild type and *Adap$^{-/-}$* mice were infected with influenza A virus strain A/Puerto Rico/8/1934 H1N1 and 14 days post infection, antigen-pulsed (NP$_{366-374}$) and unpulsed differentially CFSE-stained splenocytes from wild type donor mice were *i.v.* injected into the mice. 12 hours later, splenocytes were isolated and the previously transferred cells were identified by flow cytometry. The assay was performed according to the protocol found in section 3.2.8.

As expected, pulsed splenocytes transferred into mice that were not infected were not lysed by CTLs. On the other hand, the peptide-loaded target cells were reduced by 71.71 ± 2.631 % (mean ± SEM) in wild type mice previously infected with the virus. Of note, also the *Adap$^{-/-}$* mice were able to eliminate 78.17 ± 1.464 % (mean ± SEM) of the target cells presenting

the pathogen-specific antigen, showing no significant difference to the wild type mice (Figure 4.12). This indicates that $Adap^{-/-}$ CD8$^+$ T cells are fully competent to eliminate infected target cells.

Taken together the presented data suggests that while CD4$^+$ T cells rely strongly on ADAP for their activation and function, their CD8$^+$ counterparts are clearly less affected by ADAP deficiency. Their activation and expansion is comparable to wild type control mice in *in vitro* and *in vivo* assays. Although the expression of IFN-γ and early production of granzyme B are significantly impaired, this had no effect on their ability to clear pathogens, as shown by clearance of *L. monocytogenes* in the adoptive transfer model and unimpaired CTL response after an influenza A infection.

4.3 The role of ADAP in the immune response against the intracellular pathogen *L. monocytogenes*

With the above described evidence that $Adap^{-/-}$ CD8$^+$ T cells are only marginally affected with regard to their activation, function and cytotoxicity, analysis of the effects of total ADAP deficiency *in vivo* during an infection with *L. monocytogenes* was performed. To this end, wild type and $Adap^{-/-}$ mice were infected with the bacterium and several metrics, such as weight loss, survival, histology, cellular infiltration into organs, cell activation status and serum cytokine concentrations were determined.

4.3.1 Weight loss and survival of $Adap^{-/-}$ mice following *L. monocytogenes* infection

In order to assess the effects of total ADAP deficiency on mice following an infection with the intracellular pathogen *L. monocytogenes*, the weight loss during the course of the infection as well as the overall survival of the mice was determined. Wild type and $Adap^{-/-}$ mice were infected via the tail vein with approx. $5 \cdot 10^4$ CFU for males and approx. $2.5 \cdot 10^4$ CFU for females. For a detailed description of the procedure refer to sections 3.1.2 and 3.2.9. Different infection doses were applied to male and female mice, since it has been reported that a sex-dependent differential expression of IL-10 leads to increased susceptibility to *L. monocytogenes* infection in females [275]. The mice were monitored and weighed daily. In case of reaching a disease score too high according to the criteria listed in section 3.2.9, mice were euthanized before the final termination of the experiment.
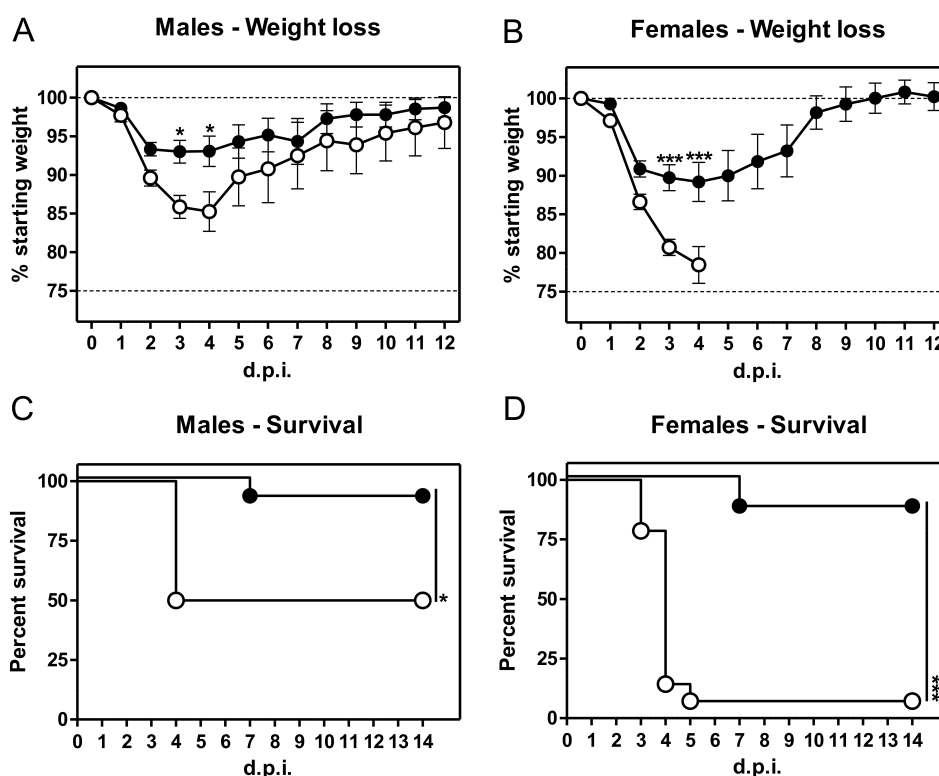
Figure 4.13: Weight loss and survival of wild type and *Adap*$^{-/-}$ mice following *L. monocytogenes* infection. Male and female wild type (■) and *Adap*$^{-/-}$ (□) mice were infected with *L. monocytogenes* and weighed and monitored daily. (A) Male and (B) female *Adap*$^{-/-}$ mice lost significantly more weight during the course of the infection. The graph for female knock-out animals stops on day 4 post infection, since only one mouse survived beyond this point. The survival of (C) male and (D) female *Adap*$^{-/-}$ mice was drastically reduced compared to the wild type control mice. Statistical analysis was performed using two-way ANOVA with Bonferroni's *post hoc* test for the weight loss data and Mantel-Cox log-rank test for the survival data. Males: *Adap*$^{+/+}$, N = 13; *Adap*$^{-/-}$, N = 12. Females: *Adap*$^{+/+}$, N = 8; *Adap*$^{-/-}$, N = 14. Data represented as means ± SEM. *$p \leq 0.05$, **$p \leq 0.01$, ***$p \leq 0.001$.

Male *Adap*$^{-/-}$ mice lost significantly more weight than wild type control animals during the early phase of the infection (4 d.p.i.: *Adap*$^{+/+}$: 93.0 ± 1.47, *Adap*$^{-/-}$: 85.9 ± 1.49; mean % starting weight ± SEM), which is indicative of a more severe disease course (Figure 4.13A). This was even more pronounced for female mice. Here, the *Adap*$^{-/-}$ mice dramatically lost weight during the early phase of the infection (4 d.p.i.: *Adap*$^{+/+}$: 89.2 ± 2.54, *Adap*$^{-/-}$: 78.5 ± 2.38) and almost all mice died within 4 days post infection. Weight data from the only mouse that survived the infection was excluded from the analysis (Figure 4.13B). The survival of the knock-out animals, regardless of sex, was severely reduced. Male *Adap*$^{-/-}$ mice showed a survival probability of only 50 % compared to 92 % for the wild type control animals (Figure 4.13C). For the female *Adap*$^{-/-}$ mice the difference was even more pronounced, with a survival rate of only 7 % after 14 days for the *Adap*$^{-/-}$ and 88 % for the wild type mice (Figure 4.13D). Even more interesting, most of the knock-out mice died rather early, i.e. between day 3 and 5 post infection. Table A.11 summarizing the weight loss data can be found in appendix
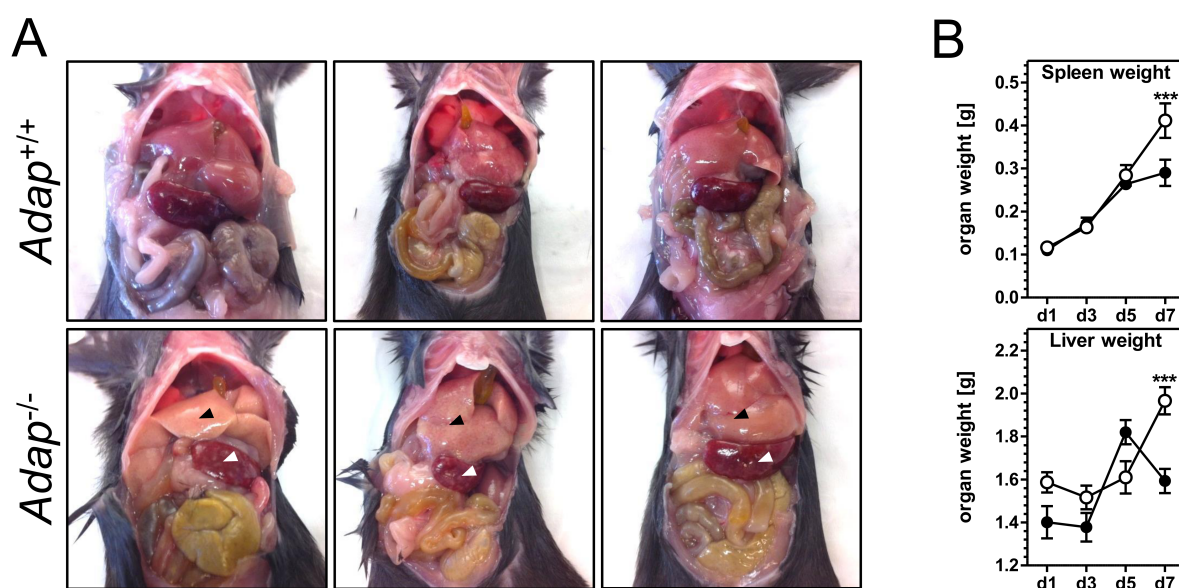
Figure 4.14: Liver and spleen weights and *in situ* pathology after *L. monocytogenes* infection. (A) Female wild type and $Adap^{-/-}$ mice were infected with approx. $1 \cdot 10^4$ CFU and sacrificed 3 days post infection. Pictures of the internal organs were taken to document the liver (▲) and spleen (△) pathology that was drastically more severe in the $Adap^{-/-}$ animals. Three individual mice are shown for each genotype. (B) Male wild type (■) and $Adap^{-/-}$ (□) mice were infected with approx. $2.5 \cdot 10^4$ CFU and the weights of spleens and livers was determined at certain time points. Statistical analysis was performed using two-way ANOVA with Bonferroni's *post hoc* test. $Adap^{+/+}$, N = 9–10; $Adap^{-/-}$, N = 8. Data represented as means ± SEM. *$p \leq 0.05$, **$p \leq 0.01$, ***$p \leq 0.001$.

A.2.10.

Together, these results prompted us to perform a more detailed analysis of the immune response in the $Adap^{-/-}$ mice during the course of a *L. monocytogenes* infection, especially at the early phase following infection where the differences between $Adap^{-/-}$ and wild type mice were most obvious.

4.3.2 Liver and spleen pathology *in situ*

The next step was to have a closer look at the organs that are initially infected by *L. monocytogenes*: spleen and liver. To this end, female mice were infected with approx. $1 \cdot 10^4$ CFU as described before. The infection dose was lowered to make sure that the animals would survive for time frame selected for performing the analysis. 3 days post infection the mice were euthanized, followed by opening of the abdomen for *in situ* exposure, macroscopic examination and photographic documentation of the organs. Furthermore, organs of uninfected mice, as well as from mice 1, 3, 5 and 7 days post infection were excised and weighed.

Three days post infection $Adap^{-/-}$ animals displayed severe and macroscopically visible liver pathology. Blood circulation in the livers seemed to have broken down and the organ itself

appeared spotted. The spleens were characterized by white lesions that resembled granuloma (Figure 4.14A). Overall the organs of interest were severely more affected after infection with the pathogen in $Adap^{-/-}$ mice than in the wild type control animals. Furthermore, the masses of the spleens increased significantly more at day 7 post infection in the knock-out mice compared to wild type controls. A similar increase in mass was observable for the livers of the $Adap^{-/-}$ animals (Figure 4.14B). Table A.12 summarizing the masses of the organs can be found in appendix A.2.11.

4.3.3 Bacterial burden in $Adap^{-/-}$ mice

Since the above mentioned *in situ* observations indicate enhanced pathology in $Adap^{-/-}$ mice following the *L. monocytogenes* infection, assessment of the bacterial burden in spleen and liver was done in order to see whether the organ damage correlated with higher numbers of bacteria in $Adap^{-/-}$ mice. To this end, male wild type and $Adap^{-/-}$ mice were infected with approx. $2.5 \cdot 10^4$ CFU and sacrificed after 1, 3, 5 or 7 days post infection. The bacterial burden was assessed by the method described in section 3.1.8.

One day post infection the mice showed almost identical bacterial colonization in spleens and livers, regardless of the ADAP genotype. However, three days post infection $Adap^{-/-}$ mice showed higher bacterial burden in spleens and livers. While at this time point bacterial growth appeared to be controlled in wild type mice, the number of bacteria still increased in $Adap^{-/-}$ animals. Five days post infection the bacterial burden decreased drastically in wild type spleens and livers. Pathogen load also decreased in $Adap^{-/-}$ mice but to a significantly lesser extent, indicating inefficient pathogen control. Interestingly, seven days post infection, both wild type and $Adap^{-/-}$ mice had practically eradicated the bacteria from their spleens. The same trend was detectable in the livers of the animals, although not in the same magnitude (Figure 4.15A and B, for spleen and liver respectively). Table A.13 summarizing the $\log_{10}$-transformed CFU data can be found in appendix A.2.12.

Together, these data further indicate impairment of the early immune response to the infection in $Adap^{-/-}$ mice. On the other hand, in case the infection dose is low enough to ensure overall survival of the mice, the later immune responses (past day 5 post infection) appear to be sufficient to eliminate the pathogens, since the bacterial numbers in $Adap^{-/-}$ mice decline to levels comparable to that found in the wild type control animals.

4.3.4 Histological analysis of spleen and liver

Due to the above described higher pathology and bacterial burdens in spleens and livers of $Adap^{-/-}$ mice infected organs were next subjected to histopathological examinations. To this
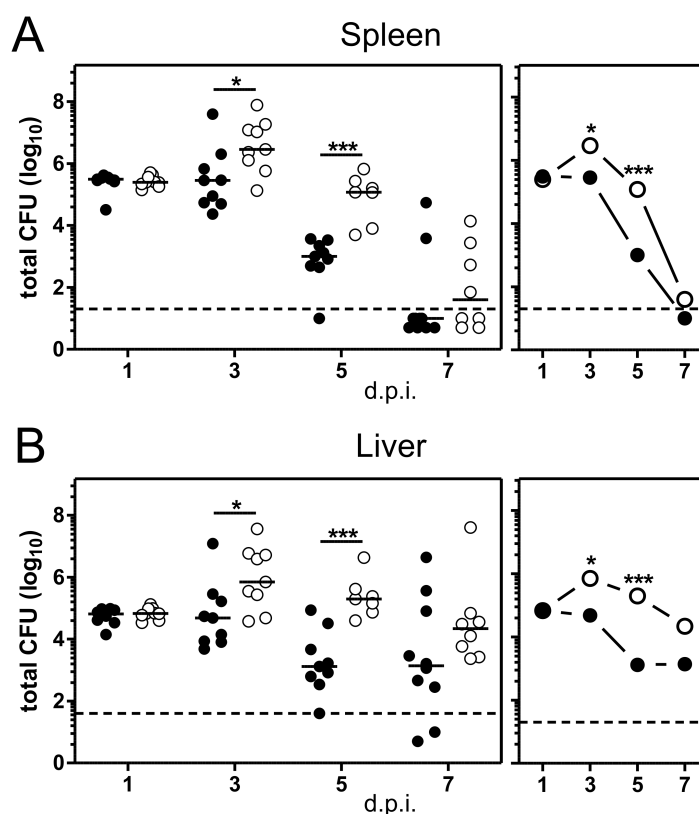
Figure 4.15: Bacterial burden after *L. monocytogenes* infection. Male wild type (■) and *Adap*$^{-/-}$ (□) mice were infected with approx. $2.5 \cdot 10^4$ CFU and after certain time points post infection sacrificed to determine the bacterial loads in their (A) spleens and (B) livers. The dashed line represents the limit of detection. The second graph of each panel shows the same data as the scatter plot, but is reduced to show only the medians in order to better demonstrate the kinetics of the bacterial burden in the respective organ. Statistical analysis was performed after $\log_{10}$-transformation using two-way ANOVA with Bonferroni's *post hoc* test. *Adap*$^{+/+}$, N = 9–10; *Adap*$^{-/-}$, N = 8. Data represented as medians. $^*p \leq 0.05$, $^{**}p \leq 0.01$, $^{***}p \leq 0.001$.

end male wild type and *Adap*$^{-/-}$ mice were infected with approx. $2.5 \cdot 10^4$ CFU and three days post infection the animals were sacrificed and their spleens and livers carefully excised. The organs were transferred to 4 % paraformaldehyde for fixation and sent to Dr. Oliva Kershaw at the Freie Universität Berlin, where histological sections were prepared. These were subjected to standard hematoxylin and eosin (H&E) staining and scored.

Histological examination revealed that compared to wild type animals, livers of *Adap*$^{-/-}$ mice showed more foci with leukocyte aggregates (Figure 4.16A) three days post infection. In spleens of wild type mice the white pulp — identifiable by the darker bluish staining — showed areas of necrotic lesions, but the basic structure of the white and red pulp was generally intact. In direct contrast, the base structure of spleens from *Adap*$^{-/-}$ animals was destroyed by vast areas of necrotic lesions (Figure 4.16B). Of note, the enlargement of the knock-out spleens following *Listeria* infection that was already indicated by the increased organ weight (Figure
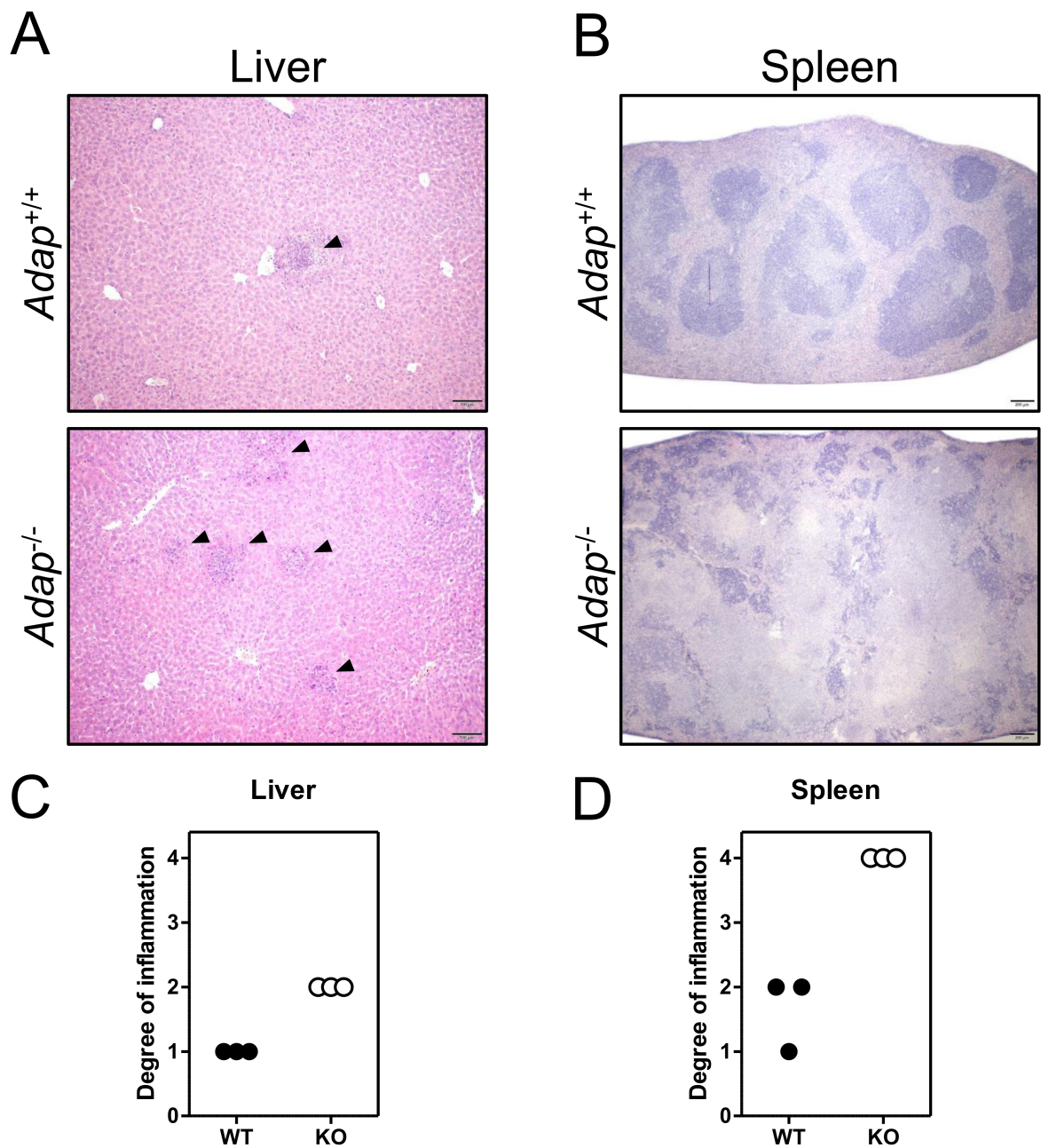
Figure 4.16: H&E histology of _L. monocytogenes_ infected livers and spleens 3 days post infection. Male wild type (■) and $Adap^{-/-}$ (□) mice were infected with approx. $2.5 \cdot 10^4$ CFU and three days post infection sacrificed to retrieve their spleens and livers. These organs were stored in 4 mL 4 % paraformaldehyde and later sectioned for histology and analyzed by H&E staining. The histological scoring was performed by Dr. Olivia Kershaw, a trained animal pathologist. (A) Liver histology revealed rare leukocyte aggregates (▲) in the livers of wild type animals, while knock-out mice showed more of these foci. (B) Spleens of wild type mice had some necrotic lesions in the white pulp area — recognizable by the bluish color — however, spleens of $Adap^{-/-}$ mice showed immensely large necrotic areas that actually destroyed the basic structure (defined areas of white and red pulp). The black bar at the bottom right corner of each panel represents a distance of 100 µm for the liver sections and 200 µm for the spleen sections. Scoring of (C) livers and (D) spleens revealed a higher degree of inflammation in $Adap^{-/-}$ mice organs; especially in the spleen.

4.14B) became also visible in the sections. Furthermore scoring for the degree of inflammation revealed clearly higher scores for the knock-out animals in both organs; however the difference between wild type and $Adap^{-/-}$ was most pronounced in the spleens (Figure 4.16C and D for liver and spleen, respectively). Together these findings indicate not only severe spleen pathology in $Adap^{-/-}$ mice very early during the course of the infection, but also increased leukocyte infiltration and/or proliferation in the liver as indicated by the higher number of leukocyte foci.

4.3.5 Leukocyte infiltration and cytokine production

The higher numbers of leukocytes in the livers of $Adap^{-/-}$ mice after *L. monocytogenes* infection — as indicated by histology — was of interest and was further investigated. For this, leukocytes from spleens and livers were isolated and their absolute numbers were determined at various time points after the infection. As expected, the absolute number of leukocytes increased in spleen — approx. twofold — during the course of the infection and reached its maximum between day 5 to day 7. There were no significant differences detectable between wild type and $Adap^{-/-}$ animals at any given time point, although there was a tendency at day seven post infection for more leukocytes in $Adap^{-/-}$ spleens. However, the picture was quite different in the liver. The number of leukocytes found in the liver also increased from negligible to quite high numbers during the course of the infection. Of note, on day 5 post infection the leukocyte numbers in livers of $Adap^{-/-}$ mice significantly exceeded the numbers found in their wild type littermates. Even more interesting, while on day 7 post infection the leukocyte numbers in wild type livers already decreased substantially, the number of leukocytes still increased in the livers of $Adap^{-/-}$ mice (Figure 4.17A). Table A.14 summarizing the data collected during these experiments can be found in appendix A.2.13.

Measurement of serum levels of *alanine transaminase* (ALT) is a standard clinical biomarker used to assess liver inflammation. In C57BL/6J mice, levels higher than 30 international units per liter (IU · L^{-1}) are considered elevated and indicative of liver damage [276]. 3 days post infection cardiac blood of *Listeria*-infected wild type and $Adap^{-/-}$ mice was collected and the ALT levels in the serum were determined. As expected, infected wild type animals had elevated levels of 82.72 ± 10.34 IU · L^{-1} (mean $\pm$ SEM). Of note, $Adap^{-/-}$ mice exhibited much higher serum ALT levels of 253.8 ± 78.40 IU · L^{-1} (mean $\pm$ SEM). Although the difference between the two groups did not reach statistical significance ($p = 0.0625$), the increased serum ALT levels in $Adap^{-/-}$ mice compared to wild type control animals (Figure 4.17B) were indicative for a more severe liver damage following *Listeria* infection in these animals.

Next, serum cytokines were analyzed by cytometric bead arrays. In this setting the amounts of TNF-α, IL-6, IFN-γ, IL-12p70 and TGF-β were of special interest. Since not all mice
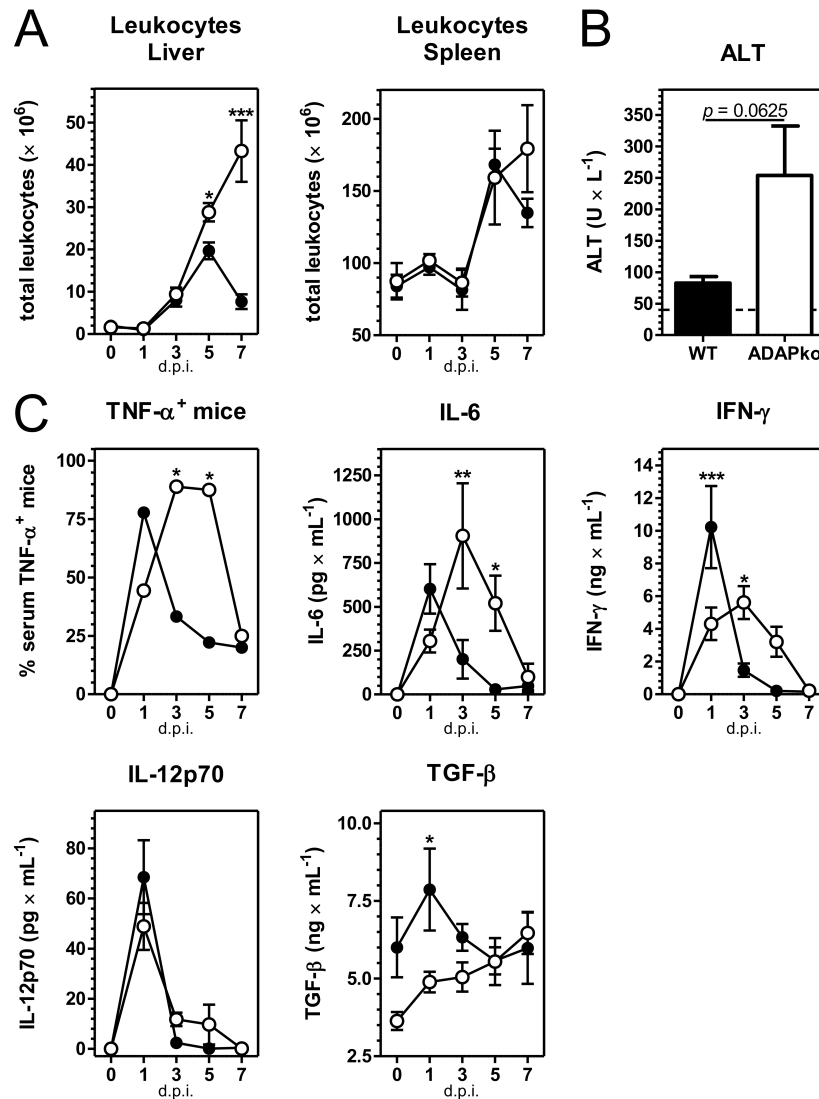
Figure 4.17: General response of wild type and $Adap^{-/-}$ mice to *L. monocytogenes* infection. Male wild type (■) and $Adap^{-/-}$ (□) mice were infected with approx. $2.5 \cdot 10^4$ CFU and sacrificed 1, 3, 5 and 7 days post infection (uninfected control mice served for time point 0) and general aspects of their immune response were analyzed. (A) Absolute leukocyte numbers in livers and spleens at the above mentioned time points were assessed by counting isolated cells in a hemocytometer. Especially at the latest time point significantly higher numbers of leukocytes were found in the livers of knock-out mice. (B) Serum ALT levels 3 days post infection were determined. The dashed line indicates the threshold of 30 $IU \cdot L^{-1}$. Levels higher than this are considered elevated and indicative of liver damage. $Adap^{-/-}$ mice showed greatly increased ALT levels after infection. (C) Serum cytokine concentrations of TNF-α, IL-6, IFN-γ and IL-12p70 were assessed by use of a cytometric bead array, while TGF-β levels were determined by ELISA. The data for TNF-α is depicted as the percentage of animals that were serum-positive for it at a given time point. In general, $Adap^{-/-}$ mice showed a delayed but sustained cytokine response compared to wild type mice. TGF-β levels were already reduced in uninfected knock-out mice and increased slowly during the course of the infection. Statistical analysis for absolute leukocyte numbers and serum levels of IL-6, IFN-γ, IL-12p70 and TGF-β was performed using two-way ANOVA with Bonferroni's *post hoc* test. Statistical analysis for ALT levels was performed using Student's unpaired two-tailed *t*-test. Analysis for the frequency of TGF-β serum-positive animals was performed using Fisher's exact test. All data (except for TGF-β) are represented as means ± SEM. N for (A), (B) and TGF-β is 5 per group. N for other cytokines is 8–9 per group. $*p \leq 0.05$, $**p \leq 0.01$, $***p \leq 0.001$.

responded with detectable serum levels of TNF-α, only the frequency of TNF-α serum-positive mice was determined. While TNF-α was not detectable in uninfected $Adap^{-/-}$ and wild type mice, more wild type mice were serum-positive for it than $Adap^{-/-}$ mice 1 day post infection. In direct contrast, almost all wild type animals were serum-negative for TNF-α by day 3 and 5 post infection, while almost 100 % of the $Adap^{-/-}$ mice were serum-positive. On day 7 post infection, no significant differences were detectable between the groups. The concentration of IL-6 in the sera of the animals showed a similar kinetic during the course of the infections. While the knock-out group initially showed a delayed IL-6 response compared to their wild type counterparts, their IL-6 response was more sustained. A similar picture was also seen for the serum concentrations of IFN-γ: initially lower in $Adap^{-/-}$ mice, but longer active. Interestingly, when the sera of the mice were analyzed for their amounts of the T_H1 signature cytokine IL-12p70, no differences were detectable between wild type and knock-out mice; both rose quickly on day 1 post infection and immediately decreased again. Analysis for TGF-β, on the other hand, showed that already uninfected $Adap^{-/-}$ mice had lower levels of this regulatory cytokine in their sera. While its concentration rose quickly following *Listeria* infection in the wild type animals, in knock-out mice it increased only very slowly (Figure 4.17B). Table A.15 containing the cytokine data can be found in appendix A.2.14.

Overall, this data shows that $Adap^{-/-}$ mice show massive infiltration of leukocytes into or proliferation of leukocytes in their livers, display higher immunopathology in this organ, and show a delayed but sustained cytokine production in response to a *L. monocytogenes* infection. These findings suggested having a closer look at the identity and number of the leukocyte populations present in the affected organs. Cells considered to be of interest were neutrophils, monocytes, CD8$^+$ T cells and NK cells. Also chemokines that are known to attract the cell types were of interest and were assessed in sera of infected animals.

4.3.6 Neutrophil and monocyte infiltrates

The absolute numbers of neutrophils and monocytes in livers and spleens during the course of the infection were determined following isolation of leukocytes from the organs (see section 3.1.5), staining of the cells with specific cell markers and subsequently analyzing their frequency by flow cytometry. On the basis of the as well determined absolute leukocyte cell numbers per organ the absolute neutrophil and monocyte numbers were calculated (see section 3.2.10). Neutrophil and monocyte numbers in spleens and livers of $Adap^{-/-}$ and wild type mice were assessed prior to infection and 1, 2, 3, 5 and 7 days post infection. Furthermore, the serum concentrations of the neutrophil attracting chemokine CXCL1 — also known as KC — and the monocyte attracting chemokine CCL2 — also known as MCP-1 — were assessed by cytometric bead array as described in section 3.2.11.
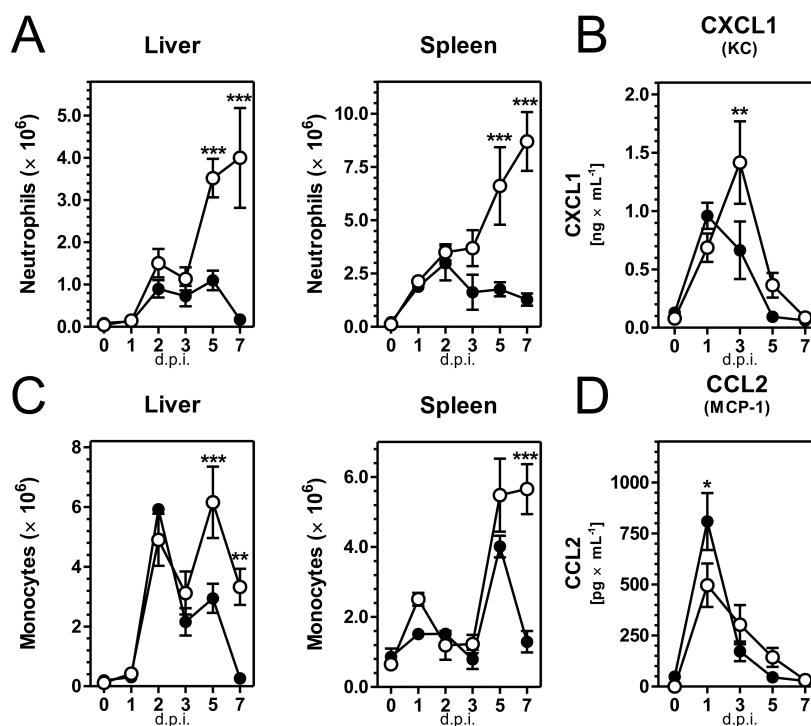
**Figure 4.18: Neutrophil and monocyte numbers in spleen and liver and their attracting chemokines in serum after *L. monocytogenes* infection.** Male wild type ($\blacksquare$) and $Adap^{-/-}$ ($\square$) mice were infected with approx. $2.5 \cdot 10^4$ CFU of *L. monocytogenes* and sacrificed after 1, 2, 3, 5, and 7 days post infection to harvest spleens and livers as well as take cardiac blood. Uninfected mice were used as day 0 controls. (A), (C) Leukocytes were isolated from liver and spleen, stained against cell markers for (A) neutrophils and (C) monocytes, and their frequencies determined by flow cytometry. From these frequencies the absolute numbers of the cells were calculated. While the early phase of the infection was comparable between wild type and $Adap^{-/-}$ mice, $Adap^{-/-}$ mice showed drastically increased neutrophil and monocyte numbers in both organs 5 and 7 days post infection. (B), (D) Cardiac blood was taken and serum samples were prepared. The concentrations of the neutrophil attracting chemokine CXCL1 (B) and the monocyte attracting chemokine CCL2 (D) were determined by cytometric bead array. CXCL1 was higher in knock-out mice 3 days post infection and tended to stay increased, while CCL2 was lower 1 day post infection. Statistical analysis was performed using two-way ANOVA with Bonferroni's *post hoc* test. N for cell numbers in (A) and (C) was 4–5. N for chemokine concentrations in (B) and (D) was 4 for uninfected and 8–9 for the infected time points. $*p \leq 0.05$, $**p \leq 0.01$, $***p \leq 0.001$.

In the livers of wild type animals neutrophil numbers rose quickly to $8.976 \pm 2.067 \cdot 10^5$ (mean $\pm$ SEM) on day 2 post infection, and remained stable until day 5, after which it almost decreased to pre-infection levels. The picture was quite different for the $Adap^{-/-}$ animals. After day 3 post infection the number of neutrophils in the livers increased more than 20-fold, reaching $4.000 \pm 1.180 \cdot 10^6$ cells compared to $1.726 \pm 0.2587 \cdot 10^5$ in wild type mice. Similar results were obtained for neutrophil numbers in the spleen. While in wild type animals the numbers for this cell type reached its peak 1 day post infection with $2.980 \pm 0.8027 \cdot 10^6$ followed by a steadily decline of neutrophil numbers during the further course of the infection, neutrophil numbers in the spleens of $Adap^{-/-}$ animals dramatically increased beyond this point, reaching $8.700 \pm 1.376 \cdot 10^6$ on day 7 post infection, compared to $1.278 \pm 0.284 \cdot 10^6$

in wild type animals. Figure 4.18A shows the neutrophil number kinetics during the course of the infections. In concordance with neutrophil numbers, the serum concentration of the neutrophil attracting chemokine CXCL1 was similar in wild type and $Adap^{-/-}$ mice until day 1 post infection. However, the concentration in the $Adap^{-/-}$ mice was significantly higher at day 3 post infection, with 1415 ± 353.3 pg $\cdot$ mL^{-1} compared to 663.5 ± 247.3 pg $\cdot$ mL^{-1} in wild type animals. Even though the serum concentration of the chemokine declined in both animals beyond this time point, it tended to stay higher in the knock-out mice (Figure 4.18B).

Monocyte dynamics showed a more complex pattern during the course of the infection. Irrespective of the genotype the monocyte number in the liver reached a first peak at day 2 post infection. In both, wild type and $Adap^{-/-}$ mice, the monocyte number had decreased on day 3 — with no significant differences — and increased again on day 5, but this time to a much higher extent in the $Adap^{-/-}$ mice ($Adap^{+/+}$: $2.942 \pm 0.4900 \cdot 10^6$; $Adap^{-/-}$: $6.155 \pm 1.196 \cdot 10^6$). The monocyte numbers in the liver decreased again on day 7 post infection but remained more than 10-fold higher in the knock-out mice compared to wild type control animals ($Adap^{+/+}$: $2.620 \pm 0.4674 \cdot 10^5$; $Adap^{-/-}$: $3.325 \pm 0.6046 \cdot 10^6$). In the spleens of the animals the monocyte numbers remained largely constant early after infection before they rapidly increased on day 5, irrespective of the ADAP genotype. Strikingly, while the cell numbers drastically decreased on day 7 in wild type animals, it remained high in the spleens of $Adap^{-/-}$ mice ($Adap^{+/+}$: $1.292 \pm 0.3049 \cdot 10^6$; $Adap^{-/-}$: $5.655 \pm 0.7154 \cdot 10^6$). The kinetics of monocyte numbers in spleens and livers are graphically depicted in Figure 4.18C. Cytometric bead array analysis revealed that the serum concentration of monocyte attracting chemokine CCL2 increased quickly, reaching its peak on day 1 post infection. Interestingly, at that time point the $Adap^{-/-}$ mice exhibited significantly lower CCL2 levels in the serum ($Adap^{+/+}$: 808.7 ± 139.4 pg $\cdot$ mL^{-1}; $Adap^{-/-}$: 496.5 ± 106.6 pg $\cdot$ mL^{-1}). However, CCL2 serum concentration tended to remain higher in the rest of the analyzed time points (Figure 4.18D). Table A.16 in appendix A.2.15 summarizes the cell number data for neutrophils and monocytes and Table A.17 in appendix A.2.16 shows the data for CXCL1 and CCL2.

Together, these finding show that during the later phase of the infection (days 5 and 7) massive numbers of neutrophils and monocytes migrate into the livers and spleens of $Adap^{-/-}$ mice, while at this time their numbers had already decreased substantially in their wild type littermates. The serum concentrations of neutrophil and monocyte attracting chemokines were lower in the $Adap^{-/-}$ mice at early time points but remained elevated during the later course of the infection.

4.3.7 CD8$^+$ T cells in wild type and *Adap*$^{-/-}$ mice

Another cell subset of interest during an infection with *Listeria* is CD8$^+$ T cells. As described already above, male wild type and *Adap*$^{-/-}$ mice were infected with approx. $2.5 \cdot 10^4$ CFU and sacrificed after 3, 5 or 7 days post infection. Uninfected mice served as controls for day 0. Spleens and livers of the mice were harvested and the leukocytes were isolated. These cells were subjected to fluorescent staining for flow cytometry in order to identify CD8$^+$ T cells and subsequently analyze activation and functional markers. Furthermore, cardiac blood was collected followed by serum preparation to be analyzed for chemokines as described above.

When spleens and livers of wild type and *Adap*$^{-/-}$ mice were analyzed for the absolute numbers of CD8$^+$ T cells that were present there during the course of the infection, spleens showed an initial decrease in the CD8$^+$ T cell numbers on 3 days post infection. However, starting on day 5 the numbers strongly increased and outnumbered the CD8$^+$ T cells present in the organ prior to the infection. However, significant differences between genotypes were not detectable. Quite the opposite was found in the liver of the infected mice. While CD8$^+$ T cells numbers increased in both genotypes 5 days post infection, a considerably and significantly higher number (more than 3-fold) of these cells were found in the livers of *Adap*$^{-/-}$ mice on day 7 post infection (*Adap*$^{+/+}$: $2.872 \pm 0.8170 \cdot 10^6$; *Adap*$^{-/-}$: $10.855 \pm 1.434 \cdot 10^6$; Figure 4.19A). Table A.18 in appendix A.2.17 summarizes the data obtained in these experiments.

Analysis of the serum concentrations of two T$_H$1 signature chemokines, CXCL10 (IP-10) and CXCL9 (MIG), revealed similar kinetics as observed before. The early CXCL10 response (day 1 post infection) was clearly weaker in *Adap*$^{-/-}$ mice (*Adap*$^{+/+}$: 1654 ± 231.5 pg $\cdot$ mL^{-1}; *Adap*$^{-/-}$: 998.9 ± 180.1 pg $\cdot$ mL^{-1}) and the same was true for CXCL9 (*Adap*$^{+/+}$: 440.3 ± 73.29 pg $\cdot$ mL^{-1}; *Adap*$^{-/-}$: 191.9 ± 49.91 pg $\cdot$ mL^{-1}). However, at later time points post infection the chemokine responses tended to be stronger in *Adap*$^{-/-}$ than in the wild type mice (Figure 4.19B). This emphasizes the delayed but sustained cytokine response in ADAP-deficient mice visible already in the earlier described analyses. Data obtained for the chemokine levels are summarized in Table A.19 in appendix A.2.18.

CD8$^+$ T cells were further characterized regarding their activation status by staining for selected activation and functional markers. As described earlier, CD69 is an activation marker that is rapidly upregulated in response to TCR engagement (see section 1.1.8). The number of activated (CD69$^+$) CD8$^+$ T cells rose during the course of the infection in spleens and livers, irrespective of the ADAP genotype. Strikingly, while the number of activated CD8$^+$ T cells reached a plateau in the livers of wild type animals on day 5 post infection, their numbers were further increased in *Adap*$^{-/-}$ mice on day 7 (*Adap*$^{+/+}$: $0.890 \pm 0.2210 \cdot 10^6$; *Adap*$^{-/-}$: $1.481 \pm 0.2769 \cdot 10^6$). In contrast, wild type animals exhibited higher numbers of activated CD8$^+$ T cells in their spleens at this late time point (*Adap*$^{+/+}$: $10.93 \pm 0.8450 \cdot 10^6$; *Adap*$^{-/-}$:
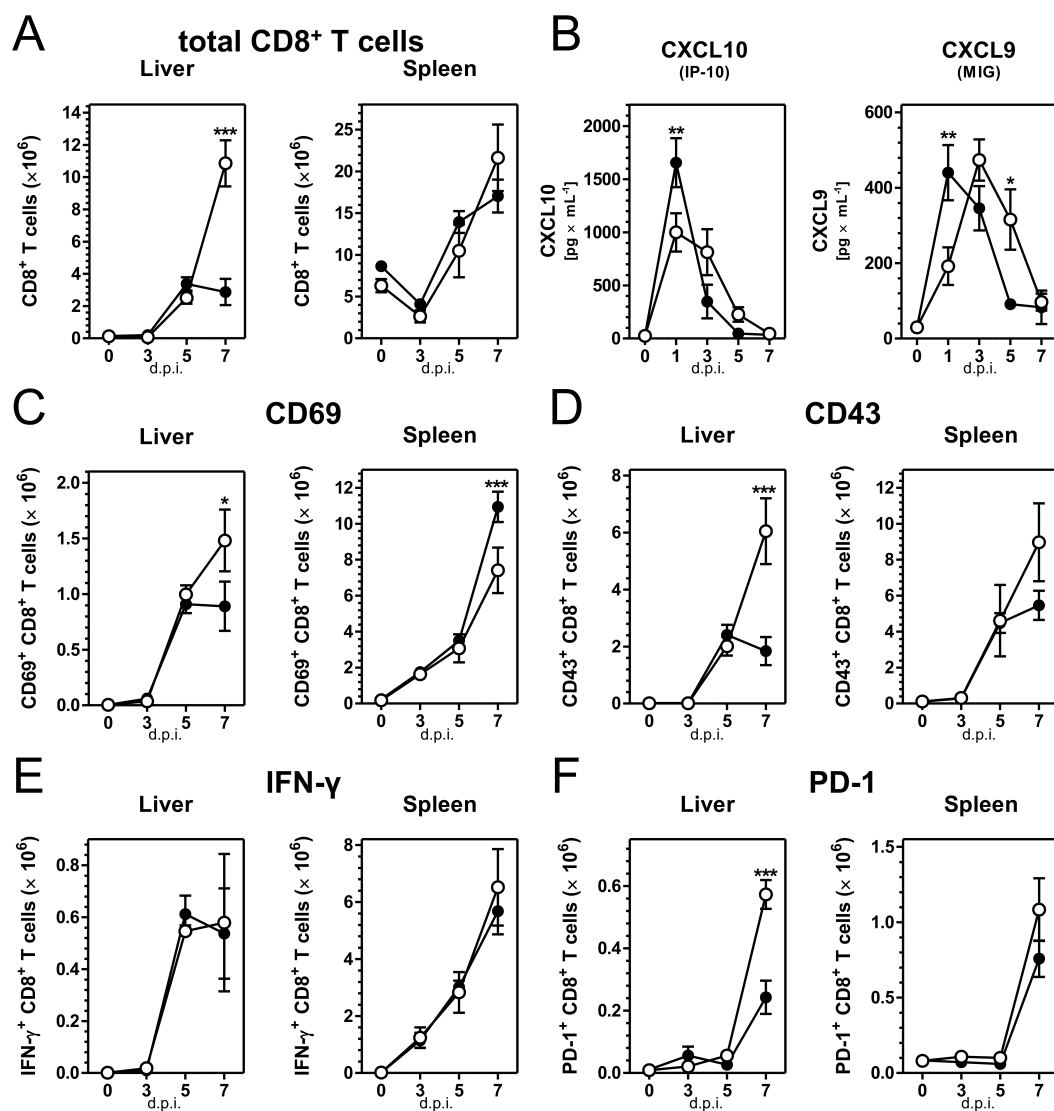
Figure 4.19: CD8$^+$ T cells during *L. monocytogenes* infection. Male wild type (■) and *Adap$^{-/-}$* (□) mice were infected with approx. $2.5 \cdot 10^4$ CFU and sacrificed after 3, 5 or 7 days to retrieve livers, spleens and cardiac blood. Uninfected mice served as controls for day 0. (A) Leukocytes from the organs of interest were isolated and stained for identification of CD8$^+$ T cells and from the flow cytometrically determined frequencies absolute cell numbers were calculated. While CD8$^+$ T cell numbers in spleens rose in both genotypes over the course of the infection, livers of *Adap$^{-/-}$* mice showed massive numbers of these cells 7 days post infection. (B) Cytometric bead array analysis revealed the same chemokine kinetics as described earlier; namely a delayed but sustained response in the *Adap$^{-/-}$* animals. The CD8$^+$ T cell compartment was further analyzed for the number of (C) CD69, (D) CD43, (E) IFN-γ and (F) PD-1 expressing cells. More CD69$^+$CD8$^+$ T cells were found in livers of *Adap$^{-/-}$* mice, while the contrary was observed in the spleens of the animals. Livers and spleens showed more cells positive for the memory marker CD43. No differences, irrespective of the organ, were detectable when analyzed for IFN-γ. More PD-1 expressing cells were found in livers, and by trend, also in the spleens. Statistical analysis was performed using two-way ANOVA with Bonferroni's *post hoc* test. N for (A), (C), (D), (E) and (F) was 4–5. N for chemokine concentrations in (B) was 4 for uninfected and 8–9 for the infected time points. *$p \leq 0.05$, **$p \leq 0.01$, ***$p \leq 0.001$.

$7.412 \pm 1.268 \cdot 10^6$) (Figure 4.19C). The data collected from this experiment are summarized in Table A.20 in appendix A.2.19.

CD43 is commonly used as a marker to evaluate the size of the effector CD8$^+$ T cell population. As expected, numbers of CD43$^+$CD8$^+$ effector T cells increased during the course of the infection in spleens and livers of wild type and $Adap^{-/-}$ mice. The kinetic followed a similar pattern as observed before for CD69$^+$ CD8$^+$ T cells, and their numbers reached a plateau in the livers of wild type animals on day 5 post infection. Moreover, as seen for the activation marker CD69, the number of CD43$^+$ effector CD8$^+$ T cells was further increased in $Adap^{-/-}$ mice on day 7 post infection ($Adap^{+/+}$: $1.842 \pm 0.4931 \cdot 10^6$; $Adap^{-/-}$: $6.046 \pm 1.152 \cdot 10^6$). However, the CD43$^+$CD8$^+$ T cell numbers at this time point were also higher in the spleen of $Adap^{-/-}$ mice ($Adap^{+/+}$: $5.460 \pm 0.8099 \cdot 10^6$; $Adap^{-/-}$: $8.972 \pm 2.164 \cdot 10^6$), although not reaching significance (Figure 4.19D). Table A.21 in appendix A.2.20 summarizes the determined cell numbers.

Since the expression of the cytokine IFN-γ is a hallmark of effector CD8$^+$ T cells, the number of cells that express it during *Listeria* infection was assessed in livers and spleens of wild type and $Adap^{-/-}$ mice. Although the absolute number of CD8$^+$ T cells in livers of $Adap^{-/-}$ animals was much greater than in wild type control mice (Figure 4.19A) and moreover, also the number of activated and functionally active cells was found to be higher (Figure 4.19C and D) in this particular organ in $Adap^{-/-}$ mice, no differences in the absolute numbers of IFN-γ^+CD8$^+$ T cells were detectable between the genoptypes. The same was true for the spleens of the animals (Figure 4.19E). Interestingly, in contrast to absolute cell numbers the frequency of IFN-γ-producing CD8$^+$ T cells was significantly higher at day 3 in the spleens — and by trend also in the livers — of the $Adap^{-/-}$ animals, while on day 7 post infection the frequency of these cells was lower in the livers of $Adap^{-/-}$ mice (data not shown). IFN-γ-producing CD8$^+$ T cell numbers are summarized in Table A.22 in appendix A.2.21.

The T cell exhaustion marker PD-1 (briefly discussed in section 1.1.7) usually becomes upregulated on T cells during an infection in order to calm down effector cells and to prevent exaggerated immune responses. PD-1 upregulation usually happens in the later phase of the immune response. To clarify whether this regulatory process would be affected in $Adap^{-/-}$ mice, the number of PD-1$^+$ CD8$^+$ T cells was assessed by flow cytometry. As expected, in livers and in spleens the numbers of PD-1 expressing CD8$^+$ T cells remained rather low up to day 5 post infection. On day 7 post infection thes numbers considerably increased in the livers of the animals, but to a much greater extent in the $Adap^{-/-}$ mice ($Adap^{+/+}$: $0.2428 \pm 0.05338 \cdot 10^6$; $Adap^{-/-}$: $0.5728 \pm 0.04608 \cdot 10^6$). By trend, this effect was also observed in the spleens (Figure 4.19F). Table A.23 summarizing the PD-1$^+$CD8$^+$ T cell numbers can be found in appendix A.2.22.

Taken together, this data show that especially during the later phase of the infection, more

CD8$^+$ T cells are found in the spleens and livers of $Adap^{-/-}$ mice. Furthermore, a more detailed analysis based on assessing CD69 and CD43 expression revealed elevated numbers of activated/effector CD8$^+$ T cells present in *Listeria* infected organs of $Adap^{-/-}$ mice. Moreover, CD8$^+$ T cells in the infected $Adap^{-/-}$ animals were more prone to exhaustion as indicated by elevated numbers of PD-1 expressing CD8$^+$ T cells. Interestingly, the number of CD8$^+$ T cells producing the hallmark effector cytokine IFN-γ was not affected by ADAP deficiency, at least on the basis of assessing absolute IFN-γ^+CD8$^+$ T cell numbers.

4.3.8 NK cells during the course of the infection

As discussed in the introduction, NK cells play multifaceted roles in the early immune response against *L. monocytogenes*. To elucidate the effects of ADAP deficiency on NK cell-mediated immunity, NK cell numbers as well as their activation and maturation phenotypes were characterized by flow cytometric analysis (see section 3.2.10) in spleens and livers at selected time points after the infection with the intracellular pathogen.

The absolute numbers of NK cells in the liver increased during the course of the infection until day 5 before it decreased again by day 7. Differences between wild type and $Adap^{-/-}$ mice were only detectable at day 5 post infection, where wild type animals exhibited significantly more NK cells in their livers ($Adap^{+/+}$: $1.910 \pm 0.3132 \cdot 10^6$; $Adap^{-/-}$: $1.214 \pm 0.1507 \cdot 10^6$). Splenic NK cell numbers decreased drastically on day 2 and recovered on day 5 post infection. The general kinetic was similar for wild type and $Adap^{-/-}$ mice. However, $Adap^{-/-}$ mice already displayed lower NK cell numbers in the spleens in the steady state, i.e. in the absence of infection. Moreover, their recovery in terms of absolute cell numbers at the later phase of the infection was far less pronounced than in wild type control mice(Figure 4.20A). Taken together, this suggests that NK cell numbers are decreased in spleens and liver of $Adap^{-/-}$ mice at certain time points during a *Listeria* infection. For data collected in these experiments refer to Table A.24 in appendix A.2.23.

CD69 is not only an excellent activation marker for CD8$^+$ T cells, but also serves this purpose for the analysis of NK cells. When liver NK cells were analyzed for their CD69 expression, an increased frequency of CD69$^+$ NK cells was detectable until day 1 post infection in wild type mice, while in $Adap^{-/-}$ mice it even further increased until day 3 post infection, where also a significant difference was observed ($Adap^{+/+}$: 21.47 ± 4.576 %; $Adap^{-/-}$: 51.59 ± 5.112 %). A similar kinetic for CD69 expression was found in the spleens of the animals. The frequency of CD69$^+$ NK cells increased massively until day 2 post infection. While the frequency decreased again in wild type spleens at day 3 post infection, it remained elevated in $Adap^{-/-}$ mice ($Adap^{+/+}$: 23.15 ± 3.059 %; $Adap^{-/-}$: 53.38 ± 5.901 %) where it did not decrease until day 5 post infection (Figure 4.20B). These findings suggest that NK cell activation during Listeria
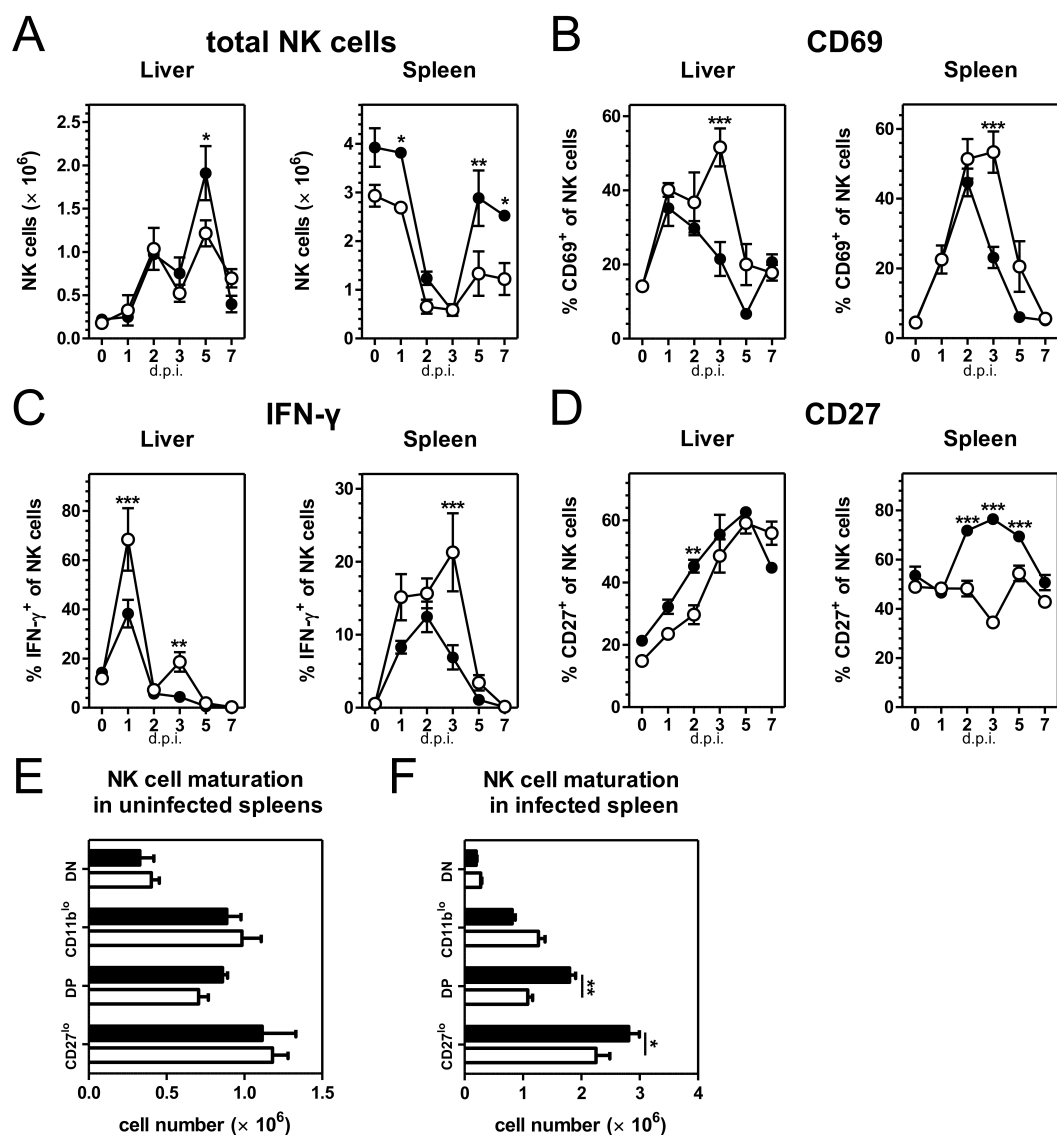
Figure 4.20: NK cells during *L. monocytogenes* infection. Male wild type (■) and $Adap^{-/-}$ (□) mice were infected with approx. $2.5 \cdot 10^4$ CFU and sacrificed after 1, 2, 3, 5 or 7 days to retrieve livers and spleens. Uninfected mice served as controls for day 0. Leukocytes were isolated from the retrieved organs and stained with αNKp46 to identify NK cells. Furthermore the cells were stained for maturation and activation markers. (A) NK cell absolute numbers in the analyzed organs were calculated from the frequencies assessed by flow cytometry with the absolute leukocyte numbers. Liver NK cells numbers were higher on day 5 post infection in $Adap^{+/+}$ mice, while splenic NK cell numbers were higher in wild types at the start and end of the infection. (B) The frequency of CD69$^+$ NK cells, a hallmark of activation, increased quickly during the early phase of the infection in the livers and spleens, but $Adap^{-/-}$ mice showed a prolonged response. (C) IFN-γ$^+$ NK cell frequency increased massively on day 1 in livers, but to a much greater extent in the $Adap^{-/-}$ mice. A similar response was observed in the spleens, however, it was more sustained. (D) CD27 expression positively correlates with effector function of NK cells and the frequency of CD27$^+$ NK cells increased in livers of both genotypes, but to a slightly greater extent in the wild type mice. In spleens only wild type mice responded with an increase in the frequency of CD25$^+$ NK cells. (E) and (F) show absolute numbers of different maturation stages of NK cells in the spleens prior to and 1 day after the infection respectively. While no differences were observed before the animals were infected, after infection knock-out mice had less DP and CD27^{lo}. Statistical analysis was performed using two-way ANOVA with Bonferroni's *post hoc* test. N for (A), was 4–5. N for (B), (C), and (D) was 5–8 ($Adap^{+/+}$) and 4–7 ($Adap^{-/-}$). N for (E) and (F) was 5. $*p \le 0.05$, $**p \le 0.01$, $***p \le 0.001$.

infectionis more sustained in $Adap^{-/-}$ mice. A summary of the CD69$^+$ NK cell frequencies can be found in Table A.25 in appendix A.2.24.

As discussed earlier, NK cells are the primary source for IFN-γ during the early phase of the infection. In order to analyze the effects of ADAP deficiency on IFN-γ production by NK cells in livers and spleens during the course of a *Listeria* infection, the frequency of IFN-γ^+ NK cells was determined. Already 1 day post infection a considerable portion of NK cells in the liver was expressing IFN-γ. Interestingly, the frequency of IFN-γ^+ NK cells was significantly higher in the $Adap^{-/-}$ mice ($Adap^{+/+}$: 38.28 $\pm$ 5.612 %; $Adap^{-/-}$: 68.42 $\pm$ 12.67 %). In wild type mice the number of IFN-γ producing cells had already decreased to pre-infection levels on day 2 post infection and remained low in the following. However, $Adap^{-/-}$ animals displayed a second significant increase in IFN-γ^+ NK cells on day 3 post infection ($Adap^{+/+}$: 4.426 $\pm$ 1.280 %; $Adap^{-/-}$: 18.66 $\pm$ 3.964 %), although to a much lesser extent than the preceding one. Regarding the splenic NK cells, the activation response was more prolonged reaching its peak in wild type animals on day 2 post infection. $Adap^{-/-}$ mice again showed a more sustained response, reaching the peak of IFN-γ^+ NK cells on 3 days post infection. Here the difference in numbers of IFN-γ^+ NK cells between $Adap^{-/-}$ and wild type mice also reached significance ($Adap^{+/+}$: 6.896 $\pm$ 1.661 %; $Adap^{-/-}$: 21.29 $\pm$ 5.344 %). Thus, the prolonged activation — as indicated by CD69 expression — is also reflected in the more sustained production of IFN-γ by NK cells in ADAP-deficient mice (Figure 4.20C). Table A.26 summarizing the data collected in this set of experiments is located in appendix A.2.25.

Since the expression of CD27 on NK cells correlates with effector function, analysis for this parameter was performed on splenic and hepatic NK cells during the infection. In livers, both wild type and $Adap^{-/-}$ mice displayed an increase in the frequency of CD27$^+$ NK cells during the infection. However, in $Adap^{-/-}$ animals the CD27$^+$ NK cell frequency increase appeared to be delayed. In the spleens of wild type animals the frequency rose from day 2 to day 5 post infection, but returned to pre-infection levels on day 7. Surprisingly, NK cells from $Adap^{-/-}$ mice completely failed to up-regulate CD27 (Figure 4.20D), a finding that directly contradicts the elevated IFN-γ^+ NK cell frequency in *Listeria* infected ADAP-deficient mice that was detected before (Figure 4.20C). Table A.27 summarizing the relevant date from this experiment can be found in appendix A.2.26.

In addition to serving as an NK cell activation marker, CD27 is also used as a marker to analyze the maturation of NK cells. In combination with CD11b four distinct maturation stages of NK cells can be identified according to Chiossone, et *al.* [277]: (i) CD11b^{lo}CD27^{lo} (double negative; DN) NK cells represent the initial state of the maturation process, (ii) CD11b^{lo}CD27^{hi} (CD11b^{lo}) also represent an immature state that is followed by (iii) CD11b^{hi}CD27^{hi} (double positive; DP) NK cells that exhibit the strongest effector function, and (iv) CD11b^{hi}CD27^{lo} (CD27^{lo}) NK cells represent the end stage of NK cell maturation and are prone to apoptosis.

In order to analyze the maturation of the NK cells during a *Listeria* infection in wild type and $Adap^{-/-}$ mice the cells were analyzed for their CD11b and CD27 expression profile on day 1 post infection. First, the maturation status in the spleen was assessed in the steady-state prior to the infection. This revealed no significant differences between the genotypes (Figure 4.20E). One day after the infection this picture changed. While the number of DP NK cells approx. doubled in wild type spleens, it only slightly increased in the $Adap^{-/-}$ mice ($Adap^{+/+}$: $1.800 \pm 0.103 \cdot 10^6$; $Adap^{-/-}$: $1.080 \pm 0.085 \cdot 10^6$). Moreover, the number of CD27^{lo} NK cells increased to a larger extent in the spleens of the wild type than in the $Adap^{-/-}$ mice ($Adap^{+/+}$: $2.812 \pm 0.184 \cdot 10^6$; $Adap^{-/-}$: $2.250 \pm 0.239 \cdot 10^6$) (Figure 4.20F). The absolute cell numbers assessed for the maturation analysis are summarized in Table A.28 in appendix A.2.27.

Taken together, upon *Listeria* infection more of the NK cells in $Adap^{-/-}$ mice appear to be activated and are producing IFN-γ, but strikingly, they fail to upregulate CD27 expression (especially in the spleen). Moreover, NK cell maturation seems to be impaired in ADAP-deficient mice as indicated by reduced numbers of DP and CD27^{lo} NK cells in the spleens of $Adap^{-/-}$ mice 1 day post *Listeria* infection.

5

Discussion

The data compiled in the frame of this thesis and described in the previous chapter show interesting roles for the adaptor protein and will be discussed in the following sections according to the aims that were set at the beginning:

Aim 1 Identifying potential differences between $CD4^+$ and $CD8^+$ T cells in terms of their dependency on ADAP for their activation and function.

Aim 2 Deciphering the role of ADAP in pathogen-specific immunity during an infection with *L. monocytogenes*.

5.1 The Adaptor Protein ADAP plays a pivotal role in $CD4^+$ T cell activation but is largely dispensable for $CD8^+$ T cell function

A lot of data has been compiled in recent years and ADAPs importance in T cell signaling is well established. Also, the role of ADAP in the development, selection and resulting cellularity of $CD4^+$ and $CD8^+$ T cells in the periphery has been extensively studied. Interestingly though, most studies did not distinguish between $CD4^+$ and $CD8^+$ T cells when analyzing functional aspects. Therefore, the first part of the thesis focused on deciphering the role of ADAP in T cell activation and function in a subset specific manner.

5.1.1 *In vitro* evidence for differential significance of on ADAP in CD4$^+$ and CD8$^+$ T cells

When the impact of ADAP deficiency on the response of the different T cell subsets to TCR stimulation was analyzed, the results were unexpected. Previous studies performed on the entire polyclonal CD4$^+$ and CD8$^+$ T cell population revealed that TCR-induced activation strongly relies on the presence of ADAP [23, 22]. However, these analyses did not distinguish between different T cell subsets and thereby obviously blanked that predominantly *Adap*$^{-/-}$ CD4$^+$ T cells show impaired response to *in vitro* TCR activation while *Adap*$^{-/-}$ CD8$^+$ T cell responses remain largely normal in these settings (Figure 4.6A-D). The only exception observed in this study was the upregulation of the early activation marker CD69, which was also affected by loss of ADAP in CD8$^+$ T cells. However, CD62L shedding, CD25 upregulation and proliferation of CD8$^+$ T cells were not significantly affected by ADAP deficiency.

It has been reported that adhesion of *Adap*$^{-/-}$ T cells to ICAM-1 is reduced when the cells were either stimulated via the TCR or the chemokine receptors CCR7 and CXCR4 [272, 37, 271]. When binding to ICAM-1 was analyzed in the CD4$^+$ vs. CD8$^+$ T cell subset, TCR-activated (αCD3ϵ) *Adap*$^{-/-}$ CD4$^+$ T cells showed markedly reduced adhesion, while their CD8$^+$ counterparts were indistinguishable from the wild type controls. This further emphasizes that CD8$^+$ T cell function is less dependent on ADAP. Interestingly, when stimulated via either CCR7 or CXCR4, loss of ADAP markedly decreased adhesion to ICAM-1 of both T cells subsets (Figure 4.7A and B).

Differences in signaling, activation and adhesion of CD4$^+$ and CD8$^+$ T cells have been attributed before to the overall lower expression level of CD3 on CD8$^+$ T cells [270, 268, 269]. Assays performed in the frame of this thesis revealed that CD8$^+$ T cells expressed lower amounts of CD3 on their surfaces when compared to their CD4$^+$ counterparts. Interestingly, *Adap*$^{-/-}$ T cells, independent of their subtype, expressed slightly less CD3 compared to the wild type control cells (Fig. 1C). Nevertheless, these findings cannot explain the differential dependence of the T cell subsets on ADAP.

The most plausible explanation for the observed T cell subset specific differences might be based on their differential dynamics of antigen recognition [278, 279, 280]. While CD4$^+$ T cells require sustained TCR signaling for optimal activation and progression to effector function [281, 282, 283], their CD8$^+$ counterparts only require a brief encounter with cognate antigen, basically putting them into a self-reliant autopilot mode [284, 285, 286, 287]. The data presented here provide evidence that ADAP is important for mediating these sustained and strong TCR signals, required for proper CD4$^+$ T cell activation and function. Moreover, irrespective of the T cell subtype ADAP seems to be a crucial part in the downstream signaling of chemokine receptors leading to integrin activation.

In order to minimize potential effects resulting from the polyclonal nature of the T cell pool, the results obtained in the activation experiments were reproduced using the OT-I and OT-II TCR-transgenic model. While $Adap^{-/-}$ OT-I TCR-transgenic mice produced sufficient numbers of $CD8^+$ T cells (comparable to their wild type counterparts), $Adap^{-/-}$ OT-II TCR-transgenic mice unfortunately produced extremely low numbers of $CD4^+$ T cells (Figure 4.3A), which made the model not feasible for further experiments. However, this also highlights the importance of ADAP in the selection process of T cells, as already shown in other TCR-transgenic models, such as H-Y and AND [11, 65], emphasizing ADAPs distinct importance for $CD4^+$ T cells. Mueller, et al. [69] on the other hand generated $Adap^{-/-}$ DO11.10 mice ($CD4^+$ T cell model) and were able to conduct experiments. The DO11.10 TCR recognizes the same peptide ($OVA_{323-339}$) as the OT-II receptor, even though the animals differ in their genetic background (BALB/c and C57BL/6 respectively) [288, 289]. A possible explanation for the finding that $Adap^{-/-}$ DO11.10 animals produced sufficient numbers of $CD4^+$ T cells might be the approximately 1000-fold higher affinity (100 nmol $\cdot$ L^{-1} vs. 100 µmol $\cdot$ L^{-1}) of the respective TCR, that seems to compensate for the lack of ADAP [290].

When OT-I TCR-transgenic $CD8^+$ T cells were activated *in vitro* with the cognate peptide $OVA_{257-264}$, less of the ADAP-deficient $CD8^+$ T cells compared to their ADAP-sufficient counterparts responded to activation with CD25 upregulation. However, this difference became evident only at minute amounts of antigen (< 100 pg $\cdot$ mL^{-1}). All other tested parameters (CD62L, CD69 and proliferation) were not dependent on ADAP in $CD8^+$ T cells, since there were no significant differences detectable in the absence of the adapter molecule (Figure 4.8A-D). Interestingly, in the aforementioned $CD4^+$ DO11.10 model, CD25 and CD69 expression, as well as proliferation, were markedly decreased in $Adap^{-/-}$ $CD4^+$ T cells, especially at lower antigen concentrations [69].

5.1.2 *In vivo* data on the role of ADAP in $CD8^+$ T cells

Extending the investigation to an *in vivo* adoptive transfer model using the intracellular pathogen *L. monocytogenes* as a carrier for ovalbumin (LmOVA; including the OT-I peptide), *in vitro* findings were further confirmed. Fewer $Adap^{-/-}$ OT-I TCR-transgenic $CD8^+$ T cells expressed CD25 following *in vivo* antigen encounter, while all other analyzed markers showed little to no difference between $Adap^{-/-}$ and wild type T cells (Figure 4.9A-D). Interestingly, although $Adap^{-/-}$ $CD8^+$ T cells showed a slight impairment in their early proliferative response, this was compensated at later post *in vivo* antigen encounter where their actual number exceeded that of their wild type counterparts (Figure 4.9D). The initially reduced number of CD25 expressing cells, and thus an impaired early response to the T cell growth factor IL-2, might explain the initial proliferative defects of the knock-out cells. Furthermore, in this *in vivo* setting, cells were also stained for the effector molecules IFN-γ and granzyme

B. At the early time point following *in vivo* activation, less $Adap^{-/-}$ CD8$^+$ T cells expressed granzyme B, but this difference was lost at the later time point (Figure 4.10A). Interestingly, less $Adap^{-/-}$ CD8$^+$ T cells responded with production of the effector cytokine IFN-γ (Figure 4.10B). Nevertheless, despite reduced IFN-γ production the $Adap^{-/-}$ CD8$^+$ T cells were not impaired in bacterial clearance as demonstrated by the effective control of the bacterial burden in the infected mice (Figure 4.10C).

These data were further confirmed using infections with recombinant influenza A virus expressing OVA$_{257-264}$. A recent study has shown that TGF-β signaling in CD8$^+$ T cells during influenza A virus infection is very much dependent on ADAP. $Adap^{-/-}$ mice showed reduced survival, massive production of proinflammatory cytokines and infiltration of CD8$^+$ T cells into the infected lung. Interestingly, although there was plenty of CD8$^+$ T cells present in the lung, the cells were unable to clear the pathogen. It is important to note that the authors did not provide any data on the activation status and function of the CD8$^+$ T cells present in the infected animals. Thus, the question whether or not ADAP deficiency affects the CD8$^+$ T cells phenotype and function during infections had not been addressed [62]. Here, using the adoptive CD8$^+$ T cell transfer model that allows for the specific analysis of $Adap^{-/-}$ CD8$^+$ T cells in an otherwise $Adap^{+/+}$ host, hardly any phenotypic differences between $Adap^{-/-}$ and wild type CD8$^+$ T cells were detectable in the influenza-infected lung, despite a markedly decreased frequency of IFN-γ-producing CD8$^+$ T cells.

Mueller, et al. [69] also reported data from adoptive CD4$^+$ T cell transfers. In support of our findings, i.e. that CD4$^+$ T cells are more dependent on ADAP than CD8$^+$ T cells. In their transfer model $Adap^{-/-}$ CD4$^+$ T cells proliferated and expanded less than their wild type counterparts when they were activated *in vivo* by treatment of the recipient mice with cognate OVA-peptide and LPS. This further substantiates the argument of this thesis for differential dependency on ADAP between T cell subsets. Interestingly, they reported no differences for the expression of CD25, CD69 and CD62L.

5.1.3 ADAP-dependent induction of transcription factors

Why in certain *in vitro* and *in vivo* settings the expression of CD69, CD25 and IFN-γ are affected by loss of ADAP in CD8$^+$ T cells, while expression of the other assessed markers was not, remains elusive. One possible explanation is based on the fact, that the promotor regions of both CD25 and IFN-γ are strikingly similar [291] and that their transcription requires a concerted action of the transcription factors AP-1, NF-κB, NFAT1 and T-bet [292, 293, 294, 295, 296, 297]. Cell cycle progression and subsequent proliferation strongly depends on NF-κB activation, mediated by the CBM signalosome [19]. Induction of CD69, on the other hand, seems to rely solely on NFAT. Taken together, this suggests that ADAP might be dispensable

for the activation of transcription factors AP-1 and NF-κB, but might play a vital role for NFAT1-mediated transcription in CD8$^+$ T cells.

Rajasekaran, et *al.* have recently shown that, while cytokine production in NK cells after NKG2D and CD137 stimulation is strongly dependent on ADAP-mediated formation of the CBM signalosome, cytotoxicity of the cells does not rely on the adaptor protein [82]. *In vitro* analysis of the cytotoxicity against allogenic target cells also revealed no differences between wild type and *Adap*$^{-/-}$ cytotoxic lymphocytes [114]. Since granzyme B production – a hallmark of CD8$^+$ T cells cytotoxicity – is not affected by ADAP deficiency while IFN-γ expression is severely decreased in both *in vivo* infection models studied within this thesis, it is reasonable to speculate that similar mechanisms are as well at play in CD8$^+$ T cells.

5.1.4 Therapeutic implications of the subset-specific effect

This thesis presents comprehensive *in vitro* as well as *in vivo* data showing that CD4$^+$ and CD8$^+$ T cells differentially rely on ADAP-mediated signaling downstream of the TCR. While CD4$^+$ T cells are strongly dependent on ADAP in terms of their TCR-mediated activation, proliferation, adhesion and thymic selection, CD8$^+$ T cells are hardly affected by ADAP deficiency and retain most of their function. This might highlight ADAP as a potential molecular target for T cell subset-specific therapeutic interventions. Since autoreactive CD4$^+$ T cells are well known to orchestrate detrimental immune responses in autoimmune diseases such as multiple sclerosis and rheumatoid arthritis, a general ADAP inhibitor would severely affect CD4$^+$ T cell function thereby potentially reducing disease burden, while at the same time CD8$^+$ T cell responses including tumor surveillance and pathogen control, would largely remain unaffected. Specific inhibitors for certain ADAP phosphorylation sites known to facilitate binding of other molecules of the TCR signaling machineries (see section 1.1.1), would allow fine tuning of certain aspects of the immune system, such as leukocyte proliferation, adhesion and migration, or cytokine production. Its multifaceted immunological functions in addition to its differential importance in CD4$^+$ and CD8$^+$ T cell subsets makes ADAP an ideal therapeutic drug target.

5.2 ADAP is involved in immuneregulatory processes during *L. monocytogenes* infection

In frame of this thesis, *in vivo L. monocytogenes* infections were used to analyze the impact of ADAP deficiency on pathogen-specific immunity. As described in the introduction (see section 1.2), infection with this bacterium represents a well-established model system that

enormously contributed to our current understanding of innate and adaptive immune responses to intracellular pathogens. Thus, studying the role of ADAP in several aspects of immunity to pathogens, the *Listeria* infection model allows for the sound interpretation of the obtained data on the basis of previous publications in the field. Moreover, the adaptive immune response to intracellular pathogens is strictly dependent on CD8$^+$ T cells, i.e. the leukocyte population analyzed in great detail in the first part of the thesis.

5.2.1 Summary of results

Infection with *L. monocytogenes* revealed considerable enhanced susceptibility of $Adap^{-/-}$ mice compared to wild type control animals. This became apparent by increased weight loss and overall decreased survival of the ADAP-deficient mice (Figure 4.13A-C). Macroscopic examination of the mice 3 days post *Listeria* infection revealed severe liver and spleen pathology (Figure 4.14A) in $Adap^{-/-}$ animals. Moreover, increase in organ weights during infections, which is a surrogate indicator for strong inflammatory responses and edema, was significantly higher in $Adap^{-/-}$ spleens and livers during the later phase of the infection (especially day 7) (Figure 4.14B). A more detailed histological analysis substantiated the *in situ* findings. Histology of the spleens of $Adap^{-/-}$ mice 3 days post infection revealed massive pathology, with total destruction of the physiological splenic structure (Figure 4.16B). Moreover, livers from $Adap^{-/-}$ mice showed significantly more leukocyte aggregation foci (Figure 4.16A) and elevated ALT serum levels were indicative of more severe liver pathology in ADAP-deficient mice following *Listeria* infection (Figure 4.17B). Determination of bacterial burdens in liver and spleen during the course of the infection revealed unexpected results. While the numbers of bacteria in the analyzed organs were found to be similar early after infection, $Adap^{-/-}$ mice had significantly more bacteria in their spleens and livers on day 3 and 5 post infection. However, late phase bacterial burdens (day 7) were strongly decreased in both genotypes with no significant differences between the groups (Figure 4.15A and B).

Analysis of leukocyte numbers in spleens revealed no significant differences between wild type and knock-out animals. However, $Adap^{-/-}$ mice showed a drastic increase of leukocytes in the liver in the later phase of the infection (Figure 4.17A). Detailed analysis of the nature of the infiltrating cell types revealed that mostly CD8$^+$ T cells (Figure 4.19A), neutrophils (Figure 4.18A) and monocytes (Figure 4.18C) were causative for the high leukocyte numbers in the livers of knock-out animals. Interestingly, although the total leukocyte numbers in spleens were not significantly different between the two genotypes, $Adap^{-/-}$ mice exhibited significantly more neutrophils and monocytes at day 7 post infection in this organ (Figure 4.18A and C). However, this was not the case for CD8$^+$ T cells (Figure 4.18A).

The key proinflammatory cytokines TNF-α, IFN-γ and IL-6 showed a delayed, but slightly

sustained, kinetic in $Adap^{-/-}$ mice following *Listeria* infection. The T_H1 signature cytokine IL-12 (identified as the active heterodimer IL-12p70) on the other hand was not differentially regulated in $Adap^{-/-}$ compared to wild type mice. Of note, the serum level of the immuneregulatory cytokine TGF-β was already lower in uninfected $Adap^{-/-}$ mice, compared to their wild type counterparts and increased only very slowly during the course of the infection (Figure 4.17C).

Besides cytokines, also serum chemokines were analyzed in the steady state and following *Listeria* infection. The neutrophil recruiting chemoattractant CXCL1 (KC) tended to be lower in the serum of $Adap^{-/-}$ animals one day post infection, but was significantly higher on day 3 post infection, when compared to the wild type control mice (Figure 4.18B). Recruitment of monocytes is mainly elicited by CCL2 (MCP-1). $Adap^{-/-}$ mice showed significantly decreased serum levels one day post infection and similar concentrations later on (Figure 4.18D).

T cell recruiting chemokines were analyzed as well and since the adaptive immunity against *L. monocytogenes* is dominated by T_H1-mediated responses, the chemokines CXCL9 (MIG) and CXCL10 (IP-10) were of primary interest. One day post infection $Adap^{-/-}$ mice displayed significantly lower serum levels of these chemokines compared to control animals. In wild type mice these cytokines dropped down again, while they remained elevated in $Adap^{-/-}$ mice, which was especially true for CXCL9 (Figure 4.19B).

Activation of the CD8$^+$ T cells was assessed by CD69 expression and significantly more activated cells were found in the liver of $Adap^{-/-}$ mice compared to the wild type controls. However, the direct opposite was found in the spleens of the animals, where less activated cells were detectable in the knock-out mice (Figure 4.19C). Effector and memory cells were determined by expression of CD43, and more of these cells were found in the livers and spleens of $Adap^{-/-}$ mice (Figure 4.19D). Interestingly, no differences between the groups were found in the number of IFN-γ-producing CD8$^+$ T cells in neither spleen nor liver (Figure 4.19E). However, the amount of CD8$^+$ T cells expressing the exhaustion marker PD-1 was greater in spleens and livers of $Adap^{-/-}$ animals compared to wild type controls (Figure 4.19F).

A more detailed analysis was also performed for NK cells during the course of a *L. monocytogenes* infection. While the number of NK cells gradually increased during the infection in livers of both wild type and $Adap^{-/-}$ mice before returning to normal levels on day 7 post infection, NK cell numbers decreased drastically in the spleens in the middle phase of the infection (Figure 4.20A). When the NK cells were analyzed for the expression of the activation markers CD69 and IFN-γ, it became evident that more of the NK cells in $Adap^{-/-}$ mice exhibited an activated phenotype during the course of the infection, as indicated by the fact that more of them expressed CD69 and produced IFN-γ (Figure 4.20B and C respectively). Interestingly, splenic NK cells from $Adap^{-/-}$ mice completely failed to upregulate CD27 in response to the infection (Figure 4.20D). Analysis of NK cell maturation revealed no differences between the

genotypes during steady state condition, i.e. in the absence of infection. However, one day after *Listeria* infection less of the more mature CD11b^{hi}CD27^{hi} and CD11b^{hi}CD27^{lo} NK cells were found in the spleens of the *Adap*$^{-/-}$ animals (Figure 4.20E and F).

5.2.2 ADAP plays an important role during the innate immune response

The significant higher weight loss and increased mortality of *Adap*$^{-/-}$ mice during the early phase of the infection are indicative of a pivotal role for the adapter protein in the innate immune response against *L. monocytogenes*. This is further substantiated by increased bacterial loads in spleens and livers of the deficient animals on day 3 and 5 post infection. Importantly, the number of bacteria in spleens and liver one day after the infection was the same in ADAP-deficient and wild type mice. This suggests equally efficient uptake of the pathogen by CD8^{+}CD11c^{+} DCs, that have been reported to function as carriers to the periarteriolar lymphoid sheaths from where the bacterium can disseminate systemically [207, 194, 208]. Furthermore, platelets have also been shown to be involved in this process [209, 195], and ADAP plays important roles in platelet function as demonstrated by the fact that ADAP deficiency leads to thrombocytopenia in mice (see section 1.1.8). Nevertheless, altered platelet function in ADAP-deficient animals does not seem to affect the shuttling of bacteria to the spleen and their subsequent systemic spreading, as indicated by a comparably high bacterial burden in the liver of both mouse groups.

However, the higher bacterial loads observed in livers and spleens on day 3 and 5 post infection indicate, that ADAP-deficient mice are impaired in their ability to control the pathogen during this early phase of the infection. The observed effects at these early time points can hardly be attributed to effects of ADAP deficiency on adaptive immune responses, since T cell are not present in sufficient numbers during this early phase of the infection [157]. Thus, a closer look at cells of the innate immune response was taken in order to decipher the mechanisms underlying the observed phenotype.

As briefly described in the introduction (see section 1.2.2), monocytes play an important role during the first few days of the infection. However, impaired pathogen control in *Adap*$^{-/-}$ mice cannot be attributed to a decreased number of monocytes in the infected organs during this time period, since no significant differences were detectable between the groups (Figure 4.18C). The same was true for another leukocyte subset with direct bactericidal capacity, i.e. neutrophils. A third leukocyte population implicated in the innate defense against *L. monocytogenes* is NK cells. In the livers of the animals, no differences in NK cell numbers were detectable during this early phase of the infection. Moreover, although ADAP-deficient mice exhibited reduced NK cell numbers in the spleen during the steady state, their numbers

were found to be similar compared to wild type mice on day 2 and 3 post infection. Thus, there was no evidence that differences in the absolute number of NK cells would be causative for the increased susceptibility and elevated bacterial burdens in $Adap^{-/-}$ mice during the early phase of the infection.

As discussed in the introduction (see section 1.2.2), specific depletion of neutrophils during infection with *L. monocytogenes* led to increased susceptibility and mortality especially if higher infection doses were applied [197]. Interestingly, the survival curves in neutrophil-deficient animals depicted by the authors of this publication very much resemble the ones determined for $Adap^{-/-}$ mice in frame of this thesis, with neutrophil-depleted as well as $Adap^{-/-}$ animals dying early on during *Listeria* infection. Furthermore, the bacterial burdens measured in spleens and livers are comparable between these two studies. Together, these data not only directly indicate the overall importance of neutrophils during the early phase of listeriosis, but at the same time support the hypothesis that ADAP deficiency negatively affects neutrophil-mediated immunity. As mentioned above, this cannot be attributed to aberrant neutrophil numbers in the affected organs, but rather by their functional impairment. Whether this would involve phagocytosis, NETosis (generation of NETs), production of soluble factors like cytokines (e.g. TNF-α) or lipid mediators (leukotrienes, prostaglandins), or intracellular killing, remains unclear and needs further investigation in the future.

Serum cytokine profile provides some further insights into the mechanisms underlying enhanced susceptibility of $Adap^{-/-}$ mice to *Listeria* infection. As mentioned earlier (see section 1.2.2), TNF-α produced by macrophages and monocytes stimulates NK cells to produce considerable amounts of IFN-γ, which in turn is able to boost the intracellular killing ability of the aforementioned cells. Of note, less $Adap^{-/-}$ mice were seropositive for TNF-α one day after infection, and seronegative mice also exhibited significantly lower IFN-γ levels in their sera at that time point (Figure 4.17C). Potential failures in this TNF-α/IFN-γ-dependent feedback loop and as a consequence reduced bactericidal capacity of macrophages and monocytes could explain the increased bacterial loads in ADAP-deficient animals. However, while the frequency of TNF-α seropositive wild type mice and the amounts of IFN-γ in their sera strongly decreases after this point, more $Adap^{-/-}$ animals exhibited TNF-α in their sera and also produced more IFN-γ in response to infection. This discrepancy is puzzling and might indicate other immune mechanisms that are impaired in ADAP-deficient mice. Furthermore, detailed analysis of NK cells revealed that in $Adap^{-/-}$ mice more of the NK cells responded with IFN-γ-production one day post infection. Closer analysis of the mean fluorescent intensities (MFI) revealed no differences in cytokine production between wild type and $Adap^{-/-}$ NK cells (data not shown). Since this type of analysis can be misleading, further analysis of supernatants of activated NK cells are needed to draw sound conclusions.

Although for now no compelling conclusions can be drawn by the acquired date, the effect

of ADAP deficiency on the innate immune response against *L. monocytogenes* is nevertheless obvious and profound. Further investigation is needed to decipher in greater detail the role of ADAP in this branch of the immune system.

5.2.3 ADAP-deficiency leads to a dysregulated immune response

Beyond day 3 post infection, the number of monocytes and neutrophils increased drastically in $Adap^{-/-}$ mice, while the numbers of NK cells were significantly lower in both affected organs. Especially the observed massive neutrophil infiltration into the livers and the spleens of $Adap^{-/-}$ mice was unexpected, since previously published data showed that neutrophils lacking ADAP were impaired in their transmigration behavior into tissue. Yet, this study used ischemia-induced renal injury to study neutrophil transmigration into the kidneys [41]. Whether the results obtained in frame of this thesis are comparable to those of the aforementioned study is questionable, since in contrast to our study their model was based on characterizing neutrophil migration in the context of sterile inflammation. *Listeria* infection on the other hand results in direct or indirect activation of a plethora of immune cells and, subsequently, a complex cellular and molecular interplay. These differences in the experimental systems could very explain rather diverse effects observed on the impact of ADAP deficiency on neutrophil migration behavior.

NK cells might be responsible for the dysregulated neutrophil infiltration. Preliminary data from our lab generated using a conditional NKp46$^{\text{cre}}$ × ADAP$^{\text{flox}}$ mouse model were ADAP is exclusively absent in NK cells revealed equally pronounced migration of neutrophils to the livers of *L. monocytogenes* infected mice (data not shown). Due to the specific feature of the mouse model, this can only be attributed to effects of ADAP deficiency in NK cells, since all other cells are capable of expressing ADAP. How ADAP in NK cells mediates neutrophil recruitment following pathogen encounter remains elusive. Though it has been shown that massive IFN-γ production by NK cells impedes neutrophil transmigration during listeriosis due to downregulation of CXCR2 on these cells [182], this is most likely not the case in the ADAP-deficient setting, since serum levels of the cytokine are actually higher in the $Adap^{-/-}$ mice during that phase of the infection. Furthermore, FACS analysis provided evidence that indeed more NK cells produced IFN-γ. These contradicting data suggest other mechanisms underlying NK cell-mediated regulation of neutrophil recruitment to inflamed tissue and indicate that ADAP in NK cells is definitely involved in these. There is growing evidence that NK cells can also serve a regulatory function in certain pathological settings, e.g. neuroinflammation, and it has been speculated, that they also do this during listeriosis [224, 225]. The data presented in this thesis provides some additional support for this hypothesis.

Not only the late phase accumulation of neutrophils and monocytes in the livers and spleens of infected $Adap^{-/-}$ mice is of interest, but also the observed massively increased numbers of CD8$^+$ T cells found in the livers of the ADAP-deficient mice post day 5 after the infection. Whether these cells are extensively recruited into the liver or whether they excessively proliferate within the infected organ remains elusive. In general, serum cytokine analysis revealed a strong induction of a T$_H$1-like immune response, exemplified by high amounts of the according signature cytokines IFN-γ and IL-12p70 and signature chemokines such as CXCL9 (MIG) and CXCL10 (IP-10). This comes as no surprise and has been discussed in the introduction (see section 1.2.3). However, compared to wild type mice, $Adap^{-/-}$ mice had a tendency of exhibiting higher chemokine levels 3 and 5 days post infection. This was also true for the T cell attracting chemokine CCL5. Nevertheless, the serum concentrations of these chemokines were all at baseline levels, irrespective of the mouse genotype, 7 days post infection, i.e. the time point when the highest number of CD8$^+$ T cells was found in the livers of the $Adap^{-/-}$ animals. Thus, differences in CCL5 serum concentrations cannot explain these massive differences in CD8$^+$ T cell numbers between the mouse genotypes. However, it needs to be taken into account that the chemokine concentrations in the infected organs have not been determined and they might indeed differ from the serum levels.

The observed aberrant early serum IFN-γ levels might also provide an explanation for the massive CD8$^+$ T cell numbers found in the liver of $Adap^{-/-}$ mice at the later stage of the *L. monocytogenes* infection. It has been reported that early IFN-γ is important for the pre-programming of the contraction phase of CD8$^+$ T cells during listeriosis [238]. This means without sufficient levels of this cytokine at the beginning of the infection, apoptosis of effector CD8$^+$ T cells is reduced in the later phase of the infection. This correlates very well with the time frame of the atypical CD8$^+$ T cell accumulation in the livers of $Adap^{-/-}$ mice. Hence, it is possible that the lower IFN-γ serum levels on day one post infection could have a negative influence on the contraction phase later on and that this might result in the massively increased number of CD8$^+$ T cells detected in the infected livers of $Adap^{-/-}$ mice. Further analysis is needed to confirm this hypothesis.

Another explanation for the observed phenotype in infected $Adap^{-/-}$ mice might come from so called *intrahepatic myeloid-cell aggregates for T cell population expansion* (iMATEs). These accumulations of specialized myeloid cells that share characteristic features with DCs and are derived from monocytes, have been shown to strongly promote CD8$^+$ T cells function and proliferation in the livers of hepatitis B virus (HBV) infected mice, mainly by protecting them from the tolerogenic environment of the liver. The induction of these structures was reliant on TLR9 signaling [298]. Analysis of $Tlr9^{-/-}$ mice infected with *L. monocytogenes* showed slightly increased susceptibility to the pathogen, proofing that TLR9 plays also a role in the defense against it [299]. Histology of livers from $Adap^{-/-}$ mice infected with *L. monocytogenes* revealed multiple leukocyte foci and in significantly higher frequency than in wild type littermates. If

these foci are indeed iMATEs, this could explain the enormous expansion of CD8$^+$ T cells in the $Adap^{-/-}$ animals during the later stage of the infection. However, more data is needed to support this hypothesis.

Next to the abnormally high CD8$^+$ T cell numbers observed in the infected organs of $Adap^{-/-}$ mice, detailed analysis of these cells revealed that they exhibit a comparably higher activation status (identified by CD69 expression) and display elevated effector function (identified by CD43 expression), at least in the livers of the ADAP-deficient animals. In contrast, in the spleen of the $Adap^{-/-}$ mice less CD69$^+$CD8$^+$ T cells were found, while there was a tendency for more CD43$^+$CD8$^+$ T cells. Interestingly, the same numbers of IFN-γ-producing cells were found in the livers and spleens of the $Adap^{-/-}$ animals compared to wild type controls, which means that in the livers of $Adap^{-/-}$ mice a smaller fraction of the CD8$^+$ T cells produced IFN-γ. This is in accordance with the data shown in the first part of this thesis, where CD8$^+$ T cell function is hardly dependent on ADAP, except for IFN-γ production (Figure 4.10B and Figure 4.11E).

Together with the data from neutrophils and monocytes, this suggests that although ADAP has been identified as an important mediator for adhesion and migration, ADAP deficiency does not seem to impair cell migration behavior during an infection. Most of the published data was collected from *in vitro* experiments or *in vivo* studies using models for sterile inflammation. Only Li, et *al.* [62] have so far provided data from infection experiments and they reported as well that they found higher numbers of CD8$^+$ T cells in the lungs of influenza A virus infected ADAP-deficient animals. This fits well with the data collected in frame of this thesis. The authors did not provide functional data for the ADAP-deficient CD8$^+$ T cells. Thus, this thesis is the first report on this in an infection model. Moreover, the authors reported that the $Adap^{-/-}$ mice were more susceptible to the infection and this was most likely due to severe immune pathology. They also provided cytokine data that supported this assumption by showing a severe cytokine storm in the influenza infected ADAP-deficient mice. The cause for this phenotype, according to the authors, was impaired TGF-β-production and signaling, a cytokine important for the downregulation of immune responses.

This is well in line with the effects seen in the $Adap^{-/-}$ mice infected with *L. monocytogenes*. In support of that, data from this thesis show that already under steady state conditions, i.e. before the infection, $Adap^{-/-}$ mice exhibit less TGF-β in their plasma than their wild type counterparts and, moreover, during the course of the infection, TGF-β plasma levels increased slower in ADAP-deficient than in wild type animals. The above mentioned reduced numbers of platelets in $Adap^{-/-}$ mice might be mechanistically involved in this abnormal cytokine response, since platelets have been shown to store high amounts of TGF-β in their α-granules [300]. One might speculate that the immune response — especially during the later stage of the infection – is insufficiently controlled in $Adap^{-/-}$ mice and thus leads to severe immune

pathology. CD8^{+} T cells, but especially neutrophils, are known to cause tissue damage if not properly controlled. So far, ADAP has mainly been considered as a proinflammatory mediator. However, increasing evidence suggests that ADAP is crucially involved as well in regulatory mechanism. Data compiled within this thesis provide further direct evidence for the immune regulatory role of this multifunctional adapter molecule during infections.

References

[1] Togni, M., Lindquist, J., Gerber, A., Kölsch, U., Hamm-Baarke, A., Kliche, S. & Schraven, B. The role of adaptor proteins in lymphocyte activation. *Molecular immunology* **41**, 615–630 (2004).

[2] Hořejší, V., Zhang, W. & Schraven, B. Transmembrane adaptor proteins: organizers of immunoreceptor signalling. *Nature Reviews Immunology* **4**, 603–616 (2004).

[3] Jordan, M. S., Singer, A. L. & Koretzky, G. A. Adaptors as central mediators of signal transduction in immune cells. *Nature immunology* **4**, 110–116 (2003).

[4] Veale, M., Raab, M., Li, Z., da Silva, A. J., Kraeft, S.-K., Weremowicz, S., Morton, C. C. & Rudd, C. E. Novel isoform of lymphoid adaptor FYN-T-binding protein (FYB-130) interacts with SLP-76 and up-regulates interleukin 2 production. *Journal of Biological Chemistry* **274**, 28427–28435 (1999).

[5] Musci, M. A., Hendricks-Taylor, L. R., Motto, D. G., Paskind, M., Kamens, J., Turck, C. W. & Koretzky, G. A. Molecular cloning of SLAP-130, an SLP-76-associated substrate of the T cell antigen receptor-stimulated protein tyrosine kinases. *Journal of Biological Chemistry* **272**, 11674–11677 (1997).

[6] Altschul, S. F., Madden, T. L., Schäffer, A. A., Zhang, J., Zhang, Z., Miller, W. & Lipman, D. J. Gapped BLAST and PSI-BLAST: a new generation of protein database search programs. *Nucleic acids research* **25**, 3389–3402 (1997).

[7] Fostel, L. V., Dluzniewska, J., Shimizu, Y., Burbach, B. J. & Peterson, E. J. ADAP is dispensable for NK cell development and function. *Int Immunol* **18**, 1305–1314 (2006).

[8] Kasirer-Friede, A., Cozzi, M. R., Mazzucato, M., De Marco, L., Ruggeri, Z. M. & Shattil, S. J. Signaling through GP Ib-IX-V activates αIIbβ3 independently of other receptors. *Blood* **103**, 3403–3411 (2004).

[9] Coppolino, M. G., Krause, M., Hagendorff, P., Monner, D. A., Trimble, W., Grinstein, S., Wehland, J. & Sechi, A. S. Evidence for a molecular complex consisting of Fyb/SLAP, SLP-76, Nck, VASP and WASP that links the actin cytoskeleton to Fcγ receptor signalling during phagocytosis. *Journal of Cell Science* **114**, 4307–4318 (2001).

[10] Da Silva, A. J., Li, Z., De Vera, C., Canto, E., Findell, P. & Rudd, C. E. Cloning of a novel T-cell protein FYB that binds FYN and SH2-domain-containing leukocyte protein 76 and modulates interleukin 2 production. *Proceedings of the National Academy of Sciences* **94**, 7493–7498 (1997).

[11] Dluzniewska, J., Zou, L., Harmon, I. R., Ellingson, M. T. & Peterson, E. J. Immature hematopoietic cells display selective requirements for adhesion-and degranulation-promoting adaptor protein in development and homeostatsis. *European journal of immunology* **37**, 3208–3219 (2007).

[12] Boerth, N. J., Judd, B. A. & Koretzky, G. A. Functional association between SLAP-130 and SLP-76 in Jurkat T cells. *Journal of Biological Chemistry* **275**, 5143–5152 (2000).

[13] Raab, M., Kang, H., da Silva, A., Zhu, X. & Rudd, C. E. FYN-T-FYB-SLP-76 interactions define a T-cell receptor ζ/CD3-mediated tyrosine phosphorylation pathway that up-regulates interleukin 2 transcription in T-cells. *Journal of Biological Chemistry* **274**, 21170–21179 (1999).

[14] Sylvester, M., Kliche, S., Lange, S., Geithner, S., Klemm, C., Schlosser, A., Großmann, A., Stelzl, U., Schraven, B., Krause, E. & others. Adhesion and degranulation promoting adapter protein (ADAP) is a central hub for phosphotyrosine-mediated interactions in T cells. *PLoS One* **5**, e11708 (2010).

[15] Heuer, K., Arbuzova, A., Strauss, H., Kofler, M. & Freund, C. The helically extended SH3 domain of the T cell adaptor protein ADAP is a novel lipid interaction domain. *Journal of molecular biology* **348**, 1025–1035 (2005).

[16] Heuer, K., Kofler, M., Langdon, G., Thiemke, K. & Freund, C. Structure of a helically extended SH3 domain of the T cell adapter protein ADAP. *Structure* **12**, 603–610 (2004).

[17] Krause, M., Sechi, A. S., Konradt, M., Monner, D., Gertler, F. B. & Wehland, J. Fyn-binding protein (Fyb)/SLP-76–associated protein (SLAP), Ena/vasodilator-stimulated phosphoprotein (VASP) proteins and the Arp2/3 complex link T cell receptor (TCR) signaling to the actin cytoskeleton. *The Journal of cell biology* **149**, 181–194 (2000).

[18] Heuer, K., Sylvester, M., Kliche, S., Pusch, R., Thiemke, K., Schraven, B. & Freund, C. Lipid-binding hSH3 domains in immune cell adapter proteins. *Journal of molecular biology* **361**, 94–104 (2006).

[19] Srivastava, R., Burbach, B. J., Mitchell, J. S., Pagán, A. J. & Shimizu, Y. ADAP regulates cell cycle progression of T cells via control of cyclin E and Cdk2 expression through two distinct CARMA1-dependent signaling pathways. *Molecular and cellular biology* **32**, 1908–1917 (2012).

[20] Medeiros, R. B., Burbach, B. J., Mueller, K. L., Srivastava, R., Moon, J. J., Highfill, S., Peterson, E. J. & Shimizu, Y. Regulation of NF-κB activation in T cells via association of the adapter proteins ADAP and CARMA1. *Science* **316**, 754–758 (2007).

[21] Witte, A., Degen, J., Baumgart, K., Waldt, N., Kuropka, B. & others. Emerging Roles of ADAP, SKAP55, and SKAP-HOM for Integrin and NF-κB Signaling in T cells. *J Clin Cell Immunol S* **12**, 2 (2012).

[22] Griffiths, E. K., Krawczyk, C., Kong, Y. Y., Raab, M., Hyduk, S. J., Bouchard, D., Chan, V. S., Kozieradzki, I., Oliveira-Dos-Santos, A. J., Wakeham, A., Ohashi, P. S., Cybulsky, M. I., Rudd, C. E. & Penninger, J. M. Positive regulation of T cell activation and integrin adhesion by the adapter Fyb/Slap. *Science* **293**, 2260–2263 (2001).

[23] Peterson, E. J., Woods, M. L., Dmowski, S. A., Derimanov, G., Jordan, M. S., Wu, J. N., Myung, P. S., Liu, Q. H., Pribila, J. T., Freedman, B. D., Shimizu, Y. & Koretzky, G. A. Coupling of the TCR to integrin activation by Slap-130/Fyb. *Science* **293**, 2263–2265 (2001).

[24] Marie-Cardine, A., Hendricks-Taylor, L. R., Boerth, N. J., Zhao, H., Schraven, B. & Koretzky, G. A. Molecular interaction between the Fyn-associated protein SKAP55 and the SLP-76-associated phosphoprotein SLAP-130. *Journal of Biological Chemistry* **273**, 25789–25795 (1998).

[25] Huang, Y., Norton, D. D., Precht, P., Martindale, J. L., Burkhardt, J. K. & Wange, R. L. Deficiency of ADAP/Fyb/SLAP-130 destabilizes SKAP55 in Jurkat T cells. *Journal of Biological Chemistry* **280**, 23576–23583 (2005).

[26] Burbach, B. J., Srivastava, R., Medeiros, R. B., O'Gorman, W. E., Peterson, E. J. & Shimizu, Y. Distinct regulation of integrin-dependent T cell conjugate formation and NF-κB activation by the adapter protein ADAP. *The Journal of Immunology* **181**, 4840–4851 (2008).

[27] Togni, M., Swanson, K., Reimann, S., Kliche, S., Pearce, A., Simeoni, L., Reinhold, D., Wienands, J., Neel, B., Schraven, B. & others. Regulation of in vitro and in vivo immune functions by the cytosolic adaptor protein SKAP-HOM. *Molecular and cellular biology* **25**, 8052–8063 (2005).

[28] Kliche, S., Breitling, D., Togni, M., Pusch, R., Heuer, K., Wang, X., Freund, C., Kasirer-Friede, A., Menasche, G., Koretzky, G. A. & others. The ADAP/SKAP55 signaling module regulates T-cell receptor-mediated integrin activation through plasma membrane targeting of Rap1. *Molecular and cellular biology* **26**, 7130–7144 (2006).

[29] Wang, H., Liu, H., Lu, Y., Lovatt, M., Wei, B. & Rudd, C. E. Functional defects of SKAP-55-deficient T cells identify a regulatory role for the adaptor in LFA-1 adhesion. *Molecular and cellular biology* **27**, 6863–6875 (2007).

[30] Smith-Garvin, J. E., Koretzky, G. A. & Jordan, M. S. T cell activation. *Annual review of immunology* **27**, 591 (2009).

[31] Acuto, O., Di Bartolo, V. & Michel, F. Tailoring T-cell receptor signals by proximal negative feedback mechanisms. *Nature Reviews Immunology* **8**, 699–712 (2008).

[32] Lafuente, E. M., van Puijenbroek, A. A., Krause, M., Carman, C. V., Freeman, G. J., Berezovskaya, A., Constantine, E., Springer, T. A., Gertler, F. B. & Boussiotis, V. A. RIAM, an Ena/VASP and Profilin ligand, interacts with Rap1-GTP and mediates Rap1-induced adhesion. *Developmental cell* **7**, 585–595 (2004).

[33] Katagiri, K., Maeda, A., Shimonaka, M. & Kinashi, T. RAPL, a Rap1-binding molecule that mediates Rap1-induced adhesion through spatial regulation of LFA-1. *Nature immunology* **4**, 741–748 (2003).

[34] Kinashi, T. Intracellular signalling controlling integrin activation in lymphocytes. *Nature Reviews Immunology* **5**, 546–559 (2005).

[35] Raab, M., Wang, H., Lu, Y., Smith, X., Wu, Z., Strebhardt, K., Ladbury, J. E. & Rudd, C. E. T cell receptor inside-out pathway via signaling module SKAP1-RapL regulates T cell motility and interactions in lymph nodes. *Immunity* **32**, 541–556 (2010).

[36] Katagiri, K., Imamura, M. & Kinashi, T. Spatiotemporal regulation of the kinase Mst1 by binding protein RAPL is critical for lymphocyte polarity and adhesion. *Nature immunology* **7**, 919–928 (2006).

[37] Kliche, S., Worbs, T., Wang, X., Degen, J., Patzak, I., Meineke, B., Togni, M., Moser, M., Reinhold, A., Kiefer, F. & others. CCR7-mediated LFA-1 functions in T cells are regulated by 2 independent ADAP/SKAP55 modules. *Blood* **119**, 777–785 (2012).

[38] Moser, M., Bauer, M., Schmid, S., Ruppert, R., Schmidt, S., Sixt, M., Wang, H.-V., Sperandio, M. & Fässler, R. Kindlin-3 is required for $\beta 2$ integrin–mediated leukocyte adhesion to endothelial cells. *Nature medicine* **15**, 300–305 (2009).

[39] Dios-Esponera, A., de Val, S. I., Sevilla-Movilla, S., García-Verdugo, R., García-Bernal, D., Arellano-Sánchez, N., Cabañas, C. & Teixidó, J. Positive and negative regulation by SLP-76/ADAP and Pyk2 of chemokine-stimulated T-lymphocyte adhesion mediated by integrin $\alpha 4 \beta 1$. *Molecular biology of the cell* **26**, 3215–3228 (2015).

[40] García-Bernal, D., Wright, N., Sotillo-Mallo, E., Nombela-Arrieta, C., Stein, J. V., Bustelo, X. R. & Teixidó, J. Vav1 and Rac control chemokine-promoted T lymphocyte adhesion mediated by the integrin $\alpha 4 \beta 1$. *Molecular biology of the cell* **16**, 3223–3235 (2005).

[41] Block, H., Herter, J. M., Rossaint, J., Stadtmann, A., Kliche, S., Lowell, C. A. & Zarbock, A. Crucial role of SLP-76 and ADAP for neutrophil recruitment in mouse kidney ischemia-reperfusion injury. *The Journal of experimental medicine* **209**, 407–421 (2012).

[42] Blonska, M. & Lin, X. CARMA1-mediated NF-κB and JNK activation in lymphocytes. *Immunological reviews* **228**, 199–211 (2009).

[43] Wang, H., McCann, F. E., Gordan, J. D., Wu, X., Raab, M., Malik, T. H., Davis, D. M. & Rudd, C. E. ADAP–SLP-76 binding differentially regulates supramolecular activation cluster (SMAC) formation relative to T cell–APC conjugation. *The Journal of experimental medicine* **200**, 1063–1074 (2004).

[44] Cheng, J., Montecalvo, A. & Kane, L. P. Regulation of NF-κB induction by TCR/CD28. *Immunologic research* **50**, 113–117 (2011).

[45] Thome, M., Charton, J. E., Pelzer, C. & Hailfinger, S. Antigen receptor signaling to NF-κB via CARMA1, BCL10, and MALT1. *Cold Spring Harbor perspectives in biology* **2**, a003004 (2010).

[46] Srivastava, R., Burbach, B. J. & Shimizu, Y. NF-κB activation in T cells requires discrete control of IKKα/β phosphorylation and IKKγ ubiquitination by the ADAP adapter protein. *Journal of Biological Chemistry* jbc–M109 (2010).

[47] Sechi, A. S., Buer, J., Wehland, J. & Probst-Kepper, M. Changes in actin dynamics at the T-cell/APC interface: implications for T-cell anergy? *Immunological reviews* **189**, 98–110 (2002).

[48] Barda-Saad, M., Braiman, A., Titerence, R., Bunnell, S. C., Barr, V. A. & Samelson, L. E. Dynamic molecular interactions linking the T cell antigen receptor to the actin cytoskeleton. *Nature immunology* **6**, 80–89 (2005).

[49] Dombroski, D., Houghtling, R. A., Labno, C. M., Precht, P., Takesono, A., Caplen, N. J., Billadeau, D. D., Wange, R. L., Burkhardt, J. K. & Schwartzberg, P. L. Kinase-independent functions for Itk in TCR-induced regulation of Vav and the actin cytoskeleton. *The Journal of Immunology* **174**, 1385–1392 (2005).

[50] Wardenburg, J. B., Pappu, R., Bu, J.-Y., Mayer, B., Chernoff, J., Straus, D. & Chan, A. C. Regulation of PAK activation and the T cell cytoskeleton by the linker protein SLP-76. *Immunity* **9**, 607–616 (1998).

[51] Cannon, J. L., Labno, C. M., Bosco, G., Seth, A., McGavin, M. H., Siminovitch, K. A., Rosen, M. K. & Burkhardt, J. K. Wasp recruitment to the T cell: APC contact site occurs independently of Cdc42 activation. *Immunity* **15**, 249–259 (2001).

[52] Nolz, J. C., Gomez, T. S., Zhu, P., Li, S., Medeiros, R. B., Shimizu, Y., Burkhardt, J. K., Freedman, B. D. & Billadeau, D. D. The WAVE2 complex regulates actin cytoskeletal reorganization and CRAC-mediated calcium entry during T cell activation. *Current biology* **16**, 24–34 (2006).

[53] Nolz, J. C., Medeiros, R. B., Mitchell, J. S., Zhu, P., Freedman, B. D., Shimizu, Y. & Billadeau, D. D. WAVE2 regulates high-affinity integrin binding by recruiting vinculin and talin to the immunological synapse. *Molecular and cellular biology* **27**, 5986–6000 (2007).

[54] Zeng, R., Cannon, J. L., Abraham, R. T., Way, M., Billadeau, D. D., Bubeck-Wardenberg, J. & Burkhardt, J. K. SLP-76 coordinates Nck-dependent Wiskott-Aldrich syndrome protein recruitment with Vav-1/Cdc42-dependent Wiskott-Aldrich syndrome protein activation at the T cell-APC contact site. *The Journal of Immunology* **171**, 1360–1368 (2003).

[55] Pauker, M. H., Reicher, B., Fried, S., Perl, O. & Barda-Saad, M. Functional cooperation between the proteins Nck and ADAP is fundamental for actin reorganization. *Molecular and cellular biology* **31**, 2653–2666 (2011).

[56] Li, M. O., Wan, Y. Y., Sanjabi, S., Robertson, A.-K. L. & Flavell, R. A. Transforming growth factor-β regulation of immune responses. *Annu. Rev. Immunol.* **24**, 99–146 (2006).

[57] Annes, J. P., Munger, J. S. & Rifkin, D. B. Making sense of latent TGFβ activation. *Journal of cell science* **116**, 217–224 (2003).

[58] Yu, Q. & Stamenkovic, I. Cell surface-localized matrix metalloproteinase-9 proteolytically activates TGF-β and promotes tumor invasion and angiogenesis. *Genes & development* **14**, 163–176 (2000).

[59] Mu, D., Cambier, S., Fjellbirkeland, L., Baron, J. L., Munger, J. S., Kawakatsu, H., Sheppard, D., Broaddus, V. C. & Nishimura, S. L. The integrin $\alpha v \beta 8$ mediates epithelial homeostasis through MT1-MMP–dependent activation of TGF-$\beta 1$. *The Journal of cell biology* **157**, 493–507 (2002).

[60] Rifkin, D. B. & Sheppard, D. The integrin v 6 binds and activates latent TGF 1: a mechanism for regulating pulmonary inflammation and fibrosis. *Cell* **96**, 319–328 (1999).

[61] Wipff, P.-J. & Hinz, B. Integrins and the activation of latent transforming growth factor $\beta 1$–an intimate relationship. *European journal of cell biology* **87**, 601–615 (2008).

[62] Li, C., Jiao, S., Wang, G., Gao, Y., Liu, C., He, X., Zhang, C., Xiao, J., Li, W., Zhang, G., Wei, B., Chen, H. & Wang, H. The Immune Adaptor ADAP Regulates Reciprocal TGF-$\beta 1$-Integrin Crosstalk to Protect from Influenza Virus Infection. *PLoS Pathog* **11**, e1004824 (2015).

[63] Francisco, L. M., Sage, P. T. & Sharpe, A. H. The PD-1 pathway in tolerance and autoimmunity. *Immunological reviews* **236**, 219–242 (2010).

[64] Li, C., Li, W., Xiao, J., Jiao, S., Teng, F., Xue, S., Zhang, C., Sheng, C., Leng, Q., Rudd, C. E., Wei, B. & Wang, H. ADAP and SKAP55 deficiency suppresses PD-1 expression in CD8+ cytotoxic T lymphocytes for enhanced anti-tumor immunotherapy. *EMBO Mol Med* **7**, 754–769 (2015).

[65] Wu, J. N., Gheith, S., Bezman, N. A., Liu, Q.-H., Fostel, L. V., Swanson, A. M., Freedman, B. D., Koretzky, G. A. & Peterson, E. J. Adhesion-and degranulation-promoting adapter protein is required for efficient thymocyte development and selection. *The Journal of Immunology* **176**, 6681–6689 (2006).

[66] Sprent, J. & Surh, C. D. Normal T cell homeostasis: the conversion of naive cells into memory-phenotype cells. *Nature immunology* **12**, 478–484 (2011).

[67] Fiege, J. K., Burbach, B. J. & Shimizu, Y. Negative Regulation of Memory Phenotype CD8 T Cell Conversion by Adhesion and Degranulation–Promoting Adapter Protein. *The Journal of Immunology* **195**, 3119–3128 (2015).

[68] Hu, J. & August, A. Naive and innate memory phenotype CD4+ T cells have different requirements for active Itk for their development. *The Journal of Immunology* **180**, 6544–6552 (2008).

[69] Mueller, K. L., Thomas, M. S., Burbach, B. J., Peterson, E. J. & Shimizu, Y. Adhesion and degranulation-promoting adapter protein (ADAP) positively regulates T cell sensitivity to antigen and T cell survival. *The Journal of Immunology* **179**, 3559–3569 (2007).

[70] Freiberg, B. A., Kupfer, H., Maslanik, W., Delli, J., Kappler, J., Zaller, D. M. & Kupfer, A. Staging and resetting T cell activation in SMACs. *Nature immunology* **3**, 911–917 (2002).

[71] Davis, D. M. Assembly of the immunological synapse for T cells and NK cells. *Trends in immunology* **23**, 356–363 (2002).

[72] Dustin, M. L. & Shaw, A. S. Costimulation: building an immunological synapse. *Science* **283**, 649–650 (1999).

[73] Monks, C. R., Freiberg, B. A., Kupfer, H., Sciaky, N. & Kupfer, A. Three-dimensional segregation of supramolecular activation clusters in T cells. *Nature* **395**, 82–86 (1998).

[74] Mitchell, J. S., Burbach, B. J., Srivastava, R., Fife, B. T. & Shimizu, Y. Multistage T Cell–Dendritic Cell Interactions Control Optimal CD4 T Cell Activation through the ADAP-SKAP55–Signaling Module. *The Journal of Immunology* **191**, 2372–2383 (2013).

[75] Diefenbach, A., Jamieson, A. M., Liu, S. D., Shastri, N. & Raulet, D. H. Ligands for the murine NKG2D receptor: expression by tumor cells and activation of NK cells and macrophages. *Nature immunology* **1**, 119–126 (2000).

[76] Lanier, L. L. Natural killer cell receptor signaling. *Current opinion in immunology* **15**, 308–314 (2003).

[77] Idris, A. H., Smith, H. R., Mason, L. H., Ortaldo, J. R., Scalzo, A. A. & Yokoyama, W. M. The natural killer gene complex genetic locus Chok encodes Ly-49D, a target recognition receptor that activates natural killing. *Proceedings of the National Academy of Sciences* **96**, 6330–6335 (1999).

[78] Bloch-Queyrat, C., Fondanèche, M.-C., Chen, R., Yin, L., Relouzat, F., Veillette, A., Fischer, A. & Latour, S. Regulation of natural cytotoxicity by the adaptor SAP and the Src-related kinase Fyn. *The Journal of experimental medicine* **202**, 181–192 (2005).

[79] Orange, J. S., Wang, B., Terhorst, C. & Biron, C. A. Requirement for natural killer cell-produced interferon gamma in defense against murine cytomegalovirus infection and enhancement of this defense pathway by interleukin 12 administration. *The Journal of experimental medicine* **182**, 1045–1056 (1995).

[80] Seaman, W., Sleisenger, M., Eriksson, E. & Koo, G. Depletion of natural killer cells in mice by monoclonal antibody to NK-1.1. Reduction in host defense against malignancy without loss of cellular or humoral immunity. *The Journal of Immunology* **138**, 4539–4544 (1987).

[81] May, R. M., Okumura, M., Hsu, C.-J., Bassiri, H., Yang, E., Rak, G., Mace, E. M., Philip, N. H., Zhang, W., Baumgart, T., Orange, J. S., Nichols, K. E. & Kambayashi, T. Murine natural killer immunoreceptors use distinct proximal signaling complexes to direct cell function. *Blood* **121**, 3135–3146 (2013).

[82] Rajasekaran, K., Kumar, P., Schuldt, K. M., Peterson, E. J., Vanhaesebroeck, B., Dixit, V., Thakar, M. S. & Malarkannan, S. Signaling by Fyn-ADAP via the Carma1-Bcl-10-MAP3K7 signalosome exclusively regulates inflammatory cytokine production in NK cells. *Nat Immunol* **14**, 1127–1136 (2013).

[83] Gerbec, Z. J., Thakar, M. S. & Malarkannan, S. The Fyn–ADAP axis: cytotoxicity versus cytokine production in killer cells. *Frontiers in immunology* **6** (2015).

[84] Togni, M., Engelmann, S., Reinhold, D., Schraven, B. & Reinhold, A. The adapter protein ADAP is required for selected dendritic cell functions. *Cell Communication and Signaling* **10**, 1 (2012).

[85] Laki, K. Our ancient heritage in blood clotting and some of its consequences. *Annals of the New York Academy of Sciences* **202**, 297–307 (1972).

[86] Sakariassen, K., Bolhuis, P. & Sixma, J. Human blood platelet adhesion to artery subendothelium is mediated by factor VIII–von Willebrand factor bound to the subendothelium (1979).

[87] Savage, B., Almus-Jacobs, F. & Ruggeri, Z. M. Specific synergy of multiple substrate–receptor interactions in platelet thrombus formation under flow. *Cell* **94**, 657–666 (1998).

[88] Savage, B., Saldívar, E. & Ruggeri, Z. M. Initiation of platelet adhesion by arrest onto fibrinogen or translocation on von Willebrand factor. *Cell* **84**, 289–297 (1996).

[89] Kasirer-Friede, A., Moran, B., Nagrampa-Orje, J., Swanson, K., Ruggeri, Z. M., Schraven, B., Neel, B. G., Koretzky, G. & Shattil, S. J. ADAP is required for normal αIIbβ3 activation by VWF/GP Ib-IX-V and other agonists. *Blood* **109**, 1018–1025 (2007).

[90] Marie-Cardine, A., Verhagen, A. M., Eckerskorn, C. & Schraven, B. SKAP-HOM, a novel adaptor protein homologous to the FYN-associated protein SKAP55. *FEBS letters* **435**, 55–60 (1998).

[91] Kasirer-Friede, A., Kang, J., Kahner, B., Ye, F., Ginsberg, M. H. & Shattil, S. J. ADAP interactions with talin and kindlin promote platelet integrin αIIbβ3 activation and stable fibrinogen binding. *Blood* **123**, 3156–3165 (2014).

[92] Jarvis, G., Bihan, D., Hamaia, S., Pugh, N., Ghevaert, C., Pearce, A., Hughes, C., Watson, S., Ware, J., Rudd, C. & others. A role for adhesion and degranulation-promoting adapter protein in collagen-induced platelet activation mediated via integrin α2β1. *Journal of Thrombosis and Haemostasis* **10**, 268–277 (2012).

[93] Kasirer-Friede, A., Ruggeri, Z. M. & Shattil, S. J. Role for ADAP in shear flow–induced platelet mechanotransduction. *Blood* **115**, 2274–2282 (2010).

[94] Foster, P. S., Mould, A. W., Yang, M., Mackenzie, J., Mattes, J., Hogan, S. P., Mahalingam, S., Mckenzie, A. N., Rothenberg, M. E., Young, I. G. & others. Elemental signals regulating eosinophil accumulation in the lung. *Immunological reviews* **179**, 173–181 (2001).

[95] Hogan, S. P., Mould, A. W., Young, J. M., Rothenberg, M. E., Ramsay, A. J., Matthaei, K., Young, I. G. & Foster, P. S. Cellular and molecular regulation of eosinophil trafficking to the lung. *Immunology and cell biology* **76**, 454–460 (1998).

[96] Park, C., Choi, Y., Ki, S., Moon, S., Jeong, S., Uh, S. & Kim, Y. Granulocyte macrophage colony-stimulating factor is the main cytokine enhancing survival of eosinophils in asthmatic airways. *European Respiratory Journal* **12**, 872–878 (1998).

[97] Czech, W., Krutmann, J., Budnik, A., Schöpf, E. & Kapp, A. Induction of intercellular adhesion molecule 1 (ICAM-1) expression in normal human eosinophils by inflammatory cytokines. *Journal of Investigative Dermatology* **100**, 417–423 (1993).

[98] Hubbard, A. K. & Rothlein, R. Intercellular adhesion molecule-1 (ICAM-1) expression and cell signaling cascades. *Free Radical Biology and Medicine* **28**, 1379–1386 (2000).

[99] Roebuck, K. A. & Finnegan, A. Regulation of intercellular adhesion molecule-1 (CD54) gene expression. *Journal of Leukocyte Biology* **66**, 876–888 (1999).

[100] Van de Stolpe, A. & Van der Saag, P. Intercellular adhesion molecule-1. *Journal of Molecular Medicine* **74**, 13–33 (1996).

[101] Chihara, J., Yamamoto, T., Kurachi, D., Kakazu, T., Higashimoto, I. & Nakajima, S. Possible release of eosinophil granule proteins in response to signaling from intercellular adhesion molecule-1 and its ligands. *International archives of allergy and immunology* **108**, 52–54 (1995).

[102] Horie, S., Okubo, Y., Hossain, M., Momose, T., Suzuki, J., Isobe, M. & Sekiguchi, M. Intercellular adhesion molecule-1 on eosinophils is involved in eosinophil protein X release induced by cytokines. *Immunology* **90**, 301–307 (1997).

[103] Takafuji, S., Shoji, S., Ito, K., Yamamoto, K. & Nakagawa, T. Eosinophil degranulation in the presence of lung fibroblasts. *International archives of allergy and immunology* **117**, 52–54 (1998).

[104] Takashi, S., Okubo, Y. & Horie, S. Contribution of CD54 to human eosinophil and neutrophil superoxide production. *Journal of Applied Physiology* **91**, 613–622 (2001).

[105] Pazdrak, K., Young, T. W., Stafford, S., Olszewska-Pazdrak, B., Straub, C., Starosta, V., Brasier, A. & Kurosky, A. Cross-talk between ICAM-1 and GM-CSF receptor signaling modulates eosinophil survival and activation. *The Journal of Immunology* **180**, 4182–4190 (2008).

[106] Woodcock, J. M., Bagley, C. J. & Lopez, A. F. The functional basis of granulocyte-macrophage colony stimulating factor, interleukin-3 and interleukin-5 receptor activation, basic and clinical implications. *The international journal of biochemistry & cell biology* **31**, 1017–1025 (1999).

[107] Alenghat, F. J., Baca, Q. J., Rubin, N. T., Pao, L. I., Matozaki, T., Lowell, C. A., Golan, D. E., Neel, B. G. & Swanson, K. D. Macrophages require Skap2 and Sirpα for integrin-stimulated cytoskeletal rearrangement. *Journal of cell science* **125**, 5535–5545 (2012).

[108] Thomas, S. M. & Brugge, J. S. Cellular functions regulated by Src family kinases. *Annual review of cell and developmental biology* **13**, 513–609 (1997).

[109] Lowe, C., Yoneda, T., Boyce, B. F., Chen, H., Mundy, G. R. & Soriano, P. Osteopetrosis in Src-deficient mice is due to an autonomous defect of osteoclasts. *Proceedings of the National Academy of Sciences* **90**, 4485–4489 (1993).

[110] Horne, W., Neff, L., Chatterjee, D., Lomri, A., Levy, J. & Baron, R. Osteoclasts express high levels of pp60c-src in association with intracellular membranes. *The Journal of cell biology* **119**, 1003–1013 (1992).

[111] Koga, S., Yogo, K., Yoshikawa, K., Samori, H., Goto, M., Uchida, T., Ishida, N. & Takeya, T. Physical and functional association of c-Src and adhesion and degranulation promoting adaptor protein (ADAP) in osteoclastogenesis in vitro. *Journal of Biological Chemistry* **280**, 31564–31571 (2005).

[112] Levin, C., Koren, A., Pretorius, E., Rosenberg, N., Shenkman, B., Hauschner, H., Zalman, L., Khayat, M., Salama, I., Elpeleg, O. & others. Deleterious mutation in the FYB gene is associated with congenital autosomal recessive small-platelet thrombocytopenia. *Journal of Thrombosis and Haemostasis* **13**, 1285–1292 (2015).

[113] Tian, J., Pabst, O., Römermann, D., Skubich, S., Förster, R., Beckmann, J., Chen, J.-H. & Hoffmann, M. W. Inactivation of T-cell receptor-mediated integrin activation prolongs allograft survival in ADAP-deficient mice. *Transplantation* **84**, 400–406 (2007).

[114] Tian, J., Rodriguez-Barbosa, J.-I., Pabst, O., Roemermann, D., Foerster, R., Beckmann, J. & Hoffmann, M. W. ADAP deficiency combined with costimulation blockade synergistically protects intestinal allografts. *Transplant International* **23**, 71–79 (2010).

[115] Elster, E. A., Xu, H., Tadaki, D. K., Montgomery, S., Burkly, L. C., Berning, J. D., Baumgartner, R. E., Cruzata, F., Marx, R., Harlan, D. M. & others. Treatment with the humanized CD154-specific monoclonal antibody, hu5C8, prevents acute rejection of primary skin allografts in nonhuman primates. *Transplantation* **72**, 1473–1478 (2001).

[116] Murakami, M., Ito, H., Harada, E., Enoki, T., Sykes, M. & Hamano, K. Long-term survival of xenogeneic heart grafts achieved by costimulatory blockade and transient mixed chimerism. *Transplantation* **82**, 275–281 (2006).

123

[117] McMichael, A. J. HIV vaccines. *Annu. Rev. Immunol.* **24**, 227–255 (2006).

[118] Letvin, N. L., Barouch, D. H. & Montefiori, D. C. Prospects for vaccine protection against HIV-1 infection and AIDS. *Annual review of immunology* **20**, 73–99 (2002).

[119] Imbeault, M., Giguere, K., Ouellet, M. & Tremblay, M. J. Exon level transcriptomic profiling of HIV-1-infected CD4+ T cells reveals virus-induced genes and host environment favorable for viral replication. *PLoS pathogens* **8**, e1002861 (2012).

[120] Kinoshita, S., Su, L., Amano, M., Timmerman, L. A., Kaneshima, H. & Nolan, G. P. The T cell activation factor NF-ATc positively regulates HIV-1 replication and gene expression in T cells. *Immunity* **6**, 235–244 (1997).

[121] Stevenson, M., Stanwick, T., Dempsey, M. & Lamonica, C. HIV-1 replication is controlled at the level of T cell activation and proviral integration. *The EMBO journal* **9**, 1551 (1990).

[122] Wang, J.-H., Kwas, C. & Wu, L. Intercellular adhesion molecule 1 (ICAM-1), but not ICAM-2 and-3, is important for dendritic cell-mediated human immunodeficiency virus type 1 transmission. *Journal of virology* **83**, 4195–4204 (2009).

[123] Sowinski, S., Jolly, C., Berninghausen, O., Purbhoo, M. A., Chauveau, A., Köhler, K., Oddos, S., Eissmann, P., Brodsky, F. M., Hopkins, C. & others. Membrane nanotubes physically connect T cells over long distances presenting a novel route for HIV-1 transmission. *Nature cell biology* **10**, 211–219 (2008).

[124] Martin, N., Welsch, S., Jolly, C., Briggs, J. A., Vaux, D. & Sattentau, Q. J. Virological synapse-mediated spread of human immunodeficiency virus type 1 between T cells is sensitive to entry inhibition. *Journal of virology* **84**, 3516–3527 (2010).

[125] Chen, P., Hübner, W., Spinelli, M. A. & Chen, B. K. Predominant mode of human immunodeficiency virus transfer between T cells is mediated by sustained Env-dependent neutralization-resistant virological synapses. *Journal of virology* **81**, 12582–12595 (2007).

[126] Groot, F., Welsch, S. & Sattentau, Q. J. Efficient HIV-1 transmission from macrophages to T cells across transient virological synapses. *Blood* **111**, 4660–4663 (2008).

[127] Groot, F., Kuijpers, T. W., Berkhout, B. & De Jong, E. C. Dendritic cell-mediated HIV-1 transmission to T cells of LAD-1 patients is impaired due to the defect in LFA-1. *Retrovirology* **3**, 75 (2006).

[128] Jolly, C., Kashefi, K., Hollinshead, M. & Sattentau, Q. J. HIV-1 cell to cell transfer across an Env-induced, actin-dependent synapse. *The Journal of experimental medicine* **199**, 283–293 (2004).

[129] Jolly, C., Booth, N. J. & Neil, S. J. Cell-cell spread of human immunodeficiency virus type 1 overcomes tetherin/BST-2-mediated restriction in T cells. *Journal of virology* **84**, 12185–12199 (2010).

[130] McDonald, D., Wu, L., Bohks, S. M., KewalRamani, V. N., Unutmaz, D. & Hope, T. J. Recruitment of HIV and its receptors to dendritic cell-T cell junctions. *Science* **300**, 1295–1297 (2003).

[131] Wei, B., Lei, H., Abbink, T., Groppelli, E., Lim, D., Thaker, Y., Gao, W., Zhai, R., Wang, J., Lever, A., Jolly, C., Wang, H. & Rudd, C. Immune adaptor ADAP in T cells regulates HIV-1 transcription and cell-cell viral spread via different co-receptors. *Retrovirology* **10** (2013).

[132] Nomi, T., Sho, M., Akahori, T., Hamada, K., Kubo, A., Kanehiro, H., Nakamura, S., Enomoto, K., Yagita, H., Azuma, M. & others. Clinical significance and therapeutic potential of the programmed death-1 ligand/programmed death-1 pathway in human pancreatic cancer. *Clinical Cancer Research* **13**, 2151–2157 (2007).

[133] Hamanishi, J., Mandai, M., Iwasaki, M., Okazaki, T., Tanaka, Y., Yamaguchi, K., Higuchi, T., Yagi, H., Takakura, K., Minato, N. & others. Programmed cell death 1 ligand 1 and tumor-infiltrating CD8+ T lymphocytes are prognostic factors of human ovarian cancer. *Proceedings of the National Academy of Sciences* **104**, 3360–3365 (2007).

[134] Topalian, S. L., Hodi, F. S., Brahmer, J. R., Gettinger, S. N., Smith, D. C., McDermott, D. F., Powderly, J. D., Carvajal, R. D., Sosman, J. A., Atkins, M. B. & others. Safety, activity, and immune correlates of anti–PD-1 antibody in cancer. *New England Journal of Medicine* **366**, 2443–2454 (2012).

[135] Brahmer, J. R., Tykodi, S. S., Chow, L. Q., Hwu, W.-J., Topalian, S. L., Hwu, P., Drake, C. G., Camacho, L. H., Kauh, J., Odunsi, K. & others. Safety and activity of anti–PD-L1 antibody in patients with advanced cancer. *New England Journal of Medicine* **366**, 2455–2465 (2012).

[136] Dotti, G. Blocking PD-1 in cancer immunotherapy. *Blood* **114**, 1457–1458 (2009).

[137] Ha, S.-J., Mueller, S. N., Wherry, E. J., Barber, D. L., Aubert, R. D., Sharpe, A. H., Freeman, G. J. & Ahmed, R. Enhancing therapeutic vaccination by blocking PD-1–mediated inhibitory signals during chronic infection. *The Journal of experimental medicine* **205**, 543–555 (2008).

[138] Miller, S. D., Karpus, W. J. & Davidson, T. S. Experimental autoimmune encephalomyelitis in the mouse. *Current protocols in immunology* 15–1 (2007).

[139] Veldhoen, M., Hocking, R. J., Flavell, R. A. & Stockinger, B. Signals mediated by transforming growth factor-β initiate autoimmune encephalomyelitis, but chronic inflammation is needed to sustain disease. *Nature immunology* **7**, 1151–1156 (2006).

[140] Korn, T., Reddy, J., Gao, W., Bettelli, E., Awasthi, A., Petersen, T. R., Bäckström, B. T., Sobel, R. A., Wucherpfennig, K. W., Strom, T. B. & others. Myelin-specific regulatory T cells accumulate in the CNS but fail to control autoimmune inflammation. *Nature medicine* **13**, 423–431 (2007).

[141] Engelmann, S., Togni, M., Thielitz, A., Reichardt, P., Kliche, S., Reinhold, D., Schraven, B. & Reinhold, A. T Cell–Independent Modulation of Experimental Autoimmune Encephalomyelitis in ADAP-Deficient Mice. *The Journal of Immunology* **191**, 4950–4959 (2013).

[142] Tisch, R. & McDevitt, H. Insulin-dependent diabetes mellitus. *Cell* **85**, 291–297 (1996).

[143] Höglund, P., Mintern, J., Waltzinger, C., Heath, W., Benoist, C. & Mathis, D. Initiation of autoimmune diabetes by developmentally regulated presentation of islet cell antigens in the pancreatic lymph nodes. *The Journal of experimental medicine* **189**, 331–339 (1999).

[144] King, C., Ilic, A., Koelsch, K. & Sarvetnick, N. Homeostatic expansion of T cells during immune insufficiency generates autoimmunity. *Cell* **117**, 265–277 (2004).

[145] Gonzalez, A., Andre-Schmutz, I., Carnaud, C., Mathis, D. & Benoist, C. Damage control, rather than unresponsiveness, effected by protective DX5+ T cells in autoimmune diabetes. *Nature immunology* **2**, 1117–1125 (2001).

[146] Kishimoto, H. & Sprent, J. A defect in central tolerance in NOD mice. *Nature immunology* **2**, 1025–1031 (2001).

[147] Lühder, F., Katz, J., Benoist, C. & Mathis, D. Major histocompatibility complex class II molecules can protect from diabetes by positively selecting T cells with additional specificities. *The Journal of experimental medicine* **187**, 379–387 (1998).

[148] Marleau, A. M. & Sarvetnick, N. T cell homeostasis in tolerance and immunity. *Journal of leukocyte biology* **78**, 575–584 (2005).

[149] Zou, L., Mendez, F., Martin-Orozco, N. & Peterson, E. J. Defective positive selection results in T cell lymphopenia and increased autoimmune diabetes in ADAP-deficient BDC2. 5-C57BL/6 mice. *European journal of immunology* **38**, 986–994 (2008).

[150] Katz, J. D., Wang, B., Haskins, K., Benoist, C. & Mathis, D. Following a diabetogenic T cell from genesis through pathogenesis. *Cell* **74**, 1089–1100 (1993).

[151] Murray, E. G. D., Webb, R. A. & Swann, M. B. R. A disease of rabbits characterised by a large mononuclear leucocytosis, caused by a hitherto undescribed bacillus Bacterium monocytogenes (n. sp.). *The Journal of Pathology and Bacteriology* **29**, 407–439 (1926).

[152] Pirie, J. H. A new disease of veld rodents,Tiger river disease. *Publ S Afr Inst Med Res* **3**, 163–187 (1927).

[153] Carbonnelle, B., Cottin, J., Parvery, F., Chambreuil, G., Kouyoumdjian, S., Le Lirzin, M., Cordier, G. & Vincent, F. [Epidemic of listeriosis in Western France (1975–1976)]. *Revue d'epidemiologie et de sante publique* **26**, 451–467 (1979).

[154] Schlech III, W. F., Lavigne, P. M., Bortolussi, R. A., Allen, A. C., Haldane, E. V., Wort, A. J., Hightower, A. W., Johnson, S. E., King, S. H., Nicholls, E. S. & others. Epidemic listeriosisevidence for transmission by food. *New england journal of medicine* **308**, 203–206 (1983).

[155] Stavru, F., Archambaud, C. & Cossart, P. Cell biology and immunology of Listeria monocytogenes infections: novel insights. *Immunological reviews* **240**, 160–184 (2011).

[156] Kuo, S. C. & McGrath, J. L. Steps and fluctuations of Listeria monocytogenes during actin-based motility. *Nature* **407**, 1026–1029 (2000).

[157] Pamer, E. G. Immune responses to Listeria monocytogenes. *Nature Reviews Immunology* **4**, 812–823 (2004).

[158] Crim, S. M., Iwamoto, M., Huang, J. Y., Griffin, P. M., Gilliss, D., Cronquist, A. B., Cartter, M., Tobin-DAngelo, M., Blythe, D., Smith, K. & others. Incidence and trends of infection with pathogens transmitted commonly through foodFoodborne Diseases Active Surveillance Network, 10 US sites, 2006–2013. *MMWR Morb Mortal Wkly Rep* **63**, 328–32 (2014).

[159] Scallan, E., Hoekstra, R. M., Angulo, F. J., Tauxe, R. V., Widdowson, M.-A., Roy, S. L., Jones, J. L. & Griffin, P. M. Foodborne illness acquired in the United Statesmajor pathogens. *Emerg Infect Dis* **17** (2011).

[160] Watson, R. & others. Listeriosis remains a cause for concern in Europe. *BMJ* **338** (2009).

[161] Mackaness, G. Cellular resistance to infection. *The Journal of experimental medicine* **116**, 381–406 (1962).

[162] Mackaness, G. The immunological basis of acquired cellular resistance. *The Journal of experimental medicine* **120**, 105–120 (1964).

[163] Bierne, H., Sabet, C., Personnic, N. & Cossart, P. Internalins: a complex family of leucine-rich repeat-containing proteins in Listeria monocytogenes. *Microbes and Infection* **9**, 1156–1166 (2007).

[164] Mengaud, J., Ohayon, H., Gounon, P., Mège, R.-M. & Cossart, P. E-cadherin is the receptor for internalin, a surface protein required for entry of L. monocytogenes into epithelial cells. *Cell* **84**, 923–932 (1996).

[165] Shen, Y., Naujokas, M., Park, M. & Ireton, K. InlB-dependent internalization of Listeria is mediated by the Met receptor tyrosine kinase. *Cell* **103**, 501–510 (2000).

[166] Lecuit, M., Dramsi, S., Gottardi, C., Fedor-Chaiken, M., Gumbiner, B. & Cossart, P. A single amino acid in E-cadherin responsible for host specificity towards the human pathogen Listeria monocytogenes. *The EMBO journal* **18**, 3956–3963 (1999).

[167] Veiga, E. & Cossart, P. Listeria hijacks the clathrin-dependent endocytic machinery to invade mammalian cells. *Nature cell biology* **7**, 894–900 (2005).

[168] Glomski, I. J., Gedde, M. M., Tsang, A. W., Swanson, J. A. & Portnoy, D. A. The Listeria monocytogenes hemolysin has an acidic pH optimum to compartmentalize activity and prevent damage to infected host cells. *The Journal of cell biology* **156**, 1029–1038 (2002).

[169] Welch, M., Iwamatsu, A. & Mitchison, T. Actin polymerization is induced by Arp2/3 protein complex at the surface of Listeria monocytogenes. *Nature* (1996).

[170] Gouin, E., Welch, M. D. & Cossart, P. Actin-based motility of intracellular pathogens. *Current opinion in microbiology* **8**, 35–45 (2005).

[171] Kocks, C., Gouin, E., Tabouret, M., Berche, P., Ohayon, H. & Cossart, P. L. monocytogenes-induced actin assembly requires the actA gene product, a surface protein. *Cell* **68**, 521–531 (1992).

[172] Kocks, C., Hellio, R., Gounon, P., Ohayon, H. & Cossart, P. Polarized distribution of Listeria monocytogenes surface protein ActA at the site of directional actin assembly. *Journal of cell science* **105**, 699–710 (1993).

[173] Robbins, J. R., Skrzypczynska, K. M., Zeldovich, V. B., Kapidzic, M. & Bakardjiev, A. I. Placental syncytiotrophoblast constitutes a major barrier to vertical transmission of Listeria monocytogenes. *PLoS Pathog* **6**, e1000732 (2010).

[174] Drevets, D. A., Jelinek, T. A. & Freitag, N. E. Listeria monocytogenes-infected phagocytes can initiate central nervous system infection in mice. *Infection and immunity* **69**, 1344–1350 (2001).

[175] Unanue, E. R. Studies in listeriosis show the strong symbiosis between the innate cellular system and the T-cell response. *Immunological reviews* **158**, 11–25 (1997).

[176] Bancroft, G. J., Schreiber, R. D. & Unanue, E. R. Natural immunity: AT-cell-independent pathway of macrophage activation, defined in the scid mouse. *Immunological reviews* **124**, 5–24 (1991).

[177] Conlan, J. Early pathogenesis of Listeria monocytogenes infection in the mouse spleen. *Journal of medical microbiology* **44**, 295–302 (1996).

[178] Zenewicz, L. A. & Shen, H. Innate and adaptive immune responses to Listeria monocytogenes: a short overview. *Microbes and Infection* **9**, 1208–1215 (2007).

[179] Harty, J. T. & Bevant, M. J. Specific immunity to Listeria monocytogenes in the absence of IFNγ. *Immunity* **3**, 109–117 (1995).

[180] Buchmeier, N. A. & Schreiber, R. D. Requirement of endogenous interferon-gamma production for resolution of Listeria monocytogenes infection. *Proceedings of the National Academy of Sciences* **82**, 7404–7408 (1985).

[181] Tripp, C. S., Wolf, S. F. & Unanue, E. R. Interleukin 12 and tumor necrosis factor alpha are costimulators of interferon gamma production by natural killer cells in severe combined immunodeficiency mice with listeriosis, and interleukin 10 is a physiologic antagonist. *Proceedings of the National Academy of Sciences* **90**, 3725–3729 (1993).

[182] Viegas, N., Andzinski, L., Wu, C.-F., Komoll, R.-M., Gekara, N., Dittmar, K. E., Weiss, S. & Jablonska, J. IFN-γ production by CD27+ NK cells exacerbates Listeria monocytogenes infection in mice by inhibiting granulocyte mobilization. *European journal of immunology* **43**, 2626–2637 (2013).

[183] Xanthoulea, S., Pasparakis, M., Kousteni, S., Brakebusch, C., Wallach, D., Bauer, J., Lassmann, H. & Kollias, G. Tumor necrosis factor (TNF) receptor shedding controls thresholds of innate immune activation that balance opposing TNF functions in infectious and inflammatory diseases. *The Journal of experimental medicine* **200**, 367–376 (2004).

[184] Rothe, J., Lesslauer, W., Lötscher, H., Lang, Y., Koebel, P., Köntgen, F., Althage, A., Zinkernagel, R., Steinmetz, M. & Bluethmann, H. Mice lacking the tumour necrosis factor receptor 1 are resistant to TNF-mediated toxicity but highly susceptible to infection by Listeria monocytogenes. *Nature* **364**, 798–802 (1993).

[185] Pfeffer, K., Matsuyama, T., Kündig, T. M., Wakeham, A., Kishihara, K., Shahinian, A., Wiegmann, K., Ohashi, P. S., Krönke, M. & Mak, T. W. Mice deficient for the 55 kd tumor necrosis factor receptor are resistant to endotoxic shock, yet succumb to L. monocytogenes infection. *Cell* **73**, 457–467 (1993).

[186] Stockinger, S., Materna, T., Stoiber, D., Bayr, L., Steinborn, R., Kolbe, T., Unger, H., Chakraborty, T., Levy, D. E., Müller, M. & others. Production of type I IFN sensitizes macrophages to cell death induced by Listeria monocytogenes. *The Journal of Immunology* **169**, 6522–6529 (2002).

[187] Carrero, J. A., Calderon, B. & Unanue, E. R. Type I interferon sensitizes lymphocytes to apoptosis and reduces resistance to Listeria infection. *The Journal of experimental medicine* **200**, 535–540 (2004).

[188] O'Connel, R., Saha, S., Vaidya, S., Bruhn, K., Miranda, G., Zarnegar, B., Perry, A., Nguyen, B., Lane, T. & Taniguchi, T. Type I interferon production enhances susceptibility to Listeria monocytogenes. *J. Exp. Med.* **200**, 437–445 (2004).

[189] Auerbuch, V., Brockstedt, D. G., Meyer-Morse, N., O'Riordan, M. & Portnoy, D. A. Mice lacking the type I interferon receptor are resistant to Listeria monocytogenes. *The Journal of experimental medicine* **200**, 527–533 (2004).

[190] Segal, A. W. How neutrophils kill microbes. *Annual review of immunology* **23**, 197 (2005).

[191] Serbina, N. V., Salazar-Mather, T. P., Biron, C. A., Kuziel, W. A. & Pamer, E. G. TNF/iNOS-producing dendritic cells mediate innate immune defense against bacterial infection. *Immunity* **19**, 59–70 (2003).

[192] Endres, R., Luz, A., Schulze, H., Neubauer, H., Fütterer, A., Holland, S. M., Wagner, H. & Pfeffer, K. Listeriosis in p47phox-/- and TRp55-/- mice: protection despite absence of ROI and susceptibility despite presence of RNI. *Immunity* **7**, 419–432 (1997).

[193] Shiloh, M. U., MacMicking, J. D., Nicholson, S., Brause, J. E., Potter, S., Marino, M., Fang, F., Dinauer, M. & Nathan, C. Phenotype of mice and macrophages deficient in both phagocyte oxidase and inducible nitric oxide synthase. *Immunity* **10**, 29–38 (1999).

[194] Neuenhahn, M., Kerksiek, K. M., Nauerth, M., Suhre, M. H., Schiemann, M., Gebhardt, F. E., Stemberger, C., Panthel, K., Schröder, S., Chakraborty, T. & others. CD8α+ dendritic cells are required for efficient entry of Listeria monocytogenes into the spleen. *Immunity* **25**, 619–630 (2006).

[195] Waite, J. C., Leiner, I., Lauer, P., Rae, C. S., Barbet, G., Zheng, H., Portnoy, D. A., Pamer, E. G. & Dustin, M. L. Dynamic imaging of the effector immune response to listeria infection in vivo. *PLoS Pathog* **7**, e1001326 (2011).

[196] Brinkmann, V., Reichard, U., Goosmann, C., Fauler, B., Uhlemann, Y., Weiss, D. S., Weinrauch, Y. & Zychlinsky, A. Neutrophil extracellular traps kill bacteria. *science* **303**, 1532–1535 (2004).

[197] Carr, K. D., Sieve, A. N., Indramohan, M., Break, T. J., Lee, S. & Berg, R. E. Specific depletion reveals a novel role for neutrophil-mediated protection in the liver during Listeria monocytogenes infection. *European journal of immunology* **41**, 2666–2676 (2011).

[198] Miyamoto, M., Emoto, M., Emoto, Y., Brinkmann, V., Yoshizawa, I., Seiler, P., Aichele, P., Kita, E. & Kaufmann, S. H. Neutrophilia in LFA-1-deficient mice confers resistance to listeriosis: possible contribution of granulocyte-colony-stimulating factor and IL-17. *The Journal of Immunology* **170**, 5228–5234 (2003).

[199] Leist, M., Gantner, F., Bohlinger, I., Germann, P. G., Tiegs, G. & Wendel, A. Murine hepatocyte apoptosis induced in vitro and in vivo by TNF-alpha requires transcriptional arrest. *The Journal of Immunology* **153**, 1778–1788 (1994).

[200] Leist, M., Gantner, F., Jilg, S. & Wendel, A. Activation of the 55 kDa TNF receptor is necessary and sufficient for TNF-induced liver failure, hepatocyte apoptosis, and nitrite release. *The Journal of Immunology* **154**, 1307–1316 (1995).

[201] Yin, J. & Ferguson, T. A. Identification of an IFN-γ-producing neutrophil early in the response to Listeria monocytogenes. *The Journal of Immunology* **182**, 7069–7073 (2009).

[202] Hsieh, C.-S., Macatonia, S. E., Tripp, C. S., Wolf, S. F., O'Garra, A. & Murphy, K. M. Development of TH1 CD4+ T cells through IL-12 produced by Listeria-induced macrophages. *Science* **260**, 547–549 (1993).

[203] Havell, E. A. Production of tumor necrosis factor during murine listeriosis. *The Journal of Immunology* **139**, 4225–4231 (1987).

[204] Serbina, N. V., Kuziel, W., Flavell, R., Akira, S., Rollins, B. & Pamer, E. G. Sequential MyD88-independent and-dependent activation of innate immune responses to intracellular bacterial infection. *Immunity* **19**, 891–901 (2003).

[205] Kurihara, T., Warr, G., Loy, J. & Bravo, R. Defects in macrophage recruitment and host defense in mice lacking the CCR2 chemokine receptor. *The Journal of experimental medicine* **186**, 1757–1762 (1997).

[206] MacMicking, J. D., Nathan, C., Hom, G., Chartrain, N., Fletcher, D. S., Trumbauer, M., Stevens, K., Xie, Q.-w., Sokol, K., Hutchinson, N. & others. Altered responses to bacterial infection and endotoxic shock in mice lacking inducible nitric oxide synthase. *Cell* **81**, 641–650 (1995).

[207] Muraille, E., Giannino, R., Guirnalda, P., Leiner, I., Jung, S., Pamer, E. G. & Lauvau, G. Distinct in vivo dendritic cell activation by live versus killed Listeria monocytogenes. *European journal of immunology* **35**, 1463–1471 (2005).

[208] Aoshi, T., Carrero, J. A., Konjufca, V., Koide, Y., Unanue, E. R. & Miller, M. J. The cellular niche of Listeria monocytogenes infection changes rapidly in the spleen. *European journal of immunology* **39**, 417–425 (2009).

129

[209] Verschoor, A., Neuenhahn, M., Navarini, A. A., Graef, P., Plaumann, A., Seidlmeier, A., Nieswandt, B., Massberg, S., Zinkernagel, R. M., Hengartner, H. & others. A platelet-mediated system for shuttling blood-borne bacteria to CD8 [alpha]+ dendritic cells depends on glycoprotein GPIb and complement C3. *Nature immunology* **12**, 1194–1201 (2011).

[210] Shen, Y., Kawamura, I., Nomura, T., Tsuchiya, K., Hara, H., Dewamitta, S. R., Sakai, S., Qu, H., Daim, S., Yamamoto, T. & others. Toll-like receptor 2-and MyD88-dependent phosphatidylinositol 3-kinase and Rac1 activation facilitates the phagocytosis of Listeria monocytogenes by murine macrophages. *Infection and immunity* **78**, 2857–2867 (2010).

[211] Seki, E., Tsutsui, H., Tsuji, N. M., Hayashi, N., Adachi, K., Nakano, H., Futatsugi-Yumikura, S., Takeuchi, O., Hoshino, K., Akira, S. & others. Critical roles of myeloid differentiation factor 88-dependent proin-flammatory cytokine release in early phase clearance of Listeria monocytogenes in mice. *The Journal of Immunology* **169**, 3863–3868 (2002).

[212] Edelson, B. T. & Unanue, E. R. MyD88-dependent but Toll-like receptor 2-independent innate immunity to Listeria: no role for either in macrophage listericidal activity. *The Journal of Immunology* **169**, 3869–3875 (2002).

[213] Özören, N., Masumoto, J., Franchi, L., Kanneganti, T.-D., Body-Malapel, M., Ertürk, İ., Jagirdar, R., Zhu, L., Inohara, N., Bertin, J. & others. Distinct roles of TLR2 and the adaptor ASC in IL-1β/IL-18 secretion in response to Listeria monocytogenes. *The Journal of Immunology* **176**, 4337–4342 (2006).

[214] Ting, J. P. & Davis, B. K. CATERPILLER: a novel gene family important in immunity, cell death, and diseases. *Annu. Rev. Immunol.* **23**, 387–414 (2005).

[215] Inohara, N., Ogura, Y., Fontalba, A., Gutierrez, O., Pons, F., Crespo, J., Fukase, K., Inamura, S., Kusumoto, S., Hashimoto, M. & others. Host Recognition of Bacterial Muramyl Dipeptide Mediated through NOD2 IMPLICATIONS FOR CROHN S DISEASE. *Journal of Biological Chemistry* **278**, 5509–5512 (2003).

[216] Kobayashi, K. S., Chamaillard, M., Ogura, Y., Henegariu, O., Inohara, N., Nunez, G. & Flavell, R. A. Nod2-dependent regulation of innate and adaptive immunity in the intestinal tract. *Science* **307**, 731–734 (2005).

[217] Mariathasan, S., Weiss, D. S., Newton, K., McBride, J., O'Rourke, K., Roose-Girma, M., Lee, W. P., Weinrauch, Y., Monack, D. M. & Dixit, V. M. Cryopyrin activates the inflammasome in response to toxins and ATP. *Nature* **440**, 228–232 (2006).

[218] Kang, S.-J., Liang, H.-E., Reizis, B. & Locksley, R. M. Regulation of hierarchical clustering and activation of innate immune cells by dendritic cells. *Immunity* **29**, 819–833 (2008).

[219] Humann, J., Bjordahl, R., Andreasen, K. & Lenz, L. L. Expression of the p60 autolysin enhances NK cell activation and is required for Listeria monocytogenes expansion in IFN-γ-responsive mice. *The Journal of Immunology* **178**, 2407–2414 (2007).

[220] Lucas, M., Schachterle, W., Oberle, K., Aichele, P. & Diefenbach, A. Dendritic cells prime natural killer cells by trans-presenting interleukin 15. *Immunity* **26**, 503–517 (2007).

[221] Humann, J. & Lenz, L. L. Activation of naive NK cells in response to Listeria monocytogenes requires IL-18 and contact with infected dendritic cells. *The Journal of Immunology* **184**, 5172–5178 (2010).

[222] Schmidt, R. L., Filak, H. C., Lemon, J. D., Potter, T. A. & Lenz, L. L. A LysM and SH3-domain containing region of the Listeria monocytogenes p60 protein stimulates accessory cells to promote activation of host NK cells. *PLoS Pathog* **7**, e1002368 (2011).

[223] Teixeira, H. C. & Kaufmann, S. Role of NK1. 1+ cells in experimental listeriosis. NK1+ cells are early IFN-gamma producers but impair resistance to Listeria monocytogenes infection. *The Journal of Immunology* **152**, 1873–1882 (1994).

[224] Williams, M. A., Schmidt, R. L. & Lenz, L. L. Early events regulating immunity and pathogenesis during Listeria monocytogenes infection. *Trends in immunology* **33**, 488–495 (2012).

[225] Hao, J., Liu, R., Piao, W., Zhou, Q., Vollmer, T. L., Campagnolo, D. I., Xiang, R., La Cava, A., Van Kaer, L. & Shi, F.-D. Central nervous system (CNS)–resident natural killer cells suppress Th17 responses and CNS autoimmune pathology. *The Journal of experimental medicine* **207**, 1907–1921 (2010).

[226] Belz, G. T., Shortman, K., Bevan, M. J. & Heath, W. R. CD8α+ dendritic cells selectively present MHC class I-restricted noncytolytic viral and intracellular bacterial antigens in vivo. *The Journal of Immunology* **175**, 196–200 (2005).

[227] Medzhitov, R. Toll-like receptors and innate immunity. *Nature Reviews Immunology* **1**, 135–145 (2001).

[228] Jung, S., Unutmaz, D., Wong, P., Sano, G.-I., De los Santos, K., Sparwasser, T., Wu, S., Vuthoori, S., Ko, K., Zavala, F. & others. In vivo depletion of CD11c+ dendritic cells abrogates priming of CD8+ T cells by exogenous cell-associated antigens. *Immunity* **17**, 211–220 (2002).

[229] Bhardwaj, V., Kanagawa, O., Swanson, P. E. & Unanue, E. R. Chronic Listeria infection in SCID mice: requirements for the carrier state and the dual role of T cells in transferring protection or suppression. *The Journal of Immunology* **160**, 376–384 (1998).

[230] Moon, J. J., Chu, H. H., Pepper, M., McSorley, S. J., Jameson, S. C., Kedl, R. M. & Jenkins, M. K. Naive CD4+ T cell frequency varies for different epitopes and predicts repertoire diversity and response magnitude. *Immunity* **27**, 203–213 (2007).

[231] Casrouge, A., Beaudoing, E., Dalle, S., Pannetier, C., Kanellopoulos, J. & Kourilsky, P. Size estimate of the $\alpha\beta$ TCR repertoire of naive mouse splenocytes. *The Journal of Immunology* **164**, 5782–5787 (2000).

[232] Blattman, J. N., Antia, R., Sourdive, D. J., Wang, X., Kaech, S. M., Murali-Krishna, K., Altman, J. D. & Ahmed, R. Estimating the precursor frequency of naive antigen-specific CD8 T cells. *The Journal of experimental medicine* **195**, 657–664 (2002).

[233] Murali-Krishna, K., Altman, J. D., Suresh, M., Sourdive, D. J., Zajac, A. J., Miller, J. D., Slansky, J. & Ahmed, R. Counting antigen-specific CD8 T cells: a reevaluation of bystander activation during viral infection. *Immunity* **8**, 177–187 (1998).

[234] Butz, E. A. & Bevan, M. J. Massive expansion of antigen-specific CD8+ T cells during an acute virus infection. *Immunity* **8**, 167–175 (1998).

[235] Badovinac, V. P. & Harty, J. T. CD8+ T-cell homeostasis after infection: setting the curve. *Microbes and infection* **4**, 441–447 (2002).

[236] Mercado, R., Vijh, S., Allen, S. E., Kerksiek, K., Pilip, I. M. & Pamer, E. G. Early programming of T cell populations responding to bacterial infection. *The Journal of Immunology* **165**, 6833–6839 (2000).

[237] Pearce, E. L. & Shen, H. Generation of CD8 T cell memory is regulated by IL-12. *The Journal of Immunology* **179**, 2074–2081 (2007).

[238] Badovinac, V. P., Tvinnereim, A. R. & Harty, J. T. Regulation of antigen-specific CD8+ T cell homeostasis by perforin and interferon-γ. *Science* **290**, 1354–1357 (2000).

[239] White, D. W., Badovinac, V. P., Kollias, G. & Harty, J. T. Cutting edge: antilisterial activity of CD8+ T cells derived from TNF-deficient and TNF/perforin double-deficient mice. *The Journal of Immunology* **165**, 5–9 (2000).

[240] Harty, J. & Bevan, M. Specific immunity to listeria monocytogenes in the absence of IFN gamma. *Immunity* **3**, 109–117 (1995).

[241] White, D. W. & Harty, J. T. Perforin-deficient CD8+ T cells provide immunity to Listeria monocytogenes by a mechanism that is independent of CD95 and IFN-γ but requires TNF-α. *The Journal of Immunology* **160**, 898–905 (1998).

[242] Condotta, S. A., Richer, M. J., Badovinac, V. P. & Harty, J. T. 5 Probing CD8 T Cell Responses with Listeria monocytogenes Infection. *Advances in immunology* **113**, 51 (2012).

[243] Badovinac, V. P., Porter, B. B. & Harty, J. T. CD8+ T cell contraction is controlled by early inflammation. *Nature immunology* **5**, 809–817 (2004).

[244] Porter, B. B. & Harty, J. T. The onset of CD8+-T-cell contraction is influenced by the peak of Listeria monocytogenes infection and antigen display. *Infection and immunity* **74**, 1528–1536 (2006).

[245] Schmidt, N. W., Butler, N. S., Badovinac, V. P. & Harty, J. T. Extreme CD8 T cell requirements for anti-malarial liver-stage immunity following immunization with radiation attenuated sporozoites. *PLoS Pathog* **6**, e1000998 (2010).

[246] Harty, J. T. & Badovinac, V. P. Shaping and reshaping CD8+ T-cell memory. *Nature Reviews Immunology* **8**, 107–119 (2008).

[247] Kaech, S. M., Hemby, S., Kersh, E. & Ahmed, R. Molecular and functional profiling of memory CD8 T cell differentiation. *Cell* **111**, 837–851 (2002).

[248] Schmidt, N. W., Podyminogin, R. L., Butler, N. S., Badovinac, V. P., Tucker, B. J., Bahjat, K. S., Lauer, P., Reyes-Sandoval, A., Hutchings, C. L., Moore, A. C. & others. Memory CD8 T cell responses exceeding a large but definable threshold provide long-term immunity to malaria. *Proceedings of the National Academy of Sciences* **105**, 14017–14022 (2008).

[249] Wherry, E. J., Teichgräber, V., Becker, T. C., Masopust, D., Kaech, S. M., Antia, R., Von Andrian, U. H. & Ahmed, R. Lineage relationship and protective immunity of memory CD8 T cell subsets. *Nature immunology* **4**, 225–234 (2003).

[250] Badovinac, V. P. & Harty, J. T. Programming, demarcating, and manipulating CD8+ T-cell memory. *Immunological reviews* **211**, 67–80 (2006).

[251] Sallusto, F., Lenig, D., Förster, R., Lipp, M. & Lanzavecchia, A. Two subsets of memory T lymphocytes with distinct homing potentials and effector functions. *Nature* **401**, 708–712 (1999).

[252] Kursar, M., Bonhagen, K., Köhler, A., Kamradt, T., Kaufmann, S. H. & Mittrücker, H.-W. Organ-specific CD4+ T cell response during Listeria monocytogenes infection. *The Journal of Immunology* **168**, 6382–6387 (2002).

[253] Shedlock, D. J., Whitmire, J. K., Tan, J., MacDonald, A. S., Ahmed, R. & Shen, H. Role of CD4 T cell help and costimulation in CD8 T cell responses during Listeria monocytogenes infection. *The Journal of Immunology* **170**, 2053–2063 (2003).

[254] Mielke, M., Ehlers, S. & Hahn, H. T cell subsets in DTH, protection and granuloma formation in primary and secondary Listeria infection in mice: superior role of Lyt-2+ cells in acquired immunity. *Immunology letters* **19**, 211–215 (1988).

[255] Daugelat, S., Ladel, C. H., Schoel, B. & Kaufmann, S. Antigen-specific T-cell responses during primary and secondary Listeria monocytogenes infection. *Infection and immunity* **62**, 1881–1888 (1994).

[256] Sun, J. C. & Bevan, M. J. Defective CD8 T cell memory following acute infection without CD4 T cell help. *Science* **300**, 339–342 (2003).

[257] Sun, J. C., Williams, M. A. & Bevan, M. J. CD4+ T cells are required for the maintenance, not programming, of memory CD8+ T cells after acute infection. *Nature immunology* **5**, 927–933 (2004).

[258] Janssen, E. M., Droin, N. M., Lemmens, E. E., Pinkoski, M. J., Bensinger, S. J., Ehst, B. D., Griffith, T. S., Green, D. R. & Schoenberger, S. P. CD4+ T-cell help controls CD8+ T-cell memory via TRAIL-mediated activation-induced cell death. *Nature* **434**, 88–93 (2005).

[259] Kursar, M., Bonhagen, K., Fensterle, J., Köhler, A., Hurwitz, R., Kamradt, T., Kaufmann, S. H. & Mittrücker, H.-W. Regulatory CD4+ CD25+ T cells restrict memory CD8+ T cell responses. *The Journal of experimental medicine* **196**, 1585–1592 (2002).

[260] Ertelt, J. M., Rowe, J. H., Johanns, T. M., Lai, J. C., McLachlan, J. B. & Way, S. S. Selective priming and expansion of antigen-specific Foxp3- CD4+ T cells during Listeria monocytogenes infection. *The Journal of Immunology* **182**, 3032–3038 (2009).

[261] Ochsenbein, A. F., Fehr, T., Lutz, C., Suter, M., Brombacher, F., Hengartner, H. & Zinkernagel, R. M. Control of early viral and bacterial distribution and disease by natural antibodies. *Science* **286**, 2156–2159 (1999).

[262] Shen, H., Whitmire, J. K., Fan, X., Shedlock, D. J., Kaech, S. M. & Ahmed, R. A specific role for B cells in the generation of CD8 T cell memory by recombinant Listeria monocytogenes. *The Journal of Immunology* **170**, 1443–1451 (2003).

[263] Cotter, M. J. & Muruve, D. A. Isolation of neutrophils from mouse liver: A novel method to study effector leukocytes during inflammation. *J Immunol Methods* **312**, 68–78 (2006).

[264] Weston, S. A. & Parish, C. R. New fluorescent dyes for lymphocyte migration studies. Analysis by flow cytometry and fluorescence microscopy. *J Immunol Methods* **133**, 87–97 (1990).

[265] Lyons, A. B. & Parish, C. R. Determination of lymphocyte division by flow cytometry. *J Immunol Methods* **171**, 131–137 (1994).

[266] Oehen, S. & Brduscha-Riem, K. Differentiation of naive CTL to effector and memory CTL: correlation of effector function with phenotype and cell division. *The Journal of Immunology* **161**, 5338–5346 (1998).

[267] Giraldo, J., Vivas, N. M., Vila, E. & Badia, A. Assessing the (a) symmetry of concentration-effect curves: empirical versus mechanistic models. *Pharmacology & therapeutics* **95**, 21–45 (2002).

[268] Hentati, E., Gruy, F., Iobagiu, C., Lambert, C. & others. Variability of CD3 membrane expression and T cell activation capacity. *Cytometry Part B: Clinical Cytometry* **78**, 105–114 (2010).

[269] Lambert, C. & Genin, C. CD3 bright lymphocyte population reveal $\gamma\delta$ T cells. *Cytometry Part B: Clinical Cytometry* **61**, 45–53 (2004).

[270] Valle, A., Barbagiovanni, G., Jofra, T., Stabilini, A., Perol, L., Baeyens, A., Anand, S., Cagnard, N., Gagliani, N., Piaggio, E. & others. Heterogeneous CD3 Expression Levels in Differing T Cell Subsets Correlate with the In Vivo Anti-CD3–Mediated T Cell Modulation. *The Journal of Immunology* **194**, 2117–2127 (2015).

[271] Lettau, M., Kliche, S., Kabelitz, D. & Janssen, O. The adapter proteins ADAP and Nck cooperate in T cell adhesion. *Molecular immunology* **60**, 72–79 (2014).

[272] Horn, J., Wang, X., Reichardt, P., Stradal, T. E., Warnecke, N., Simeoni, L., Gunzer, M., Yablonski, D., Schraven, B. & Kliche, S. Src homology 2-domain containing leukocyte-specific phosphoprotein of 76 kDa is mandatory for TCR-mediated inside-out signaling, but dispensable for CXCR4-mediated LFA-1 activation, adhesion, and migration of T cells. *The Journal of Immunology* **183**, 5756–5767 (2009).

[273] Bender, B. S., Croghan, T., Zhang, L. & Small, P. Transgenic mice lacking class I major histocompatibility complex-restricted T cells have delayed viral clearance and increased mortality after influenza virus challenge. *The Journal of experimental medicine* **175**, 1143–1145 (1992).

[274] Topham, D., Tripp, R. & Doherty, P. CD8+ T cells clear influenza virus by perforin or Fas-dependent processes. *The Journal of Immunology* **159**, 5197–5200 (1997).

[275] Pasche, B., Kalaydjiev, S., Franz, T. J., Kremmer, E., Gailus-Durner, V., Fuchs, H., de Angelis, M. H., Lengeling, A. & Busch, D. H. Sex-dependent susceptibility to Listeria monocytogenes infection is mediated by differential interleukin-10 production. *Infection and immunity* **73**, 5952–5960 (2005).

[276] Fernández, I., Peña, A., Del Teso, N., Pérez, V. & Rodríguez-Cuesta, J. Clinical biochemistry parameters in C57BL/6J mice after blood collection from the submandibular vein and retroorbital plexus. *Journal of the American Association for Laboratory Animal Science* **49**, 202–206 (2010).

[277] Chiossone, L., Chaix, J., Fuseri, N., Roth, C., Vivier, E. & Walzer, T. Maturation of mouse NK cells is a 4-stage developmental program. *Blood* **113**, 5488–5496 (2009).

[278] Seder, R. A. & Ahmed, R. Similarities and differences in CD4+ and CD8+ effector and memory T cell generation. *Nature immunology* **4**, 835–842 (2003).

[279] Foulds, K. E., Zenewicz, L. A., Shedlock, D. J., Jiang, J., Troy, A. E. & Shen, H. Cutting edge: CD4 and CD8 T cells are intrinsically different in their proliferative responses. *The Journal of Immunology* **168**, 1528–1532 (2002).

[280] Rabenstein, H., Behrendt, A. C., Ellwart, J. W., Naumann, R., Horsch, M., Beckers, J. & Obst, R. Differential kinetics of antigen dependency of CD4+ and CD8+ T cells. *The Journal of Immunology* **192**, 3507–3517 (2014).

[281] Schrum, A. G. & Turka, L. A. The proliferative capacity of individual naive CD4+ T cells is amplified by prolonged T cell antigen receptor triggering. *The Journal of experimental medicine* **196**, 793–803 (2002).

[282] Celli, S., Lemaître, F. & Bousso, P. Real-time manipulation of T cell-dendritic cell interactions in vivo reveals the importance of prolonged contacts for CD4+ T cell activation. *Immunity* **27**, 625–634 (2007).

[283] Obst, R., van Santen, H.-M., Mathis, D. & Benoist, C. Antigen persistence is required throughout the expansion phase of a CD4+ T cell response. *The Journal of experimental medicine* **201**, 1555–1565 (2005).

[284] Williams, M. A. & Bevan, M. J. Shortening the infectious period does not alter expansion of CD8 T cells but diminishes their capacity to differentiate into memory cells. *The Journal of Immunology* **173**, 6694–6702 (2004).

[285] Bevan, M. J. & Fink, P. J. The CD8 response on autopilot. *Nature immunology* **2**, 381–382 (2001).

[286] Kaech, S. M. & Ahmed, R. Memory CD8+ T cell differentiation: initial antigen encounter triggers a developmental program in naive cells. *Nature immunology* **2**, 415–422 (2001).

[287] Masopust, D., Kaech, S. M., Wherry, E. J. & Ahmed, R. The role of programming in memory T-cell development. *Current opinion in immunology* **16**, 217–225 (2004).

[288] Shimonkevitz, R., Colon, S., Kappler, J. W., Marrack, P. & Grey, H. M. Antigen recognition by H-2-restricted T cells. II. A tryptic ovalbumin peptide that substitutes for processed antigen. *The Journal of Immunology* **133**, 2067–2074 (1984).

[289] Barnden, M. J., Allison, J., Heath, W. R. & Carbone, F. R. Defective TCR expression in transgenic mice constructed using cDNA-based alpha-and beta-chain genes under the control of heterologous regulatory elements. *Immunology and cell biology* **76**, 34–40 (1998).

[290] Robertson, J. M., Jensen, P. E. & Evavold, B. D. DO11. 10 and OT-II T cells recognize a C-terminal ovalbumin 323–339 epitope. *The Journal of Immunology* **164**, 4706–4712 (2000).

[291] Penix, L., Weaver, W. M., Pang, Y., Young, H. & Wilson, C. Two essential regulatory elements in the human interferon gamma promoter confer activation specific expression in T cells. *The Journal of experimental medicine* **178**, 1483–1496 (1993).

[292] Sullivan, B. M., Juedes, A., Szabo, S. J., von Herrath, M. & Glimcher, L. H. Antigen-driven effector CD8 T cell function regulated by T-bet. *Proceedings of the National Academy of Sciences* **100**, 15818–15823 (2003).

[293] Kiani, A., Garcı a Cózar, F. J., Habermann, I., Laforsch, S., Aebischer, T., Ehninger, G. & Rao, A. Regulation of interferon-γ gene expression by nuclear factor of activated T cells. *Blood* **98**, 1480–1488 (2001).

[294] Sica, A., Dorman, L., Viggiano, V., Cippitelli, M., Ghosh, P., Rice, N. & Young, H. A. Interaction of NF-κB and NFAT with the interferon-γ promoter. *Journal of Biological Chemistry* **272**, 30412–30420 (1997).

[295] Sweetser, M. T., Hoey, T., Sun, Y.-L., Weaver, W. M., Price, G. A. & Wilson, C. B. The roles of nuclear factor of activated T cells and ying-yang 1 in activation-induced expression of the interferon-γ promoter in T cells. *Journal of Biological Chemistry* **273**, 34775–34783 (1998).

[296] Xu, X., Sun, Y.-L. & Hoey, T. Cooperative DNA binding and sequence-selective recognition conferred by the STAT amino-terminal domain. *Science* **273**, 794–797 (1996).

[297] Ye, J., Cippitelli, M., Dorman, L., Ortaldo, J. R. & Young, H. A. The nuclear factor YY1 suppresses the human gamma interferon promoter through two mechanisms: inhibition of AP1 binding and activation of a silencer element. *Molecular and Cellular Biology* **16**, 4744–4753 (1996).

[298] Huang, L.-R., Wohlleber, D., Reisinger, F., Jenne, C. N., Cheng, R.-L., Abdullah, Z., Schildberg, F. A., Odenthal, M., Dienes, H.-P., van Rooijen, N. & others. Intrahepatic myeloid-cell aggregates enable local proliferation of CD8+ T cells and successful immunotherapy against chronic viral liver infection. *Nature immunology* **14**, 574–583 (2013).

[299] Stockinger, S., Kastner, R., Kernbauer, E., Pilz, A., Westermayer, S., Reutterer, B., Soulat, D., Stengl, G., Vogl, C., Frenz, T. & others. Characterization of the interferon-producing cell in mice infected with Listeria monocytogenes. *PLoS Pathog* **5**, e1000355 (2009).

[300] Assoian, R., Komoriya, A., Meyers, C. A., Miller, D. M. & Sporn, M. B. Transforming growth factor-beta in human platelets. Identification of a major storage site, purification, and characterization. *Journal of Biological Chemistry* **258**, 7155–7160 (1983).

A
Appendix

A.1 Gating strategies

A.1.1 Adaptive cellularity in conventional $Adap^{-/-}$ mice
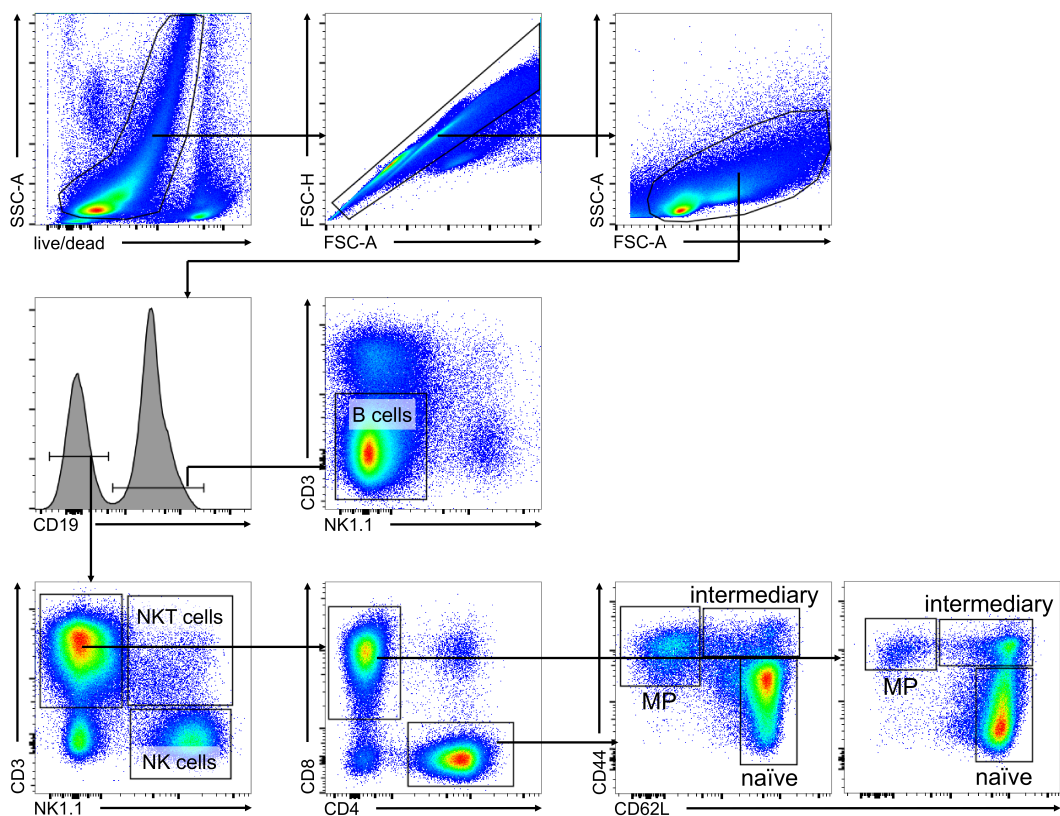
Figure A.1: Gating strategy: Adaptive cellularity and activation status in conventional $Adap^{-/-}$ mice.

A.1.2 Myeloid cellularity in conventional *Adap*$^{-/-}$ mice
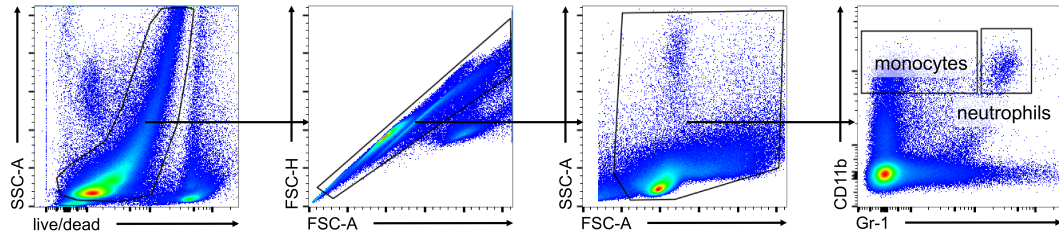
Figure A.2: Gating strategy: Myeloid cellularity and activation status in conventional *Adap*$^{-/-}$ mice.

A.1.3 ADAP expression in lymphocytes
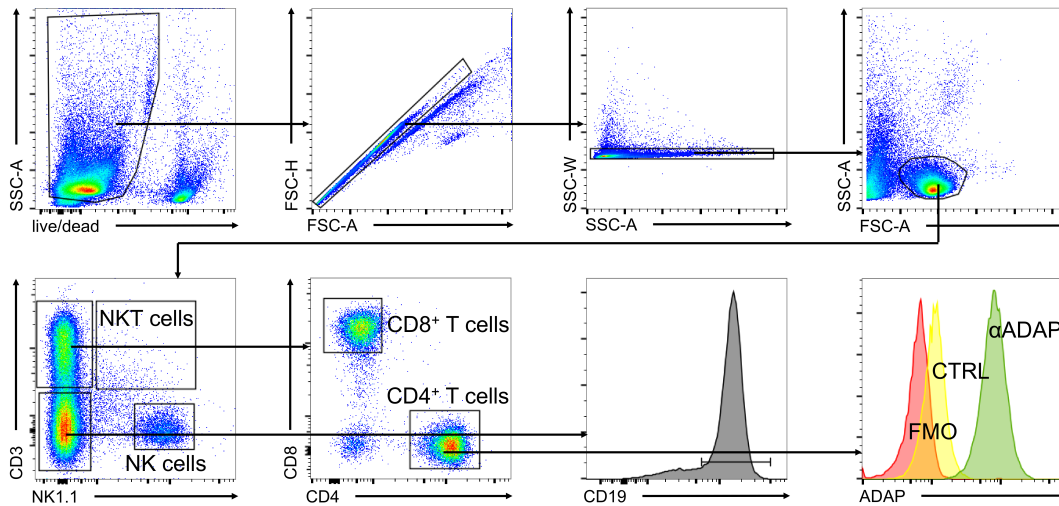
Figure A.3: Gating strategy: Flow cytometric determination of ADAP expression in lymphocytes.

A.1.4 *In vitro* activation and proliferation of $Adap^{-/-}$ T cells
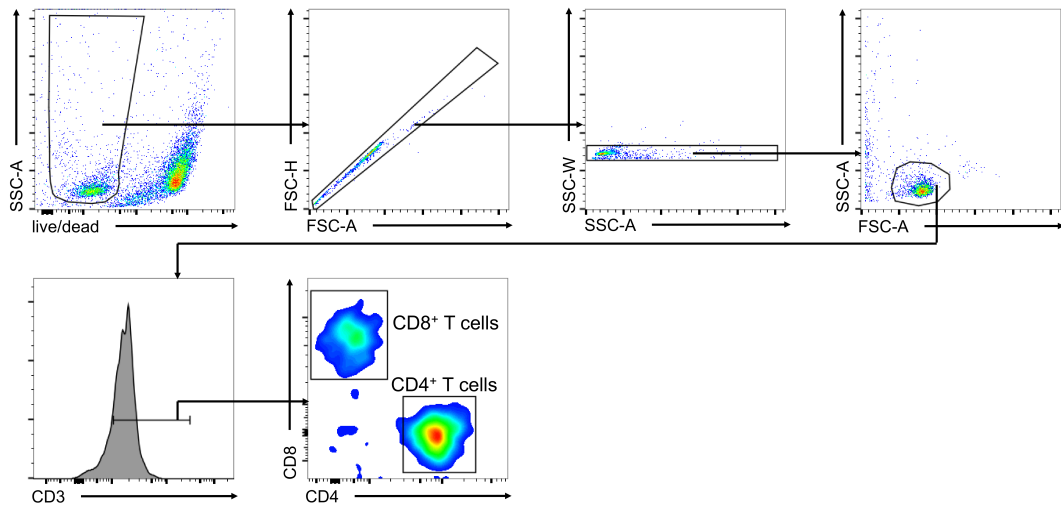
Figure A.4: Gating strategy: *In vitro* activation and proliferation of $Adap^{-/-}$ T cells.

A.1.5 *In vitro* activation and proliferation of OT-I $CD8^{+}$ T cells
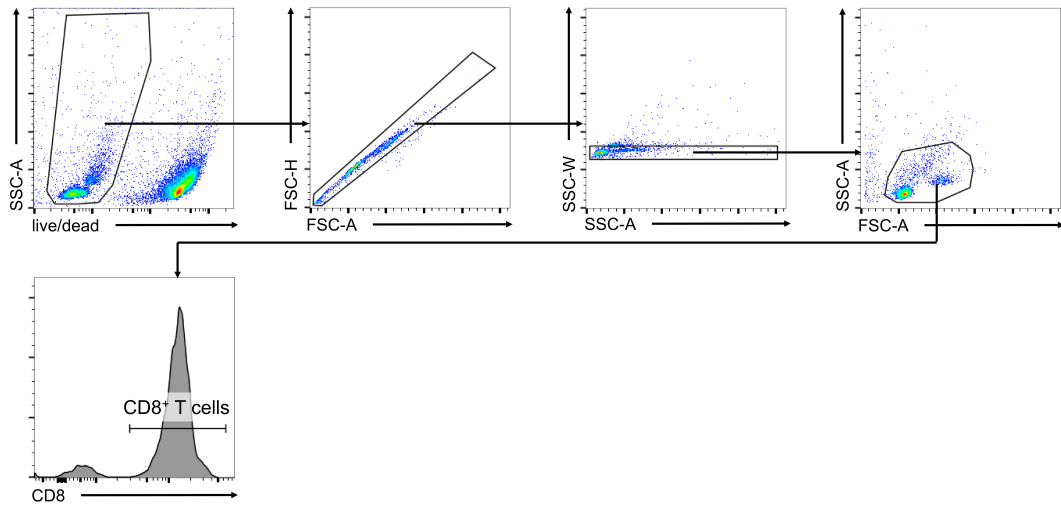
Figure A.5: Gating strategy: *In vitro* activation and proliferation of OT-I $CD8^{+}$ T cells.

A.1.6 Adoptive Transfer of $Adap^{-/-}$ OT-I CD8$^+$ T cells with LmOVA infection
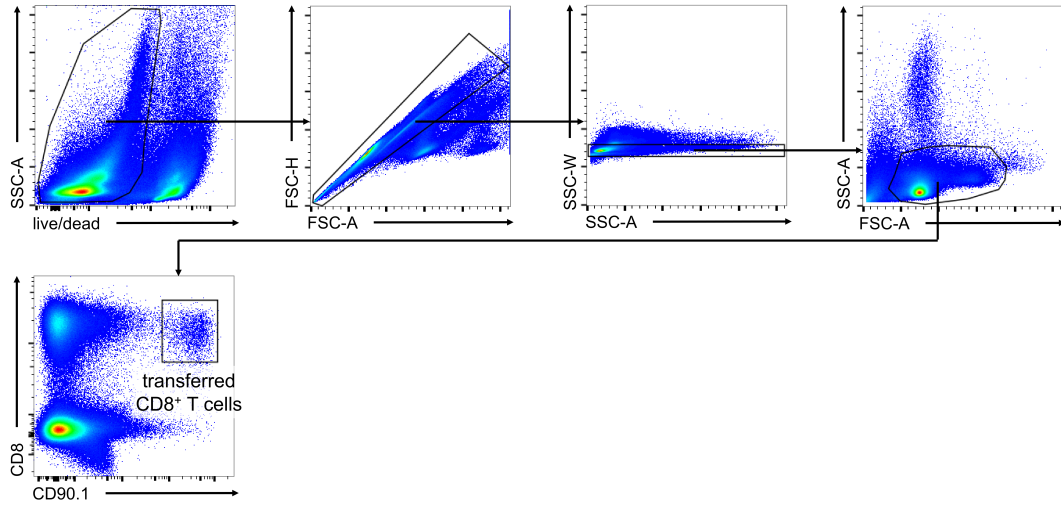
Figure A.6: Gating strategy: Adoptive Transfer of $Adap^{-/-}$ OT-I CD8$^+$ T cells with LmOVA infection.

A.1.7 *In vivo* cytotoxicity of CD8$^+$ T cells in $Adap^{-/-}$ mice
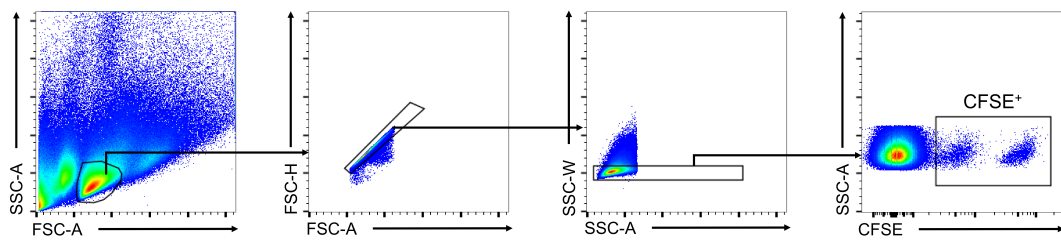
Figure A.7: Gating strategy: *In vivo* cytotoxicity of CD8$^+$ T cells in $Adap^{-/-}$ mice.

A.1.8 Identification of leukocyte subsets in infected mice
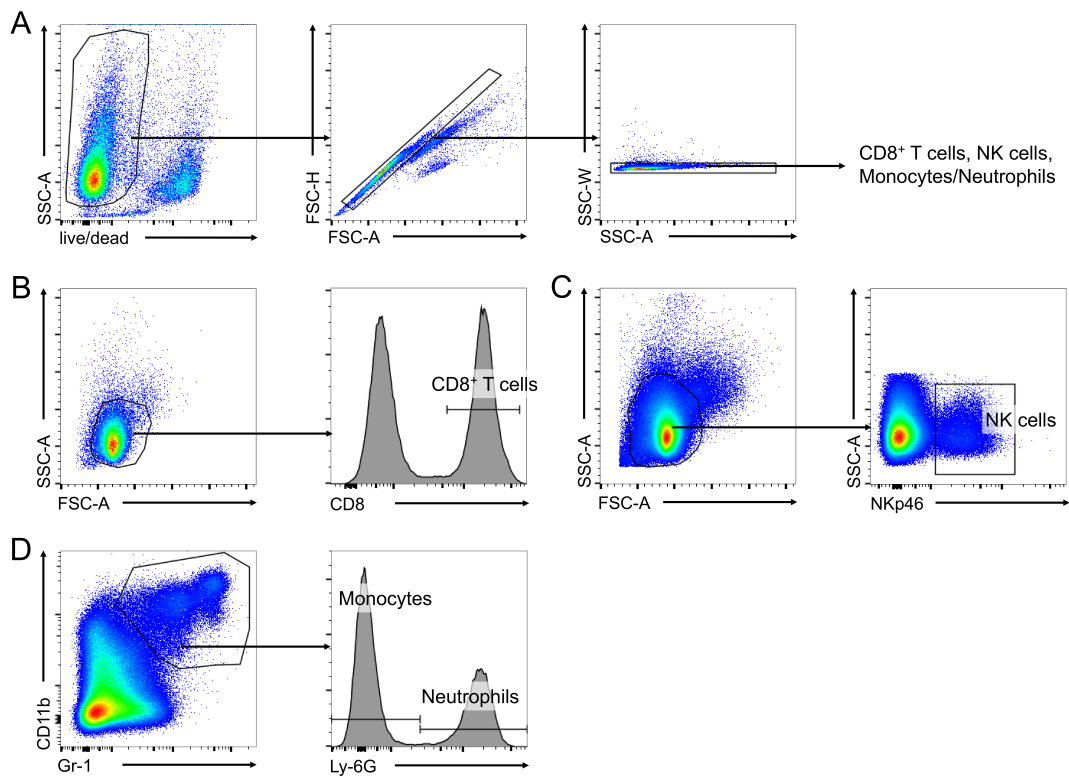
Figure A.8: Gating strategy: Identification of leukocyte subsets in infected mice. (A) Live/dead and singlet gating was performed identical for all other subset gating strategies. Gatings after (A) for (B) CD8$^+$ T cells, (C) NK cells, and (D) neutrophils and monocytes.

A.1.9 Cytometric bead array analysis of serum cytokines
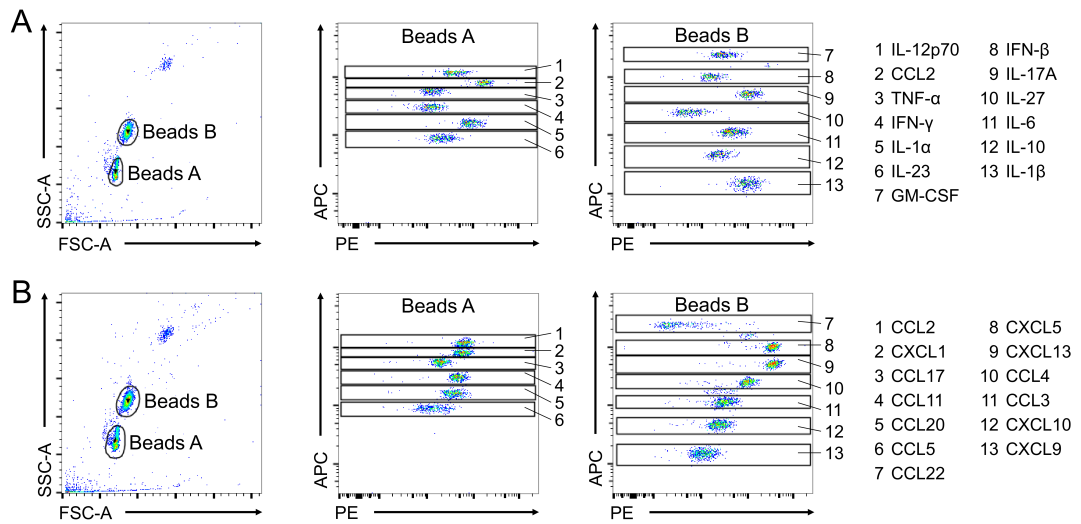
Figure A.9: Gating strategy: Identification of leukocyte subsets in infected mice. Gating strategies for BioLegend LEGENDplex™ (A) *Mouse Inflammation Panel* and (B)*Mouse Proinflammatory Chemokine Panel.*

A.2 Data tables

A.2.1 Cellularity of $Adap^{-/-}$ mice

Table A.1: Data table: Absolute cell numbers lymphocytes, neutrophils and monocytes in $Adap^{-/-}$ **mice.** $\bar{x}$ represents means of absolute cell numbers. $Adap^{+/+}$, N = 4; $Adap^{-/-}$, N = 5. Statistical analysis was performed using unpaired, two-tailed Student's t-test.

	Spleen				
	$Adap^{+/+}$		$Adap^{-/-}$		
	$\bar{x}$ ($\times 10^6$)	$\pm$ SEM	$\bar{x}$ ($\times 10^6$)	$\pm$ SEM	p value
total leukocytes	177.8	14.92	229.6	18.84	0.0773
$CD4^+$ *T cells*	29.70	3.021	34.08	2.542	0.3004
$CD8^+$ *T cells*	7.205	0.5481	4.826	0.3700	0.0074
NKT cells	2.798	0.3907	3.920	0.4155	0.0955
NK cells	9.643	0.7140	11.36	1.281	0.3136
B cells	82.60	5.230	115.5	10.25	0.0338
Neutrophils	0.4830	0.09969	1.464	0.5886	0.1883
Monocytes	1.660	0.07627	2.856	0.4728	0.0625

	Blood				
	$Adap^{+/+}$		$Adap^{-/-}$		
	$\bar{x}$ ($\times 10^4$)	$\pm$ SEM	$\bar{x}$ ($\times 10^4$)	$\pm$ SEM	p value
total leukocytes	158.5	20.46	217.8	37.09	0.2359
$CD4^+$ *T cells*	23.65	3.874	26.74	4.905	0.6500
$CD8^+$ *T cells*	5.643	0.9162	5.932	0.9201	0.8324
NKT cells	5.088	0.6274	4.218	0.8549	0.4610
NK cells	35.63	4.626	42.92	6.431	0.4112
Neutrophils	2.453	0.6270	13.67	2.688	0.0085
Monocytes	3.383	0.6555	11.35	1.450	0.0026

	inLN				
	$Adap^{+/+}$		$Adap^{-/-}$		
	$\bar{x}$ ($\times 10^4$)	$\pm$ SEM	$\bar{x}$ ($\times 10^4$)	$\pm$ SEM	p value
total leukocytes	231.5	77.54	256.2	90.68	0.8470
$CD4^+$ *T cells*	76.15	27.12	79.62	27.36	0.9318
$CD8^+$ *T cells*	58.13	18.71	36.40	10.13	0.3144
NKT cells	3.229	1.498	3.264	1.274	0.9862
NK cells	2.426	0.8348	2.514	0.7667	0.9403

Table A.2: Data table: Frequencies of naïve, intermediary and memory phenotpye (MP) T cells in wild type and $Adap^{-/-}$ animals. $\bar{x}$ represents means of frequencies in %. $Adap^{+/+}$, N = 4; $Adap^{-/-}$, N = 5. Statistical analysis was performed using unpaired, two-tailed Student's t-test and two-way ANOVA with Bonferroni's *post-hoc* test for CD43 expression.

Spleen					
	$Adap^{+/+}$		$Adap^{-/-}$		
	$\bar{x}$ [%]	$\pm$ **SEM**	$\bar{x}$ [%]	$\pm$ **SEM**	p **value**
naïve $CD4^+$ T cells	75.23	5.922	63.82	3.312	0.1187
intermediary $CD4^+$ T cells	4.885	0.2996	6.848	0.1866	0.0007
MP $CD4^+$ T cells	11.90	2.324	21.26	1.633	0.0115
naïve $CD8^+$ T cells	75.63	4.125	53.18	2.722	0.0022
intermediary $CD8^+$ T cells	14.25	0.7354	35.54	1.203	≤ 0.0001
MP $CD8^+$ T cells	2.253	0.4092	3.842	0.2742	0.0123

Blood					
	$Adap^{+/+}$		$Adap^{-/-}$		
	$\bar{x}$ [%]	$\pm$ **SEM**	$\bar{x}$ [%]	$\pm$ **SEM**	p **value**
naïve $CD4^+$ T cells	80.13	1.171	38.30	7.730	0.0021
intermediary $CD4^+$ T cells	3.618	0.2375	4.662	0.9735	0.3834
MP $CD4^+$ T cells	9.745	0.5520	12.05	1.512	0.2367
naïve $CD8^+$ T cells	73.75	0.9946	34.96	3.784	≤ 0.0001
intermediary $CD8^+$ T cells	14.13	0.5721	37.84	1.327	≤ 0.0001
MP $CD8^+$ T cells	8.248	0.7012	11.12	0.8064	0.0352

inLN					
	$Adap^{+/+}$		$Adap^{-/-}$		
	$\bar{x}$ [%]	$\pm$ **SEM**	$\bar{x}$ [%]	$\pm$ **SEM**	p **value**
naïve $CD4^+$ T cells	88.50	0.5050	88.84	0.7339	0.7291
intermediary $CD4^+$ T cells	3.393	0.4020	2.798	0.1508	0.1735
MP $CD4^+$ T cells	3.590	0.2593	3.688	0.1801	0.758
naïve $CD8^+$ T cells	84.20	0.7692	67.06	1.460	≤ 0.0001
intermediary $CD8^+$ T cells	11.98	0.6223	28.10	1.328	≤ 0.0001
MP $CD8^+$ T cells	0.4450	0.05454	1.068	0.2732	0.0872

CD43 expression					
	$Adap^{+/+}$		$Adap^{-/-}$		
	$\bar{x}$ [%]	$\pm$ **SEM**	$\bar{x}$ [%]	$\pm$ **SEM**	p **value**
naïve $CD8^+$ T cells	0.3125	0.01601	0.5380	0.03153	> 0.05
MP $CD8^+$ T cells	28.70	3.967	39.70	3.006	≤ 0.05

A.2.2 CD8$^+$ T cell cellularity in $Adap^{-/-}$ × OT-I × CD90.1 mice

Table A.3: Data table: CD8$^+$ T cell cellularity in $Adap^{-/-}$ × OT-I × CD90.1 mice. $\bar{x}$ represents means of absolute cell numbers. $Adap^{+/+}$, N = 4; $Adap^{-/-}$, N = 4. Statistical analysis was performed using two-way ANOVA with Bonferroni's *post-hoc* test.

	Spleen				
	$Adap^{+/+}$		$Adap^{-/-}$		
	$\bar{x}$ (×10^6)	± SEM	$\bar{x}$ (×10^6)	± SEM	p value
Total OT-I CD8$^+$ T cells	12.43	2.356	14.28	0.8440	> 0.05
MP OT-I CD8$^+$ T cells	14.72	4.375	8.702	1.285	> 0.05

	Thymus				
	$Adap^{+/+}$		$Adap^{-/-}$		
	$\bar{x}$ (×10^6)	± SEM	$\bar{x}$ (×10^6)	± SEM	p value
Total OT-I CD8$^+$ T cells	1.660	0.4091	0.4043	0.09061	≤ 0.001
MP OT-I CD8$^+$ T cells	0.1171	0.06110	0.03465	0.01132	> 0.05

A.2.3 ADAP expression levels in lymphocytes

Table A.4: Data table: ADAP expression levels in lymphocytes of $Adap^{+/+}$, $Adap^{+/-}$ and $Adap^{-/-}$ mice. $\bar{x}$ represents means of fold over pre-immunization controls. $Adap^{+/+}$, N = 14; $Adap^{+/-}$, N = 5; $Adap^{-/-}$, N = 10. Statistical analysis was performed using two-way ANOVA with Bonferroni's *post-hoc* test.

	ADAP Expression					
	$Adap^{+/+}$		$Adap^{+/-}$		$Adap^{+/-}$	
	$\bar{x}$	± SEM	$\bar{x}$	± SEM	$\bar{x}$	± SEM
CD4$^+$ T cells	7.766	0.2448	5.630	0.1496	1.103	0.04475
CD8$^+$ T cells	7.261	0.2403	5.500	0.1236	1.215	0.05550
NK cells	5.990	0.2531	3.792	0.08351	1.109	0.04518
NKT cells	5.947	0.2005	4.454	0.06030	1.082	0.02977
B cells	1.010	0.03143	1.124	0.03982	1.193	0.04182

A.2.4 CD3ε expression levels

Table A.5: Data table: CD3ε expression levels in $Adap^{+/+}$ and $Adap^{-/-}$ T cells. $\bar{x}$ represents means of gMFIs. $Adap^{+/+}$, N = 4; $Adap^{-/-}$, N = 5. Statistical analysis was performed using two-way ANOVA with Bonferroni's *post-hoc* test.

	CD3ε expression				
	$Adap^{+/+}$		$Adap^{-/-}$		
	$\bar{x}$ (×10^3)	± SEM	$\bar{x}$ (×10^3)	± SEM	p value
CD4$^+$ T cells	2.832	0.02918	2.269	0.04296	≤ 0.001
CD8$^+$ T cells	1.648	0.02007	1.338	0.02194	≤ 0.001

A.2.5 Activation and proliferation of $Adap^{-/-}$ CD4$^+$ and CD8$^+$ T cells

Table A.6: Data table: Activation and proliferation of $Adap^{-/-}$ T cells. $\bar{x}$ represents means of % positive cells. $Adap^{+/+}$, N = 7; $Adap^{-/-}$, N = 5. Statistical analysis was performed using two-way ANOVA with Bonferroni's *post-hoc* test.

	CD69				
	$Adap^{+/+}$		$Adap^{-/-}$		
	$\bar{x}$ [%]	$\pm$ SEM	$\bar{x}$ [%]	$\pm$ SEM	p value
CD4$^+$ T cells					
unstimulated	2.659	0.8938	2.028	0.4184	> 0.05
24 h	81.20	4.527	37.81	10.75	≤ 0.001
72 h	74.90	5.206	29.07	7.581	≤ 0.001
CD8$^+$ T cells					
unstimulated	7.697	1.879	6.348	1.428	> 0.05
24 h	76.40	10.20	39.96	11.22	≤ 0.01
72 h	61.01	4.835	40.06	6.705	> 0.05

	CD62L				
	$Adap^{+/+}$		$Adap^{-/-}$		
	$\bar{x}$ [%]	$\pm$ SEM	$\bar{x}$ [%]	$\pm$ SEM	p value
CD4$^+$ T cells					
unstimulated	46.67	3.454	51.24	5.800	> 0.05
24 h	83.70	3.039	56.54	4.290	≤ 0.001
72 h	81.24	3.332	49.98	4.353	≤ 0.001
CD8$^+$ T cells					
unstimulated	17.51	1.375	17.56	3.729	> 0.05
24 h	57.16	5.351	40.88	8.972	> 0.05
72 h	68.00	3.762	66.08	4.010	> 0.05

	CD25				
	$Adap^{+/+}$		$Adap^{-/-}$		
	$\bar{x}$ [%]	$\pm$ SEM	$\bar{x}$ [%]	$\pm$ SEM	p value
CD4$^+$ T cells					
unstimulated	1.419	0.3294	1.636	0.3711	> 0.05
24 h	64.93	8.841	23.81	11.36	≤ 0.01
72 h	97.11	1.017	60.18	15.03	≤ 0.01
CD8$^+$ T cells					
unstimulated	0.5243	0.1541	0.7560	0.1445	> 0.05
24 h	50.51	9.967	22.90	9.988	> 0.05
72 h	87.39	6.204	74.46	13.86	> 0.05

	Proliferation				
	$Adap^{+/+}$		$Adap^{-/-}$		
	$\bar{x}$ [%]	$\pm$ SEM	$\bar{x}$ [%]	$\pm$ SEM	p value
CD4$^+$ T cells 72 h	95.72	1.445	54.27	14.84	≤ 0.001
CD8$^+$ T cells 72 h	89.46	5.079	79.93	11.29	> 0.05

A.2.6 Adhesion of CD4$^+$ and CD8$^+$ wild type and *Adap*$^{-/-}$ T cells

Table A.7: Data table: Adhesion of CD4$^+$ and CD8$^+$ wild type and *Adap*$^{-/-}$ T cells. $\bar{x}$ represents means of % adherent cells. *Adap*$^{+/+}$, N = 6; *Adap*$^{-/-}$, N = 6. Statistical analysis was performed using two-way ANOVA with Bonferroni's *post-hoc* test.

	***In vitro* adhesion**				
	***Adap*$^{+/+}$**		***Adap*$^{-/-}$**		
	$\bar{x}$ [%]	$\pm$ **SEM**	$\bar{x}$ [%]	$\pm$ **SEM**	p **value**
CD4$^+$ T cells					
none	8.017	1.284	9.033	0.9838	> 0.05
1 µg αCD3	21.80	1.453	13.63	0.7424	≤ 0.05
5 µg αCD3	43.88	2.430	28.58	1.500	≤ 0.001
10 µg αCD3	49.55	2.025	37.62	2.083	≤ 0.001
500 ng $\cdot$ mL^{-1} CCL21	26.95	2.468	12.13	1.436	≤ 0.001
100 ng $\cdot$ mL^{-1} CXCL12	39.48	2.103	20.20	1.593	≤ 0.001
50 ng $\cdot$ mL^{-1} PMA	41.27	2.383	41.17	2.217	> 0.05
50 mM MnCl$_2$	54.17	2.128	53.02	1.983	> 0.05
CD8$^+$ T cells					
none	8.600	0.7085	10.17	0.9611	> 0.05
1 µg αCD3	23.32	1.056	18.92	1.202	> 0.05
5 µg αCD3	35.68	1.069	33.23	1.776	> 0.05
10 µg αCD3	48.07	1.494	46.20	1.385	> 0.05
500 ng $\cdot$ mL^{-1} CCL21	25.95	2.211	11.42	1.407	≤ 0.001
100 ng $\cdot$ mL^{-1} CXCL12	40.93	2.634	17.87	1.169	≤ 0.001
50 ng $\cdot$ mL^{-1} PMA	39.40	2.565	39.72	3.3189	> 0.05
50 mM MnCl$_2$	48.60	1.261	45.57	2.379	> 0.05

A.2.7 Activation and proliferation of monoclonal wild type and $Adap^{-/-}$ CD8$^+$ OT-I TCR-transgenic T cells *in vitro*

Table A.8: Data table: **Activation and proliferation of monoclonal wild type and** $Adap^{-/-}$**CD8$^+$OT-I × CD90.1-I TCR-transgenic T cells *in vitro*.** $\bar{x}$ represents means of % positive cells. $Adap^{+/+}$, N = 4; $Adap^{-/-}$, N = 4. Statistical analysis was performed using two-way ANOVA with Bonferroni's *post-hoc* test.

	CD69 (24 h)				
	$Adap^{+/+}$		$Adap^{-/-}$		
	$\bar{x}$ [%]	$\pm$ SEM	$\bar{x}$ [%]	$\pm$ SEM	p value
vehicle	2.368	1.301	1.653	0.5494	> 0.05
$OVA_{257-264}$					
10 pg $\cdot$ mL^{-1}	81.73	8.236	73.27	10.61	> 0.05
100 pg $\cdot$ mL^{-1}	81.07	10.17	84.16	11.50	> 0.05
1000 pg $\cdot$ mL^{-1}	79.54	12.74	83.02	14.31	> 0.05

	CD62L (24 h)				
	$Adap^{+/+}$		$Adap^{-/-}$		
	$\bar{x}$ [%]	$\pm$ SEM	$\bar{x}$ [%]	$\pm$ SEM	p value
vehicle	28.17	8.568	13.92	4.924	> 0.05
$OVA_{257-264}$					
10 pg $\cdot$ mL^{-1}	77.26	4.717	61.94	4.187	> 0.05
100 pg $\cdot$ mL^{-1}	79.85	5.557	61.07	3.639	> 0.05
1000 pg $\cdot$ mL^{-1}	83.03	5.090	62.94	3.434	> 0.05

	CD25 (72 h)				
	$Adap^{+/+}$		$Adap^{-/-}$		
	$\bar{x}$ [%]	$\pm$ SEM	$\bar{x}$ [%]	$\pm$ SEM	p value
vehicle	0.3225	0.02496	0.3250	0.1097	> 0.05
$OVA_{257-264}$					
10 pg $\cdot$ mL^{-1}	80.97	4.842	36.37	9.593	$\leq$ 0.001
100 pg $\cdot$ mL^{-1}	93.20	3.749	83.18	4.307	> 0.05
1000 pg $\cdot$ mL^{-1}	97.47	1.813	91.27	2.305	> 0.05

	Proliferation (72 h)				
	$Adap^{+/+}$		$Adap^{-/-}$		
	$\bar{x}$ [%]	$\pm$ SEM	$\bar{x}$ [%]	$\pm$ SEM	p value
vehicle	4.430	1.484	1.398	0.5283	> 0.05
$OVA_{257-264}$					
10 pg $\cdot$ mL^{-1}	86.63	2.400	83.45	4.057	> 0.05
100 pg $\cdot$ mL^{-1}	83.07	4.161	88.22	3.346	> 0.05
1000 pg $\cdot$ mL^{-1}	86.24	2.593	85.44	4.153	> 0.05

A.2.8 Activation and effector function analysis *in vivo* of OT-I TCR-transgenic CD8$^+$ T cells in an adoptive transfer model with *Lm*OVA infection

Table A.9: Data table: Activation and effector function analysis *in vivo* of OT-I TCR-transgenic CD8$^+$ T cells in an adoptive transfer model with *L. monocytogenes* infection. $\bar{x}$ represents means of % positive or identified transferred cells. $Adap^{+/+}$, N = 6; $Adap^{-/-}$, N = 6–7. Statistical analysis was performed using two-way ANOVA with Bonferroni's *post-hoc* test.

	Adoptive Transfer with *L. monocytogenes* infection				
	$Adap^{+/+}$		$Adap^{-/-}$		
	$\bar{x}$ [%]	$\pm$ SEM	$\bar{x}$ [%]	$\pm$ SEM	p value
CD43$^+$					
2 d.p.i.	23.95	5.727	15.82	2.848	> 0.05
4 d.p.i.	71.70	1.812	67.12	0.4715	> 0.05
CD44^{hi}					
2 d.p.i.	36.35	0.7775	49.09	1.881	≤ 0.001
4 d.p.i.	80.73	2.078	77.08	1.204	> 0.05
CD25$^+$					
2 d.p.i.	26.85	1.838	15.99	2.029	≤ 0.001
4 d.p.i.	3.880	0.6790	2.250	0.3939	> 0.05
Proliferated					
2 d.p.i.	33.05	1.827	23.91	3.702	≤ 0.05
4 d.p.i.	99.47	0.1022	99.28	0.07032	> 0.05
Frequency					
2 d.p.i.	0.2583	0.02774	0.2571	0.01769	> 0.05
4 d.p.i.	8.645	0.9581	12.83	1.062	≤ 0.001
Granzyme B$^+$					
2 d.p.i.	28.42	2.041	18.44	2.102	≤ 0.05
4 d.p.i.	61.13	3.547	57.17	6.230	> 0.05
IFN-γ$^+$					
2 d.p.i.	52.90	1.839	49.01	2.336	> 0.05
4 d.p.i.	85.58	1.173	57.42	3.493	≤ 0.001

A.2.9 Activation and effector function analysis *in vivo* of OT-I TCR-transgenic CD8$^+$ T cells in an adoptive transfer model with IAV-OVA infection

Table A.10: Data table: Activation and effector function analysis *in vivo* of OT-I TCR-transgenic CD8$^+$ T cells in an adoptive transfer model with IAV-OVA infection. $\bar{x}$ represents means of % positive or identified transferred cells. $Adap^{+/+}$, N = 6; $Adap^{-/-}$, N = 8. Statistical analysis was performed using Student's *t*-test.

	Adoptive Transfer with IAV-OVA infection				
	$Adap^{+/+}$		$Adap^{-/-}$		
	$\bar{x}$ [%]	$\pm$ SEM	$\bar{x}$ [%]	$\pm$ SEM	p value
CD43$^+$	81.40	2.275	74.68	1.537	0.0258
CD44^{hi}	61.10	5.545	67.06	2.738	0.3171
Proliferated	99.97	0.02108	99.91	0.02266	0.1161
Frequency	17.75	3.391	22.95	3.221	0.2944
Granzyme B$^+$	66.83	1.642	74.50	3.868	0.1307
IFN-γ$^+$	62.12	1.870	41.84	3.576	0.0007

A.2.10 Weight loss after infection with *L. monocytogenes*

Table A.11: Data table: Weight loss of male and female mice after *L. monocytogenes* infection. $\bar{x}$ represents means of % of the weight prior to infection. Male mice: $Adap^{+/+}$, N = 13; $Adap^{-/-}$, N = 12; female mice; $Adap^{+/+}$, N = 8; $Adap^{-/-}$, N = 14. Statistical analysis was performed using repeated measures two-way ANOVA with Bonferroni's *post hoc* test. Analysis was only performed until day 4 post infection, since to many $Adap^{-/-}$ mice had died after that time point.

	Weight loss of male mice during *L. monocytogenes* infection				
	$Adap^{+/+}$		$Adap^{-/-}$		
	$\bar{x}$ [%]	$\pm$ SEM	$\bar{x}$ [%]	$\pm$ SEM	p value
Days post infection					
0	100.0	*n/a*	100.0	*n/a*	*n/a*
1	98.63	0.6645	97.71	0.8454	> 0.05
2	93.33	0.8717	89.59	1.022	> 0.05
3	93.00	1.469	85.87	1.485	≤ 0.05
4	93.06	1.967	85.26	2.563	≤ 0.05
5	94.32	2.150	89.75	3.740	> 0.05
6	95.16	2.172	90.80	4.386	> 0.05
7	94.33	2.966	92.50	4.304	> 0.05
8	97.29	1.926	94.43	3.893	> 0.05
9	97.80	1.585	93.89	3.729	> 0.05
10	97.79	1.584	95.41	3.618	> 0.05
11	98.53	1.405	96.11	3.644	> 0.05
12	98.71	1.277	96.78	3.337	> 0.05

	Weight loss of female mice during *L. monocytogenes* infection				
	$Adap^{+/+}$		$Adap^{-/-}$		
	$\bar{x}$ [%]	$\pm$ SEM	$\bar{x}$ [%]	$\pm$ SEM	p value
Days post infection					
0	100.0	*n/a*	100.0	*n/a*	*n/a*
1	99.30	0.6875	97.10	0.6278	> 0.05
2	90.86	1.048	86.61	0.9871	> 0.05
3	89.74	1.687	80.71	1.045	≤ 0.001
4	89.19	2.540	78.46	2.378	≤ 0.001
5	89.99	3.263	*n/a*	*n/a*	*n/a*
6	91.84	3.523	*n/a*	*n/a*	*n/a*
7	93.21	3.361	*n/a*	*n/a*	*n/a*
8	98.16	2.165	*n/a*	*n/a*	*n/a*
9	99.25	2.230	*n/a*	*n/a*	*n/a*
10	100.03	1.956	*n/a*	*n/a*	*n/a*
11	100.8	1.549	*n/a*	*n/a*	*n/a*
12	100.2	1.804	*n/a*	*n/a*	*n/a*

A.2.11 Weights of spleen and livers during *L. monocytogenes* infection

Table A.12: Data table: Weights of spleens and livers during *L. monocytogenes* infection. $\bar{x}$ represents means of organ weights in g. $Adap^{+/+}$, N = 9–10; $Adap^{-/-}$, N = 8. Statistical analysis was performed using two-way ANOVA with Bonferroni's *post hoc* test.

	$Adap^{+/+}$		$Adap^{-/-}$		
	$\bar{x}$ [g]	$\pm$ **SEM**	$\bar{x}$ [g]	$\pm$ **SEM**	p **value**
Days post infection					
1	0.11	0.0062	0.12	0.0082	> 0.05
3	0.17	0.015	0.16	0.011	> 0.05
5	0.26	0.0093	0.28	0.024	> 0.05
7	0.29	0.030	0.41	0.040	≤ 0.001
Liver weights during *L. monocytogenes* infection					
1	1.40	0.075	1.59	0.047	> 0.05
3	1.38	0.067	1.52	0.055	> 0.05
5	1.82	0.056	1.61	0.075	> 0.05
7	1.59	0.057	1.97	0.063	≤ 0.001

Table header row (spanning): Spleen weights during L. monocytogenes infection

A.2.12 Bacterial burden in spleens and livers

Table A.13: Data table: Bacterial burden in spleens and livers during *L. monocytogenes* infection. $\bar{x}$ represents means of $\log_{10}$-transformed CFU numbers. $Adap^{+/+}$, N = 8–10; $Adap^{-/-}$, N = 7–9. Statistical analysis was performed on the transformed data using two-way ANOVA with Bonferroni's *post hoc* test.

	$Adap^{+/+}$		$Adap^{-/-}$		
	$\bar{x}$	$\pm$ **SEM**	$\bar{x}$	$\pm$ **SEM**	p **value**
Days post infection					
1	5.39	0.113	5.43	0.0599	> 0.05
3	5.49	0.332	6.57	0.281	≤ 0.05
5	2.87	0.258	4.89	0.297	≤ 0.001
7	1.51	0.452	1.94	0.474	> 0.05
Bacterial burden in livers during *L. monocytogenes* infection					
1	4.73	0.102	4.83	0.0621	> 0.05
3	4.76	0.355	5.97	0.337	≤ 0.05
5	3.25	0.337	5.36	0.246	≤ 0.001
7	3.36	0.597	4.52	0.480	> 0.05

Table header row (spanning): Bacterial burden in spleens during L. monocytogenes infection

A.2.13 Absolute leukocyte numbers in livers and spleens

Table A.14: Data table: Leukocyte numbers in spleens and livers during *L. monocytogenes* infection. $\bar{x}$ represents means of absolute cell numbers. $Adap^{+/+}$, N = 5; $Adap^{-/-}$, N = 5. Statistical analysis was performed using two-way ANOVA with Bonferroni's *post hoc* test.

Leukocyte numbers in livers during *L. monocytogenes* infection					
	$Adap^{+/+}$		$Adap^{-/-}$		
	$\bar{x}$ ($\times 10^6$)	$\pm$ SEM	$\bar{x}$ ($\times 10^6$)	$\pm$ SEM	p value
Days post infection					
0	1.946	0.3219	1.637	0.2235	> 0.05
1	0.9326	0.1675	1.322	0.5759	> 0.05
3	8.032	1.537	9.452	1.533	> 0.05
5	19.70	1.977	28.80	2.167	≤ 0.05
7	7.650	1.719	43.28	7.286	≤ 0.001

Leukocyte numbers in spleens during *L. monocytogenes* infection					
	$Adap^{+/+}$		$Adap^{-/-}$		
	$\bar{x}$ ($\times 10^6$)	$\pm$ SEM	$\bar{x}$ ($\times 10^6$)	$\pm$ SEM	p value
Days post infection					
0	84.02	7.947	87.42	12.62	> 0.05
1	97.22	5.287	101.8	4.505	> 0.05
3	81.46	13.88	86.46	9.693	> 0.05
5	168.2	11.08	159.3	32.46	> 0.05
7	134.8	9.861	179.3	30.15	> 0.05

A.2.14 Serum cytokine levels

Table A.15: Data table: Cytokines in serum during *L. monocytogenes* infection. $\bar{x}$ represents means of cytokine concentrations in the sera. $Adap^{+/+}$, N = 4–10; $Adap^{-/-}$, N = 4–9. Statistical analysis was performed using two-way ANOVA with Bonferroni's *post hoc* test, except for TNF-α which was analyzed with Fisher's exact test.

	Frequency of TNF-α serum-positive mice during *L. monocytogenes* infection				
	$Adap^{+/+}$		**$Adap^{-/-}$**		
	Frequency [%]	**Relation**	**Frequency [%]**	**Relation**	**p value**
Days post infection					
0	0.0	0/4	0.0	0/4	> 0.05
1	77.8	7/9	44.4	4/9	> 0.05
3	33.3	3/9	88.9	8/9	≤ 0.05
5	22.2	2/9	87.5	7/8	≤ 0.05
7	20.0	2/10	25.0	2/8	> 0.05

	IL-6 concentration in serum during *L. monocytogenes* infection				
	$\bar{x}$ [pg · mL^{-1}]	**± SEM**	**$\bar{x}$ [pg · mL^{-1}]**	**± SEM**	**p value**
Days post infection					
0	0.0000	0.0000	0.6150	0.6150	> 0.05
1	602.2	140.7	305.1	65.46	> 0.05
3	200.7	110.6	904.6	300.4	≤ 0.01
5	28.18	14.58	520.3	157.0	≤ 0.05
7	48.59	37.10	99.99	75.55	> 0.05

	IFN-γ concentration in serum during *L. monocytogenes* infection				
	$\bar{x}$ [ng · mL^{-1}]	**± SEM**	**$\bar{x}$ [ng · mL^{-1}]**	**± SEM**	**p value**
Days post infection					
0	0.009375	0.005810	0.01244	0.007200	> 0.05
1	10.23	2.512	4.305	0.9922	≤ 0.001
3	1.469	0.4045	5.611	1.006	≤ 0.05
5	0.2075	0.04974	3.209	0.9179	> 0.05
7	0.1533	0.1132	0.2244	0.1217	> 0.05

	IL-12p70 concentration in serum during *L. monocytogenes* infection				
	$\bar{x}$ [pg · mL^{-1}]	**± SEM**	**$\bar{x}$ [pg · mL^{-1}]**	**± SEM**	**p value**
Days post infection					
0	0.0000	0.0000	0.0000	0.0000	> 0.05
1	68.50	14.78	48.86	9.381	> 0.05
3	2.3278	0.8552	11.73	2.719	> 0.05
5	0.04000	0.04000	9.674	7.947	> 0.05
7	0.3500	0.2494	0.07875	0.07875	> 0.05

	TGF-β concentration in serum during *L. monocytogenes* infection				
	$\bar{x}$ [ng · mL^{-1}]	**± SEM**	**$\bar{x}$ [ng · mL^{-1}]**	**± SEM**	**p value**
Days post infection					
0	6.005	0.9614	3.633	0.2903	> 0.05
1	7.866	1.319	4.888	0.3336	≤ 0.05
3	6.329	0.4285	5.050	0.4702	> 0.05
5	5.574	0.4377	5.551	0.7559	> 0.05
7	5.980	1.151	6.471	0.6761	> 0.05

A.2.15 Neutrophil and monocyte numbers in spleens and livers

Table A.16: Data table: Neutrophil and monocyte numbers in spleens and livers during *L.* *monocytogenes* infection. $\bar{x}$ represents means of cell numbers. $Adap^{+/+}$, N = 4–5; $Adap^{-/-}$, N = 4–5. Statistical analysis was performed using two-way ANOVA with Bonferroni's *post hoc* test.

	$Adap^{+/+}$		$Adap^{-/-}$		
	$\bar{x}$ ($\times 10^6$)	$\pm$ **SEM**	$\bar{x}$ ($\times 10^6$)	$\pm$ **SEM**	*p* value
Neutrophil and monocyte numbers in liver					
Days post infection					
Neutrophils					
0	0.08956	0.03931	0.04492	0.008458	> 0.05
1	0.1292	0.02450	0.1464	0.05254	> 0.05
2	0.8976	0.2067	1.506	0.3370	> 0.05
3	0.7280	0.2425	1.133	0.2730	> 0.05
5	1.099	0.2324	3.520	0.4557	$\leq$ 0.001
7	0.1726	0.02587	4.000	1.180	$\leq$ 0.001
Monocytes					
0	0.1947	0.05623	0.1151	0.01637	> 0.05
1	0.3070	0.05848	0.4198	0.1797	> 0.05
2	5.926	0.1572	4.900	0.8695	> 0.05
3	2.154	0.4605	3.120	0.7233	> 0.05
5	2.942	0.4899	6.155	1.196	$\leq$ 0.001
7	0.2620	0.04674	3.325	0.6046	$\leq$ 0.01
Neutrophil and monocyte numbers in spleen					
Neutrophils					
0	0.2182	0.1016	0.1188	0.01590	> 0.05
1	1.886	0.1405	2.130	0.1675	> 0.05
2	2.980	0.8027	3.498	0.3764	> 0.05
3	1.623	0.8226	3.690	0.8399	> 0.05
5	1.762	0.3287	6.613	1.8182	$\leq$ 0.001
7	1.278	0.2837	8.700	1.376	$\leq$ 0.001
Monocytes					
0	0.8612	0.2347	0.6524	0.03350	> 0.05
1	1.510	0.1493	2.508	0.1845	> 0.05
2	1.518	0.1549	1.190	0.4124	> 0.05
3	0.7920	0.2740	1.227	0.2619	> 0.05
5	4.012	0.3071	5.483	1.0445	> 0.05
7	1.292	0.3049	5.655	0.7154	$\leq$ 0.001

A.2.16 CXCL1 and CCL2 levels in serum

Table A.17: Data table: CXCL1 and CCL2 levels in serum during *L. monocytogenes* infection.
$\bar{x}$ represents means of cytokine concentration. $Adap^{+/+}$, N = 4 (uninfected), 9 (infected); $Adap^{-/-}$, N = 4 (uninfected), 9 (infected). Statistical analysis was performed using two-way ANOVA with Bonferroni's *post hoc* test.

Serum concentration of CXCL1 (KC) during *L. monocytogenes* infection					
	$Adap^{+/+}$		$Adap^{-/-}$		
	$\bar{x}$ [ng $\cdot$ mL^{-1}]	$\pm$ SEM	$\bar{x}$ [ng $\cdot$ mL^{-1}]	$\pm$ SEM	p value
Days post infection					
0	0.1289	0.01447	0.07939	0.009067	> 0.05
1	0.9596	0.1120	0.6855	0.1221	> 0.05
3	0.6635	0.2473	1.415	0.3533	$\leq$ 0.01
5	0.09292	0.01624	0.3643	0.1057	> 0.05
7	0.06288	0.005529	0.08715	0.02629	> 0.05

Serum concentration of CCL2 (MCP-1) during *L. monocytogenes* infection					
	$\bar{x}$ [pg $\cdot$ mL^{-1}]	$\pm$ SEM	$\bar{x}$ [pg $\cdot$ mL^{-1}]	$\pm$ SEM	p value
0	48.04	8.725	0.7780	0.7780	> 0.05
1	808.7	139.4	496.5	106.6	$\leq$ 0.05
3	172.6	47.94	302.9	95.95	> 0.05
5	45.39	9.558	143.0	46.59	> 0.05
7	27.94	7.166	31.66	11.60	> 0.05

A.2.17 CD8$^+$ T cell numbers in spleen and liver

Table A.18: Data table: CD8$^+$ T cell numbers in spleen and liver during *L. monocytogenes* infection. $\bar{x}$ represents means of cell numbers. $Adap^{+/+}$, N = 4–5; $Adap^{-/-}$, N = 4–5. Statistical analysis was performed using two-way ANOVA with Bonferroni's *post hoc* test.

Liver CD8$^+$ T cells during *L. monocytogenes* infection					
	$Adap^{+/+}$		$Adap^{-/-}$		
	$\bar{x}$ ($\times 10^6$)	$\pm$ SEM	$\bar{x}$ ($\times 10^6$)	$\pm$ SEM	p value
Days post infection					
0	0.1414	0.01959	0.1301	0.01950	> 0.05
3	0.1941	0.06154	0.06398	0.02165	> 0.05
5	3.374	0.4082	2.505	0.3602	> 0.05
7	2.872	0.8173	10.86	1.434	$\leq$ 0.001

Splenic CD8$^+$ T cells during *L. monocytogenes* infection					
0	8.642	0.4261	6.310	0.7968	> 0.05
3	4.080	0.4499	2.622	0.7277	> 0.05
5	13.93	1.303	10.47	3.152	> 0.05
7	17.04	1.963	21.62	3.9834	> 0.05

A.2.18 Serum concentrations of CXCL10 and CXCL9

Table A.19: Data table: Serum concentrations of CXCL10 and CXCL9 during *L. monocytogenes* infection. $\bar{x}$ represents means of serum concentrations. $Adap^{+/+}$, N = 4 (uninfected), 9 (infected); $Adap^{-/-}$, N = 4 (uninfected), 9 (infected). Statistical analysis was performed using two-way ANOVA with Bonferroni's *post hoc* test.

	Serum concentration of CXCL10 (IP-10) during *L. monocytogenes* infection				
	$Adap^{+/+}$		$Adap^{-/-}$		
	$\bar{x}$ [pg · mL^{-1}]	$\pm$ SEM	$\bar{x}$ [pg · mL^{-1}]	$\pm$ SEM	p value
Days post infection					
0	26.56	1.975	24.42	1.107	> 0.05
1	1654	231.5	998.9	180.1	≤ 0.01
3	347.9	158.7	812.4	215.7	> 0.05
5	46.52	5.043	226.5	67.33	> 0.05
7	34.52	12.23	44.43	12.80	> 0.05
	Serum concentration of CXCL9 (MIG) during *L. monocytogenes* infection				
0	29.97	4.649	29.59	5.092	> 0.05
1	440.3	73.29	191.9	49.91	≤ 0.01
3	345.8	58.91	473.6	54.88	> 0.05
5	90.89	10.80	315.8	79.96	≤ 0.05
7	82.90	44.49	96.73	22.48	> 0.05

A.2.19 CD69$^+$ CD8$^+$ T cells in livers and spleens

Table A.20: Data table: CD69$^+$ CD8$^+$ T cell numbers in spleen and liver during *L. monocytogenes* infection. $\bar{x}$ represents means of cell numbers. $Adap^{+/+}$, N = 4–5; $Adap^{-/-}$, N = 4–5. Statistical analysis was performed using two-way ANOVA with Bonferroni's *post hoc* test.

	Liver CD69$^+$ CD8$^+$ T cells during *L. monocytogenes* infection				
	$Adap^{+/+}$		$Adap^{-/-}$		
	$\bar{x}$ (×10^6)	$\pm$ SEM	$\bar{x}$ (×10^6)	$\pm$ SEM	p value
Days post infection					
0	0.005022	0.001034	0.005198	0.0007482	> 0.05
3	0.06078	0.01966	0.03652	0.008525	> 0.05
5	0.9088	0.08056	0.9955	0.08268	> 0.05
7	0.8898	0.2208	1.481	0.2769	≤ 0.05
	Splenic CD69$^+$ CD8$^+$ T cells during *L. monocytogenes* infection				
0	0.2422	0.02899	0.1786	0.01626	> 0.05
3	1.750	0.2855	1.628	0.3104	> 0.05
5	3.488	0.1719	3.068	0.7818	> 0.05
7	10.93	0.8448	7.413	1.268	≤ 0.001

A.2.20 CD43$^+$ CD8$^+$ T cells in livers and spleens

Table A.21: Data table: CD43$^+$ CD8$^+$ T cell numbers in spleen and liver during *L. monocytogenes* infection. $\bar{x}$ represents means of cell numbers. *Adap*$^{+/+}$, N = 4–5; *Adap*$^{-/-}$, N = 4–5. Statistical analysis was performed using two-way ANOVA with Bonferroni's *post hoc* test.

	Liver CD43$^+$ CD8$^+$ T cells during *L. monocytogenes* infection				
	Adap$^{+/+}$		*Adap*$^{-/-}$		
	$\bar{x}$ ($\times 10^6$)	$\pm$ SEM	$\bar{x}$ ($\times 10^6$)	$\pm$ SEM	*p* value
Days post infection					
0	0.01503	0.001723	0.01338	0.001343	> 0.05
3	0.01547	0.004288	0.01207	0.001920	> 0.05
5	2.404	0.3610	2.013	0.3310	> 0.05
7	1.842	0.4931	6.046	1.152	≤ 0.001
	Splenic CD43$^+$ CD8$^+$ T cells during *L. monocytogenes* infection				
0	0.1056	0.01512	0.1176	0.01257	> 0.05
3	0.2836	0.03282	0.3036	0.05831	> 0.05
5	4.478	0.5523	4.610	1.983	> 0.05
7	5.460	0.8099	8.972	2.164	> 0.05

A.2.21 IFN-γ^+ CD8$^+$ T cells in livers and spleens

Table A.22: Data table: IFN-γ^+ CD8$^+$ T cell numbers in spleen and liver during *L. monocytogenes* infection. $\bar{x}$ represents means of cell numbers. *Adap*$^{+/+}$, N = 4–5; *Adap*$^{-/-}$, N = 4–5. Statistical analysis was performed using two-way ANOVA with Bonferroni's *post hoc* test.

	Liver IFN-γ^+ CD8$^+$ T cells during *L. monocytogenes* infection				
	Adap$^{+/+}$		*Adap*$^{-/-}$		
	$\bar{x}$ ($\times 10^6$)	$\pm$ SEM	$\bar{x}$ ($\times 10^6$)	$\pm$ SEM	*p* value
Days post infection					
0	0.001942	0.0004049	0.001433	0.0002369	> 0.05
3	0.01027	0.005192	0.01835	0.005431	> 0.05
5	0.6118	0.07108	0.5463	0.02219	> 0.05
7	0.5370	0.1741	0.5790	0.2644	> 0.05
	Splenic IFN-γ^+ CD8$^+$ T cells during *L. monocytogenes* infection				
0	0.01606	0.004051	0.01684	0.001979	> 0.05
3	1.143	0.2672	1.241	0.3573	> 0.05
5	3.016	0.2213	2.828	0.7143	> 0.05
7	5.678	0.8145	6.515	1.340	> 0.05

A.2.22 PD-1$^+$ CD8$^+$ T cells in livers and spleens

Table A.23: Data table: PD-1$^+$ CD8$^+$ T cell numbers in spleen and liver during *L. monocytogenes* infection. $\bar{x}$ represents means of cell numbers. $Adap^{+/+}$, N = 4–5; $Adap^{-/-}$, N = 4–5. Statistical analysis was performed using two-way ANOVA with Bonferroni's *post hoc* test.

	$Adap^{+/+}$		$Adap^{-/-}$		
	$\bar{x}$ ($\times 10^6$)	$\pm$ SEM	$\bar{x}$ ($\times 10^6$)	$\pm$ SEM	p value
Days post infection					
0	0.01078	0.001407	0.009115	0.0008484	> 0.05
3	0.05603	0.02835	0.02089	0.006839	> 0.05
5	0.02654	0.003318	0.05603	0.01243	> 0.05
7	0.2428	0.05338	0.5728	0.04608	≤ 0.001

Splenic PD-1$^+$ CD8$^+$ T cells during *L. monocytogenes* infection

0	0.08305	0.01983	0.08088	0.01447	> 0.05
3	0.07158	0.01039	0.1084	0.008763	> 0.05
5	0.05994	0.006560	0.1002	0.01908	> 0.05
7	0.7578	0.1208	1.083	0.2080	> 0.05

A.2.23 Absolute NK cell numbers in livers and spleens

Table A.24: Data table: Absolute NK cell numbers in spleen and liver during *L. monocytogenes* infection. $\bar{x}$ represents means of cell numbers. $Adap^{+/+}$, N = 5; $Adap^{-/-}$, N = 4–5. Statistical analysis was performed using two-way ANOVA with Bonferroni's *post hoc* test.

	$Adap^{+/+}$		$Adap^{-/-}$		
	$\bar{x}$ ($\times 10^6$)	$\pm$ SEM	$\bar{x}$ ($\times 10^6$)	$\pm$ SEM	p value
Days post infection					
0	0.2196	0.03186	0.1780	0.02463	> 0.05
1	0.2477	0.05993	0.3246	0.1755	> 0.05
2	0.9718	0.04577	1.036	0.2432	> 0.05
3	0.7514	0.1850	0.5228	0.09883	> 0.05
5	1.910	0.3132	1.2145	0.1508	≤ 0.05
7	0.3978	0.09648	0.6960	0.1049	> 0.05

Splenic NK cells during *L. monocytogenes* infection

0	3.922	0.3957449	2.932	0.2227644	> 0.05
1	3.816	0.1130752	2.686	0.0786511	≤ 0.05
2	1.2376	0.1364322	0.6546	0.1433725	> 0.05
3	0.5624	0.05916891	0.587	0.1200379	> 0.05
5	2.882	0.5704682	1.33375	0.455912	≤ 0.01
7	2.524	0.06368674	1.22225	0.3270857	≤ 0.05

A.2.24 CD69$^+$ NK cell frequency in livers and spleens

Table A.25: Data table: CD69$^+$ NK cell frequency in spleen and liver during *L. monocytogenes* infection. $\bar{x}$ represents means of percent CD69$^+$ NK cells. *Adap*$^{+/+}$, N = 5–8; *Adap*$^{-/-}$, N = 4–7. Statistical analysis was performed using two-way ANOVA with Bonferroni's *post hoc* test.

| | Liver CD69$^+$ NK cell frequency during *L. monocytogenes* infection | | | | |
| | *Adap*$^{+/+}$ | | *Adap*$^{-/-}$ | | |
Days post infection	$\bar{x}$ [%]	$\pm$ SEM	$\bar{x}$ [%]	$\pm$ SEM	*p* value
0	14.28	0.8169	14.12	0.6741	> 0.05
1	35.16	4.747	40.10	1.823	> 0.05
2	29.78	1.921	36.74	8.010	> 0.05
3	21.47	4.576	51.59	5.112	$\leq$ 0.001
5	6.674	0.4646	20.01	5.533	> 0.05
7	20.62	2.128	17.78	2.102	> 0.05
	Splenic CD69$^+$ NK cell frequency during *L. monocytogenes* infection				
0	4.802	0.3323	4.506	0.4762	> 0.05
1	22.22	0.7344	22.56	4.024	> 0.05
2	44.68	3.960	51.42	5.674	> 0.05
3	23.15	3.059	53.38	5.901	$\leq$ 0.001
5	6.036	1.469	20.55	7.255	> 0.05
7	5.122	0.5303	5.630	0.7742	> 0.05

A.2.25 IFN-γ^+ NK cell frequency in livers and spleens

Table A.26: Data table: IFN-γ^+ NK cell frequency in spleen and liver during *L. monocytogenes* infection. $\bar{x}$ represents means of percent IFN-γ^+ NK cells. *Adap*$^{+/+}$, N = 5–8; *Adap*$^{-/-}$, N = 4–7. Statistical analysis was performed using two-way ANOVA with Bonferroni's *post hoc* test.

| | Liver IFN-γ^+ NK cell frequency during *L. monocytogenes* infection | | | | |
| | *Adap*$^{+/+}$ | | *Adap*$^{-/-}$ | | |
Days post infection	$\bar{x}$ [%]	$\pm$ SEM	$\bar{x}$ [%]	$\pm$ SEM	*p* value
0	14.26	1.874	11.90	1.642	> 0.05
1	38.28	5.612	68.42	12.67	$\leq$ 0.001
2	5.726	0.5923	7.238	1.745	> 0.05
3	4.426	1.280	18.66	3.964	$\leq$ 0.01
5	0.5960	0.08430	1.850	0.5716	> 0.05
7	0.2760	0.05653	0.2540	0.05372	> 0.05
	Splenic IFN-γ^+ NK cell frequency during *L. monocytogenes* infection				
0	0.3700	0.08000	0.5560	0.04665	> 0.05
1	8.282	0.8678	15.14	3.159	> 0.05
2	12.45	2.0913	15.66	2.033	> 0.05
3	6.896	1.6611	21.29	5.344	$\leq$ 0.001
5	1.086	0.2773	3.418	1.048	> 0.05
7	0.1002	0.01867	0.1474	0.0323	> 0.05

A.2.26 CD27$^+$ NK cell frequency in livers and spleens

**Table A.27: Data table: CD27$^+$ NK cell frequency in spleen and liver during *L. monocytogenes*
infection.** $\bar{x}$ represents means of percent CD27$^+$ NK cells. *Adap*$^{+/+}$, N = 5–8; *Adap*$^{-/-}$, N = 4–7.
Statistical analysis was performed using two-way ANOVA with Bonferroni's *post hoc* test.

| | Liver CD27$^+$ NK cell frequency during *L. monocytogenes* infection | | | | |
| | *Adap*$^{+/+}$ | | *Adap*$^{-/-}$ | | |
	$\bar{x}$ [%]	$\pm$ SEM	$\bar{x}$ [%]	$\pm$ SEM	p value
Days post infection					
0	21.31	1.129	14.84	1.707	> 0.05
1	32.22	2.271	23.51	1.126	> 0.05
2	45.24	2.074	29.68	3.032	≤ 0.01
3	55.42	6.309	48.53	5.352	> 0.05
5	62.58	1.132	59.10	3.345	> 0.05
7	44.72	1.338	55.84	3.698	> 0.05
	Splenic CD27$^+$ NK cell frequency during *L. monocytogenes* infection				
0	53.48	3.678	48.96	2.287	> 0.05
1	46.56	2.331	48.28	0.9805	> 0.05
2	71.78	1.384	48.20	3.171	≤ 0.001
3	76.44	0.8140	34.46	1.218	≤ 0.001
5	69.42	1.220	54.38	3.185	≤ 0.001
7	50.68	3.087	42.80	2.203	> 0.05

A.2.27 NK cell maturation in livers and spleens

**Table A.28: Data table: NK cell maturation in spleen and liver during *L. monocytogenes*
infection.** $\bar{x}$ represents means of absolute cell numbers. *Adap*$^{+/+}$, N = 5; *Adap*$^{-/-}$, N = 5. Statistical
analysis was performed using two-way ANOVA with Bonferroni's *post hoc* test.

| | NK cell maturation stages prior to *L. monocytogenes* infection | | | | |
| | *Adap*$^{+/+}$ | | *Adap*$^{-/-}$ | | |
	$\bar{x}$ ($\times 10^6$)	$\pm$ SEM	$\bar{x}$ ($\times 10^6$)	$\pm$ SEM	p value
Maturation stage					
DN	0.3279	0.08982	0.4014	0.05172	> 0.05
CD11b^{lo}	0.8871	0.09125	0.9846	0.1230	> 0.05
DP	0.8593	0.03290	0.7060	0.06271	> 0.05
CD27^{lo}	1.115	0.2161	1.180	0.09999	> 0.05
	NK cell maturation stages 1 day post *L. monocytogenes* infection				
DN	0.1992	0.01188	0.2752	0.02113	> 0.05
CD11b^{lo}	0.8166	0.05218	1.264	0.1129	> 0.05
DP	1.800	0.1028	1.080	0.08452	≤ 0.01
CD27^{lo}	2.812	0.1839	2.250	0.2386	≤ 0.05

A.3 Scientific contributions

A.3.1 List of publications

1. **Gerald P Parzmair**, Marcus Gereke, Oxana Haberkorn, Michaela Annemann, Lisa Podlasly, Stefanie Kliche, Annegret Reinhold, Burkhart Schraven & Dunja Bruder. The adaptor protein ADAP plays a pivotal role in CD4$^+$ T cell activation but is largely dispensable for CD8$^+$ T cell-mediated pathogen clearance. *Journal of Leukocyte Biology*, [in revision].

2. Robert B Frei, Petra Luschnig, **Gerald P Parzmair**, Miriam Peinhaupt, Silke Schranz, Alexander Fauland, Craig E Wheelock, Akos Heinemann & Eva M Sturm. Cannabinoid receptor 2 augments eosinophil responsiveness and aggravates allergen-induced pulmonary inflammation in mice. *Allergy*, Feb 2016.

3. Eva M. Sturm, **Gerald P Parzmair**, Balzs Radnai, Robert B. Frei, Gunter J. Sturm, Astrid Hammer, Rufina Schuligoi, Irmgard Th Lippe & Akos Heinemann. Phosphoinositidedependent protein kinase 1 (PDK1) mediates potent inhibitory effects on eosinophils. *Eur J Immunol*, **45**(5):15481559, May 2015.

4. Eva M Sturm, Balazs Radnai, Katharina Jandl, Angela Stancic, **Gerald P Parzmair**, Christoph Högenauer, Patrizia Kump, Heimo Wenzl, Wolfgang Petritsch, Thomas R Pieber, Rufina Schuligoi, Gunther Marsche, Nerea Ferreirs, Akos Heinemann & Rudolf Schicho. Opposing roles of prostaglandin D2 receptors in ulcerative colitis. *J Immunol*, **193**(2):82739, Jul 2014.

5. Julia Kargl, Nariman Balenga, **Gerald P Parzmair**, Andrew J Brown, Akos Heinemann & Maria Waldhoer. The cannabinoid receptor CB1 modulates the signaling properties of the lysophosphatidylinositol receptor GPR55. *J Biol Chem*, **287**(53):4423448, Dec 2012.

6. Viktoria Konya, Andreas Ullen, Nora Kampitsch, Anna Theiler, Sonia Philipose, **Gerald P Parzmair**, Gunther Marsche, Bernhard A Peskar, Rufina Schuligoi, Wolfgang Sattler & Akos Heinemann. Endothelial E-type prostanoid 4 receptors promote barrier function and inhibit neutrophil trafficking. *J Allergy Clin Immunol*, Jun 2012.

7. Pia Tschische, Elisabeth Moser, Dawn Thompson, Henry F Vischer, **Gerald P Parzmair**, Veronika Pommer, Wolfgang Platzer, Thomas Schwarzbraun, Helmut Schaider, Martine J Smit, Lene Martini, Jennifer L Whistler & Maria Waldhoer. The G-protein coupled receptor associated sorting protein GASP-1 regulates the signalling and trafficking of the viral chemokine receptor US28. *Traffic*, **11**(5):660674, May 2010.

A.3.2 Meeting abstracts

1. Eva Sturm, **Gerald P Parzmair**, Petra Luschnig-Schratl, Viktoria Konya & Akos Heinemann. [Meeting Abstract] Protein kinase C-zeta is involved in the inhibition of eosinophil migration. *BMC Pharmacology*, **9**(Suppl 2):A34, 2009.

2. **Gerald P Parzmair**, Wolfgang Platzer, Henry Vischer, Martine Smit & Maria Waldhoer. [Meeting Abstract] The far carboxy-terminus of the viral encoded chemokine receptor US28 binds to the sorting protein GASP-1 in vitro. *BMC Pharmacology*, **8**:11, 2008. 10.1186/1471-2210-8-S1-A26.

3. **Gerald P Parzmair**, Wolfgang Platzer & Maria Waldhoer. [Meeting Abstract] Mapping the interaction sites of the viral encoded chemokine receptor US28 and the sorting protein GASP-1. *BMC Pharmacology*, **7**:11, 2007. 10.1186/1471-2210-7-S2-A12.

A.3.3 Congress attendance and public presentations

1. **Gerald P Parzmair**, Marcus Gereke, Oxana Haberkorn, Annegret Reinhold, Maxi Heyner, Olivia Kershaw, Burkhart Schraven & Dunja Bruder. The potential regulatory roles of the adaptor protein ADAP in immune responses against the intracellular pathogen *Listeria monocytogenes*. **Oral presentation**. *8th International PhD Symposium of the HZI Infection Research Graduate School*. 10th of December 2015. Braunschweig, Germany.

2. **Gerald P Parzmair**, Marcus Gereke, Maxi Heyner, Oxana Haberkorn, Lothar Jänsch, Burkhart Schraven & Dunja Bruder. The potential regulatory roles of the adaptor protein ADAP in the innate immune response against the intracellular pathogen *Listeria monocytogenes*. **Poster Presentation**. *1st Allergy Meets Infection International Symposium*. 8th – 11th of November 2015. Lübeck, Germany.

3. **Gerald P Parzmair**, Marcus Gereke, Burkhart Schraven & Dunja Bruder.The adaptor protein ADAP is dispensable in the CD8$^+$ T cell mediated immune response against the intracellular pathogen *Listeria monocytogenes*. **Oral and poster presentation**. *44th Annual Meeting of the German Society for Immunology*. 17th – 21st of September 2014. Bonn, Germany.

A.4 Selbständigkeitserklärung

Gerald Peter Parzmair, M.Sc., B.Sc.
Virchowstr. 38
38118 Braunschweig, Deutschland

Erklärung

Hiermit erkläre ich, dass ich die von mir eingereichte Dissertation zu dem Thema

The Role of the Adaptor Protein ADAP in different T cell Subsets and Pathogen-specific Immune Responses against *Listeria monocytogenes*

selbständig verfasst, nicht schon als Dissertation verwendet habe und die benutzten Hilfsmittel und Quellen vollständig angegeben wurden.

Weiterhin erkläre ich, dass ich weder diese noch eine andere Arbeit zur Erlangung des akademischen Grades *doctor rerum naturalium* (Dr. rer. nat.) an anderen Einrichtungen eingereicht habe

Magdeburg, am 27. September 2016   Gerald Peter Parzmair, M.Sc., B.Sc.

A.5 Curriculum vitae

Persönliche Daten

Name:	Gerald Peter Parzmair
Geburtsdatum:	14.12.1981
Geburtsort:	Hallein, Österreich
Staatszugehörigkeit:	Österreich

Bildungsgang

2001   **Matura**, *Bundesgymnasium und Bundesrealgymnasium Hallein*, 5400 Hallein, Österreich.
Hochschulreifeprüfung

2002–2009   **Bachelor of Science (B.Sc.)**, *Paris Lodron Universität Salzburg*, 5020 Salzburg, Österreich.
Studiengang: Biologie/Genetik

2009–2012   **Master of Science (M.Sc.)**, *Paris Lodron Universität Salzburg*, 5020 Salzburg, Österreich.
Studiengang: Biologie/Genetik
Masterarbeit: "The Effects of Cannabidiol and Structural Analogues on Polymorphonuclear Leukocyte Function"
Betreuer: Prof. Dr. Akos Heinemann and Prof. Dr. Josef Thalhamer

2012–2016   **Doktorand**, *Otto-von-Guericke-Universität Magdeburg*, 39106 Magdeburg, Deutschland.
Dissertation: "The Role of the Adaptor Protein ADAP in different T cell Subsets and Pathogen-specific Immune Responses against *Listeria monocytogenes*"
Betreuer: Prof. Dr. Dunja Bruder und Prof. Dr. Burkhart Schraven

Praktika

2006   **Arbeitsgruppe Prof. Dr. Robert Schwarzenbacher**, *Paris Lodron Universität Salzburg*, 5020 Salzburg, Österreich.
Strukturbiologie

2007–2008   **Arbeitsgruppe Dr. Maria Waldhör**, *Medizinische Universität Graz*, 8020 Graz, Österreich.
Signaltransduktion, Protein-Affinitätsstudien.